



ScuDo

Scuola di Dottorato ~ Doctoral School

WHAT YOU ARE, TAKES YOU FAR



Doctoral Dissertation
Doctoral Program in Mechanical Engineering (32th Cycle)

Powered exoskeleton for trunk assistance in industrial tasks

PhD Candidate

Elisa Panero

* * * * *

Supervisor

Prof. Laura Gastaldi

Doctoral Examination Committee:

Prof. Francesco Bottiglione, Politecnico di Bari, Bari, Italia
Prof. Fabrizio Billi, University of California, Los Angeles, California

Politecnico di Torino
June 2020

This thesis is licensed under a Creative Commons License, Attribution - Noncommercial - NoDerivative Works 4.0 International: see www.creativecommons.org. The text may be reproduced for non-commercial purposes, provided that credit is given to the original author.

I hereby declare that, the contents and organisation of this dissertation constitute my own original work and does not compromise in any way the rights of third parties, including those relating to the security of personal data.

.....
Elisa Panero
Turin, June 2020

Acknowledgment

I would like to express my sincere gratitude to my supervisors Prof. Laura Gastaldi for providing her strong guidance, suggestions and support along my Ph.D. experience. She reveals to be a precious mentor, a colleague, a friend and, sometimes, a mum.

The realization of this project could not have been accomplished without the support of Prof. Stefano Paolo Pastorelli: he gave me the chance to improve my knowledge and to grow my professional and personal figure.

I would like to thank Prof. Francesco Bottiglione and Prof. Fabrizio Billi for accepting the opportunity to revise my Doctoral Dissertation and for their constructive and stimulating comments.

If I said that my Ph.D. has been an easy route, it would be a lie. However, it gave me unique emotions and unforgettable memories.

Thanks to all my colleagues that are always ready to sustain and support me: the next-door office, the XXXII cycle, the fifth floor DIMEAS.

Thanks to “Amici di G” for giving me the strength to smile, always.

Thanks to Dario, the most unexpected and passionate “April Fool”.

Finally, a sincere thanks to Carla, Antonio and Silvia, my safe haven, forever and ever.

Ringraziamenti

Il mio primo ringraziamento va alla mia Tutor Prof. Laura Gastaldi, per la sua forte guida, i suoi suggerimenti ed il suo supporto durante tutto il mio percorso di Dottorato. Laura è stata per me una mentore, ma anche collega, amica e mamma.

Non sarebbe stato possibile portare a termine il progetto senza il supporto del Prof. Stefano Paolo Pastorelli. Con i suoi insegnamenti, mi ha permesso di crescere professionalmente, ma anche come persona.

Vorrei ringraziare i revisori Prof. Francesco Bottiglione e Prof. Fabrizio Billi per aver accettato l'incarico e per i loro costruttivi commenti e stimoli per approfondire la ricerca.

Mentirei se dicessi che il mio Dottorato è stato un percorso facile. Eppure, mi ha regalato irripetibili emozioni ed indelebili ricordi.

Grazie ai colleghi dell'ufficio accanto, ai colleghi del XXXII ciclo, al DIMEAS quinto piano, a tutte le persone che sono state sempre pronte a supportarmi e sopportarmi.

Grazie agli "Amici di G" per avermi dato la forza di sorridere, sempre.

Grazie a Dario, il "Pesce d'Aprile" più inaspettato e travolgente.

Infine, un grazie sincero a Carla, Antonio e Silvia, il mio porto sicuro, da sempre e per sempre.

Ad Elisa,

*Che il tuo dolce sorriso possa
accompagnarti in ogni tuo traguardo.*

Summary

Within Industry 4.0, the robotic innovations and applications focus on the simultaneous presence of robots and workers sharing the same workstation. The role of robots has changed during the last decades, starting from substituting workers in heavy and hard tasks to assisting them in performing works. Merging robotics and human skills, as creativity and decision-making, seems to be a promising solution for many tasks that cannot be totally automated. In this contest also wearable robotics is introduced in manufacturing and industrial fields. Occupational health and safety are principal objects of interest due to the impact of work-related accidents and diseases on the work population. Among those, low back pain and injuries are the most common.

Industrial exoskeletons are robotic, mechanical devices directly worn by the users. The principal aim of an industrial exoskeleton is the partial reduction of the muscular efforts of the operator during working gesture. The exoskeleton can be defined as a personal daily use equipment and, for this reason, the acceptability and wearability by the operators gain crucial importance in design and development.

The aim of the present PhD thesis is the analysis, design and development of a powered exoskeleton prototype for the trunk support in industrial tasks of lifting and manual handling.

After briefly introducing the biomechanics and physiology of the human spine, the kinematics and dynamics connected to the risk of injuries are analysed. Then a literature review of current trunk support exoskeletons is conducted with the attempt to highlight current open challenges. Due to the specific function of the assistive device, ergonomic guidelines and lifting strategies are explored.

Mechanical and assistance characteristics of a passive commercial trunk-support exoskeleton are analyzed. Experimental tests are conducted to evaluate the device performances and to stress the benefits and drawbacks of the system in order to point out possible improvements.

A model-based approach is selected for the investigation of human-exoskeleton interaction, with attention to the effects of the wearable device on human body biomechanical loads. 3D multibody models of the human body, exoskeleton and interface are implemented. The simulation analyses of different exoskeleton configurations and the biomechanical investigation of human joint efforts allow the final characterization of a suitable architecture and assistance law for the powered system. The new system should be able to recognize the lifting strategy adopted by the user and to differentiate the assistance based on human body kinematics. The support strategy is designed to be user and task specific.

Based on experimental and computational analyses, the powered prototype of the trunk support exoskeleton is developed. Both the mechanical and control architectures are object of the present study.

The mechanical design and the implementation of the powered system are deeply presented, starting from the identification of the maximum supplied torque. Mechanical components are selected with the attempt to provide the required assistance performance with limited encumbrance and weight of the final structure. The exoskeleton supplies assistance to the user through electric actuators and a proper designed powered joint. The study presents the CAD design of different solutions in order to ensure compactness and lightweight of the final proposal.

The control system is based on two loops: model-based control (high level) for the definition of the desired torque and torque control (low level) for the closed loop on the motor output. The hardware system and the selected electronic components are defined for the implementation of the exoskeleton two-level control architecture.

CONCEPTUAL MAP of the Thesis

State of the art

Analysis of the past evolution in Robotics application, the introduction of wearable device in industrial environment, the current commercial and research proposals for the assistance of workers in lifting tasks.



Principal Aim of the PhD project: development of a powered trunk support exoskeleton prototype for the recognition of lifting strategies

Passive system

Analysis of the Laevo mechanical & design structure

Analysis of assistance mechanism & interaction with user in terms of size and wearability

Investigation of exo performance in lifting strategies & user's acceptance

Modelling simulation

Development of human, interface & exoskeleton 3D models

Biomechanical analysis of human joints efforts & interaction forces

Investigation of different exo configurations

Maps of exoskeleton torque assistance

Powered system: control architecture

Analysis of assistive strategies for wearable device

Model based strategy & torque control: description of the architecture

Analysis & selection of electronic components

Impedance control with SEA: analysis, modeling and design

Powered system: mechanical concept

Project of needed torque & contact force threshold

Analysis & selection of mechanical components

Mechanical design for the integration of motorized exo joint

Mechanical end-strokes definition

Powered device: final solution implementation

Conclusion

Summary of the principal results, future plans for the experimental validation of the implemented exoskeleton system and possible improvements.

Contents

List of Tables	IX
List of Figures.....	XI
List of Acronyms	XIX
1. INTRODUCTION	1
2. STATE OF ART	5
2.1. Exoskeleton in the industrial environment	5
2.2. Biomechanics of the human spine	12
2.3. Human lifting strategies.....	19
2.4. Ergonomic regulations and guidelines.....	22
2.5. Current trunk exoskeleton solutions	24
2.6. Experimental applications.....	37
3. MAIN GOALS AND THESIS CONTRIBUTION	53
4. PASSIVE SYSTEM: Biomechanical evaluation.....	57
4.1. The Laevo exoskeleton	57
4.1.1 Mechanical structure	58
4.1.2 Exoskeleton assistance	61
4.1.3 Exoskeleton wearability	63
4.2. Experimental test	65
4.2.1 Principal aim	65
4.2.2 Material & Methods	66
4.2.3 Results and discussion.....	73
4.2.4 Conclusion.....	80
4.2.5 Future perspectives.....	81
5. MODELING APPROACH.....	83
5.1. The computational approach.....	83
5.2. 3D multibody models.....	84
5.2.1 Human model	84

5.2.2	Exoskeleton model	92
5.2.3	Interface model.....	93
5.2.4	Dynamic simulation	93
6.	SIMULATION ANALYSIS	95
6.1.	Influence of exoskeleton hinge joint positioning.....	96
6.2.	Comparison of two mechanical designs for a passive exoskeleton 104	
6.3.	Simulation maps for differentiating lifting strategies	116
7.	POWERED PROTOTYPE: the actuation and control scheme	127
7.1.	Introduction.....	127
7.2.	Actuation solutions for wearable robotics	128
7.3.	Exoskeleton actuator selection.....	130
7.4.	Control Architecture: model-based strategy and torque control....	132
7.5.	Electronic components.....	133
7.6.	Serial elastic actuator	135
7.6.1	Spring design.....	137
7.7.	Conclusion	146
8.	POWERED PROTOTYPE: the mechanical concept	147
8.1.	From Passive to Powered Exoskeleton.....	147
8.2.	Actuation system.....	148
8.2.1	Pressure thresholds.....	148
8.2.2	Evaluation of the demanded torque.....	150
8.2.3	Selection of the mechanical components	151
8.3.	Angular sensors.....	156
8.3.1	Inertial sensors analysis.....	156
8.3.2	Measurement of trunk-thigh angle	158
8.3.3	Measurement of the thigh flexion	159
8.4.	Powered joint design.....	162
8.4.1	From the first to the final solution.....	162
8.4.2	Design solutions	164
8.4.3	The transmission mechanism	167
8.4.4	Mechanical end-strokes definition	170
8.4.5	Mechanical description of the final proposal	176

8.5.	Mechanical components connection.....	178
8.6.	Exoskeleton assembly.....	179
9.	CONCLUSIONS.....	187
9.1.	Study results.....	187
9.2.	Future perspectives.....	188
10.	References.....	190
A.	Appendix: Anatomical reference position.....	201
B.	Appendix: ISO reference guidelines.....	210
C.	Appendix: a standardized rating scale for subjective evaluation.....	216

List of Tables

Table 2.5.1 List of passive trunk exoskeletons.	26
Table 2.5.2 List of active trunk exoskeletons.....	33
Table 2.6.1: List of experimental tests on wearable trunk support exoskeletons.....	43
Table 4.2.1: Labelling and description of the markers set positioned on the human body, exoskeleton and laboratory tools.....	69
Table 4.2.2: Subjective evaluation in different tasks of perceived efforts (Borg scale), perceived local discomfort, perceived local pressure, with and without the exo	78
Table 5.2.1: Human body anthropometry and inertial parameters.....	87
Table 6.2.1: Kinematic sketches of the several human lifting strategies reproduced in the simulation and detailed angles description for the human trunk and lower body joints.	106
Table 6.2.2: Comparison of the two passive exoskeleton structure (Single and Double Support) in terms of biomechanical effects on human variables.	114
Table 6.3.1: Manikin motion schematization and maximum human joint angles.	123
Table 7.2.1: Description of the most common actuators solution for the development of powered exoskeleton, stressing the advantages and the drawbacks.....	129
Table 7.6.1 Mechanical description of main characteristics of the selected motor for the simulation of serial elastic actuator.....	138
Table 7.6.2: Mechanical description of the main characteristics of the designed spring. The material is chrome-molybdenum-vanadium steel DIN 1.2367 (X38CrMoV5-3).....	144
Table 8.4.1: Numerical definition of the end-stroke angular range implemented in the powered prototype.....	173
Table A.1: Human body segments and joints description with relative labels.	204
Table A.2: Definition of relative motion between human segments and description of physiological ranges of motion.	205
Table B.1: Mass reference value.....	211
Table B.2: Classification of the Lifting Index in working manual and lifting tasks.	213
Table B.3: Description of the OCRA classification of risk in case of repetitive tasks. ..	214
Table B.4: Classification of the OCRA Index.....	215

List of Figures

Figure 2.1.1: Maps of the different exoskeleton classification strategies.	7
Figure 2.1.2: Examples of upper limb industrial exoskeletons. Passive upper limb exoskeleton Mate by Comau (A), passive upper limb Airframe by Levitate Technologies (B) and active PARM prototype by Kadota and colleagues (C).	8
Figure 2.1.3: Examples of trunk industrial exoskeletons. Passive trunk exoskeleton BackX by SuitX (A), passive Laevo exoskeleton by Laevo (B) and active trunk exoskeleton prototype from ROBOMATE European project (C).....	9
Figure 2.1.4: Examples of lower limb industrial exoskeletons. Passive lower limb exoskeleton Chairless Chair by Noone (A), passive lower limb exoskeleton Lex wearable chair by Astride Bionix (B) and passive lower limb Archelis by Nitto company (C).	9
Figure 2.1.5: Examples of total body industrial exoskeletons. Robot Suit Hybrid Assistive Limb HAL by Japan's Tsukuba University (A), Body Extender exoskeleton by PELCRO Laboratory of Scuola Superiore Sant'Anna (B) and AXO-SUIT modular full-body exoskeleton by EU AAL project (C).....	10
Figure 2.2.1: Sagittal, posterior and anterior views of the human spine and separation of the different vertebral regions: cervical, thoracic, lumbar and sacrum vertebrae.	12
Figure 2.2.2: Graphical representation of the principal human back muscle groups.	14
Figure 2.2.3: Graphical representation of the main human abdomen muscle groups.	14
Figure 2.2.4: Representative ranges of motion at the different regions of the human spine in flexion/extension, lateral bending and rotation movements.	15
Figure 2.2.5: Simplified free body diagram of forces at the lumbar spine (A); intradiscal pressure distribution during daily activities normalized respect to standing position loads measured by Wilke in 1998 (B).	17
Figure 2.3.1: Graphical representation of the three main lifting strategies: stooping (A), semi-squatting (B) and squatting (C) lifting techniques.	19
Figure 4.1.1: Laevo exoskeleton version 2.5. Identification of the three main parts and description of the several structural components.	58
Figure 4.1.2: Laevo exoskeleton structure. Description of the several components of the device and the free degrees of freedom integrated with the device to avoid any restrictions to physiological human body motion.	60
Figure 4.1.3: Laevo different proposed sizes and corresponding human body length.	60
Figure 4.1.4: Smart joint of the Laevo with covers (A), without covers and visible cam-spring mechanism (B), with separated mechanical components (C).	61
Figure 4.1.5: Graphical description of the cam-spring mechanism inside the smart joint and the torque-angle relation of the implemented passive assistance.....	62

Figure 4.1.6: Front view of four subjects with different height, anthropometry and gender wearing passive Laevo exoskeleton.	64
Figure 4.1.7: One female subject with a height < 1.72 m wearing the passive Laevo exoskeleton from lateral view (A-C), front view (B) and behind view (D).	65
Figure 4.2.1: Scheme of the setting for the simulation of industrial tasks dealing with the lifting and the manipulating of objects. Definition of the global coordinate system fixed to the table ($G_1G_2G_3$) and markers position on the box ($B_1B_2B_3$).	67
Figure 4.2.2: Static reference posture of the female subject with markers on human landmarks for the reconstruction of motion in the post-processing, without (A) and with (B) the exoskeleton.	68
Figure 4.2.3: Picture representing the three force sensors Flexiforce A502 (A), the three customized conditioning boxes (B), DAQ system and laptop (C).	70
Figure 4.2.4: Labview Block diagram (A) for the data acquisition from the customized pressure sensors.	70
Figure 4.2.5: Labview Front panel for the data acquisition from the customized pressure sensors.	70
Figure 4.2.6: Curve results from the calibration procedure of the three pressure sensors. Solid line refers to ascending phase of weight positioning (from lower to higher weight), while the dashed line refers to the descending phase (from higher to lower weight).	71
Figure 4.2.7: Upper limbs joints trajectory (waist, hip, knee, ankle) without (black line) and with (green line) exoskeleton, in all performed motions: static holding stoop (A), stoop lifting (B), semisquat lifting (C), squat lifting (D), free lifting (E).	73
Figure 4.2.8: Lower limbs joints trajectory (waist, hip, knee, ankle) without (black line) and with (green line) exoskeleton, in all performed motions: static holding stoop (A), stoop lifting (B), semisquat lifting (C), squat lifting (D), free lifting (E).	74
Figure 4.2.9: Joints range of motion without (black bar) and with (green bar) exoskeleton, in all performed motions: static holding stoop (A), stoop lifting (B), semisquat lifting (C), squat lifting (D), free lifting (E).	75
Figure 4.2.10: Pressure distribution on the contact area (trunk, right thigh) in all performed motions: static holding stoop (A), stoop lifting (B), semisquat lifting (C), squat lifting (D), free lifting (E).	76
Figure 4.2.11: Mean value of the subjective evaluation among different motion tasks of perceived efforts (Borg scale (A) without exoskeleton, (C) with exoskeleton), perceived local discomfort ((B) without exoskeleton, (D) with exoskeleton) and perceived local pressure ((E) with exoskeleton). Both graphical and numerical values are stressed.	79
Figure 5.2.1: 3D human body manikin from the frontal and the sagittal planes.	85
Figure 5.2.2: Matlab Simscape scheme of the human body model with segments and joints blocks description.	86
Figure 5.2.3: Matlab Simscape Multibody Contact Forces Library. Graphical representation of the contact model between the floor (Plane) and the human foot (square surface). (A) representation of the two element, relative dimensions and local coordinate system; (B) details of one square face corner modeled with a sphere.	88
Figure 5.2.4: Matlab Simscape Multibody Contact Forces Library. Linea force law (A) for the definition of contact force in the direction of penetration; (B-C) stick-slip continuous friction law for the calculation of friction force at the contact point.	89
Figure 5.2.5: Comparison of experimental and simulation pressures distribution in different foot subareas during (A) stoop, (B) semisquat and (C) squat lifting motion. Simulation curves are related to the four corners of the right foot model.	90

Figure 5.2.6: Extension torque at waist joint in (A) stoop and (B) semisquat: model curves (blue line), experimental reference mean (black dotted line) and experimental range curves (grey area).	91
Figure 5.2.7: Sketch of the human body wearing the device. Description of the main parts of the device and imscape scheme of the exoskeleton model.	92
Figure 5.2.8: Sketch of the manikin wearing the device and Simscape scheme of the interface model. Identification of the contact points.....	93
Figure 5.2.9: Simscape scheme of the connection between the three main models (A) and schematic representation of the main passages of the computational process (B).....	94
Figure 6.1.1: Human joint angle kinematics in (A) stoop and (B) semisquat lifting.	96
Figure 6.1.2: Graphical representation of the manikin movement and human joint maximum joint angles in (A) stoop and (B) semisquat lifting.	97
Figure 6.1.3: Maps of exoskeleton configurations in the three analysis: (A) random distribution of 100 hinge joint positions, (B) radial distribution of 200 positions with the displacement of only the assistance exoskeleton joint; (C) radial distribution of 200 positions with the coaxial displacement of both assistance and free exoskeleton joints... ..	98
Figure 6.1.4: Net joint moments at the waist and hip joints during (A-C) stoop and (B-D) semisquat lifting motions without wearing the exoskeleton.	99
Figure 6.1.5: Distribution of joints torque impulse and interface forces impulse during (A) stoop and (B) semisquat motion with different exoskeleton joint positions.	100
Figure 6.1.6: Interface forces (trunk/thigh) and human joints torques (waist/hip) maximum peaks during (A-C) stoop and (B-D) semisquat motion related to J ₂ positions. Graphs A-B refer to 20 Nm exo assistance, graphs C-D to 40 Nm.....	101
Figure 6.1.7: Maps of optimal and critical zones based on variables in (A-C) stoop and (B-D) semisquat motion. Green areas depict the suitable zone for the exo joint, while the red ones underline the critical areas. Graphs A-B refer to 20 Nm exo assistance, graphs C-D to 40 Nm.....	102
Figure 6.1.8: Net joint moments at the waist and hip joints during (A-C) stoop and (B-D) semisquat lifting motions.	104
Figure 6.2.1: Human lower limb joint angle kinematics in (A) stoop, (B) semisquat and (C) squat lifting.	105
Figure 6.2.2: Human lower limb joint angle kinematics in (A) stoop-squat and (B) squat-stoop lifting.	105
Figure 6.2.3: Graphical description of the two different passive exoskeleton structures and linear input characterization of the exoskeleton assistance expressing the relation between human torso angle and the maximum waist torque required with 60° of flexion.	106
Figure 6.2.4: Simulation map of the current analysis with the two exoskeletons.	107
Figure 6.2.5: Relative variation of biomechanical variables during the stoop motion when wearing the two different exoskeleton structures (blue and purple columns) compared to the physiological condition without the exoskeleton (black reference line).	108
Figure 6.2.6: Relative variation of biomechanical variables during the semisquat motion when wearing the two different exoskeleton structures (blue and purple columns) compared to the physiological condition without the exoskeleton (black reference line).	108
Figure 6.2.7: Relative variation of biomechanical variables during the squat motion when wearing the two different exoskeleton structures (blue and purple columns) compared to the physiological condition without the exoskeleton (black reference line).	109
Figure 6.2.8: Torques results at the human waist joint in (A) stoop, (B) semisquat and (C) squat. Graphs compared the 3 conditions: without (no exo), with single (SS exo) and with double (DS exo) support exoskeleton. The background highlights suitable values.....	110

Figure 6.2.9: Torques results at the human hip in stoop (A), semisquat (B) and squat (C). Graphs compared the three conditions: without (no exo), with single support (SS exo) and with double support (DS exo). The graph background highlights the range of suitable values.	111
Figure 6.2.10: Compression and shear forces at the waist ($C_W - S_W$) and hip ($C_H - S_H$) in stoop (A), semisquat (B) and squat (C). Bar graphs compared the three conditions: without (no exo), with a single (SS exo) and with double support (DS exo) exo.	112
Figure 6.2.11: Interface pressures results at the human trunk in stoop (A), semisquat (B) and squat (C). Graphs compared the two-exoskeleton conditions: with single support (SS exo) and with double support (DS exo). The graph background highlights the range of suitable values.	112
Figure 6.2.12: Interface pressures results at the human thigh in stoop (A), semisquat (B) and squat (C). Graphs compared the two-exoskeleton conditions: with single support (SS exo) and with double support (DS exo). The graph background highlights the range of suitable values.	113
Figure 6.2.13: Torques results at the human waist joint in combined motion stoop-squat (A) and squat-stoop (B). Graphs compared the three conditions: without (no exo), with single support (SS exo) and with double support (DS exo) exoskeleton. The graph background highlights the range of suitable values.	115
Figure 6.2.14: Torques results at the human hip joint in combined motion stoop-squat (A) and squat-stoop (B). Graphs compared the three conditions: without (no exo), with single support (SS exo) and with double support (DS exo) exoskeleton. The graph background highlights the range of suitable values.	115
Figure 6.3.1: Different human body poses assumed by the user without changing the absolute flexion angle of the trunk: (A) stoop, (B) stoop with extended hips, (C) semisquat; (D) squat; (E) deep squat.....	117
Figure 6.3.2: Starting from the standing posture (A), a description of principal angles involved during the three main lifting strategies: (B) stoop, (C) semisquat, (D) squat. .	117
Figure 6.3.3: Graphical schematization of the angles involved in the definition of mechanical assistance in the passive (A) and powered exoskeleton (B).	118
Figure 6.3.4: Example of assistance map based on the manikin parameters and joint loads calculation. The map represents the assistance law which must be implemented for each exoskeleton motorized joint, for the final support of 50% at the human waist.....	119
Figure 6.3.5: (A) Torque-Velocity and (B) Torque-Angle relation describing the assistance map.....	121
Figure 6.3.6: Graphical curves of the kinematic inputs for upper and lower human limbs in (A) stoop and (B) squat.....	122
Figure 6.3.7: Kinematics of (A) stoop and (B) squat motions for the waist (black line) and lower limb (light blue line) joints of the human body manikin, the absolute trunk angle (orange line) and the exoskeleton β (blue line) and α (red line) angles.	123
Figure 6.3.8: Comparison results of waist torques in the three simulated conditions (without exoskeleton, with a passive exoskeleton, with a powered exoskeleton) and exoskeletons assistance torque during (A) stoop and (B) squat motion.	124
Figure 7.3.1: Description of powered exoskeleton (motor-reducer) and human body (load) interaction.....	130
Figure 7.4.1: Concept of the torque control scheme of powered exoskeleton without the elastic element. Two main levels of control: high-level control and low-level control. .	133
Figure 7.5.1: Front (A) and lateral (B) view of the motor driver with the summary of the main characteristics.....	134

Figure 7.5.2: (A) National Instruments USB 6341 DAQ system interface and (B) National Instruments USB 8502 CAN interface communication device presentation. Graphical picture of the devices and tables summing up the main characteristics.	135
Figure 7.6.1: Serial elastic actuator schematization implemented in exoskeleton- human body interaction (A); example of control loop for the regulation of SEA (B).	136
Figure 7.6.2: Graphical schematization of the complete system with control-SEA-load (A), rotary serial elastic actuator (B) and passages for the evaluation of stiffness (C).	139
Figure 7.6.3: Bandwidth analysis simulation with different value of spring stiffness (100, 200, 300, 800 Nm/rad) in case of fixed load: the bode diagram. In the magnitude plot, the green and the red areas stress the range of torque frequencies if considering a spring stiffness of 200 Nm/rad.	141
Figure 7.6.4: Impedance analysis simulation with different value of spring stiffness (100, 200, 300, 800 Nm/rad) with applied external load: the bode diagram. The natural frequency of 5 Hz is selected in order to calculate the gain of the proportional controller.	142
Figure 7.6.5: Design of custom spring: (A) front view with inner (18 mm) and outer (100 mm) diameters, (B) lateral view with thickness (20 mm), (C) simulation design of the maximum expected load (torsional moment of 60 Nm on the external ring) with constrained inner ring, (D) Von Mises results with stressed angular displacement (20°).	143
Figure 7.6.6: Simulation results of the static analysis with imposed torsional moment on the external ring and constraints on the inner ring: (A) Von Mises stress results, (B) displacement results, (C) strain results and (D) safety factor evaluation.	145
Figure 7.6.7: Concept of the control scheme of powered exoskeleton with SEA. Three main levels of control: high level control, impedance control and low-level control.	145
Figure 8.2.1: Theoretical description of the relation between the external load applied and the duration for the definition of tissue damage (A); theoretical relation between physical activity and risk of low back pain (B).	149
Figure 8.2.2: Simulation and design of the max assistance torque: (A) relation between contact area and applied force considering maximum pressure, (B) force-torque relation considering the Laevo's dimensions, (C) comparison among waist joint moments required in lifting conditions and the dimensioned max assistance torque.	150
Figure 8.2.3: Front (A), back (B) and lateral (C-D) view of the selected Maxon motor EC60 flat. Description of the main mechanical, electric and technical characteristics.	152
Figure 8.2.4: Front (A) and back (B) view of the Circular Spline and Flexspline, front (C) and back (D) view the Wave Generator of the selected Harmonic Drive CPU-20A. Description of the main mechanical and technical characteristics and graphical representation of harmonic reducer operation.	154
Figure 8.2.5: Dimensioning data of the flange for the interface adaptation of the harmonic reducer to the maxon motor. Back (A) and front (B) view of the realized flange, graphical representation of the Harmonic Drive components and the designed flange (C).	155
Figure 8.3.1: Configuration of two inertial sensors on the human body in suitable positions for the contact with exoskeleton components: human thorax (blue circle) and human pelvis (red circle).	157
Figure 8.3.2: Experimental comparison of angular kinematics registered with inertial sensors positioned on the human thorax and human pelvis during several performed lifting simulations.	158
Figure 8.3.3: Maxon encoder Mile integrated in the Maxon motor EC60 flat for the measuring of relative angular position between trunk and thigh support. Description of the main characteristics and the output digital signal for the calculation of kinematics.	159

Figure 8.3.4: Three commercial angular solutions with through-hole configuration: (A) optical, (B) magnetic, (C) inductive encoders.....	160
Figure 8.3.5: Schematization concept of the transmission system between the exoskeleton assistance joint and the secondary encoder.....	161
Figure 8.3.6: ELAP encoder RM22Vx used for the monitoring of relative angular displacement between thigh support and pelvis belt. Graphical representation of the encoder (A-B), description of the main characteristics, technical data of dimensions and graphical report of the output analogical signal for the calculation of kinematics.	162
Figure 8.4.1: Graphical representation of the powered joint of the exoskeleton (A) and description of the components (B).	163
Figure 8.4.2: Front view of the powered joint (sagittal plane of the exoskeleton) in the four different solutions: (A) powered joint with O-ring drive belt transmission, (B) powered solution with O-ring drive belt transmission and modified flanges of connection, (C) powered solution with four-bar linkage mechanism for the motion transmission, (D) final powered solution with a freewheel mechanism for the motion transmission.	165
Figure 8.4.3: Lateral view of the powered joint in the four different solutions: (A) powered joint with O-ring drive belt transmission, (B) powered solution with O-ring drive belt transmission and modified flanges of connection, (C) powered solution with four-bar linkage mechanism for the motion transmission, (D) final powered solution with a freewheel mechanism for the motion transmission.....	166
Figure 8.4.4: Exploded view drawing of the four proposed solutions: (A) powered joint with O-ring drive belt transmission, (B) powered solution with O-ring drive belt transmission and modified flanges of connection, (C) powered solution with four-bar linkage mechanism for the motion transmission, (D) final powered solution with a freewheel mechanism for the motion transmission.....	167
Figure 8.4.5: Back view of the powered joint stressing the three proposed solutions for the transmission of rotary motion from the motor to the misaligned encoder: (A) O-ring drive belt transmission, (B) four-bar linkage mechanism, (C) freewheel mechanism.	168
Figure 8.4.6: Two different solutions for the integration of the misaligned encoder with the plate of the pelvis belt: one double row deep groove ball bearing (A) and two single row deep groove ball bearings (B).	169
Figure 8.4.7: Semi-section view of the two solutions for the encoder integration: one double row deep groove ball bearing (A), two single row deep groove ball bearings (B).	170
Figure 8.4.8: Graphical representation of the main exoskeleton components (A), range of the end-stroke in the passive Laevo solution that can be regulated (B), identification of the two end-stroke ranges that need to be defined in the powered prototype (C).	171
Figure 8.4.9: Exoskeleton map of the different angular ranges implemented in the powered system.	172
Figure 8.4.10: Validation of the exoskeleton end-stroke map during standing posture with four different subjects, two females (A-B) and two males (C-D).	173
Figure 8.4.11: Validation of the exoskeleton end-stroke map during static holding stoop posture with four different subjects, two females (A-B) and two males (C-D).	174
Figure 8.4.12: Validation of the exoskeleton end-stroke map with the first female subject during three lifting dynamic motion: stoop (A), semisquat (B), squat (C).	174
Figure 8.4.13: Validation of the exoskeleton end-stroke map with the second female subject during three lifting dynamic motion: stoop (A), semisquat (B), squat (C).	175
Figure 8.4.14: Validation of the exoskeleton end-stroke map with the first male subject during three lifting dynamic motion: stoop (A), semisquat (B), squat (C).	175

Figure 8.4.15: Validation of the exoskeleton end-stroke map with the second male subject during three lifting dynamic motion: stoop (A), semisquat (B), squat (C).	176
Figure 8.4.16: Powered exoskeleton joint solution proposed: (A) graphical representation of the integration of the powered joint into the Laevo exoskeleton, (B) lateral view of the powered joint stressing the height and lateral encumbrance.	177
Figure 8.4.17: Exploded view drawing of the powered joint: the final solution.....	177
Figure 8.4.18: Exploded lateral view drawing of the powered joint: the final solution. Labeling of the several components.....	178
Figure 8.5.1: Bench simulation of the mechanical components (motor and integrated encoder) and electronic devices (laptop, driver, can interface device and power supply) connections.....	179
Figure 8.6.1: Pelvis plate of the powered exoskeleton realized in stainless steel AISI 304. Front (A), behind (B), perspective (C) view of the plate. Zoom view (D-E) on the support for the secondary angular sensor and the free wheel.	180
Figure 8.6.2: Flange for the connection with leg pad from front (A) and behind (B) view, made in Aluminium 6082. Thigh flange, pelvis belt, washers and spacer (C).	180
Figure 8.6.3: Exoskeleton flange for the connection with the trunk support from frontal (A), behind (B) and lateral (C) view. Zoom view of the buttonhole for the end-stroke range implementation (D-E).	181
Figure 8.6.4: Positioning of the harmonic drive reducer (A), of the trunk flange (B) and particular view of motor+flange assembly (C).	181
Figure 8.6.5: Perspective views of the two powered joints assembled.	182
Figure 8.6.6: Final assembly of the powered exoskeleton.	183
Figure 8.7.1: One female subject with a height < 1.72 m wearing the powered exoskeleton from lateral view (A-C), front view (B) and behind view (D).	184
Figure 8.7.2: Detailed view of frontal (A) and lateral (B) sides during standing.	184
Figure 8.7.3: One female subject wearing the powered prototype exoskeleton and performing stoop (A), semisquat (B) and squat (C) lifting.	185
Figure A.1: Front and sagittal view of the anatomical reference position. Graphical explanation of anatomical reference direction used to describe the relative position of a specific human body part.	202
Figure A.2: Graphical representation of anatomical reference planes and anatomical reference axes in the 3D space.	203
Figure A.3: Representation of local reference systems of several human body parts with corresponding labels in the front and lateral (right and left) views.....	209
Figure B.1: Graphical list of common and crucial risk factors that must be considered for the analysis of working stations and industrial manual tasks with the main attempt to reduce and prevent the risk of overloads and injuries for the employees.	210
Figure B.2: Graph reported in the normative ISO 11228-Part 1 describing the relation between the mass of the external object and the frequency of grasping motion.	212
Figure C.1: Borg's scale and modified Borg's scale description. Explanation of the meaning of the different numbers in the ranges 6-20 and 0-10 respectively, that can be assigned by the subject during the evaluation.....	217
Figure C.2: Body part discomfort and perceived pressure scales description. Explanation of the meaning of the different numbers in the range 0-5 that can be assigned by the subject during the evaluation. Graphical maps of female (A-C) and male (B-D) human body with several body parts that can be used for the representation. A-B Graphs depicted the human body without mapping the evaluation while graphs C-D reported an example of colored mapping of local human body parts.	218

List of Acronyms

ADLs:	Daily Living Activities
CCS:	Cartesian Coordinate System
COG:	Center Of Gravity
COM:	Center Of Mass
CAN:	Controller Area Network
D/A:	Digital/Analog
DAQ:	Data AcQuisition
DC:	Direct Current
DOFs:	Degrees Of Freedom
DS:	Double Support
EMG:	Electromyography
EU-OSHA:	The European Union Information Agency for Occupational Safety and Health
FEM:	Finite Element Method
FOS:	Factor Of Safety
HAL:	Hybrid Assistive Limb
HD:	Harmonic Drive
HR:	Heart Rate
IMU:	Inertial Measure Unit
ISB:	International Society of Biomechanics
ISO:	International Organization for Standardization
JCS:	Joint Coordinate System
LBP:	Lower Back Pain
LI:	Lifting Index
MACCEPA:	Mechanically Adjustable Compliance and Controllable Equilibrium Position Actuator
MSDs:	Musculoskeletal Disorders

NIOSH:	National Institute of Occupational Safety and Health
OCP:	Optimal Control Problem
OCRA:	Occupational Repetitive Action
OSH ACT:	The Occupational Safety and Health Act of 1970
OSHA:	Occupational Safety and Health Administration
PCA:	Principal Component Analysis
PDT:	Pain Detection Threshold
PI:	Proportional Integral
PLAD:	Personal Lift Augmentation Device
PTT:	Pain Tolerance Threshold
ROM:	Range Of Motion
SEA:	Serial Elastic Actuator
SS:	Single Support
SSL:	Smart Suit Lite
TPU:	Thermoplastic polyurethane
VAS:	Visual Analog Scale
VBR:	Vertebral Body Replacements
WAD:	Wearable Assistive Device
WMRD:	Wearable Moment Restoring Device

Chapter 1

INTRODUCTION

“Robotics are beginning to cross that line from absolutely primitive motion to motion that resembles animal or human behavior.” JJ Abrams.

The significant interest in robotics development and applications is increasing in many different fields, from clinic and rehabilitation to the automation and industrial environment, from sport and physical disciplines to home and daily activities. The role of robots has changed during the past decades. Considering the medical sphere, numerous technological systems have been designed, developed and applied. Robots can help both patients and medical operators within direct or remote interaction. Assistive robotics is revealing positive improvements in the rehabilitation process, in the teleoperation and telemonitoring of patients. During the last years, their employment at home and in daily routines is catching on.

In industry and manufacturing, initially robots were introduced to substitute human operator in heavy working conditions and dangerous tasks. Nowadays, within Industry 4.0, the focus has shifted to the simultaneous presence of robots and workers sharing the same space. Indeed, there are still many workers exposed to physical workloads in precision tasks that cannot be performed by robots, since human flexibility and adaptability prove to be unique. The optimal combination of the advantages of robotics with the human skills, creativity and decision-making seems to be a promising solution for many tasks that cannot be totally automated. Wearable robotics are current solutions recently proposed for the innovative application of robotics systems in Industry 4.0. The human-device interaction is improved thanks to the robotic capabilities to follow and mimic the operator motion, without restrictions and limitations. Moreover, the occupational health and

safety are becoming principal objects of interest due to the recognized, strong and negative impact of work-related accidents and diseases on the work population. The musculoskeletal disorders (MSDs) due to material handling, repetitive movements and maintaining body postures affected both working population, both working economy. Among MSDs, the work-related low back pain and injuries are the most common.

Among the several technological solutions, the introduction of wearable device has been proposed both by academics and companies during the last years. Industrial exoskeletons are robotic, mechanical devices directly worn by the users. The principal aim of an industrial exoskeleton is the partial reduction of the muscular efforts of the operator during working gesture. The assistance would interest a specific human body part. Due to the working operations requiring large muscular efforts and fatigue, most industrial exoskeletons are developed for the assistance of human upper limbs and human back in lifting and lowering, manual handling and precision tasks. The exoskeleton can be defined as a personal daily use equipment and, for this reason, the acceptability and wearability by the operators gain crucial importance in design and development. Several factors must be considered in the project of an industrial exoskeleton:

- *Assistance.* The system has to assist the user and reduce the physical effort. It is important to differentiate the scope of industrial exoskeleton, mainly concentrated on prevention and support, from rehabilitation and military applications, where the device has to restore physiological function and enhance the human body force respectively.
- *Comfort.* In addition to the assistant benefits, it is important to reduce and prevent discomfort, perceived pressure and motion restriction. The wearer is a healthy subject able to conduct the working task also without the exoskeleton. For this reason, despite the supplied assistance, the risk of non-acceptance of the support device requires attention in the design, development and testing phases. It is important that the wearable device can follow the human motions without causing any limitations and restrictions. The mechanical transparency of the robotic system describes the minimization of resistive forces felt by the user [1].
- *Adaptation.* Industrial exoskeleton must be thought for an entire working population, that might present different size, anthropometric measures and body characteristics. For this reason, an adapted wearability of the device is a fundamental aspect that must be considered during the development.
- *Control.* Exoskeletons can be classified as passive or active device based on the type of assistance mechanism. The passive solution presents mechanical springs, dampers and suitable materials that store energy and release it in a different phase. Active ones are characterized

by electric, hydraulic or pneumatic actuators that provide external energy. Both types need to interact with the users with a precise and correct level of assistance, following the human motion and avoiding any restrictions. The kinematic design and the back-drivability of the actuation dictate the transparency of the system. Leaving out problems related to the current legislation, the complexity and dynamics of the specific working task may justify the choice between active or passive solution.

- *Modularity.* More complex solutions could consist of multiple modules, that can be used alone or combined. For example, different exoskeleton parts can be developed for the upper body and the lower body, but they can be integrated in one solution if a total body exoskeleton may be required. Due to the complexity and the increase of total weight and encumbrance, at the moment a total body exoskeleton has been proposed only in military applications.

The aim of the present PhD thesis is the analysis, design and development of a powered exoskeleton prototype for the trunk support in industrial tasks of lifting and manual handling. The exoskeleton supplies assistance to the user through electric motors and the support strategy is designed to be user and task specific. The system will be able to recognize the lifting strategy adopted by the user and, as a consequence, to differentiate the assistance based on human body kinematics. The description of the whole study will be organized in the following chapters:

- ✚ *Chapter 2.* Brief introduction of the application of robotics in industrial fields during the past decades and current ergonomic and industrial open challenges. Investigation of the biomechanics of the human spine and analysis of possible risk of injuries and overloads. Presentation of the different lifting strategies that can be adopted by the subject in lifting and manual handling industrial tasks. Literature review related to the development of trunk-support exoskeletons. Classification of commercial solutions and prototypes of trunk exoskeleton based on mechanism of assistance and summary of the several experimental validations already conducted.
- ✚ *Chapter 3.* Presentation of the current study contribution and summary of the several passages that will be discussed.
- ✚ *Chapter 4.* Description of a passive commercial trunk-support exoskeleton. Examination of the mechanical structure and the assistance mechanism. Evaluation of device performance in experimental simulation of different lifting tasks. Analysis of both subjective and objective variables. The experiment highlights the benefits and drawbacks of the system in order to point out possible improvements.

- ✚ *Chapter 5.* Model based approach for the analysis of human-device interaction. Development and validation of 3D multibody model of the human body, exoskeleton and interface.
- ✚ *Chapter 6.* Simulation analyses of different exoskeleton configurations by the variation of hinge joint positioning and the number of assistance joints between exoskeleton structural components. Biomechanical investigation of the positive and negative effects of the assistance device on the human body joints. Final characterization of a suitable assistance law for the powered system and computational validation.
- ✚ *Chapter 7.* Description and implementation of a suitable control architecture for the powered exoskeleton. Control system based on two control loops: model-based control (high level) for the definition of the desired torque and torque control (low level) for the closed loop on the motor output. Description of the hardware system and the selected electronic components for the implementation of the exoskeleton two-level control architecture. Simulation modelling, validation and analysis of a customized torsional spring for the hypothesis of serial elastic actuator.
- ✚ *Chapter 8.* Description of the mechanical design and implementation of the powered system. Identification of the maximum supplied torque, CAD design with different solutions, definition of mechanical end-stroke for the user's safety, identification and description of mechanical components and final structure prototyping and assembly.
- ✚ *Chapter 9.* Conclusions, summary of the main results and future plans of the presented study.

Chapter 2

STATE OF ART

2.1. Exoskeleton in the industrial environment

In the last decades, robotics and innovative technologies have radically changed the industrial and manufacturing environments. Both the workers' roles, the time necessary for completing specific tasks, the total cost of procedures and products have significantly evolved. In 1954, George Devol applied for the first robotic patents. Some years later, in collaboration with "the Father of Robotics" Joseph Engelberger, he founded the first company to produce robots, the *Unimation Inc.* [2]. Industrial robotics took off quite quickly in Europe, with both *ABB Robotics* [3] and *KUKA Robotics* [4] bringing robots to the European market in 1973. *ABB Robotics* introduced IRB 6, the first commercially available microprocessor-controlled robot. In the beginning, the introduction of robots in the industries consisted in replacing human roles in several manual and uncomfortable tasks, allowing higher productivity but reduced task flexibility. Robots employments allowed reducing time and cost of production, satisfying the augmented request of products. Machine and robots enabled a new reality of control and execution of production lines. Typical applications of robots in manufacturing included welding, painting, assembly, packaging, an inspection of production, testing, pick and place. Nowadays, current industrial robots are automated and capable of movements on several axes. Several degrees of autonomy characterize robotic systems. Indeed, some robots are programmed for repetitive actions without variation and with a high level of accuracy. Other robots are more flexible, with the possibility to update their orientation and guidance based on the required task. Main advantages of the industrial use of robotics are endurance, speed, accuracy and precision.

However, robots are not necessarily replacing the jobs of professionals. While some specific dangerous tasks are assigned to robotic systems, some situations find robots' contributions more beneficial in direct contact and at the service of workers. Indeed, despite the on-going trend in automation and the evident progress in mechatronics and engineering, many tasks still require human contribution and collaboration. The needed interaction with humans opens several challenges in improving the interface, the control system, and requiring a more advanced mechanical structure. As a consequence, because of the coming back of human central and active role, many workers are nowadays exposed to physical workloads and tasks, which contribute to the impact on human health and the risk of accidents.

In industry, the most frequent risk for human health is musculoskeletal disorders (MSDs) caused by material handling, maintaining hard body posture for a long time, manual managing or lifting external objects, repetitive and prolonged tasks. The human spine results in one of the most affected body parts because entailed in numerous working tasks. For this reason, the most common MSDs are work-related lower back pain (LBP) and injuries. Based on recent statistics and analysis, more than 40% of the European worker population declares that their work caused them back problems (around 63% for repetitive motions, 46% for wrong body positions and >30% for material handling) [5]. An additional aspect is the aging of the work population. The percentage of employed people over 50-years has grown from 24% to 31% during the last ten years and statistics foresees further increases [6]. This expectation enhances the requirement of reducing the risk of injuries and of promoting human well-being in working environments.

All these considerations stress the importance of assisting human activity in the industry for safety and prevention. Several health organizations as the Occupational Safety and Health Administration (OSHA) [7] and the National Institute of Occupational Safety and Health (NIOSH) [8] provide detailed guidelines for disorders prevention. At the same time, researches are working on methods to assess the risk of injury by means of subjective analysis, questionnaires, expert evaluation, and direct objective measurements.

In parallel, the identification of suitable solutions that can assist workers to reduce musculoskeletal disorders is an open challenge of current interest. Among them, exoskeletons for workers' support and assistance during specific tasks reveal to be a promising key to reduce human body physical efforts.

Exoskeletons are wearable devices that can directly interact with the user to replace muscles functionality, to offer amplified human capability or even to partially contribute to the human effort during specific and selected movements. Wearable robots are person-oriented robots. This means that interaction with humans is not limited to exchanging information and services (as in service-robotics), but it involves a closed interaction, both physical and cognitive. Based on the different characteristics, mechanical structure, functions, and applications, the exoskeletons can be classified in several ways, as depicted in Figure 2.1.1.

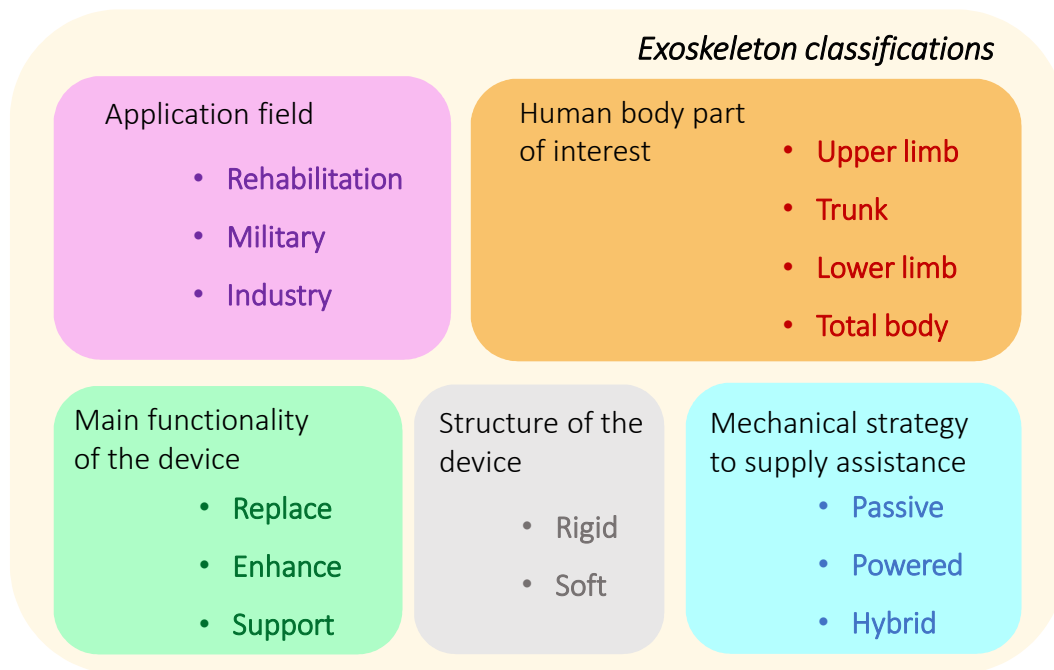


Figure 2.1.1: Maps of the different exoskeleton classification strategies.

There are many possible application fields and main functionalities. In the biomedical clinics and rehabilitation therapy, exoskeletons are principally addressed to people with motor impairments or dysfunctionalities, in order to give assistance, restore muscular activity or substitute specific human body function. In that case, the wearable device is specifically developed and realized based on the needs, comfort, and size of the patient. The interface and control system may consider not only the direct interaction with the user but also the communication with professional experts and medical figures. In military applications, the exoskeletons are defined as a class of robots that enhance the strength of users and allows actions that humans normally cannot do. In this case, the robots empower the human body, but the user maintains the total control, as in a master-slave relation. During the last years, the increased interest in adopting exoskeletons to reduce physical loading in several occupational activities has expanded in the development of both commercial products and research prototypes. Focusing on the industrial applications, the main purpose of the device consists in partially assisting the human body, reducing human physical workloads in order to prevent disorders and injuries [6, 9]. The user usually is a healthy subject, without specific impairments or dysfunctions. In industry, the human-robot interaction is characterized by *assist-as-needed*. The device must supply assistance in specific tasks or even specific phases of the task, without creating any obstructions or motion limitations to the worker.

Considering the human body part directly involved in the interaction with the device, the exoskeleton can be described as the upper limb, trunk, lower limb or

total body exoskeleton. Upper limb devices are introduced in order to assist human shoulder and elbow during specific tasks that require the workers to spend prolonged time with raised arms. For example, painting or pick-and-screw works might demand a high level of precision and long-time activity, with the onset of overloads and fatigue effects. Wearable exoskeleton that can supply forces to maintain the arms raised seems to satisfy the need to support and prevent the risk of excessive muscular and joint loads. Examples of commercial and research exoskeletons for the human upper limb are Mate by Comau (Figure 2.1.2 A) [10], Airframe by Levitate Technologies (Figure 2.1.2 B) [11] and PARM by Kadota and colleagues (Figure 2.1.2 C) [12]. While the first two are commercial exoskeletons characterized by passive elements for assistance, the PARM device is presented as an active prototype with three pneumatic artificial rubber muscles to mimic the motion of biarticular muscles.

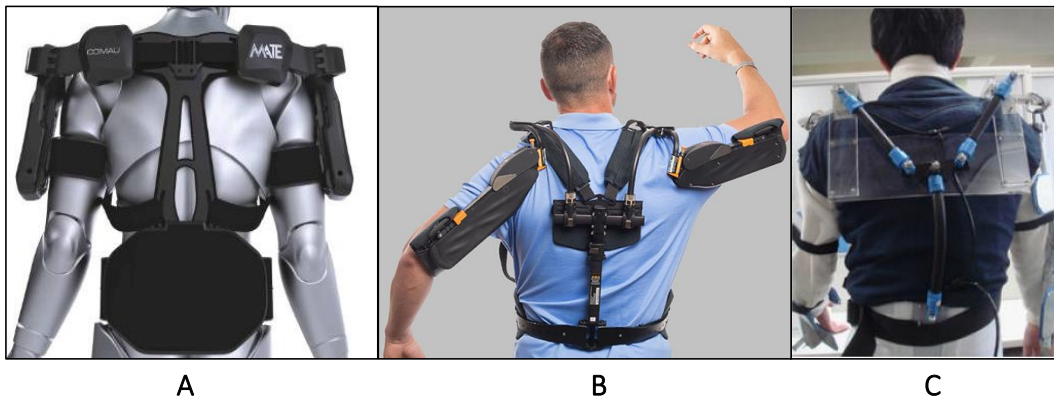


Figure 2.1.2: Examples of upper limb industrial exoskeletons. Passive upper limb exoskeleton Mate by Comau (A), passive upper limb Airframe by Levitate Technologies (B) and active PARM prototype by Kadota and colleagues (C).

Trunk exoskeletons are the most common solutions proposed in industry, with the main attempt to contribute to reducing physical efforts in manual handling and lifting. Both commercial and research solutions have been proposed in the last years, with different mechanical structure, controls systems, and interface arrangements. The company SuitX has proposed the passive system BackX [13], as depicted in Figure 2.1.3 A, while the company Laevo developed five prototypes of the exoskeleton Laevo [14], trying to improve the interaction, the wearability and the comfort of the structure. The last version of Laevo is depicted in Figure 2.1.3 B. ROBOMATE [15] is an European research project dealing with the analysis and development of a powered spinal support system for carrying and lifting external objects tasks in occupational environments. Figure 2.1.3 C depicts the first solution.

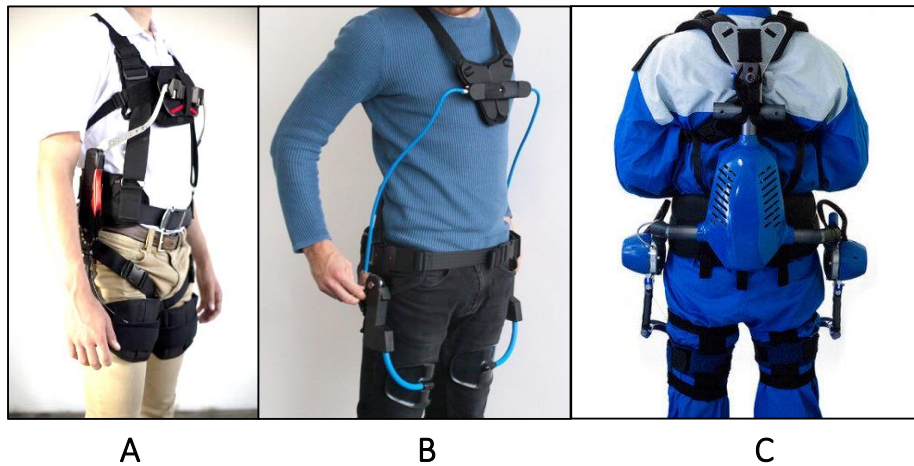


Figure 2.1.3: Examples of trunk industrial exoskeletons. Passive trunk exoskeleton BackX by SuitX (A), passive Laevo exoskeleton by Laevo (B) and active trunk exoskeleton prototype from ROBOMATE European project (C).

In the industrial environment, lower limb exoskeletons are suitable for allowing a sitting position, without the direct use of a chair, for all workers that have to spend a long day standing up. The Chairless Chair by Noone [16] proposes an ergonomic and comfortable workplace without limitations of mobility, allowing users to switch between walking, standing and sitting position with a reduction of muscle efforts and prevention of weariness. A graphical representation of the Chairless Chair is reported in Figure 2.1.4 A. Similar solutions are presented by Astride Bionix (Singapore) with the Lex wearable chair thought for resting posture in several applications [17], and Nitto (Japan) with the Archelis chair suitable for reducing leg muscle fatigue and maintain the correct posture and ideal for laparoscopic surgeons [18]. Figure 2.1.4 B and C show the two solutions respectively.



Figure 2.1.4: Examples of lower limb industrial exoskeletons. Passive lower limb exoskeleton Chairless Chair by Noone (A), passive lower limb exoskeleton Lex wearable chair by Astride Bionix (B) and passive lower limb Archelis by Nitto company (C).

Finally, a total body solution could be useful for a work task that requires a high level of stress from different muscles. The Robot Suit Hybrid Assistive Limb HAL developed by Japan's Tsukuba University and the robotics company Cyberdyne [19], the Body Extender exoskeleton proposed as research prototype by PELCRO Laboratory from Scuola Superiore Sant'Anna (Italy) [20] and the AXO-SUIT modular full body exoskeleton supported by the European project AAL Programme [21] are three examples of a wearable device that involves all the human body. The exoskeletons assist full-body motions as walking, standing, bending, industrial lifting and carrying heavy objects and performing tasks of daily living. In addition, they can find use in hospitals for nurses that need empowerment to lift patients. Bulky total weight, complex coordination of actuation and control systems characterize these exoskeletons.

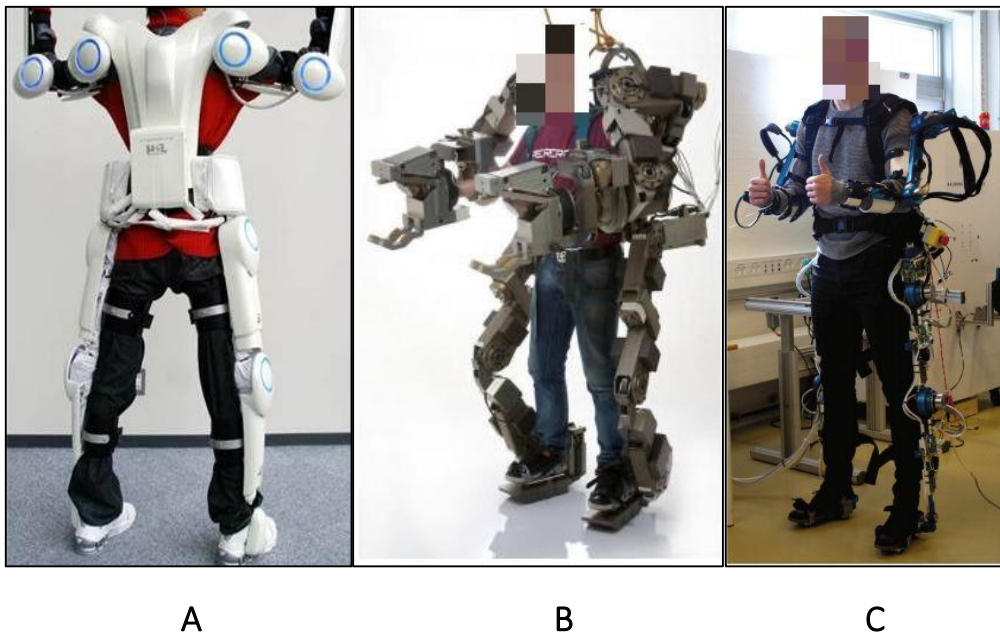


Figure 2.1.5: Examples of total body industrial exoskeletons. Robot Suit Hybrid Assistive Limb HAL by Japan's Tsukuba University (A), Body Extender exoskeleton by PELCRO Laboratory of Scuola Superiore Sant'Anna (B) and AXO-SUIT modular full-body exoskeleton by EU AAL project (C).

Moreover, based on the mechanical structure, the device can be described as rigid or soft. Rigid exoskeletons are built with rigid and articulated frames that run parallel with body segments and connect the assistance system (passive or active) to the garments worn by the user. Free joints may be added to the structure in order to increase the range of motion in space, avoiding restriction and limitation to the user, as avoiding misalignments between the exoskeleton and the human body during motion. Soft exoskeletons, also called *exosuits*, consist of garments worn on body segments in correspondence of the joint that needs support. Typically, cables, elastic bands, and straps generate assistance pulling two body segments together.

The exoskeleton results light and adaptable to several users, without drawbacks of space and obstacles. In addition, the soft structure might be worn under clothes. In the last years, some researches proposed a combined solution of soft and rigid components in order to take advantage of both solutions. An example is the recent back support prototype proposed by the SPEXOR EU project. It combines carbon fiber rods to generate and transfer forces between the user's pelvis, torso and thighs, and a traditional rigid structure actuated by a coil spring [22].

The strategy adopted to supply assistance can be another criterion for classification. The exoskeleton might be passive or active. In the first case forces and torques are generated by means of passive components, such as springs or other elastic elements. Existing passive exoskeletons employ different types of elastic elements. The most common solutions are made of gas springs, rotational springs, coil springs or even elastic bands. Recently, some devices employ flexible carbon fiber beams. The integration of passive elements to supply forces and torques allows the development of light and compact exoskeletons, but with a limited possibility to modulate the supplied assistance. Indeed, the level of assistance must be imposed during the design of the device and can be modulated in a very limited manner during the usage. Some more articulated devices allow the possibility to change the exoskeleton part that contains the assistance mechanism, but with a limited number of degrees of support. In most cases, the structure includes a mechanical on/off switch to disengage the assistance. Active exoskeleton includes powered actuators to supply forces or torques to the human body. Several solutions have been adopted, and the most common are electric motors, pneumatic actuators, hydraulic systems. The main advantages of powered solutions can be summed up as the possibility to modulate the assistance based on specific signals of motions, to directly control the interface and interaction between user and device and to satisfy the request of assistance based on user's demand. A control system must be integrated into the device in order to manage the actuation, and an external or on-board power source is necessary to activate the device. Moreover, based on the type of actuation implemented, specific mechanical arrangements and sensors must be combined with the actuator in order to obtain the desired forces/torques and to monitor signals and motions for the desired assistance. Inevitably, the structure is more complex and articulated, and has a higher weight.

To sum up, exoskeletons are wearable robots that directly interact with the user and have the main role to reduce or substitute the human physical efforts. After the initial interest in clinics and rehabilitation, exoskeletons have found applications also in military and industrial fields. The device can be classified and described based on mechanical and assistance characteristics. It is important to identify the specific function of the device in order to select and design the most suitable and comfortable structure. As the first step, because the device must be dressed by the user and interfaces with selected human body parts, a deep investigation and comprehension of anatomy and physiology of the human body result fundamental.

2.2. Biomechanics of the human spine

Considering that the aim of the present thesis is the development of a powered trunk industrial exoskeleton, the study of the anatomy and the biomechanics of the human spine is crucial. The biomechanical analysis consists in quantifying functions and forces occurring under various positions and motions. With the understanding of the natural mechanics of the spinal segments, it can be possible to stress the ranges of human motion, the conditions under which tissue damage, limits, fatigue, and overloads occur.

The human spine is a complex mechanical structure. Its main roles can be identified in protecting the spinal cord and nerves, transmitting the weight of the upper body to the pelvis, maintaining balance and posture of the total body and allowing the motion of the trunk. The spine presents four different types of vertebrae, named according to the regional position along the spinal cord: 7 cervical vertebrae, 12 thoracic vertebrae, 5 lumbar vertebrae, 5 sacral, and 4 coccygeal vertebrae. Based on the region, the vertebrae present different shape, dimension and function. A graphical representation of the human spine and the different regions is reported in Figure 2.2.1, with the three views according to the anatomical planes (sagittal, posterior and anterior).

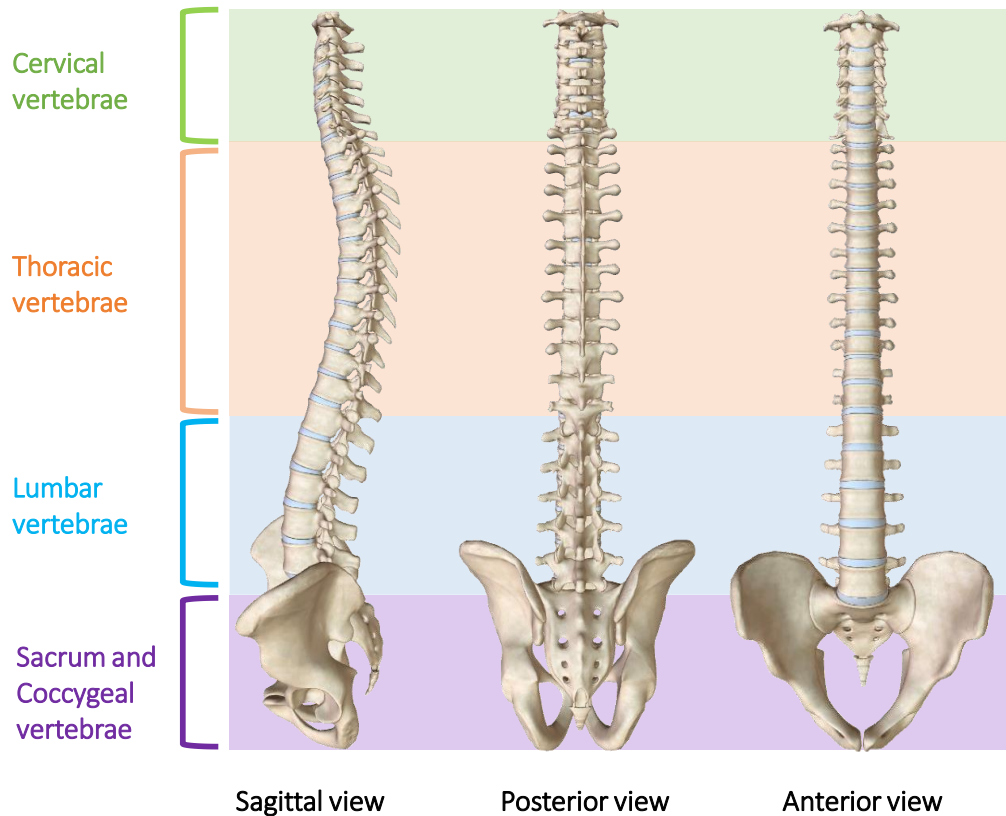


Figure 2.2.1: Sagittal, posterior and anterior views of the human spine and separation of the different vertebral regions: cervical, thoracic, lumbar and sacrum vertebrae.

The different shapes and orientations of the vertebral body contribute to restrict or permit motion in different directions. The human spine is also characterized by several physiologic curves (cervical and lumbar lordosis, thoracic and sacral kyphosis) that accommodate the different pelvic orientation during motions and contribute to maintaining the center of gravity in a balance condition. A vertebral body is stronger in the center and weaker in the posterolateral regions. This characteristic becomes crucial in loads distribution during motion. Caused by age and pathology, the porosity can increase making the vertebral body weak and more compliant [23]. For this reason, age directly influences the mobility and health of the human spine.

The vertebrae are joined by passive ligamentous restraints and kept separated by intervertebral discs. Ligaments can store energy and provide resistance to loads. The intervertebral disc structure acts as shock absorbers between vertebral bodies. It transmits the forces along the spine and allows and regulates motion between vertebrae. The disc is subjected to injury in case of high stress. Injuries and degenerations reduce the function of the disc to transmit forces, while pain sensibility is enhanced [24].

A complex architecture of muscles dynamically controls the motion of the spine, providing stability to the structure and protecting the spine during trauma. In general, the purpose of the muscles is to supply torques across joints. Two different groups can be underlined, based on the relative position with respect to the spinal cord: posterior and anterior spinal muscles. Posterior spinal muscles can be divided into intrinsic muscles, which connect the vertebrae, and extrinsic muscles, which connect vertebrae to the limbs, pelvis and ribcage. In the thoracolumbar region, the intrinsic muscles called Erector Spinae and Multifidus comprise the bulk of spinal muscles. The Erector Spinae muscle is commonly divided into three muscles: Spinalis, Longissimus and Iliocostalis. Based on the level of the spine, these muscles change their principal characteristics. The main function of Erector Spinae muscles is back dynamic extension, but they contribute also to lateral back flexion and rotation. During a static flexed position of the human back, the Erector Spinae are activated to balance the human body weight. In full flexion position, the Erector Spinae muscles become inactive because fully stretched. In that position, the flexion torque is supported by spinal ligaments. This silent condition of Erector Spinae is commonly known as the flexion-relaxation phenomenon. Latissimus Dorsi, Levator Scapulae, Rhomboids and Trapezius are superficial extrinsic muscles that connect the limbs to the trunk. Figure 2.2.2 shows the human back muscles labelling the most important muscle groups. Considering the anterior muscles of the spine, the abdominal group is composed of the Rectus Abdominis, External and Internal Oblique, and the Transverse Abdominis. Abdominal muscles contribute to the stabilization of the trunk, flexion and rotation motion of the spine [23]. Finally, the Psoas Major contributes to the flexion-extension motion of the hip joint, connecting

the human back to the human lower limbs, while the Psoas Minor is a weak flexor of the lumbar spine. Figure 2.2.3 sums up the main muscles of the human abdomen.

The biomechanical analysis of the human spine consists in the investigation of movements and forces developed between spinal components (bones, muscles, ligaments, joints) during daily living activities (ADLs) and work conditions. From the physiological point of view, the human spine range of motion is restricted to specific limits in the space. In order to describe the movements and forces applied in terms of direction and magnitude, the accurate definition of a specific coordinate system is necessary. The International Society of Biomechanics (ISB) have assumed specific references for the definition of a global coordinate system of the human body and local coordinate systems of a single human body segment, as reported in Appendix A.

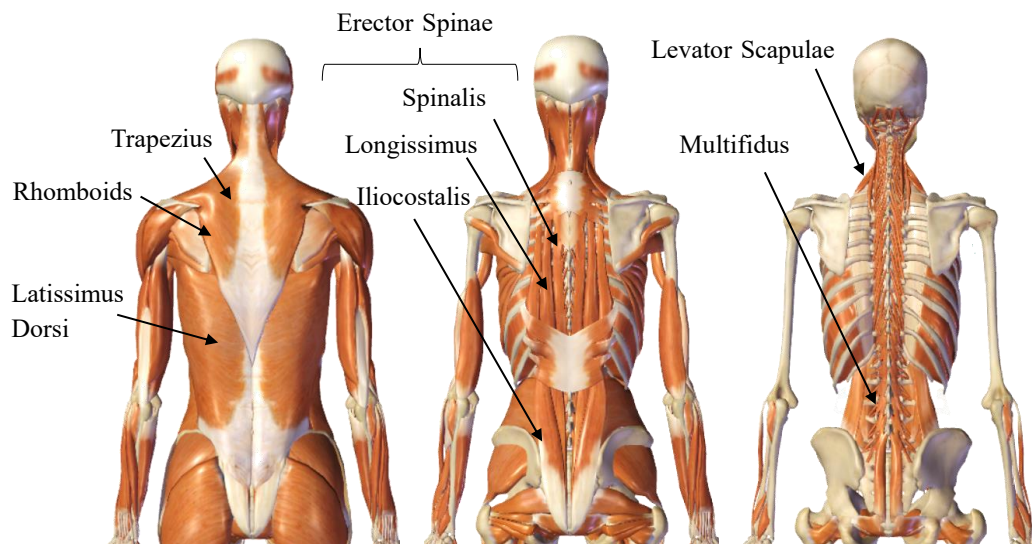


Figure 2.2.2: Graphical representation of the principal human back muscle groups.

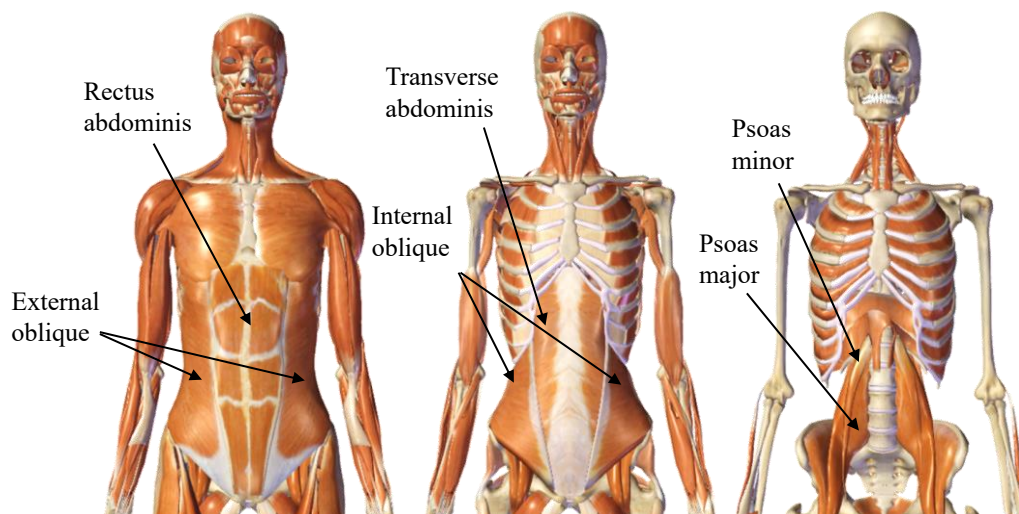


Figure 2.2.3: Graphical representation of the main human abdomen muscle groups.

Range of motion of the human spine is defined based on the global coordinate system. Flexion and extension motions are described in the sagittal plane, lateral bending in the coronal plane and rotation along the transverse plane. Daily and work activities depict a combination of motions in all three planes. The several spinal regions contribute in a different way to the 3D motion of the spine, as depicted in Figure 2.2.4 [25].

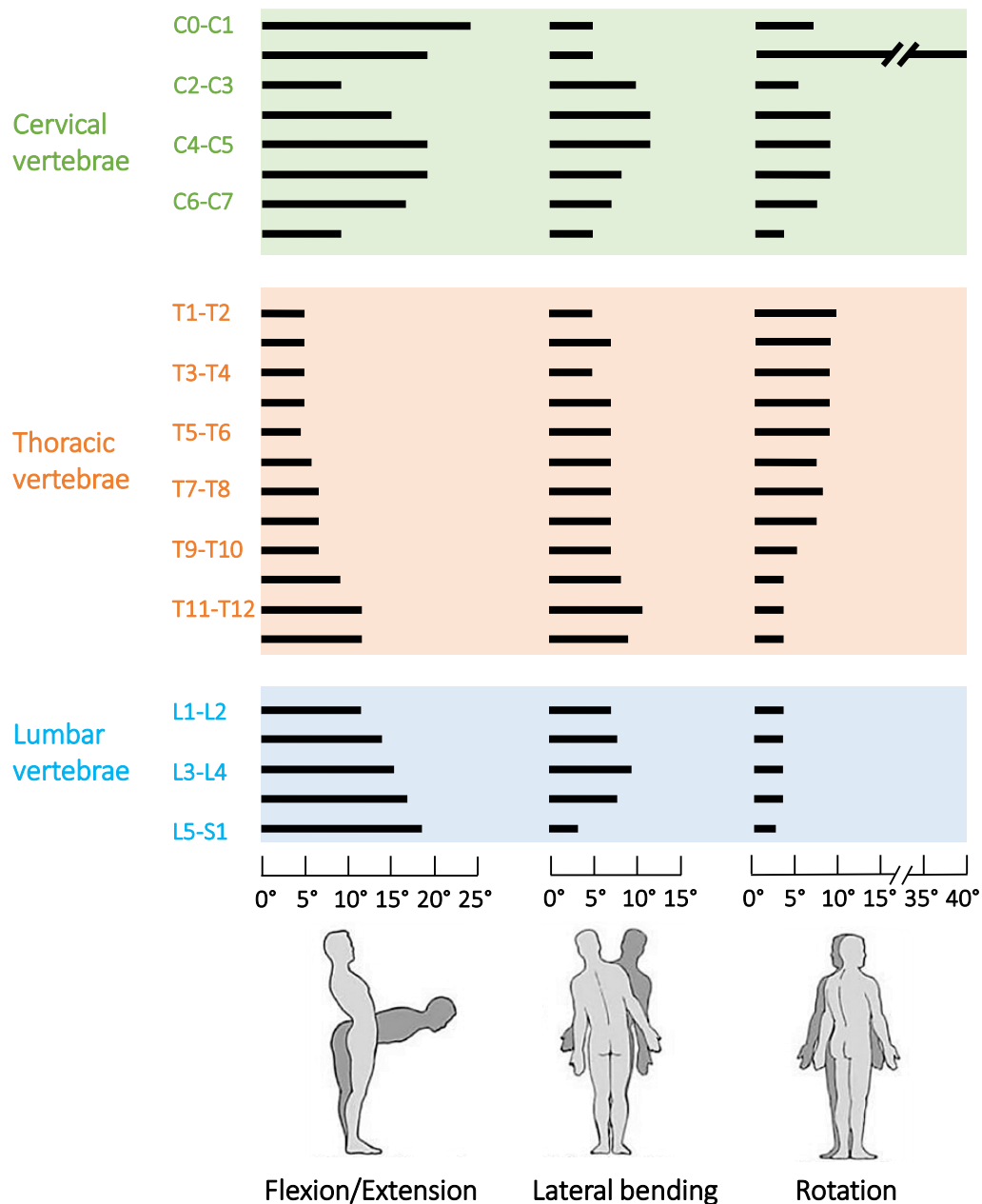


Figure 2.2.4: Representative ranges of motion at the different regions of the human spine in flexion/extension, lateral bending and rotation movements.

By the graph, it is possible to highlight the most involved spinal region during flexion and extension motion. The last lumbar vertebra (L5-S1) is considered the most loaded joint of the human spine during flexion motions and lifting tasks. For this reason, it results in the zone most affected by back pain and injuries. The thoracic region mainly contributes to the rotation of the trunk and the cervical region permits the neck movement in all directions. All the spinal regions are involved in lateral bending movements. In view of the thoracolumbar spine, the maximum degrees of motion along the three directions are 25° extension-80° flexion, 30° lateral flexion at each side, 45° rotation at each side. Considering the flexion-extension motion in the sagittal plane, two different types of joint forces can be defined along the parallel and perpendicular axes relative to the spine's length. Compression and tension forces act along the parallel direction relative to the human spine and depend on whether they compress or pull the spinal segment. These types of forces are typically developed during bending motion and lifting an external object. Considering the perpendicular direction, forces are named as shear forces. The joint forces are developed in order to contrast the weight of the upper body and the forces exerted by muscles during dynamic motions and during the maintaining of body postures. Due to the mechanical properties, dimensions and conformations, the human spine can bear large vertical loads (compression forces), thanks to a proportional distribution of the interacting forces along the area. On the other hand, the unbalance distribution of compression forces and the development of shear forces might contribute to the damage of the disc structure and cause injuries and pain. A recent study by Vecchio reported the value of 7000 N as the compression load that might cause damage in fragile spines, and the 9000 N value as reference threshold for compression tolerance in healthy subjects. On the contrary, the maximum spinal shear tolerance has been quantified in the range of 2000-2800 N [26]. Moreover, the NIOSH proposes the safety limit of 3400 N of compressive force to protect the 99% of male employees and 75% of female workers. Figure 2.2.5 A depicts a simplified representation of forces acting on the lumbar joint during a flexed posture.

As stressed in a recent review about the current knowledge on the biomechanics of the human spine [27], the compressive loads in the lumbar spine were already known in 1990, based on *in vivo* intradiscal pressure measures of Nachemson and colleagues [28, 29]. Patterns of intradiscal pressure during several daily activities were confirmed by Wilke [30, 31]. The pressure was recorded with a telemetry system for 24 hours in various lying positions, sitting positions in a chair, in an armchair, and on an ergonomic sitting ball, walking, lifting and others. Figure 2.2.5 B displays the different percentage of pressure during different human common positions normalized to intradiscal loads measured in standing posture, which resulted in 0.5 MPa [31]. The lifting technique may play a crucial role in spinal loading. Lifting an external object in stooping position (with flexed human spine and extended legs) resulted in the most loaded position with approximately 35%

higher intradiscal pressure compared with squat lifting (flexed legs), while in lying postures (both down and on side) the intradiscal pressure resulted reduced.

The direct measure of compression force in vivo experiments is difficult. For this reason, in previous studies, it was estimated by multiplying the intradiscal pressure with the corresponding disc area (between 15-20 cm²) and a correction factor [28, 32]. A more recent study adopted a telemetered instrumented vertebral body replacements (VBR) to measure the compressive forces transmitted through the device [33]. This study investigated numerous activities with the attempt to stress the motions with the highest implant force and moment in five patients. Lifting weight from ground resulted in the activity with the highest value, measuring 1650 N resultant force when lifting an external object with mass of 10 kg [33]. Other movements with a maximum resultant force larger than 1200 N included elevation keeping straight arms with an external object of 9 kg mass in hands, moving a 10 kg external mass from a lateral to a front position with respect the body and changing the body position from sitting to standing posture.

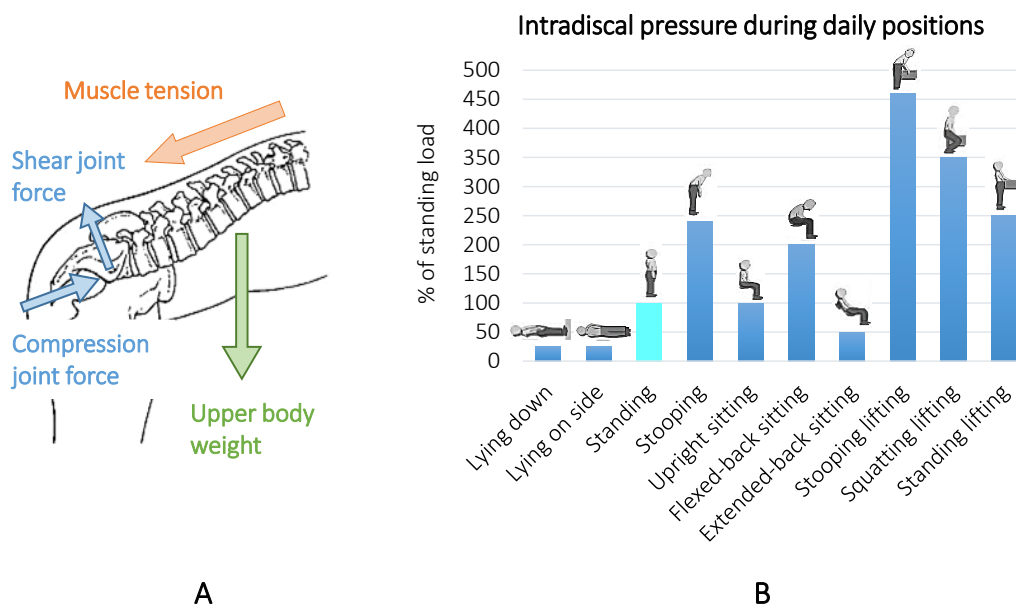


Figure 2.2.5: Simplified free body diagram of forces at the lumbar spine (A); intradiscal pressure distribution during daily activities normalized respect to standing position loads measured by Wilke in 1998 (B).

The investigation of human load distribution in several daily motions allows the identification of correct and incorrect postures to be adopted or avoided also during working activities. Previous in vivo works concentrated on the estimation of compressive forces at the lumbar zone, while a few studies measured the thoracic and cervical spine compressive loads [27, 34]. Moreover, in vivo spine loading has been investigated considering only axial compressive forces, while shear forces cannot be estimated from an intradiscal pressure because of the little pressure

change within the disc [27]. Despite the numerous in vivo experiments from previous studies, that approach appears particularly invasive and complex to implement. Moreover, the results can strongly depend on the adopted sensors for measurements, and on the anthropometric characteristics of the subject. Values should be also normalized in order to allow an inter-subject comparison. To overcome the in vivo limitations and invasive conditions, a mathematical and computational modelling approach might be considered to evaluate the joint loads in several directions. Dreischarf and colleagues have recently reviewed in vivo and computational model studies [35]. The development of accurate and complete biomechanical model of the human body is a current open challenge. The employment of models would allow the simulation of several conditions, with reduced time and cost, and the evaluation of forces that cannot be measured during experimental tests. The computational approach has been adopted in several previous biomechanical, ergonomic and wearable-robotic studies. On the other hand, the main limitation of computational approach consists in determining the correct description and assumptions of human characteristics without strong simplifications. In addition, the anthropometric measures of subjects are necessary to correctly scale and describe the model. Furthermore, kinematic and dynamic data are necessary as input models during the simulation. Several human spine models have been developed in the past, both in two and three dimensions, with different grades of complexity according to the final aims of the single study. Multi-segment spinal structure with ligaments and muscles is often considered in investigating biomedical conditions, constraints relation, non-linear materials proprieties and mechanical behaviour. In ergonomic applications and injury prevention, the net moments balance at only one joint reveals to be the most commonly adopted method. The identified reference joint schematizes the spine role of connecting the upper body part to the lower body part and it can be referred to the human hip joint. In more recent studies, the separation of human torso in two different segments, the human trunk and the human pelvis proposes the introduction of one other degree of freedom. The last lumbar vertebra, usually called waist joint, depicts the connection between trunk and pelvis. In these models, both the human waist and hip joints contribute to the development of flexion-extension motion. The other important aspect deals with the validation of the model in order to assess the accuracy of the calculated results when compared to real measurements.

Despite limits and approximations in existing measurements and models, in vivo and computational model studies have made fundamental advances in understanding and investigating the lumbar spinal loads, which is recognized as a major risk factor for low back pain. A full-detailed knowledge of lumbar spinal efforts is a crucial requirement for appropriate management of spinal disorders, effective injury prevention in ergonomics or in rehabilitation.

2.3. Human lifting strategies

The human spine is involved in several daily and working activities. Considering the holding posture, manual handling and lifting, the human spine reveals high joint moments and forces, which increase in case of external loads. Manual lifting is consistently linked with occupational injuries and musculoskeletal disorders. Due to the numerous degrees of motions, joints and segments in the human body, the same activity or position may be obtained with different kinematics and coordination of the body segments. Principally, the human lifting movement is symmetric and developed in the sagittal plane. It involves large spinal flexion and extension angles. Only in some specific tasks, the motion results asymmetrical, with a spine rotation or lateral flexion. . When it is possible, the industrial mansions try to avoid the implementation of asymmetrical movements.

The human body reaches and lifts the object with a main lumbar and/or hip flexion-extension motion, hence the main joints involved in the lifting task are the lumbar and hip joints. The combination of hip and lumbar flexion depends on the subject and determines the relative motion between legs, pelvis and lumbar spine. However, three main lifting strategies can be highlighted considering the posture adopted: stooping, semi-squatting and squatting lifting. Stoop and squat lifting depict the two extreme positions, while the semi-squatting posture is a combination of the previous two movements. The three techniques are reported in Figure 2.3.1.

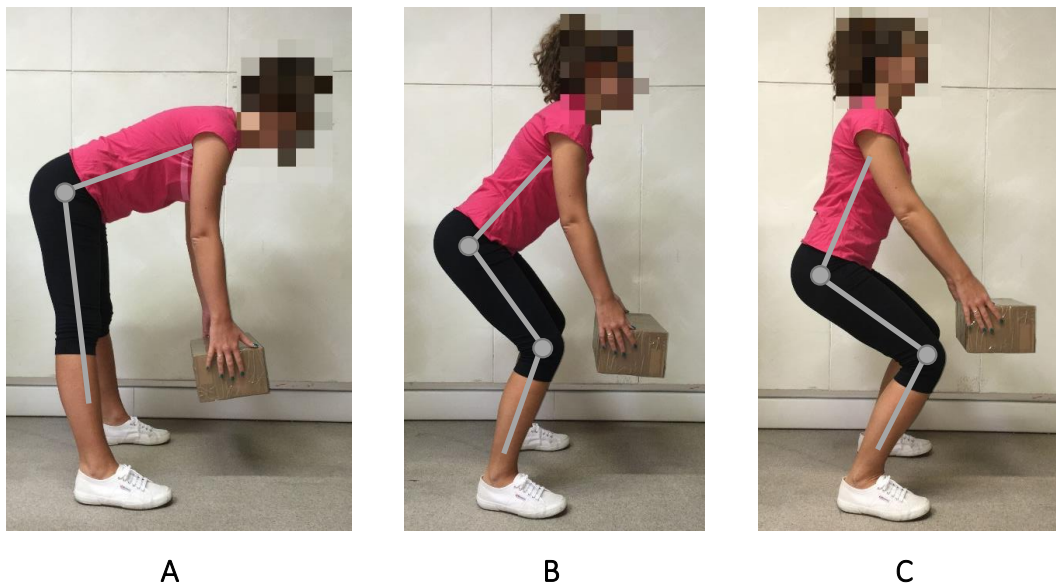


Figure 2.3.1: Graphical representation of the three main lifting strategies: stooping (A), semi-squatting (B) and squatting (C) lifting techniques.

In stooping, all the flexion/extension are developed at the lumbar and hip joints. The legs appear mostly fully extended, with knee and ankle joints in a neutral position during the movement. Figure 2.3.1 A represents the stooping motion

depicted at a specific degree of trunk inclination. Despite the concentration of efforts at the lumbar spine and the risk of lumbar joints overloads, the stoop lifting is preferred in static holding posture and prolonged tasks.

The semi-squatting lifting could be defined as a combination of stoop and squat; lower leg and lumbar joints are all involved during the motion. Legs are partially flexed, but knees and ankle joints do not reach a fully flexed position, while the flexion angle of the lumbar joint has lower values when compared to the stoop posture. In order to correctly describe the kinematics at human joints during semi-squat, the inter-joint coordination and the initial starting posture must be considered. Figure 2.3.1 B represents the semi-squatting motion. Despite the complexity of joints coordination, this strategy is often performed, both in working and daily tasks.

In the squatting, knee and ankle joints participate in the motion and, consequently, the legs are flexed, while the trunk is held in an almost vertical position. Figure 2.3.1 C represents an example of the squatting motion. This lifting technique is particularly performed in weightlifting and strength exercises, but it is also strongly suggested in industrial task of repetitive lifting objects.

As already mentioned, the investigation on which is the self-selected lifting technique adopted by workers revealed that they typically adopt the semi-squat style [36].

In the past decades, several ergonomic and academic studies have been carried out in order to describe the effect of the different lifting strategies on human loads and efforts, with the main final attempt to identify the best lifting style. Due to the controversial results, the question is still an open object of interest and discussion. In view of the high costs associated with LBP and the increase of workers affected by occupational diseases and musculoskeletal disorders, industries are promoting training courses for employees to point out incorrect positions and motions. Moreover, recent guidelines have been developed in order to provide education on appropriate postures and patterns. Nevertheless, the health effects of training programs with respect to lifting techniques result minimal [37, 38].

Traditionally, the most recommended posture is the squat style, despite this is not spontaneously adopted without specific instructions. By maintaining the trunk in a vertical position, the loads and stresses on vertebrae are better distributed along with the intervertebral disc and the risk of injury are expected to be limited. Indeed, damage to the intervertebral disc is a consequence of the accumulation of repeated or prolonged unbalance compressive and torsional loading during flexed position. Moreover, the vertical position of the trunk avoids the development of shear forces that represents an additional risk of injury. In a squat position, the shear forces are limited to the safe level of 200 N, allowing the muscle to support the moment in a neutral posture [26]. In a previous experimental investigation, peak lumbar moments are considered in squat and stoop lift performed by 15 men lifting masses from 6-32kgs. Data show a 5% lower peak lumbar moment in the first strategy with

respect to the second one [39]. The estimation of peak lumbar moment has been conducted with simulation approach and the development of a musculoskeletal human body model. For this reason, the results are strongly influenced by both the experimental data acquisition and the accuracy of the model. The main disadvantages of squat style results: the reduction of stability due to heels lifted and hence the loss of balance, the risk of injuries due to unexpected external perturbations, the overloads of other joints (knee and ankle joints), the higher metabolic cost required during movements, the greater muscular efforts of leg muscles and the impossibility to adopt that strategy in some working conditions. In addition, the perceived efforts and fatigue resulted higher compared to a stooped posture. In repetitive lifting experiments, subjects tried to reduce perceived fatigue by shifting from squat to stoop posture [40]. Workers may naturally prefer the stoop strategy because of the greater demand on the knee extensors imposed by the squat style.

Van Dieen, Jaap and colleagues resumed and described previous biomechanical studies comparing stoop and squat lifting with respect to the mechanical loads on the human back [41]. Based on these previous studies, there is not the possibility to depict the best lifting strategy that must suggested in all conditions. The direct comparison between strategies and several studies may become difficult due to the numerous external conditions that might affect the biomechanical estimated loads. Indeed, the difference in motion velocity, external object total mass, the position of the external object, the position of human upper limbs and the biomechanical models adopted are only some variables of influence. Different studies had different outcomes. The main common finding agrees on the potential positive effect of squat lifting in terms of net moments and compression forces on the spine when the external object was positioned between the feet. In all other cases, the stoop lifting motion revealed to be more suitable. Although shear forces were considered in a restricted number of investigations, squat lifting was found to be beneficial in all the different lifting conditions.

Because of the difficulties in the direct measurement of biomechanical lumbar loads, the development of biomechanical models was introduced. However, the inter-subject variability in kinematics and muscles activity introduces additional complexity, without considering possible differences in anthropometry, age, gender, physical conditions, and cognitive perceptions

To sum up, from a theoretical point of view, the squat lifting technique demonstrates lower lumbar shear stress and less stress on the passive tissues of the spine, while from the subjective perception, the stoop lifting style seems to be more natural and less fatiguing. The semi-squat lifting strategy might be a suitable compromise, both considering the kinematics of human joints, both the perceived efforts by the subject. Considering experimental tests and estimation of biomechanical human efforts, previous studies depicted the absence of a single best lifting posture that is appropriate for all work situations. Providing education and

training in general lifting guidelines and efficient biomechanical movement patterns may be a necessary approach for the prevention of low back pain and musculoskeletal disorders in workers.

2.4. Ergonomic regulations and guidelines

Italian regulations dealing with manual handling are similar in the US and the EU. In the US, the current law is *The Occupational Safety and Health Act of 1970* (OSH Act) [7], while, in the EU, the current regulation is the *Directive 90/269/CEE* [42]. In general, both laws assert the illegality for an employer of putting the physical health of their workers at risk, as his responsibility to correctly identify and prevent risks. Nevertheless, both regulations do not provide specific weight limits for lifting or carrying, neither any concrete guidelines concerning correct postures. The correct posture that needs to be assumed depends on several variables, as the industrial task, the repetition of motion frequency, and the presence/weight/position/size/shape of external loads.

In the US, each State is actually encouraged by the OSH Act to make its own safety and health program. The law, in particular the General Duty Clause, Section 5(a), states that:

“Each employer –

(1) shall furnish to each of his employee's employment and a place of employment which is free from recognized hazards that are causing or are likely to cause death or serious physical harm to his employees;

(2) shall comply with occupational safety and health standards promulgated under this Act.

(b) Each employee shall comply with occupational safety and health standards and all rules, regulations, and orders issued pursuant to this Act which is applicable to his own actions and conduct.”

If a state does not have a state plan, it must follow the Federal OSHA (Occupational Safety and Health Administration) program. OSHA is a national public health agency, which is part of the United States Department of Labor. OSHA is responsible for ensuring that employers keep their employees safe at work, for setting standards and for providing training and education. Because OSHA does not have any official regulations on the limits of lifting and carrying, NIOSH (National Institute for Occupational Safety and Health), has created a math-based lifting formula called the NIOSH Lifting Equation. It establishes the maximum load under ideal circumstances to be 23 kg, but it is important to stress that this is not a recognized law, but a guideline. Moreover, in repetitive lifting, the threshold needs to be revised.

In the EU, the employer has to consider the Manual Handling Directive 90/269/CEE, which sets the general health and safety requirements for the manual

handling loads. It was created with the intention of protecting workers, improving their health and reducing the risk of injuries.

"Employers shall take appropriate organizational measures, or shall use the appropriate means, in particular, mechanical equipment, in order to avoid the need for the manual handling of loads by workers. Where the need for the manual handling of loads by workers cannot be avoided, the employer shall take the appropriate organizational measures, use the appropriate means or provide workers with such means in order to reduce the risk involved in the manual handling of such loads".

OSHA has a crucial impact also in the EU, and it is called EU-OSHA (*The European Union Information Agency for Occupational Safety and Health*). All member states must be able to present guidelines for performing risk assessment, but only a few countries included specific weight limits in manual lifting.

The three parts of the normative *ISO 11228 Ergonomics, Manual handling* establish ergonomic recommendations for different manual handling tasks [43–45]. All the parts (Part 1. Lifting and carrying; Part 2. Pushing and pulling; Part 3. Handling of low loads at high frequency) apply to such professional and non-occupational activities. The standards provide information for designers, employers, employees and others involved in work, job and product design.

Part 1 of ISO 11228 specifies recommended limits for manual lifting and carrying while considering, respectively, the intensity, the frequency and the interval of the task. It provides guidance on the assessment of several task variables, allowing the health risks for the working population to be evaluated. It applies to manual handling of objects with a mass of 3 kg or more, and to moderate walking speed (0.5-1.0 m/s) on a horizontal level surface. It is based on 8 hours working day. Part 2 of ISO 11228 gives the recommended limitations for whole-body pushing and pulling, but it is restricted to specific conditions and applied forces. Part 3 of ISO 11228 points out ergonomic references for repetitive working tasks concerning the manual handling of low loads at high frequency. It provides directions on the assessment of risk factors commonly associated with those conditions. Those recommendations are mainly based on experimental studies regarding musculoskeletal loading, discomfort/pain and endurance/fatigue related to methods of working. Appendix B of the thesis resumes some important aspects of Part 1 and Part 3 that are meaningful for the current study.

Despite the increased attention on human well-being and health by industries and the numerous developed references from normative, directives, training programs and general guidelines, the problems of LBP and MSDs in the working population still affect many workers. Moreover, they seem to increase. One possible reason could be the fact that workers know the correct behavior, but they do not follow it. In the last years, the academy and industrial environment have concentrated on the introduction of mechanical systems and wearable devices in order to prevent the risk of damage and to reduce human efforts during tasks.

2.5. Current trunk exoskeleton solutions

During the last decade, several commercial and research prototype solutions have been developed to unload the human lumbar spine. The wearable devices are defined with different labels (“lumbar/back/hip support”, “lift assist device”, “trunk/spinal exoskeleton”), because of the not defined and standardized category for these wearable robotic tools. Despite the common aim to reduce the loads at the lumbar spine and partially support the worker during specific tasks of holding and lifting, the proposed solutions differ in terms of mechanical design, assistance mechanism, points of interface with the human body, number of actuated and free degrees of freedom and complexity of the structure. All of them apply forces/torques in the sagittal plane between the human trunk and thighs. The present section describes these solutions considering a classification based on the mechanism of assistance, distinguishing passive and active industrial trunk exoskeletons.

Passive exoskeletons. Passive exoskeletons, as previously described, are characterized by passive mechanical components for the generation of assistance, for example, elastic bands or springs. In this case, the mechanical support can store the energy produced by the user and consequently restore it when necessary. In numerous cases, thanks to the advantages of light and flexible structure, the passive exoskeleton can be used also in narrow and cumbersome workspaces, and it can be worn without the help of assistants and/or technicians. In addition, if composed by soft structure, the device can be also worn under clothes. Several passive garments were proposed in the past.

In 2006, Abdoli-E and Stevenson proposed one of the first prototype, the Personal Lift Augmentation Device (PLAD) [46]. The PLAD has been modeled on the concept of human muscles. Elastic elements have been considered as external muscle force generators. The elastic bands must be aligned parallel both to the Erector Spinae and to the leg muscles. This configuration enables a portion of the forces and moments required to the spinal column to be provided by the shoulders, pelvic girdle and knees, that represented the three points of contact with the human body. During lowering phase, the elastic components store energy that is released on the rising phase of a lift cycle, reducing the energy demand on the involved muscles. The device was tested varying the elastic bands stiffness [47], in repetitive working tasks [48], different lifting techniques [49] and 3D dynamic motions [50]. Both males and females dressed the device [51]. Kinematic and dynamic variables were considered for evaluating effects on the human body [46, 52].

Analogously to the PLAD, the Wearable Assistive Device (WAD) was proposed as a laboratory prototype [53, 54]. It consists of a lower and an upper part connected by 4 crossed and 4 parallel elastic bands. The weight of the upper and lower parts is 650 g and 850 g, respectively. The upper body element is made of a vest that covered shoulders. The use of Velcro allows the circumferential

adjustment of the limbs and trunk sizes of different users. In addition, the length of the elastic bands can be adaptable for different sizes. The use of elastic bands is adopted also in the Smart Suit Lite (SSL), proposed by Imamura and colleagues in 2011 [55] and in the assistive garment by Lamers [56].




In 2009, a passive Wearable Moment Restoring Device (WMRD) has been designed and developed in the UC Berkeley Human Engineering Laboratory [57]. The device provides attachment to the wearer via chest and shoulder harness, hip and thigh straps. The device is connected to the ground with the wearer stepping into foot bindings. This solution eliminates high contact stresses on the wearer's lower limbs. The assisting torque is generated at the hip level via a spring cable mechanism absorbing energy and returning it when the user returns to a neutral position. The assistance is delivered via a force on the wearer's upper torso through the chest/shoulder attach. A "Star-cam" mounted in correspondence of the hips provides an initial free zone allowing the user to perform tasks involving small flexion-extension angles without assistance.


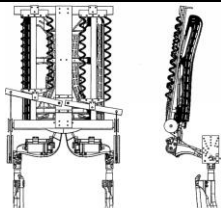


A more recent study presented the VT-Lowe [58], a wearable device developed by the Virginia Tech, in collaboration with Lowe's Inc. The innovation consists in carbon fiber beams running along the center of the human back, from the neck to the middle of the thighs. The beams are fixed at the back of the human waist. The beams are positioned parallel to the human back muscles. The kinematic differences between the exoskeleton and the human body are partially compensated by the sliders connecting shoulder harness and thigh pads to the carbon fiber beams.




Gas springs have been adopted in two current commercial passive exoskeletons, Laevo [14] and BackX [13]. The Laevo exoskeleton is made of three main parts: trunk support, pelvis belt, and thigh support. The gas spring is linked to the hinge joint connecting the trunk and thigh support, in order to develop assistance between the human trunk and thighs. A free hinge joint, coaxial with the assistive joint, connects the thigh support and the pelvis belt. Forces act through the contact points at the chest and thighs level. The total mass of the device is 2.8 kg. The BackX exoskeleton shows a similar design, with contact points at chest, pelvis and thighs, for a total mass of 3.4 kg. It can be worn with the model ShoulderX and LegX, to obtain a total body exoskeleton. Both exoskeletons have been investigated in literature researches to measure and analyze their effect on the user during work, the suitability in different human motions and the wearability with several users.

Other examples of commercial passive exoskeletons are the V22 and FLx ergoskeletons by Strongarm Technologies [59], which use cables to supply assistance in holding postures. The adopted solution allows the reduction of total weight and the limitation of spatial encumbrance. Nevertheless, the assistance is strongly affected by the tension of the cables and cannot be regulated by the users. Both exoskeleton solutions are connected to the human body at the shoulders and waist level, without interactions with the human lower limbs. Table 2.5.1 sums up the passive devices previously described, with their main characteristics.

Table 2.5.1 List of passive trunk exoskeletons.

Passive exoskeletons						
Name	Institution	Picture of the device	Assistance mechanism	Structure	Mass (kg)	Contact points
PLAD	Biomechanics and Ergonomics Lab-Queen's University, Kingston	 A line drawing of a person in a crouching position wearing a blue and white exoskeleton. The device consists of a vest-like structure with straps and bands connecting the shoulders, hips, and shanks.	Elastic bands	Soft	/	Shoulders, pelvis, shanks
WAD	Sharif University of Technology, Tehran	 A photograph of a person wearing a black and white exoskeleton while bending over. The device features a central vertical support and horizontal bands across the shoulders and thighs.	Elastic bands	Soft	1.5	Shoulders, pelvis, thighs
SSL	Research Laboratory (Japan)	 A photograph of a person wearing a white and blue exoskeleton. The device is a full-body vest with multiple straps and bands, designed to support the trunk and lower limbs.	Elastic bands	Soft	/	Shoulders, back, chest, pelvis, thighs

Assistive garment	Mechanical Engineering Department at Vanderbilt University, Nashville		Elastic bands	Soft	2	Shoulders, back, thighs
WMRD	UC Berkeley human engineering laboratory, Berkeley		Coil spring	Rigid	/	Shoulders, pelvis, thighs, shanks, feet
VT-Lowe	Virginia Tech, Blacksburg/ Lowe's Inc, Mooresville		Carbon fiber beams	Rigid	/	Shoulders, pelvis, thighs
Laevo 2.5	Laevo, Delft		Gas spring	Rigid	2.8	Trunk, pelvis, thighs

BackX	US Bionics, Berkeley		Gas spring	Rigid	3.4	Trunk, pelvis, thighs
V22 ergoskeleton	Strongarm Tech., New York		Cables	Rigid	/	Shoulders, pelvis
FLx ergoskeleton	Strongarm Tech., New York		Cables	Rigid	/	Shoulders, pelvis

Active exoskeletons. Active exoskeletons involve the presence of an external power source to generate the forces/torques of assistance. They usually allow the modulation of support during the working tasks, based on specific control variables and signals. This aspect could be a crucial advantage in order to use the device with different tasks and human motions. Moreover, the modulation of the law of assistance might be adapted to the user's needs, discomfort perception and biomechanical efforts. In previously developed industrial trunk exoskeletons, both electric and pneumatic motors have been proposed as actuation mechanism. In addition to the actuator, the device needs the integration of a control system, sensors and power supply.

In 2003, Naruse and colleagues proposed one of the first examples of powered assistive devices [60, 61]. The device is composed of five rigid metal links attached to the shoulder, back, waist and thighs of the human body. The metal links are connected together by a cable system. This is connected, with a drum, to a DC motor. By pulling the cable, the motor provides assistance to the user during lifting up and handling down external heavy objects. In a first version, the drum has been positioned behind the human limb, while in a second version, it is positioned behind the human trunk. To control the device, as input signals trunk position, provided by a potentiometer, and muscle activation, read by Electromyography (EMG) electrodes positioned on thighs, are considered.

Hara and colleagues developed the exoskeleton HAL lumbar support as the first prototype in 2010 [62]. It is made of electric actuators and control is based on kinematic variables measured using potentiometer and accelerometer, and on EMG signals of the back-muscle activation. The crucial difference between the HAL exoskeleton and the other powered trunk support exoskeletons consists in the mechanical structure and the contact with the human body. Indeed, the HAL exoskeleton interacts with the human body at the pelvis and thighs contact points, without acting at chest, trunk and/or shoulders level. After several prototypes, the system has been tested in different applications, both for care and labor support [63, 64]. The last version of HAL Lumbar support exoskeleton is provided as commercial product by Cyberdyne Inc [65].

In the same period, a research prototype was proposed particularly for the assistance of workers during static stooped posture by Luo and Yu [66]. Shoulder straps, breast band and pelvis belt are connected by means of two tension bands running parallel to the Erector Spinae. The two tension bands are linked to two pulleys positioned on to the shafts of servomotors, which are fixed to the pelvis belt. Two lower limb bands are attached from hooks (mounted under the servomotors) to the middle of the feet to balance the tension of the upper bands. Both breast and lower limb bands could be adapted to different anthropometric circumferences. An angle sensor installed on the backside of the breast band allows the monitoring of human torso flexion and stooped position. When subject sustains static forward-bent posture, the actuators rotate the pulleys to strain the tension bands to reduce the energy demand on back muscles.

In collaboration with other research institutions in a UE project, the Italian Institute of Technology has presented two versions of the active trunk device ROBOMATE [15, 67, 68]. Both prototypes use brushless motors combined with a harmonic drive to obtain the desired support torque during flexion-extension motion in the sagittal plane. In the second one, the addition of a parallel elastic element allows to store energy during motion and to reduce the dimensions and performance required to the motor. Biosensors as inertial measure unit (IMU) for kinematics and EMG forearm bracelet for muscle activation are adopted to monitor the human movements and to implement the control law. The mechanical structure presents additional free joints in order to reduce possible obstructions and discomfort in human motions in the 3D space [67].

The commercial products ATOUN model Y by ATOUN Inc. [69] and CRAY X exoskeleton by German Bionic [70] propose similar design and support assistance. The ATOUN exoskeleton presents shoulders and thigh straps and a pelvis belt for the contact with the operator, while a rigid bar parallel to the human back contains the actuation and control system. Two motors supply the required assistance torque, but the developers do not provide more information about the type of motors and the included sensors. The assistance can be regulated by the operator based on three different modes: the assist mode for pulling the upper body up, the walking mode for turning off the motors and allowing the wearer to walk, the brake mode for supporting the body to slowly perform a trunk flexion [69]. The CRAY X exoskeleton presents a similar structure, with shoulder and thigh straps for the contact with human body and the transmission of assistance, and a pelvis belt to fix the exoskeleton to the human waist. The assistance is supplied by two servo-motors positioned coaxial with the hip joints, while the included battery provides 8 hours of autonomy. The assistance torque acts in the sagittal plane, reducing the human efforts during trunk flexion-extension. No other information are provided by the developers about the control systems and the included sensors for the monitoring of human activity [70]. One other commercial product already on the market is the H-WEX exoskeleton by Hyundai. The device is connected to the user with straps on the shoulder, breast and waist. The leg brace can be positioned on the human thigh without strap in order to allow free movement. The exoskeleton has total eight degrees of freedom consisting of two one-directional active degrees for pitching of both hip joint, two passive degrees for yawing and pitch of upper body, two passive degrees for ab/adduction of each leg. A back side-plate including the battery, the controller and the actuator module is in contact with the human back. Thanks to the use of one single brushless DC flat motor combined with harmonic gear and positioned in the back of the pelvis belt, the total weight (4.5 kg) and encumbrance of the structure can be reduced. The torque assistance is transmitted to two pulleys coaxial to human hips and it acts between the human shoulders and thighs braces. The transmission system allows the splitting of the total assistance torque to the two human sides [71]. A new version of the exoskeleton, the H-WEXv2, has been proposed by the company during the last months. It presents some improvements compared to the previous one [72]. Better

control maneuverability on powered flexion/extension is provided by a new mechanism based on ball screw drive and a series elastic actuator. It maintains the advantage of allowing natural human walking with almost zero impedance.

At the end of 2019, a new semi-active prototype MRLift has been proposed by the University of Tsukuba, in Japan. The MRLift exoskeleton [73] is a lightweight solution that allows controlling the energy conversion of a passive compression spring thanks to the recent technology based on Magneto-Rheological and Electro-Rheological fluids. When the wearer leans down, the upper body's weight is converted to potential energy inside the MRLink. The core component of the MRLift is the MR damper with the embedded spring and the force retention mechanism. The MR damper is one degree of freedom linear motion system composed by a cylinder, a piston and an embedded spring. The magnetic field is generated by a coil wound around the piston. The MR fluid inside the cylinder changes the viscosity in the response of the change of the magnetic field. A Bowden cable connects the rotary joint in correspondence to the human hip joint to the piston of the mechanism. Arduino controller and a small battery are included in the back part of the structure. The proposed solution has been tested during a pilot study with a healthy male subject performing stoop movements with and without the exoskeleton, with and without picking external mass. The back muscular activity revealed a reduction thanks to the support.

In 2018-2019, several other research prototypes with electric motors have been proposed. Among them, the lower back robotic exoskeleton presented by Zhang and colleagues is made of four serial elastic actuators to support human motion both during hip flexion-extension and during adduction-abduction. The elastic element in series allowed reducing shocks and improving the human-device interaction [74]. More recently, Lee and Kim have proposed a serial elastic actuator (SEA) Lifting Assist Device [75]. In this prototype, one brushless DC motor is positioned on the back of the structure. Assist torque is transmitted to flexion-extension joints coaxial with human hip joints by a Bowden cable transmission. The waist assist exoskeleton proposed by Yong and colleagues is actuated by brushless flat motors combined with harmonic drive, but without the integration of any elastic elements. In this prototype, the assistance torque acts between the human waist and thighs [76, 77].

Few pneumatic solutions have been also presented. The Muscle Suit is a power assist commercial exoskeleton that employs McKibben actuators. It has been previously developed for supporting upper limbs in occupational tasks, and then reconfigured for lumbar support [78, 79]. It consists of an internal bladder surrounded by a braided mesh shell. When the internal bladder is pressurized, the highly pressurized air pushes against its inner surface and against the external shell, tending to increase its volume. Due to the non-extensibility, the actuator shortens according to its volume increase. In the Muscle Suit exoskeleton, the assistance acts between human shoulders and thighs. The Japanese company Innophys proposes several models [80]. It requires a compressor, a microprocessor, and electro-pneumatic controls in order to regulate the assistance. Despite the lightweight,

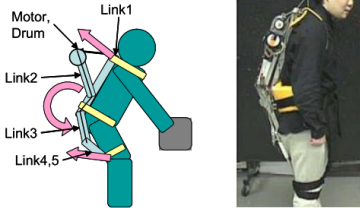



simple, and flexible structure, it needs compressed air from an external compressor unit.

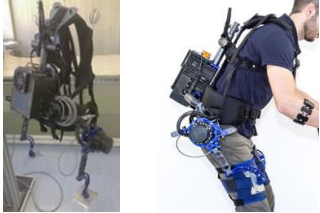



In 2016, a Wearable Power Assist Wear has been proposed as a research prototype [81]. Two types of pneumatic actuators are employed in assisting the low back movement. The first actuator is an elongation-type rubber artificial muscle and acts as external muscle to reduce the required forces. The second actuator made of thermoplastic polyurethane (TPU) balloons acts as a moment arm for the contractile force generated by the other and increases the effective torque. The required pressure is regulated by a set of valves controlled by micro-computer. The TPU material is a composite material that combines properties of rubber and plastic, with a good weight bearing capacity and impact resistance. It is commonly used to produce airbags. Acceleration, EMG and pressure sensors complete the control system for the bio-signal data acquisition. Thanks to the soft structure, the exoskeleton results lightweight, user-friendly and can be worn under the clothes. The device has been tested with the monitoring of EMG activation of back muscles and the comparison of muscular activity without and with the exoskeleton. During the test, the subjects performed a lifting task with stooping strategy. The effectiveness of the device is confirmed by the reduction of muscular activities. Despite the advantages of support, lightweight and compliance, the device must be connected to external air compressor system that could reveal to be unsuitable in common workstations. Moreover, both the air compressor and the external control system may restrict the human motion around the workplace.





One other prototype developed by the European collaboration of different academic and industrial research groups is the SPEXOR exoskeleton. Similar to previous devices, it has been thought to partially compensate the torques required in flexion-extension motion and it provides contact points with the human body at shoulders, waist and thighs. The wearable device presents two different assistance mechanisms: the Mechanically Adjustable Compliance and Controllable Equilibrium Position Actuator (MACCEPA 2.0) as torque source hip, and passive carbon fiber beams running parallel to the human spine. Because still on development, the actual prototype is made of the passive version of MACCEPA 2.0 (torsional springs) in order to conduct preliminary tests and validation of the mechanical structure [82].





Table 2.5.2 sums out the main characteristics of the active exoskeletons and depicts a graphical representation of the previously described structures.

Table 2.5.2 List of active trunk exoskeletons.

Active exoskeletons							
Name	Institution	Picture of the device	Assistance mechanism	Structure	Mass (kg)	Contact points	
Power assist device	Hokkaido University		DC motor, potentiometer, and EMG electrodes	Rigid	11	Shoulders, pelvis, thighs	
HAL lumbar support	Cyberdyne Inc, Tsukuba	 	Electric motor, potentiometer, accelerometer, EMG sensors	Rigid	3.1	Pelvis, thighs	
SWAD	University of science and technology of China		Servomotors, angle sensors	Rigid	/	Shoulders, pelvis, thighs, shanks, feet	

ROBOMATE	Italian Institute of Technology		Brushless motors, IMU sensors, EMG forearm bracelet	Rigid	11 (no battery included)	Shoulders, pelvis, thighs
ATOUN model Y	ATOUN, Nara city		Electric motors	Rigid	4.5	Shoulders, pelvis, thighs
CRAY X	German Bionic, Augsburg		Electric motors	Rigid	/	Shoulders, pelvis, thighs
HWEX	Hyundai		Brushless DC motor, pulleys, IMU	Rigid	4.5	Shoulders, pelvis, thighs

HWEXv2	Hyundai		Brushless DC motor, ball screw, SEA, IMU	Rigid	5.5	Shoulders, pelvis, thighs
SPEXOR	EU project		MACCEPA 2.0, carbon fiber beams	Rigid	6.6	Shoulders, pelvis, thighs
MRLift	University of Tsukuba		MR fluid, spring	Rigid	3	Trunk, pelvis, leg
Lower back robotic exoskeleton	North Carolina State University, Raleigh		SEA, IMU, gloves	Rigid	11 (no battery)	Shoulders, back, pelvis, thighs, shanks, feet

Waist assist exoskeleton	Chinese Academy of Science, Shenzhen		Brushless motor, IMU	Rigid	5	waist, thighs
Lifting Assist Device	Rehabilitation Engineering Research Institute, Korea		Brushless motor, Bowden cable transmission IMU	Rigid	4.4	Shoulders, back, pelvis, thighs
MUSCLE SUIT	Innophys		McKibben artificial muscle pneumatic actuator	Rigid	4.3-5.5	Shoulders, pelvis, thighs
Wearable Power Assist Wear	National Institute of Technology, Tsuyama		Pneumatic actuators, IMU, EMG and pressure sensors	Soft	/	Shoulder, waist, thighs

2.6. Experimental applications

One fundamental aspect that must be considered in developing a wearable device is the interaction with the user and the direct contact with the human body. Indeed, the interface with the user, is both at a physical and cognitive level. For this reason, after the development, the system must be verified and tested evaluating subjective and objective measurements. Moreover, during the design process, the exoskeleton is addressed to the entire work population, not to a specific subject. For this reason, an inter-subject analysis has to be considered to point out possible differences and perceptions. Considering the previous prototypes and commercial trunk exoskeletons, some experimental tests have been highlighted.

Several experiments were conducted in order to examine the effects of PLAD exoskeleton [46–51, 83]. First, the muscular activity of back muscles has been investigated in order to confirm the reduction of effort required to the human body in lifting tasks. The independent variables were the exoskeleton conditions (with or without), the weight of an external object (5-15-25 kg) and the lifting style (free, squat and stoop). EMG signals from the back and abdominal muscles have revealed the reduced lumbar EMG and the absence of significant effects on the abdominal region [46]. Due to the limitation of short-time experiments, type of motions, investigated variables and gender of the subjects (9 male participants) of the first investigation, other experiments have been implemented. By means of an EMG based model, the kinematics and dynamics at human joints were investigated. Differences in joint coordination were highlighted, with significance at waist and hip joint. The reduced waist net moment when wearing the device confirmed the positive effect of assistance, but joint shear forces resulted in higher values [83]. Experiments based on gender, fatigue and asymmetrical lifting motions were proposed with the investigation of kinematics, heart rate, endurance time, perceived effort and muscular activation variables during lifting tasks [48, 50, 51]. Results pointed out several important aspects: the reduced load in lateral bending and rotation moments in asymmetrical tasks with PLAD, no significant differences in terms of heart rate, reduced endurance time in prolonged experiments if the users did not wear the device, female participants subjected to higher fatigue compared to male and perceived discomfort at shoulders and knees contact points. The comparison between results from 15 females and 15 males depicted the absence of significant kinematic differences due to gender, investigated through the principal component analysis (PCA). Because individuals revealed greater ankle and hip flexion in combination with reduced lumbar and thoracic spine flexion, the use of PLAD has seemed to encourage squat lifting technique in spite of stoop [49].

Other devices as WAD, assist garment and VT-Lowe have been tested with the analysis of muscle activation during lifting tasks in laboratory environments [54, 56, 58]. All the studies confirmed the positive effects of the device assistance by the reduction of back muscles work. The recent comparison of commercial V22 and FLx ergoskeletons and the control condition (no device) revealed no significant biomechanical benefits of the two support devices in terms of joint loads. The

analysis considered only squat posture and was implemented by means of computational approach (EMG-driven multibody model), that could have jeopardized the results [84].

The Laevo exoskeleton can be considered one of the most well-known commercial wearable devices for the support of workers in industrial tasks. Several studies concentrated on the analysis of exoskeleton effects in reproducing numerous human body daily motions and static postures. The tests were conducted on healthy subjects with a maximum of 30 participants, and both subjective and objective outcome measures were considered. In 2016, Bosch and colleagues pointed out the reduced activity both for back and leg muscles, while the absence of significant differences in abdominal muscle activation during static holding tasks [85]. Three years later, Baltrusch and colleagues did not confirm previous discoveries [86]. Indeed, with the analysis of repetitive lifting of a 10 kg load the average peak muscular activity of the back muscles seemed to be lower when wearing the exoskeleton, but this difference was not significant in any phase of the lifting cycle. Moreover, the abdominal muscles showed significant increased activity during lifting when wearing the device. Koopman confirmed the results obtained by Baltrusch with the investigation of holding a flexed posture for a short time and at different degrees of trunk flexion [87]. One of the main possible reasons for this discrepancy in outcomes between experimental studies was supposed to be the different lifting motion tasks. As a matter of fact, all investigators agree that kinematics and coordination of human joints during lifting tasks significantly changes without and with Laevo. Participants changed the lifting technique to a stoop-like technique, with more extended knees and reduced hip flexion [85–87]. Moreover, the center of mass (COM) movement amplitude of the human body was lower, but without statistical significance. In 2018, Baltrusch registered from participants a restricted mobility and increased perceived difficulties when simulating daily tasks based on squat posture [88]. This change of movement strategy may contribute to a significant decrease in metabolic cost. These outcomes stressed the different effects of the Laevo exoskeleton compared to PLAD exoskeleton. Baltrusch has investigated the metabolic cost variable in two different studies [86, 89]. During lifting motion, the participants reduced the metabolic consumption when wearing the exoskeleton, while during the walking test the metabolic cost increased with the exoskeleton. Among the user's subjective perception and evaluation, the comparison of performing task without and with the Laevo demonstrated significant reduction of perceived muscular activity both for back and leg muscles, but an increase of pressure discomfort for chest due to the contact pad of the device [88]. A more recent investigation has stressed the effects of Laevo exoskeleton on energy expenditure during repetitive lifting, in comparison to the performance of one other passive solution, the SuitX exoskeleton [90]. Both males and females have been recruited for the test, performing both stoop and squat motions, both symmetric and asymmetric movements. The outcome measures considered not only the energy expenditure, that stressed a reduction with both exoskeletons, but also the activity of back muscles and the subjectively perceived

effort, usability rating and perceived balance. Both devices reduced the muscle activities, but with a strong dependence on the symmetry of the task. The Laevo revealed better assistance in symmetric lifting. Differences due to gender were evident. Indeed, females registered a larger reduction of muscular activities compared to males, but future researches have to be conducted in order to clarify the causes of differences (due to anthropometry, wearability or selected motion strategy). Considering the subjective judgements, participants reported medium to high levels of discomfort at the chest, waist and thigh with both structures, Laevo resulted in 38% higher chest discomfort in all task conditions. Exoskeletons revealed to be helpful during stoop motion, but slightly helpful when lifting in a squatting posture. The usability ratings showed comparable values across genders and exoskeleton types, excepted for the squatting motion, in which males reported the Laevo less suitable than the SuitX. Regarding the Laevo, the participants expressed negative considerations about shifting and moving of the chest and thigh pads. The same research group dealt with the comparison of Laevo and BackX exoskeleton during laboratory simulations of a precision manual assembly task. Muscular activity, endurance time and perceived efforts as outcomes of interest were considered [91]. The study concentrated on the evaluation of assistance during quasi-static task, pointing out minimal effects on task performance, but demonstrating benefits in terms of muscular activity reduction. In particular, the BackX exoskeleton registered higher reduction of trunk muscle activity (45%) compared to the Laevo exoskeleton (24%). The BackX exoskeleton has also been tested by Poon and colleagues with the main attempt to assess the muscle fatigue reduction in repetitive tasks. The results highlighted muscular activity reduction, but with lower percentages respect to the previous described study (around 20% of reduction). In addition, the time that subjects could hold the flexed posture after repetitive lifting session increased by 52% after wearing the device [92]. In 2019, Hensel and colleagues, during a long period of test in the workplace, highlighted different levels of discomfort based on the task [93]. In static holding posture, the Laevo reduced the discomfort at the lumbar back, while in dynamic motions the perceived discomfort increased. In both cases, the study confirmed the discomfort at chest contact. The cited study [93] reveals important considerations about the use of exoskeleton during daily working life and not only in a laboratory setting. Moreover, it tested the device for a long period, registering the subjective perception at the start and at the end of one month. Despite the initial high level of user acceptance and usability, these parameters resulted reduced after the entire trial [93]. Additional investigations by means of objective measures might be crucial in order to confirm the users' perception and to evaluate possible kinematic adaptation within time. Finally, a recent investigation about the potential use of an exoskeleton by patients and health care professionals has been presented by Baltrusch and colleagues [94]. The aim of the research concentrated on the clarification of users' perception when wearing the passive exoskeleton. Four patients affected by low back pain have been included in the test. Data analysis focused on the subjective evaluation of the device in terms of usability, wearability, comfort and limitations.

Both patients and health care professionals pointed out some limitations due to discomfort at the chest and hindrance during sitting. Improved comfort was considered as an important design requirement. Many aspects had been investigated in the past, but there are some conditions that need a deeper analysis, as the direct comparison between lifting strategies to point out the suitability of the device in several motions. Moreover, the importance of testing the device in a working setting seems to be a crucial point to consider possible encumbrances and difficulties. Moreover, the exoskeleton has been tested on healthy young male subjects. The investigation of human body effects considering gender and age variability might stress important differences and necessities.

Among the powered exoskeletons, a lower number of investigations have been conducted compared to passive systems. Most of the researches verified the application of developed prototype by means of a pilot study with only one participant [65, 66, 74, 76, 95, 96]. Despite the positive preliminary results, the device needed to be tested on a larger sample size and in several conditions. Analyses focused on the evaluation of back muscle activation. Several prototypes confirmed the decrease of muscle activation when wearing the exoskeleton [65, 66, 71, 72, 74, 79, 97]. The ROBOMATE prototype has been investigated in order to confirm its main function of assistance during lifting tasks [98], but, in addition, the tests allowed the comparison between different control strategies [99]. The first strategy is based on user kinematics monitored by inertial sensor and modulates the assistance to support the wearer's upper body. The second strategy adapts the assistance to the mass of the lifted object and is based on the electromyographic measurements of forearm muscles. A third strategy is a combination of the first two solutions. Switching between these strategies, the ROBOMATE can adjust the support to different task conditions and to individual preference. Experimental results confirmed the suitability of all strategies for the reduction of spinal muscular activities. Additionally, Tsuneyasu used a similar approach to compare torque-based and angle-based control implemented on the Muscle Suit [100], pointing out the suitability of both control strategies.

In addition to the investigation of back muscle activation [62], different analyses were implemented on HAL support [63, 64, 95, 101, 102]. Among objective measurements, the experimental verification of the device highlighted the absence of influence on the human heart rate [102] and blood pressure [64], but several analyses stressed the important effect on increased time, number of lifts, distance of load throw [63, 64]. The HAL Care Support significantly reduced the human lumbar fatigue both in the reproduction of a typical repetitive stoop lifting movement [63], and in a repeated snow-shoveling application [64]. The exoskeleton has been tested also in simulating patient transfer, highlighting a reduced VAS score when wearing the device [103]. An interesting investigation has been conducted by Kadone, Miura and colleagues, in order to investigate muscle synergies during repetitive stoop movements [101]. The study pointed out a significant change in muscle coordination when wearing the exoskeleton, with a significant reduction in EMG amplitudes of the Erector spinae. Moreover, the

muscles involved in the simulated task but not supported by the device (right and left Latissimus dorsi) demonstrated a significant reduction. A possible explanation has been stressed as the restriction of the lumbar relative movement between vertebrae caused by the design of the exoskeleton, allowing the assistive torque to be transmitted to the upper back. However, Finally, the integration of a passive elastic element into the structure to supply assistance to the user revealed to significantly reduce power consumption of the device with the maintenance of the same partial support [95].

The SPEXOR exoskeleton has been firstly tested in a pilot study with three healthy subjects, evaluating the acceptance and the subjective perception by the users. Clusters of markers have been positioned both on the exoskeleton both on the human body in order to measure the motion kinematics. Results highlighted good transparency of the exoskeleton. A correlation of 0.98 has been registered between exoskeleton and human angles. The perceived task difficulty decreased when wearing the exoskeleton and low discomfort level has been pointed out. Nevertheless, the lack of efficacy has been evaluated in walking, squatting, trunk 3D rotation and wide stance [22]. Later, an experimental study has been conducted to assess the effect of the device on reducing the metabolic cost during repetitive lifting tasks [104]. A larger group of participants has been considered. Ten men employees performed 5 minutes repetitive lifting motion, lifting and lowering an external object with a total mass of 10 kg. The participants could select the preferred lifting strategy. In addition to the metabolic cost, human joints kinematics, mechanical joints work, and back muscle activity has been considered as outcomes. Results stressed the positive effects of the exoskeleton in reducing the muscular activity and metabolic cost when wearing the device. More recent analyses have been conducted on subjects affected by low back pain [105, 106]. Several human body motions have been performed during tests and both subjective evaluations and performance improvements have been considered as outcomes. General positive results are reduced local discomfort, perceived task difficulty and improved task performances. Some drawbacks have been stressed in terms of total weight of the structure.

Table 2.6.1 sums up the main characteristics, findings and limitations of experimental tests on passive and powered devices. Despite the numerous researches dealing with the testing and analysis of human-device interaction in the occupational application, the effectiveness of wearable exoskeleton in reducing human efforts is still an open discussion. It is difficult to evaluate the suitability and efficacy of the device in real industrial and manufacturing workstations without affecting the range of motions, the encumbrances and the comfort of the user. The inter-subject variability may crucially influence the device testing results. Several subjective and objective measurements have been proposed for validation, but no standards neither experimental guidelines have been pointed out. In addition, tests have been implemented in a laboratory setting and for a short time, while only a few cases presented long-time verification on the workplace. Some discrepancies in results have been stressed due to external variables of influence or different

experimental settings/properties. Passive solutions present the main advantages of flexibility, adjustment to user sizes, easiness of usage, low weight of the total structure and possible utilization in several conditions. Nevertheless, the total amount of support must be imposed during the design of the structure and cannot be modulated during motions. Passive exoskeletons revealed to be suitable in specific tasks and human positions but created discomfort, perceived difficulties, and user's refusal in other movements. Due to the complexity of human movements and the possibility to adopt several motion strategies and joints coordination during manual handling and lifting tasks, the introduction of powered systems seems to be necessary for trunk support exoskeletons. Despite the fundamental advantage of assistance modulation based on human kinematics and human needs, the introduction of a powered mechanism requires a more complex and articulated structure. The total mass of the device may crucially increase, with possible augmented discomfort and reduced acceptance for the user. Moreover, proper control and power systems need to be implemented. The direct comparison between passive and active trunk support prototypes has not been already investigated.

Table 2.6.1: List of experimental tests on wearable trunk support exoskeletons.

EXPERIMENTAL TESTS WITH WEARABLE TRUNK SUPPORT EXOSKELETON				
MAIN PURPOSE	SUBJECTS & TASKS	VARIABLES	FINDINGS	LIMITATIONS
LAEVO [85] Analyze the effect of a passive exo during specific tasks in terms of muscle activity and endurance time	18 subjects: 9 males and 9 females. 2 tasks: - assembly work task on a table with 40° trunk flexion (10 cycles) - static holding (40° trunk flexion)	- EMG activity at low back, abdomen and legs - trunk kinematics - local perceived discomfort	- no differences in the left and right side - EMG: no significant results for abdomen, reduce activity in both tasks for back (37-44%) and legs muscles (20-24%) - discomfort: significant reduction for back, no significance for legs; significant increase for chest - legs kinematics: over-extended knees - endurance time: 3 times higher with exo	- knees over-extension - weakening of back muscles - partial support - specific tasks - limited time
LAEVO [88] Assess the effect of exo on functional performance during work-related tasks in healthy individuals	18 men 12 tasks (lifting, carrying, forward bending, walking, sit to stand, one-handed bank position, stair & ladder climbing, stooping, squatting, trunk flexion & rotation, wide stance)	- general/local discomfort - performance time	- a significant difference in objective lifting performance and perceived task difficulty for forward bending - no significant difference in objective lifting performance and perceived task difficulty for carrying and lifting - discomfort chest and leg pad - discomfort, reduce angles, increase difficulty and reduce objective performance in tasks all other tasks	- time to get habituated - laboratory setting - short total duration of the test
LAEVO [89] Assess exo effects on metabolic cost	11 men repetitive lifting & walk	- metabolic cost - energy expenditure	- decrease metabolic cost during lifting (17%) - increase metabolic cost during walking (17%)	- laboratory environment - sample size
LAEVO [93] Subjective evaluations in static & dynamic lifting for 4 weeks	30 men - static flexed position (range 20-90°) - dynamic handling (load 3-20 kg)	- perceived usefulness: discomfort - perceived ease-of-use: usability & use intention	- decrease discomfort low back in static flexion, increase in dynamic task - significant increase in discomfort at chest - usability and user acceptance decreased along weeks	- no female - only healthy men - only subjective outcomes

<p>LAEVO [87] Assess the exo effects on abdominal and back EMG, hip and waist flexion, lumbar and exo net moments</p>	<p>11 healthy men bending forward till the hands were at 5 heights (100-75-50-25-0%) and holding position (5 s). 3 times for each task, in 3 conditions: no exo, low exo, high exo</p>	<ul style="list-style-type: none"> - waist total net moments - exo and human net moments - trunk inclination - lumbar & hip flexion - EMG back muscles 	<ul style="list-style-type: none"> - hand positions influence results - reduction of hip flexion when using exo - reduction of lumbar net moments with exo - reduction of EMG activity only at specific hand height - increase of abdomen EMG activity at 0-25% hand height - flexion relaxation phenomenon (no back muscles activity) 	<ul style="list-style-type: none"> - no women - no knee investigations -no contact points investigation
<p>LAEVO [86] Assess how wearing a passive trunk exoskeleton affects metabolic costs, movement strategy and muscle activation during repetitive lifting and walking</p>	<p>11 healthy men Tasks: -5 min of repetitive lifting (10 kg) at selected velocity but preferred lifting technique -5 min of walking on treadmill at preferred speed</p>	<ul style="list-style-type: none"> - Metabolic cost - EMG back and legs - knee, hip, trunk, lumbar angles - COM of body - stride time 	<p>Lifting: -decrease metabolic cost - no significant change in kinematics. Smaller angles with exo -no significant change in COM -no significance in back muscle EMG neither legs, but significant increase in abdomen muscles with exo - changed lifting technique to a stoop-like technique with exo, reduced COM movement amplitude</p> <p>Walking: -increase metabolic cost -significant difference in walk speed & reduced stride length -no difference in EMG back and leg, difference in abdomen</p>	<ul style="list-style-type: none"> -laboratory -short time -no significance in statistics
<p>LAEVO [91] Biomechanical evaluation of two passive exoskeleton, Laevo and BackX</p>	<p>18 subjects (9 males and 9 females) Precision assembly task (pick up pegs) in 26 conditions, two passive exoskeletons</p>	<ul style="list-style-type: none"> - trunk muscular activity - task completion time - perceived effort 	<ul style="list-style-type: none"> - reduced back muscle activities in many conditions with both passive exoskeleton (45% reduction with BackX, 24% with Laevo) -minimal effects on task completion time and perceived efforts 	<ul style="list-style-type: none"> - future analysis must better characterize the task specificity

LAEVO [90] Test the efficacy of two passive exoskeletons, Laevo and SuitX	18 subjects (9 males and 9 females) Repetitive lifting/lowering task (stoop/squat, symmetry/asymmetry) with two exoskeletons	- peak-normalized muscle activity - energy expenditure (metabolic demand) - subjective assessment	- reduced trunk muscle activity with both devices, higher in symmetrical lifting, higher for females - minimal effects on the abdominal muscles -reduced energy expenditure (around 8%) - helpful in stoop, less during squat -perceived discomfort Laevo's pads - Laevo not suitable in asymmetrical lifting -restricted hip motion in the 3D space	- young adults - laboratory environment
LAEVO [94] Subjective evaluation of the device to stress the principal characteristics	12 subjects (4 patients affected by LBP and 8 health care professionals) Wear the device and try simple tasks	Subjective outcomes	- discomfort at the chest pad - difficulty in some specific movements (sitting) - hindrance to flex legs - assistance in lifting	- only subjective evaluations -small sample size group
BACK-X [92]	11 males Lifting and lowering 18 kg load at 7 lifts/minute for 4 min, with and without exo	- muscle fatigue - endurance time - oxygen consumption	- reduced peak thoracic and lumbar erector spinae muscle activity - increase of endurance time with exo - no significant increase on oxygen consumption rate	- number of subjects -limited types of task -lab setting
ROBOMATE [98] Perform an ergonomic assessment of an active trunk exo	12 males 5 trials of lifting and lowering with external load (7.5-15 kg) and exo condition (no exo with exo)	- back, abdomen, legs EMG - Perceived pressure - usability - perceived effort	- lower EMG for back and leg, but not for abdomen - significant reduction of perceived effort at trunk, no effect on perceived leg effort - higher perceived pressure at legs	- laboratory setting - short time - small sample size
ROBOMATE [99] EMG effects with several exo controls	11 males Lif object (7.5-15 kg) with/no exo	EMG at low back	-reduction of muscle activation in case of exo in all control strategies (IMU-EMG arm-hybrid)	- simplified motion

PLAD [46] Determine reduction of human back EMG muscles	9 males Lifting external object (5, 15, 25 kg) in stoop, squat and free strategy	- EMG at lumbar and abdominal muscles - pelvis & lumbar angle - peak trunk and load vertical accelerations.	- reduced lumbar EMG in all conditions - no significant change in abdomen muscles - trunk acceleration resulted different with PLAD - limited user acceptance	-Small sample size -self-selected elastic stiffness -short time -no fatigue
PLAD [83] Kinematic and kinetics analysis of PLAD exo	9 males - 30 trial varying flexion angle (15-75) and PLAD stiffness (5 K) - 9 blocks of lifting trials, each trial block 5 minutes	- EMG back and abdomen - Trunk angle - Spinal loads (EMG-assisted spine model) - joint motion at the knee, hip, and waist	- stiffness and trunk angle influenced the force from exo - exo reduced waist net joint moment - extensors EMG decreased, flexors EMG increased - reduction of joint compression force - increase of joint shear force - no time difference in lifting - significant reduction in lumbar and hip flexion	- future analysis with PCA
PLAD [50] Assess the PLAD's effectiveness for asymmetric lifting	9 males total of 54 lifts with one lift at each weight (5-15-25 kg), style (freestyle, stoop, squat), position (centre, right, left), exo condition (with, no)	- EMG back and abdomen muscles - L5 3D joint moments (dynamic model)	-The PLAD reduced mean lateral bending moments (M_y) by an average of 30%, mean rotational moments (M_z) by 24% and mean flexion-extension moments (M_x) by 19.5%. No difference due to asymmetry -discomfort at shoulders and knees -PLAD reduced muscles activity and joint moments	- small sample size - no women tested
PLAD [48] Determine if the exo could reduce localized muscular fatigue during repetitive lifting	10 men 45 min lifting task, with and without PLAD	- mean heart rate (HR) - perceived level of exertion - waist extensor moment - endurance time - EMG lumbar spine (amplitude and median power frequency)	- significant increase of HR over time, but no significance in difference between PLAD and no-PLAD - HR linked to user evaluation, with PLAD the repetitive lifting was felt less strenuous - reduction of endurance time if no PLAD - reduction of EMG activity back - decrease of median power frequency without PLAD, no noticeable decrease if with PLAD	- small sample size - laboratory - sagittal plane - possible error in measuring extensor moment with load cell

PLAD [51] Determine if the exo could reduce localized muscular fatigue during repetitive lifting in women	12 women 45 min lifting task with and without PLAD	<ul style="list-style-type: none"> - mean heart rate (HR) - perceived level of exertion - waist extensor moment - endurance time - EMG lumbar spine (amplitude and median power frequency) 	<ul style="list-style-type: none"> - significant interaction of device and time was observed for the EMG (increase of activity during time) - decrease of strength and endurance time in PLAD and no-PLAD compared to reference - no significant effect on heart rate - discomfort at knee area - females demonstrated more lumbar fatigue than males - no difference in back endurance 	<ul style="list-style-type: none"> - hip straps slip upwards and over the iliac crests in the forward bending phase - substantial levels of pain in the upper trapezius muscles
PLAD [47] Examine exo (6 stiffness conditions) effects	13 men Stoop, squat, free style lifting	<ul style="list-style-type: none"> - EMG trunk, hips and lower limbs - waist net moment - lumbo-pelvic angle 	<ul style="list-style-type: none"> - higher lumbar EMG reduction with higher stiffness -reduced legs EMG in stoop and free lifting -no significance in abdomen muscles -reduction of net waist joint moment -no effects on lumbar angle - rectus femoris and gluteus EMG increased in squat - the flexion/extension waist net moment higher in stoop 	<ul style="list-style-type: none"> - no subjective evaluation
PLAD [49] Test how the PLAD affects lifting kinematics using PCA	30 healthy participants (15 males and 15 females) Perform free style lifting, 30 cycles for trial	<ul style="list-style-type: none"> - 5 joint angles (ankle, knee, hip, lumbar spine, thoracic spine) 	<ul style="list-style-type: none"> - no significant difference due to gender - significance difference in joint flexion and rotation Individuals demonstrate greater ankle and hip flexion and less lumbar and thoracic spine flexion (squat) - no significant differences in knee flexion 	<ul style="list-style-type: none"> - no comparison between different lifting strategies
MUSCLE SUIT [79] Development and test	5 males handing external object of 10 kg above head	<ul style="list-style-type: none"> EMG at shoulder, elbow, waist 	<ul style="list-style-type: none"> - muscle suit reduced muscle power at shoulder and elbow - no waist assistance. 	<ul style="list-style-type: none"> - small sample size - small variables - no specific lifting strategies
MUSCLE SUIT [97] Test the device	3 subjects Lifting external object of 10 kg	<ul style="list-style-type: none"> EMG of low back 	<ul style="list-style-type: none"> - muscle suit reduced about 40% muscle use for all subjects 	<ul style="list-style-type: none"> - pilot study

MUSCLE SUIT [100] Develop an assistive suit with flexible pneumatic rubber artificial muscles	5 participants Upright, bending+5 s static, return to standing posture 3 conditions (angle-based control, torque-based control, no suit)	- center of gravity (COG) fluctuation - EMG back	- both control methods could reduce the EMG activity - reduction in fluctuation of COG of approximately 4 mm with the support - statistically significant differences between the torque-based control and the angle-based control	- small sample size
HAL [62] Develop the HAL to reduce the lumbar load	7 adults Lifting heavy load (10 kg) in stoop	- trunk angle - torque at lumbar joint - subject questionnaire	- the HAL reduces the lumbar load by supporting hip flexion/extension movement.	- small sample size - no comparison between lifting styles
HAL [95] Exo with passive mechanism to reduce the power consumption	1 man task of carrying external object to measure energy consumption	- lumbar moments - exo power consumption	- HAL with passive mechanism reduced the lumbar stress - the average power consumption of HAL was reduced 44% - the HAL max power consumption was reduced 45%	- only one subject - pilot study
HAL [64] Test the HAL for Care Support in reducing lumbar load in repetitive snow-shoveling	9 men repeated snow-shoveling until fatigue	- visual analog scale (VAS) - Total time - Number of scoops - Distance of snow - Heart rate - Blood pressure	- with HAL subjective lumbar fatigue after repetitive snow-shoveling movements decreased significantly - with HAL major number of scoops, longest distance and higher time - no significant difference in pulse and blood pressure	- no women - no elderly people
HAL [63] Test the decrease of the lumbar fatigue and the performance in repetitive lifting motions	11 men, 7 women repetitive stoop lifting movements of a cardboard box (12 kg) as many times as possible	- VAS - numbers of lift - time	- subjective lumbar fatigue after repetitive lifting movements with HAL for Care Support was significantly less than without HAL - increase time - increase number of lifts	- lifting motion in vertical direction - only stoop

HAL [101] Evaluate exo effect with muscle synergy analysis	13 males, 7 females 2 sessions (with and without HAL) of stoop lifting/placing until possible lift and place a small box, (for males, 12 kg, for females, 6 kg)	- VAS - number of cycles - hip kinematics - muscles synergy analysis	- significant increase of cycles - significant less perceived fatigue - no significant differences in peak hip angles - angular vel decreased from stoop to upright posture - muscle coordination patterns significantly changed - sign changes muscles not supported - significant reduction in EMG amplitudes	- no upper limb kinematics - limited number of muscles
HAL [102] Investigate exo effects on muscular activity and heart rate	14 men Freestyle symmetrical lifting task	- EMG lumbar spine - heart rate - physical effort - discomfort & range of motion (ROM)	- significant reduction of EMG - no difference in heart rate & discomfort (Borg scale) - no significant difference between the average number of repetitions during a 10-min lifting task	- laboratory - simple motion - small sample size
HAL [103] Test the use of exoskeleton for care support in a simulated patient transfer	19 subjects (16 males, 3 females) Lift a 60 kg doll from a seated position to a standing posture	- Transfer performance - VAS - EMG of trunk and hip	- reduced lumbar fatigue - increase in EMG activity of left gluteus maximus - reduced VAS score with exoskeleton	- Only vertical movement simulation - problems on data registration
SPEXOR [22] Develop & test a passive exo system with different configurations	3 healthy subjects back range of motions in stoop with 4 configurations (no exo, exo with unlocked beam, exo with locked beam, exo with rigid unlocked beam) range of daily activities	- user impression - perceived task difficulty - discomfort	- good correspondence between human and exo angles - trunk flexion reduce with 16° (flex slider exo) and 41° (rigid exo) compared with no exo condition - all cases lower peak angles - flex slider exo has bigger ROM - reduced lateral bending with rigid exo - exo unsuitable for walk, trunk rotation, squat - high perceived support, low interference - low discomfort, some problems in legs pad & hips pressure	- number of subjects
SPEXOR [104] Assess the effect of the device on	10 men employees	- metabolic cost - kinematics	- decrease of metabolic cost of lifting by 18% with exo - no sign results in kinematic range of motion - no sign variation of centre of mass motion	- lab setting - pre-defined duration

reducing metabolic cost during repetitive lifting	5 min repetitive lifting task. Lift and lower a 10 kg box from ankle height, with and without exo. Self-selected lifting strategy	- mechanical joint work - back muscle activity	- sign decrease of mean muscle activity in the back with exo	- no long period - skin artifacts influenced kinematics
SPEXOR [105] Assess functional performance and user satisfaction of workers	24 males (13 with LBP and 11 without LBP) 12 tasks (lifting, carrying, forward bending, walking, sit to stand, one-handed bank position, stair & ladder climbing, stooping, squatting, trunk flexion & rotation, wide stance)	- subjective evaluation with VAS scale - performance time	- increase in performance - reduction in local discomfort -reduced or equal perceived task difficulties	- no objective biomechanical evaluations
SPEXOR [106] Investigate the use of passive exoskeleton with LBP patients	14 patients 12 tasks (lifting, carrying, forward bending, walking, sit to stand, one-handed bank position, stair & ladder climbing, stooping, squatting, trunk flexion & rotation, wide stance)	- level of low back discomfort - task difficulty -general discomfort (VAS)	- reduced local discomfort in static forward bending - favourable effects on performance - some discomfort due to the weight of the structure	- no objective biomechanical evaluations
VT-Lowe [58] Test the effect of passive exo during lifting	12 adults Stoop, squat, free and asymmetric lifting	- EMG of back, abdomen, legs muscles - discomfort	- reduced peak and mean EMG of back and leg muscles - increased abdomen activity, but no significance - discomfort at thigh pad	- short training period - number of carbon fibers
NARUSE [65] 3D analysis of lifting motion and the exo effects	1 subject lifting object (0–20 kg) in many tasks (2 height, 2 distance, 3 orientations)	- joints angles - estimated compression force at lumbar spine - EMG erector spinae	- difference in joint angles with & without exo - reduced EMG & lumbar compression force with exo - reduced twisting angle with exo	- small sample size - pilot study - no lifting strategies analysis

V22 & FLX [84] Compare two postural support passive exo with EMG driven multibody model	10 men squat lifting exo conditions (no, exo1, exo2), combination of asymmetry and weight height	- joint kinematics (peak angle of torso, hip, knee) - Horizontal moment arm - 3D spinal loads	- significant higher angles for heavy loads & low height - no differences between exo on hip and knee joint - higher waist angle with V22 exo - significant difference due to asymmetry or height - no significant difference in spinal loads & moment arms - no significant biomechanical benefit of both ergoskeletons	- laboratory environment - only squat - no training before the test
WMRD [57] Design, build, and test a worn lower extremity exo	6 subjects (5 males, 1 female) squat lifting strategies repeated 2 times with two different weights	- EMG erector spinae - back joint forces - human device interface - device effectiveness	- 54% reduction in back muscle activity - reduced spine compression force - critical fit device - device was most comfortable if included initial free zone	- small sample size - only static sagittal lifting - only back EMG
Hyundai H-WEX [71] Design and evaluation of exo	9 males semi-squat and stoop, 15 kg load	- muscles activity of back, abdomen, legs - usability	- reduction in muscles activation if wearing exoskeleton for back and legs, while abdomen depicted an increase of value. - similar results but in stoop and squat.	- limited objective variables - small sample size
Hyundai H-WEXv2 [72] Verify the effectiveness of the waist assistance and confirm the improvements of the exoskeleton compared to the previous version	10 healthy male subjects Lift 15 load in stoop and semisquat motions With H-WEX1, with H-WEX2, without exo	- EMG signals	- reduced muscular activities when wearing the new version of the exoskeleton H-WEX2	- no kinematics evaluations - limited number of subjects - no subjective evaluations

Waist assist exoskeleton [76] Develop and test	1 subject lifting external object of 20 kg	- Heart rate	26.7% reduction of heart rate if wearing the exo	- preliminary test
WAD [54] Evaluate exo in reducing trunk EMG in static tasks	9 subjects 2 conditions (with and no), 3 trunk angles (0,30,60°), 3 loads (0,5,15 kg)	- EMG at low back and abdomen	- decreased EMG back muscles (15-30%) and some case abdominal muscles increased (14%) - no problem of comfort and usability	- no repetitive tasks to evaluate fatigue
SWAD [66] Develop and test of the proposed exo	1 subject stoop at 0-30-60-90° trunk flexion	- EMG at low back	- small EMG increase at 0°, but large EMG decrease at 30-60-90° with exo	- small sample size - localized EMG
Lower back robotic exoskeleton [74] Description and verification	1 male Lift object (0,5,15,25 kg) in squat and stoop	- Hip joint kinematics - EMG lumbar spine	- reduction of back muscles with exo both in symmetric and asymmetric tasks - the second degree of freedom (DOF) support contributed reducing EMG - no difference in hip joint due to exo in symmetrical lifting	- exo weight - joints misalignment - small sample size
Passive garments with elastic bands [56] Develop and test	8 subjects (7 males, 1 female). - Squat lifting (weight 12.7-24 kg) - stooped at 30-60-90° trunk flexion	- Kinematics (pelvis, trunk, external object) - EMG of erector spinae - Elastic band force	- mean EMG reduced in leaning position & lifting task - no significant difference in kinematics, position of external object & duration time - model predicted reduced forces at intervertebral discs	- small sample size - short time
Active exo prototype [96] Preliminary test	1 subject stoop lifting an external mass (25 kg)	- Questionnaire for wearability and mobility	- Light and easy to wear - No restricted motion - Tangible help in extension phase	- Absence of objective measure - 1 participant

Chapter 3

MAIN GOALS AND THESIS CONTRIBUTION

The current research deals with the analysis of the passive exoskeleton-human interface and the development of the prototype of a powered trunk-support exoskeleton for industrial tasks. The main novelty of the proposed exoskeleton is the capacity of differentiating and adjusting the assistance torque according to the user's kinematics, efforts, biomechanical loads, wearability and perceived comfort. The whole study can be summed up in four main steps, as following pointed out.

1. The starting point concentrates on the evaluation of a passive commercial system, the Laevo exoskeleton [14]. The analysis of the device focuses on both the mechanical investigation of the structure and on the estimation of subjective and objective measures of human-device interaction through experimental laboratory tests. A preliminary mechanical examination needs to be implemented with the attempt to underline the several parts of the structure and the adopted passive mechanism of support. The wearability of the device is analyzed with four different users, two females and two males, with the attempt to compare the possibility of adaptation to different sizes and anthropometry. During the experimental test, several lifting tasks are performed by one female subject in order to represent typical industrial workstations. Data analysis, subjective acceptance and perceived discomfort are evaluated by means of questionnaires and standardized evaluation scales. Optoelectronic systems and force sensors allow the monitoring of human kinematics and the interface pressures exchanged at the contact points, which represent the objective variables.

2. The exoskeleton-user interface is analysed also with a computational approach. 3D multibody models of the human body, of exoskeleton structure and of the interfaces between the two are developed. The human body model is implemented based on literature anthropometric measure and consists of a kinematic chain of rigid bodies (human body segments) connected by articulated joints. The exoskeleton model reproduces the mechanical structure of the passive commercial system previously investigated (Laevo exoskeleton). Starting from the passive solution, different exoskeleton configurations are developed varying the exoskeleton joint position and the number of elastic elements for the assistance torque. The interaction of the exoskeleton models with the human body is investigated in terms of biomechanical effects, stressing the positive and negative consequences on human body efforts due to the exoskeleton. Considering the final attempt to substitute the passive joint with a powered mechanism in order to compensate for the limitations and the drawbacks of the passive structure, several maps of torque assistance are designed and simulated. A proper investigation of the required assistance is conducted. Two different relative angles are considered for the differentiation of the lifting motion technique adopted by the user. The computational approach and the developed multibody models are used for the characterization and the validation of the implemented powered law of assistance.
3. The control strategy is a fundamental aspect in the development of a wearable device with a motorized system. The crucial aspect for an industrial exoskeleton is the direct interaction with the user and the necessity to correctly understand and follow the human motion (mechanical transparency), avoiding any limitations and kinematic restrictions. In the present work, different actuation systems and control laws are investigated and compared in order to define the type of actuation and the control strategy, which need to be implemented. Electric actuator is selected for the powered joint development. Control system based on two control loops and proper assistive strategies is implemented: model-based control (high level) for the definition of the desired torque and torque control (low level) for the closed loop on the motor output. The hardware system and the selected electronic components for the implementation of the exoskeleton two-level control architecture are fully described. A customized torsional spring is computationally modelled, analysed, design and validated for the hypothesis of serial elastic actuator in order to provide additional compliance and back-drivability to the system.
4. After the definition of the torque assistance law of the high control level and the identification of the torque control scheme that must be used for driving the selected motors, the following phase of the study deals with the design and the development of the powered prototype. The passive structure is integrated with electric servomotors and sensors. Electric actuators and gearboxes are selected based on needed torque, required performance,

limitation of encumbrance and restrained total weight. The integration of angular position sensors allows the monitoring of human kinematics, the differentiation among lifting strategies and the resulting assistance torque. Flanges for the connection of the upper body support and the lower body support of the exoskeleton are designed. The new mechanical components need to be suitable for the integration with the components of the passive structure that will be maintained. Mechanical end-strokes are defined based on the range of motion of the human body, in order to guarantee the wearability and the safety of the device. Once defined the whole new powered joint and realized the mechanical components, the structure is assembled. The developed prototype of the active exoskeleton assists the user with an adjustable flexion/extension torque in the sagittal plane differentiating the different human lifting strategies.

Chapter 4

PASSIVE SYSTEM: Biomechanical evaluation

4.1. The Laevo exoskeleton

The Laevo exoskeleton is a passive trunk-support device currently proposed on the market. The first concept of Laevo exoskeleton was born in the X-arm project, carried out by *InteSpring B.V.* and *Delft University of Technology* in 2010. It was originally designed to assist nurses with lifting patients, but it has revealed to be useful and applied in several working environments. The idea consisted in the realization of a lightweight and comfortable structure that can be adapted to different users and several working conditions. Nowadays, the exoskeleton is addressed to workers that must repeat bending motions, for people suffering from low back pain or those at risk of back injuries and fatigue. The minimalism and the smartness of the mechanical structure contributes to increasing acceptance, wearability, and comfort, as to reduce the encumbrance and the difficulties in adjustment to several users. From the first proposed solution, five different prototypes have been realized with the attempt to overcome limits, satisfy users' requirements and enhance the product. The progressive improvement from the first to the last version deals with several aspects: the different design of the contact pad that interacts with the human chest to improve the comfort of the interface, the integration of a mechanical level to adapt the initial position of the device, the identification of the best mechanical features of the torque assistance and the possibility to integrate different level of supports to the structure.

In the following section, the last Laevo prototype (version 2.5) is presented and described in detail.

4.1.1 Mechanical structure

The Laevo exoskeleton consists of three main parts articulated by means of hinge joints:

- Torso structure, a support part interacting with human upper body that transmits the assistance to the chest;
- Pelvis belt, that is not directly involved in the assistance but allows fixing the exoskeleton to the human pelvis;
- Thigh structure, a support part interacting with the human lower body that transmits the assistance to the thighs.

Figure 4.1.1 depicts the Laevo exoskeleton 2.5 and describes the several structural components.

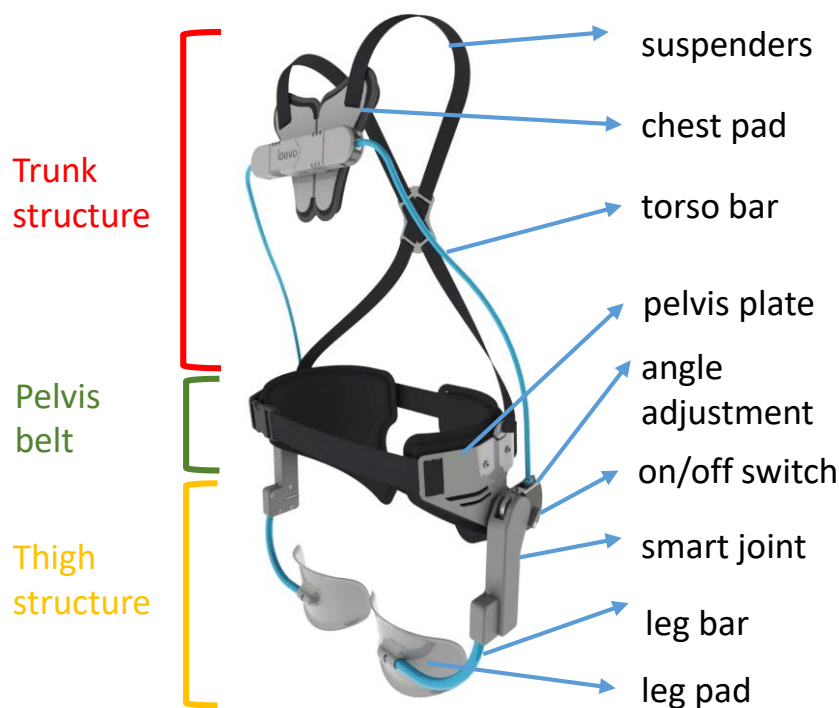


Figure 4.1.1: Laevo exoskeleton version 2.5. Identification of the three main parts and description of the several structural components.

The torso structure is composed of soft suspenders at the shoulder level and a chest pad supported by two rigid bars. The chest pad is connected to the lower part of the device, the leg structure, by means of two smart joints with spring-like characteristics. The suspenders connect the chest pad to the pelvis belt. The leg structure is composed of two rigid bars and thigh pads for the interaction with the user's legs. The Laevo exoskeleton is a symmetrical support device. The right and the left sides of leg structure present the same characteristics and can supply the same amount of assistance. The assistant device is not though to provide different supports in case of asymmetrical requirements. Each smart joint supply assistance

to the user. It has to be positioned aligned with the human hip joint. In correspondence to the smart joint, there is an on/off switch that allows activating/deactivating the support. Moreover, the angle adjustment mechanism allows the user to adapt the initial inclination of the device based on the personal anthropometry with an angular range of 0° - 35° . The variation of the starting position allows the adaptation of the exoskeleton to different chest measures and it reveals strong benefits particularly for women chest and for men with greater trunk size. The starting angular position must be defined when the user wears the device, before activating the assistance. From the selected position, the exoskeleton considers the relative angle between trunk and thigh support as the zero point. The passive system does not provide any adaptation or motion limits at the thigh support bars in closing direction. Nevertheless, a small mechanical lever fixed to the pelvis belt blocks the rotation of the thigh support bars in clockwise direction. This limitation helps the user to wear the device correctly, but it does not operate during the assistance. Finally, the third part of the device is a pelvis belt that is connected by a free hinge joint to the leg structure on both sides. This free joint does not supply assistance but allows free rotation between the two connected parts. The pelvis belt has to be worn by the user in a comfortable way but avoiding any sliding during human motion. The pelvis belt consists of both rigid plates and soft lining pads. Figure 4.1.2 highlights the contact points of exoskeleton pads with the human body. The geometry of trunk and thigh pads have changed between the five prototypes in order to better interface with the human body parts. In particular, the chest pad has a butterfly design and is furnished with soft lining to prevent the rigid contact between the human trunk and the plate. Due to the presence of muscular tissues at the thighs level, the leg pads are lacking any linings. In order to limit the restriction of physiological free motions in the 3D space when wearing the device, the exoskeleton is provided of free degrees of freedom, integrated into the trunk and thigh pads. Figure 4.1.2 shows the allowed motions of chest and thigh pads respect to a human coordinate system. The chest pad allows the rotation of the butterfly support in the frontal plane, the inclination of the rigid support for bars connection and the independent rotation of the two rigid bars connectors in the sagittal plane. The combination of these DOFs allows the subject to rotate and bend the trunk on lateral sides.

The thigh supports reveal a more rigid structure, without the integration of any mechanical DOFs to allow the hip abduction/adduction and the hip rotation. Nevertheless, each thigh pad presents a free rotation in the sagittal plane in order to contribute to the user's anthropometry adjustment. Finally, all pads can small translations along the vertical direction to prevent rigid and uncomfortable restrictions to the user.

The Laevo exoskeleton offers four different sizes, according to the user's height, in order to provide modularity and adaptation to several anthropometric measures.

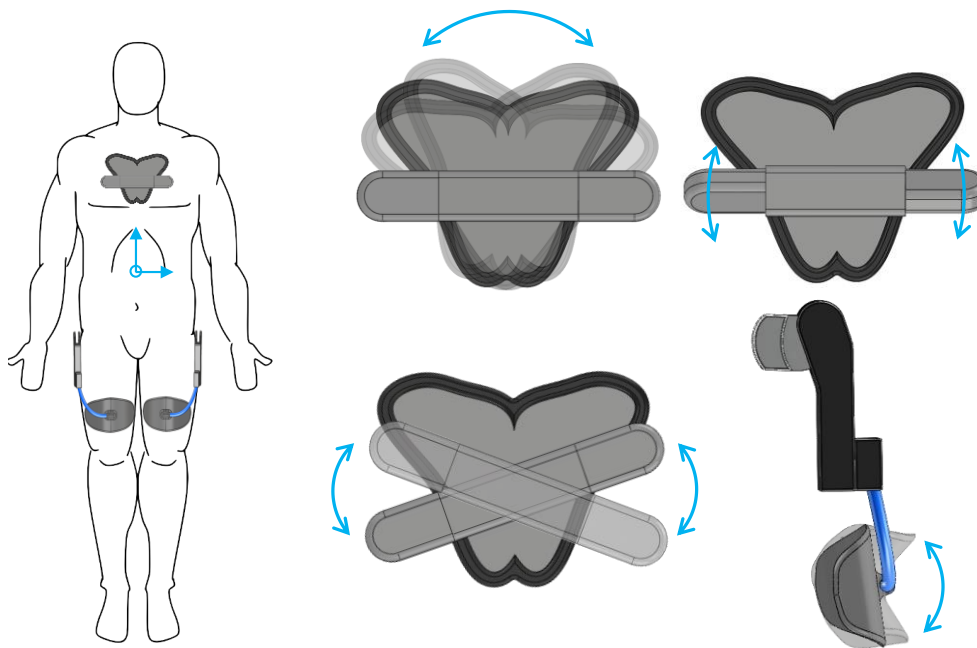


Figure 4.1.2: Laevo exoskeleton structure. Description of the several components of the device and the free degrees of freedom integrated with the device to avoid any restrictions to physiological human body motion.

The design of the exoskeleton allows modifying the size of the whole structure with few easy passages. The pelvis belt width size can be adjusted using Velcro straps. There is no regulation for the leg structure, while for the trunk support four different solutions of the bars are presented. For this reason, the component that defines the size is the trunk structure, in particular the variation of the length of trunk bars. In that way, the same structure can be used by several subjects with the only change of the trunk support bars. The current solution does not differentiate the system based on human gender, despite the direct interface with the human chest. Only the previous study by Bosch and colleagues [85] has tested the device both with males and females, but without evaluating any comparison between the two groups. Figure 4.1.3 displays the four sizes and the corresponding data of human height.



Size	Body length	Ring color
Small	Less than 1.72 m	Yellow
Medium	Between 1.72 and 1.80 m	Pink
Large	Between 1.80 and 1.88 m	Blue
Extra Large	1.88 and longer	Green

Figure 4.1.3: Laevo different proposed sizes and corresponding human body length.

4.1.2 Exoskeleton assistance

Each smart joint connecting the trunk-support and the thigh-support parts contributes to supply assistance to the user during the extension phase of trunk bending and during holding trunk-flexed posture in static tasks. It is coaxial with the free hinge joint connecting the thigh supports to the pelvis belt and has to be positioned in correspondence to the human hip joint when worn by the user. It appears as a light and small black box that contains and protects the passive assistant mechanism. Figure 4.1.4 depicts the detailed of the closed (A) and opened (B) black box and the separation of the different mechanical components of the Laevo smart joint (C).

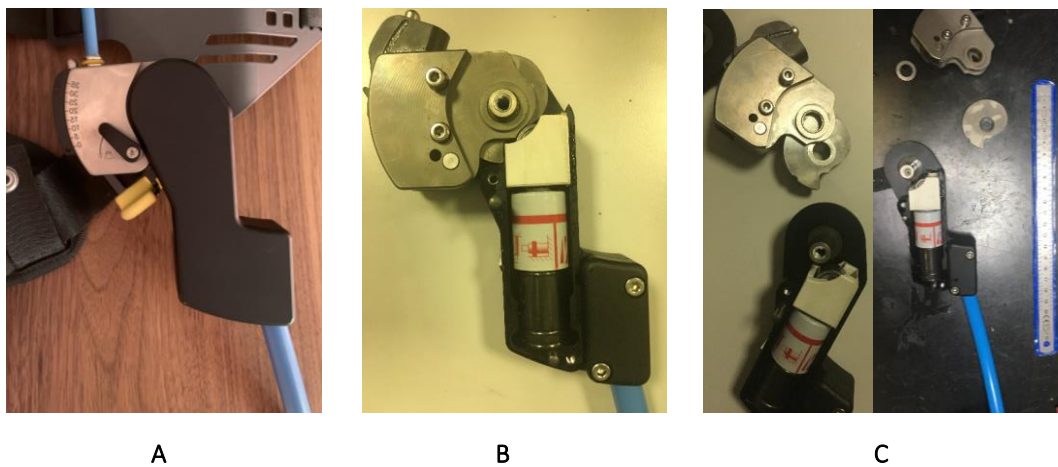


Figure 4.1.4: Smart joint of the Laevo with covers (A), without covers and visible cam-spring mechanism (B), with separated mechanical components (C).

The assistance joint is composed of a cam-spring mechanism, in particular a gas spring. The cam-spring mechanism allows the development and transmission of the assistance torque. The solution has been adopted in order to combine the rotary and linear movements. As depicted in Figure 4.1.5, starting from the static standing posture, the human torso flexion applies to the trunk support (red bar) a force perpendicular with respect to the chest pad that is transmitted, through the rigid bars, to the hinge joint (blue element). The hinge joint allows the rotation of the bars. The human flexion force develops a rotation of the cam mechanism around the hinge joint. Thanks to the continuous contact between the two mechanical elements, the cam and the spring, the rotation motion of the cam is converted in translational motion of the gas spring piston. Indeed, during the motion, the cam presses the piston of the gas spring. An analog behavior can be implemented with a standing trunk posture and flexion of human legs, due to the direct connection with the thigh support (yellow bar). On the contrary, during the extension phase, the piston of the gas spring extends supplying a support torque to the user. The piston presses on the cam and the translational motion is converted into rotational one. The torque assistance is transmitted to the human body as perpendicular pushing forces through thigh and chest pads. Due to the geometry of the

mechanism, the relation between assisting torque and trunk angle is unique. The torque-angle relation has been experimentally assessed and it is reported in Figure 4.1.5. The experimental measure has been conducted with a dynamometer for the estimation of interacting force, both during pull down and push up phases. The rotation starts from 0° flexion, that is considered as the reference standing position, and reaches the 60° flexion, that is considered as a common flexion posture assumed by the human trunk. The dynamometer is fixed to the exoskeleton chest pad and is maintained perpendicular to the segment during the movement. Angles are measured with a rigid goniometer. Considering the length of the support bars, the torque at hinge level is calculated. The obtained torque curve shows a peak value of assistance at 40° of flexion/extension, for a maximum value of 32 Nm during the pull-down phase and 18 Nm during the push-up phase.

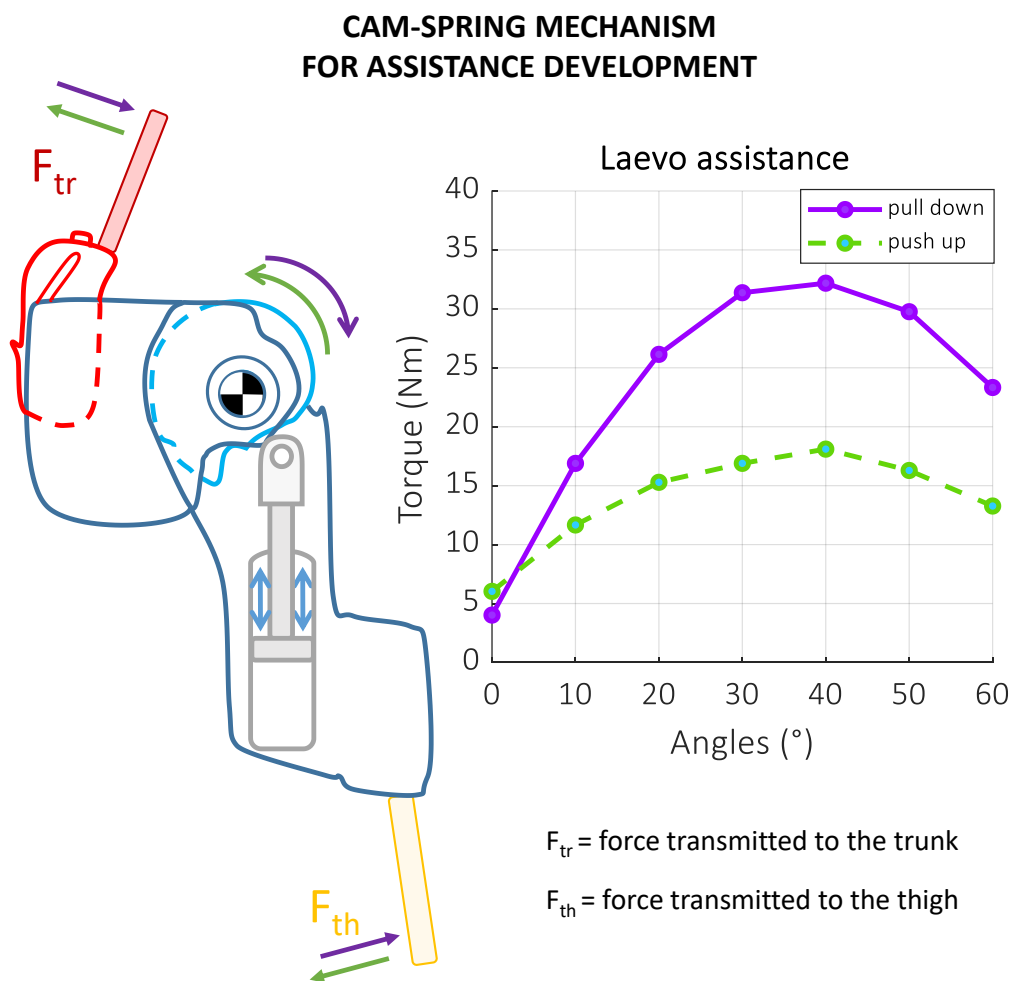


Figure 4.1.5: Graphical description of the cam-spring mechanism inside the smart joint and the torque-angle relation of the implemented passive assistance.

The result is similar to ones calculated by Koopman and colleagues in a previous experimental study, despite the different Laevo prototype adopted [87]. During the test, the assistance torque has been measured through a force transducer placed on the chest pad. A cluster of markers on the chest pad and three LEDs on

the smart joint allows evaluating the orientation of the pad and the distance vector. The previous Laevo has the possibility to regulate the assistance on two levels (high and low). The curve in Figure 4.1.5 is similar to the ones obtained with the high support level in trend, range of values and maximum registered torque. Moreover, also in that case, a substantial difference in support has been found between the push-up and pull-down phase. Indeed, the two curves identify non-symmetry characteristics of the assistance. The reason is assumed to be non-reversible phenomena, as the friction within the system. In addition to the non-symmetry, both push and pull phases highlight non-linearity of the torque-angle relation, that is due to the cam profile. This characteristic seems to be contradictory respect to the proportional increase of waist torque related to the trunk flexion. A possible reason can be identified in the flexion-relaxation phenomenon. In full flexion position (around 90°), indeed, the Erector Spinae muscles become inactive because fully stretched and the flexion torque is supported by spinal ligaments. For this reason, a decreasing support could be supplied by the device in case of trunk flexion $>60^\circ$. Moreover, a trunk flexion between 30° - 60° reveals to be the most common position assumed both in static and dynamic lifting motions. For this reason, an assistance peak is supplied in that range. The estimation of exoskeleton contribution is fundamental to quantify the percentage of human torques reduction. One fundamental aspect of the Laevo exoskeleton is the pre-load phase of the gas spring. Indeed, during the flexion phase, the human body loads the spring mechanism, with an increase of back and core muscular activity compared to the physiological effort without the exoskeleton. The need to pre-load the spring is a peculiarity of passive systems and it might create discomfort to the user.

4.1.3 Exoskeleton wearability

As previously discussed, the Laevo exoskeleton can be worn by different users, both male and female. The Laevo used in the current project is a small size. For this reason, it can be worn by subjects shorter than 1.72 m. In order to qualitatively evaluate the wearability of the structure and to stress any differences due to human anthropometry, four different subjects are selected to wear the Laevo. Figure 4.1.6 shows the front view of the four subjects wearing the exoskeleton. Two females (A-B) and two males (C-D) are considered.

Both the female's heights are consistent with the indication given by the Laevo specifications for the small size (total body height < 1.72 m), while one male is 1.72 m and the other is 1.75 m, over the suggested limit.

The belt regulations satisfy the needed adaptation of the different pelvis circumference and can be worn by all the subjects. Considering the thigh support, in all cases, the thigh pad correctly leans in correspondence of the middle of the thigh. The different circumference of the thigh might influence the correct positioning of the thigh pad, which does not allow any regulation in dimensions. Indeed, if considering the first female (A) and the second male (D), both subjects present a larger distance between feet. The adaptation of the feet position may be

due to a wrong regulation of the pelvis belt and to the difficulty of adaptation to the thigh pad dimensions. The integration with adjustable Velcro straps may improve the correct positioning and fixing of the thigh pad around the thigh circumference.



Figure 4.1.6: Front view of four subjects with different height, anthropometry and gender wearing passive Laevo exoskeleton.

The crucial difference due to height can be highlighted if considering the chest pad and the trunk support bars. Indeed, the females correctly positioned the butterfly pad in correspondence to the chest, while, despite the possibility to regulate the shoulder suspenders, the males cannot arrange the pad in the correct position. The position of chest pad results to be too low due to the small length of the trunk bars for the male over the admitted height, but also for the male with boundary height.

Figure 4.1.7 depicts subject B wearing the exoskeleton: front (B), back (D) and lateral (A-C) views are reported. The subject is selected for laboratory experimental tests. The device will be tested during lifting strategies in terms of wearability, user's acceptance, perceived discomfort and pressure, and human joint kinematics.



Figure 4.1.7: One female subject with a height < 1.72 m wearing the passive Laevo exoskeleton from lateral view (A-C), front view (B) and behind view (D).

4.2. Experimental test

4.2.1 Principal aim

Experimental laboratory tests are conducted with the principal aim to test the effectiveness of the device, to stress advantages and highlight, if existing, any possible drawbacks. As preliminary study, one female subject performs lifting tasks with different strategies, with and without the Laevo exoskeleton. For the analysis of the device performance, both subjective and objective variables are considered. The user's acceptance, perceived discomfort and perceived effort are evaluated as subjective variables, while the user's kinematics and interface pressure are measured as objective parameters. Borg's scale [107], the human body part discomfort scale and perceived pressure scale [108] are used for the subjective assessment. These scales, fully described in Appendix C, have been used in previous experimental tests with wearable devices [52, 58, 85, 88, 102]. The user's kinematics is reconstructed from markers trajectories registered with an optoelectronic system. The interface pressures are estimated with a customer pressure sensors system. Final summary considerations are compared with past experimental studies and could be the starting point for the development and analysis of the new prototype.

4.2.2 Material & Methods

Subject. One young female participant (55 kg weight, 1.65 m height, 26 years old) performs the experimental test. She declares to be not affected by any orthopedic diseases. The protocol and the aim of the experiment have been extensively explained to the subject. Some previous pre-tests have been conducted to allow the subject to familiarize with the exoskeleton, to understand the mechanism of assistance and to try the several motions.

Instrumentation. The instrumentation adopted in the study can be categorized into two groups, based on the main function: tools to simulate an industrial task in the lab, and instruments for the data acquisition. In the current analysis, the human motion is supposed symmetric between the left and right side and is primary performed in the sagittal plane, as suggested by occupational and ergonomic guidelines [44]. For this reason, only the right side of the human body is registered during motion. Concerning the first group, they can be summed up as the following list:

- One table;
- One box;
- Several small instruments with different weight (from 0.5 to 3 kg);
- Laevo exoskeleton version 2.5.

For the data acquisition, the instrumentations can be resumed:

- One self-contained and pre-calibrated Optitrack Bar V120 Trio for 3D motion capture (120Hz);
- One external camera for videos/pictures recording;
- 26 passive markers (14 mm diameter);
- 3 customized pressure sensors;
- USB-6341 data acquisition system (DAQ) from National Instruments to acquire pressure sensors data;
- Personal Laptop for data acquisition and for data elaboration;

The Optitrack bar V120 Trio is an optoelectronic motion capture system that is composed of three infrared cameras mounted on a bar. The system self-calibrates before each acquisition and defines a reference frame to which marker positions are referred. Motive software, proprietary of Optitrack, is used for data acquisition of markers 3D position. Figure 4.2.1 depicts a schematization of the setting to analyze box lifting. To define a global reference system XYZ convenient for the analysis, three markers are positioned on the corners of the table (G1G2G3) and their positions are registered during the static calibration acquisition. The x-axis has the direction of to the vector connecting point G1 and point G2, while the vector connecting point G3 and point G2 is considered as supporting axis. The z-axis is obtained from the cross product between x-axis and the support axis, and, as a

consequence, the y-axis is calculated from the cross product between z-axis and x-axis. Markers' position, as a function of time, are referred to the global coordinate system XYZ by means of a transformation matrix during the post-processing elaboration.

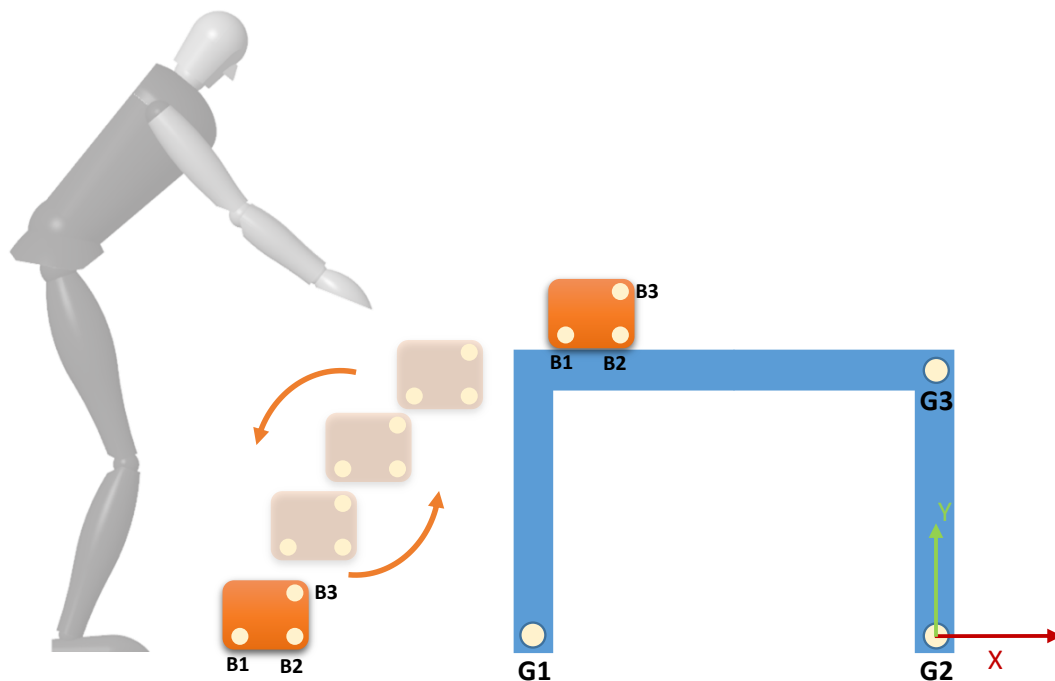


Figure 4.2.1: Scheme of the setting for the simulation of industrial tasks dealing with the lifting and the manipulating of objects. Definition of the global coordinate system fixed to the table ($G_1G_2G_3$) and markers position on the box ($B_1B_2B_3$).

A total of 26 markers are positioned on the right side of the human body, exoskeleton parts, table and box in order to register the movement. Considering the human body, the markers are positioned on landmarks of interest with the attempt to approximate human joints position and corresponding human body segments. Three clusters of markers are added to the trunk and lower limbs (thigh and shank) to compensate possible markers obstruction during the experiment. A set of three markers is positioned on the lifted box, as represented in Figure 4.2.1, with the attempt to track box translation during motion. When wearing the exoskeleton, three markers were positioned on the chest pad, smart joint and thigh pad respectively. In this case, the marker on the human anterior superior iliac spine cannot be positioned. A rigid relation is supposed between the marker and the cluster of markers on the thigh segment, allowing the reconstruction of the hip marker position. Figure 4.2.2 depicts the participant in a static reference standing posture in the sagittal plane without (Figure 4.2.2 A) and with (Figure 4.2.2 B) the exoskeleton. In that figure all the human and exoskeleton markers are visible.

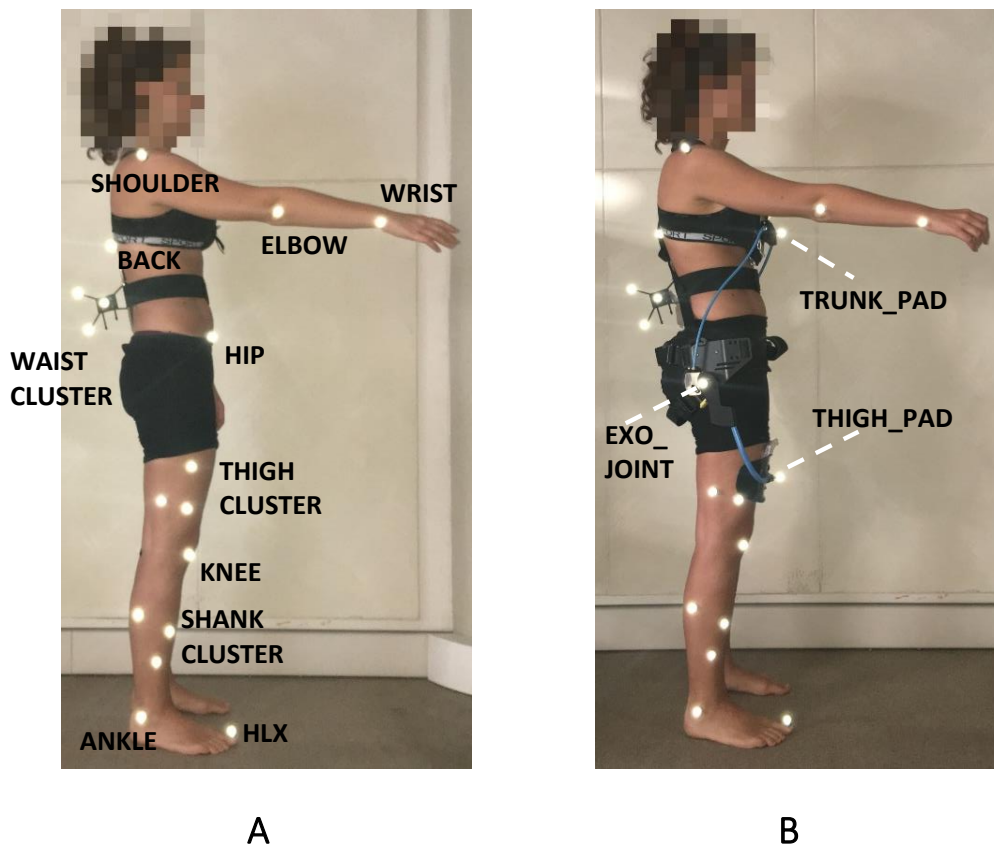


Figure 4.2.2: Static reference posture of the female subject with markers on human landmarks for the reconstruction of motion in the post-processing, without (A) and with (B) the exoskeleton.

Table 4.2.1 sums up all the markers indicating the label, the body of application (table, box, human body, exoskeleton) and the full description of each ones. Markers are grouped based on the specific body where they are positioned (table, box, exoskeleton, human body).

For the monitoring of pressures exchanged between the human body and the exoskeleton at the contact point, a customized system has been implemented. It is made of three Flexiforce A502 sensors (50*50 mm² covering area) each of which has a customized conditioning box. Each box contains a FlexiForce Quickstart Board for the detection of sensor pressure and the conditioning of the signal with an analogical circuit, and a 9V battery for the powering of the system. The output of the system is a voltage signal in the range of 0.5-5 V. Figure 4.2.3 depicts the three force sensors (A), the three conditioning boxes (B) and the whole data acquisition system (C). The output voltage from each sensor is acquired USB-634 data acquisition system from National Instruments, connected to a personal laptop by means of a USB connection. Data are collected with *Labview* software installed on the personal Laptop. Figure 4.2.4 and Figure 4.2.5 present the developed Labview code for the acquisition of pressure data from the three customized pressure sensors.

Table 4.2.1: Labelling and description of the markers set positioned on the human body, exoskeleton and laboratory tools.

MARKER SET DEFINITION AND DESCRIPTION		
Label	Body	Description
G1	GLOBAL COORDINATE SYSTEM	Point 1 of the global coordinate system
G2		Point 2¢re of the global coordinate system
G3		Point 3 of the global coordinate system
BOX1	EXTERNAL LOAD	Point 1 of the external load lifted by the subject and positioned into a corner
BOX2		Point 2 of the external load lifted by the subject and positioned into a corner
BOX3		Point 3 of the external load lifted by the subject and positioned into a corner
THIGH_PAD	EXOSKELETON	The point that identifies the centre position of exoskeleton pad in contact with human thigh
TRUNK_PAD		The point that identifies the centre position of exoskeleton pad in contact with human trunk
EXO_JOINT		The point that identifies the centre position of exoskeleton assistance hinge joint
HLX	HUMAN	Marker positioned on hallux of the human foot
ANKLE		Marker positioned on human lateral elbow malleolus; it approximates the ankle position
SHANK1		Cluster of three markers positioned oh the human shank. The main function is to identify a reference system for knee position reconstruction in case of obstruction
SHANK2		
SHANK3		
KNEE		Marker positioned on human lateral knee epicondyle; it approximates the knee position
THIGH1		Cluster of 3 markers positioned oh the human thigh. The main aim is to identify a reference system for hip reconstruction in case of obstruction
THIGH2		
THIGH3		
HIP		Marker positioned on human anterior superior iliac spine; it approximates the hip position
WAIST1		Cluster of three markers positioned oh the human back. The main function is to identify a reference system for back position reconstruction in case of obstruction
WAIST2		
WAIST3		
BACK		Marker on human trunk (T12 vertebra)
SHOULDER		Marker positioned on human acromion; it approximates the shoulder position
ELBOW		Marker positioned on human lateral elbow epicondyle; it approximates the elbow position
WRIST		Marker positioned on human lateral wrist epicondyle; it approximates the wrist position

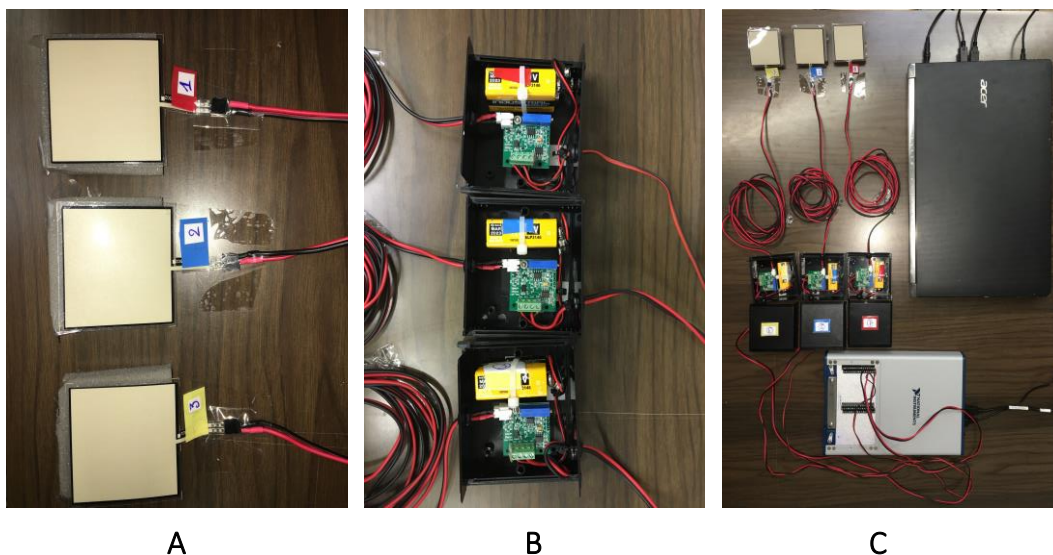


Figure 4.2.3: Picture representing the three force sensors Flexiforce A502 (A), the three customized conditioning boxes (B), DAQ system and laptop (C).

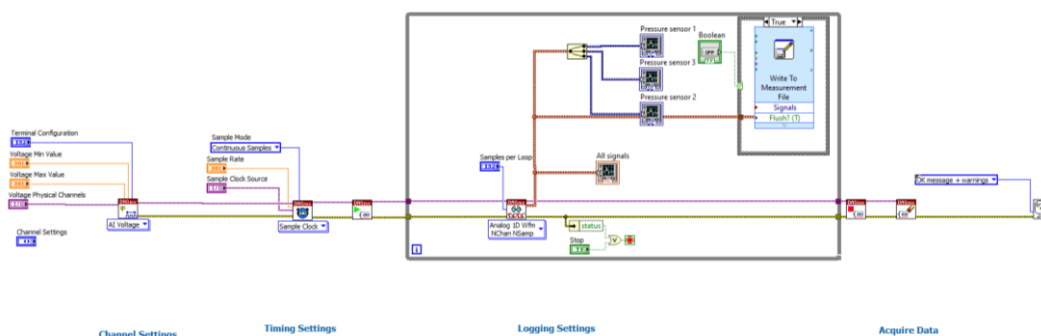


Figure 4.2.4: Labview Block diagram (A) for the data acquisition from the customized pressure sensors.

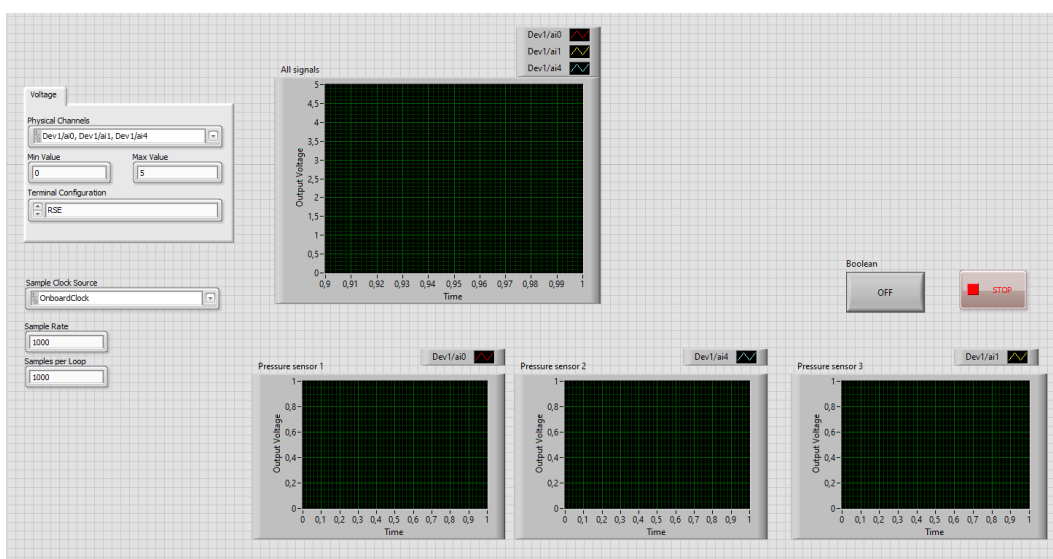


Figure 4.2.5: Labview Front panel for the data acquisition from the customized pressure sensors.

Thanks to the presence of a potentiometer on the board (15 turns, 500 k Ω) sensor' gain and output can be adjusted. The board outputs 0.5 V in case of no load, while to define the output range of interest, the sensors was calibrated with 4 known forces, as recommended by the developer's instructions. Figure 4.2.6 depicts the calibration curves obtained during the procedure from the three pressure sensors. The four identified weights are positioned at the center of the pressure sensors two times, depicting ascending and descending phases of the process.

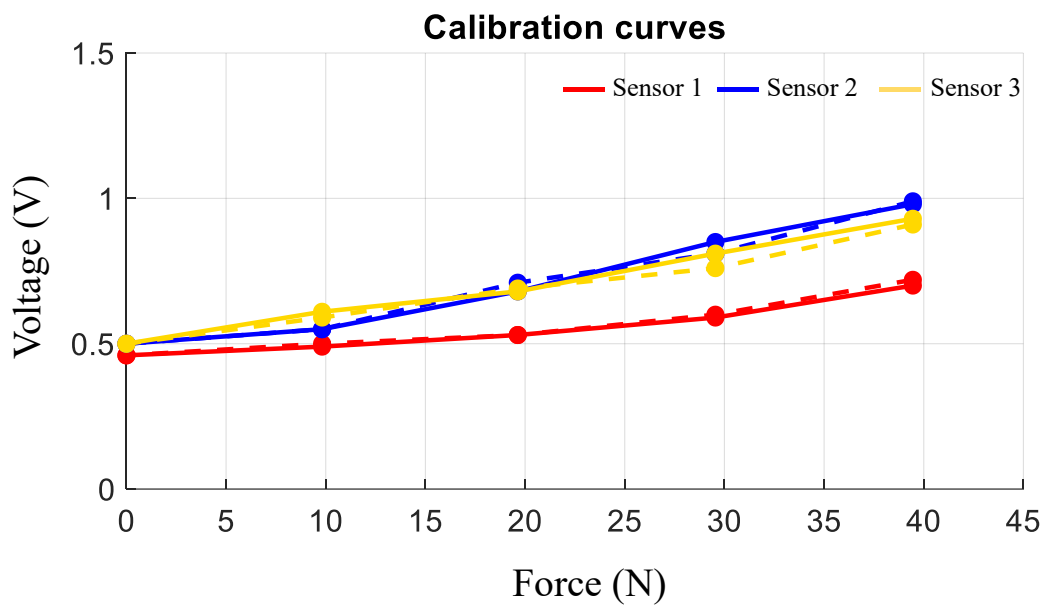


Figure 4.2.6: Curve results from the calibration procedure of the three pressure sensors. Solid line refers to ascending phase of weight positioning (from lower to higher weight), while the dashed line refers to the descending phase (from higher to lower weight).

Procedure and motion tasks. Two different tasks are performed by the subject in order to simulate the common industrial occupational task.

In the first task, named "holding stoop", the subject holds the trunk flexed in a static position while manipulating several objects leaned on the table. The legs must be maintained in an extended posture. The subject is asked to maintain the trunk flexed until the perception of effort at the back level. The inclination of the trunk respect to the vertical line is measured at the starting of registration and is around 40°- 45°. The range of flexion is selected by the subject as the most suitable position for the task performance.

In the second task, named "dynamic task" the subject starts from a standing posture, performs a descending movement to reach a box positioned on the floor at ankle height level, grasps the box, performs an ascending motion to place the box on the table then takes the box from the table, descends to return the box on the floor and returns to the starting standing posture. Four different lifting strategies are simulated in this dynamic task: stoop lifting (flexed trunk, extended legs), semisquat lifting (both flexed trunk and flexed legs), squat lifting (extended trunk and flexed leg) and free lifting (self-selected lifting strategy). Five sequential

repetitions are performed for each task and each lifting strategy. The whole test sequence is repeated by the subject without and with the device, which represents the independent variable. In this phase, no weight has been added to the box.

The several repetitions have been realized with the feet at the same distance to the table. This distance has been defined with the attempt to pose the box on the table in standing posture and with extended upper limbs. When wearing the exoskeleton, the pressure sensors have been positioned in the central position of the pad area. Due to the small size, the sensor cannot cover the whole contact area between the exoskeleton pad and the human body. For this reason, it is assumed the constant pressure distribution on the whole pad area. Moreover, due to the symmetrical movement of the lower limbs, it is considered the signal registered from the right thigh. The pressure on the left thigh is considered in case of any problems and/or error on the right thigh. For the synchronization of data acquisition between the optoelectronic system and the pressure sensors when wearing the exoskeleton, external input is implemented by the user before starting the motion. When in the upright posture, the user places the right hand on the trunk pad with a smack. In this way, the pressure sensors register a peak tension value, while the marker on the chest pad is occluded. All the tests have been performed during the same day, with 5 minutes rest among the performed lifting strategies. The registration data are collected in different data file based on the task and the selected strategy. The subjective evaluation has been performed at the end of each task. All the tasks have been performed without the device, then with the device, in a random order.

Outcome variables and Data Analysis. Both objective and subjective variables are considered for the analysis of motion and exoskeleton performance.

Joints trajectory, joints angular range of motion (ROM) and interface pressures are considered as objective values. Joints kinematics is reconstructed from the markers and compared between the case without and with the exoskeleton. Joints' angular ROM is calculated as the difference between the maximum and minimum angle registered during motion. As for the joints' trajectory, in this case, the comparison is made between the two independent conditions (without and with the exoskeleton). Finally, the pressure exerted on the contact points is calculated when wearing the device and compared among the several motions. The exerted pressure represents the interaction between human body and the exoskeleton device. For this reason, it is the result from the pushing force from the human body and the assistance torque provided by the exoskeleton. The torque transmitted at the chest pad results from the whole exoskeleton assistance, while the torque at each thigh pad is the half of the exoskeleton support. Nevertheless, the distance from the assistance joint and the contact chest pad is two times the distance to the contact thigh pad. A customized *Matlab* code is implemented for the data analysis.

For the subjective evaluation, Borg's scale [107], the human body part discomfort scale and perceived pressure scale [108] are used. After each performed motion task, the subject is interviewed about the general opinion of perceived effort and difficulty. The subject has to explain what she has felt during the performance

and indicate for each selected human body area the perceived discomfort, the level of effort and perceived muscular work, and the perceived local pressure at the contact points in case of wearing the exoskeleton. In addition to the full verbal description, the user has to assign a specific value to human body region based on the corresponding scale and the matching explanation of numerical value. As already mentioned, the full description of these scales is reported in Appendix C.

4.2.3 Results and discussion

Joints kinematics. The trajectory of reference joints of both the human upper body and lower body is depicted and compared between the two with/without exoskeleton conditions and between the several performed kinematic motions. Due to the absence of a metronome to define the velocity of the motion, some small differences can be pointed out considering the kinematics respect to time performance. Position data are referred to the global coordinate system. Figure 4.2.7 shows the trajectories of upper limb joints: shoulder, elbow and wrist joints. The graphs are divided based on the performed motion task and each graph compares the case without (black line) and with (green line) the exoskeleton. All five cyclic repetitions are reproduced in the graphs. No fundamental variation of upper limb joints positions can be highlighted. Indeed, in all kinematic conditions, the green and black curves well overlap. Moreover, no differences can be stressed comparing the different lifting motion strategies (graphs B-C-D-E).

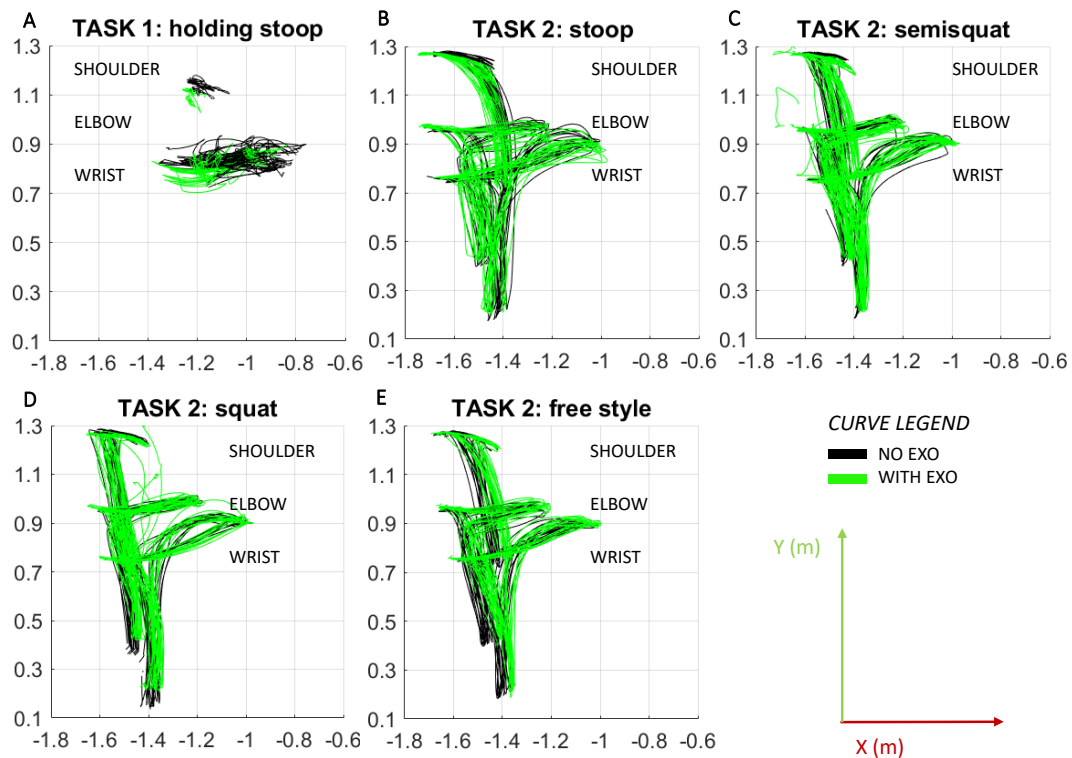


Figure 4.2.7: Upper limbs joints trajectory (waist, hip, knee, ankle) without (black line) and with (green line) exoskeleton, in all performed motions: static holding stoop (A), stoop lifting (B), semisquat lifting (C), squat lifting (D), free lifting (E).

Figure 4.2.8 depicts the joints trajectories of the human trunk and lower limbs: the waist, hip, knee and ankle reference points. As in the previous figure, the graphs are divided based on motion tasks and curves from the two exoskeleton conditions (without is the black line and with is the green line) are compared on the same graph. As for the upper limb joints, the presence of exoskeleton seems to not affect the trajectories. Black and green lines well overlap in all motion cases.

Some small differences have been registered at the hip joint during holding stoop (A) and stoop lifting (B). From the figure, it is possible to highlight the different range of human joints movement considering the same kinematic motion. In addition, it is possible to compare the range of movement of the same joint but in different motion conditions. Waist and hip joints reveal a greater range of movement compared to knee and ankle joints in all dynamic tasks (graphs B-C-D-E). The knee joint registers a greater displacement in semisquat, squat and free lifting strategies. The ankle joint, as expected, presents the same small displacement in all the performed tasks. Compared to the stoop motion, the other lifting strategies involve greater displacement, especially at the hip and knee joints.

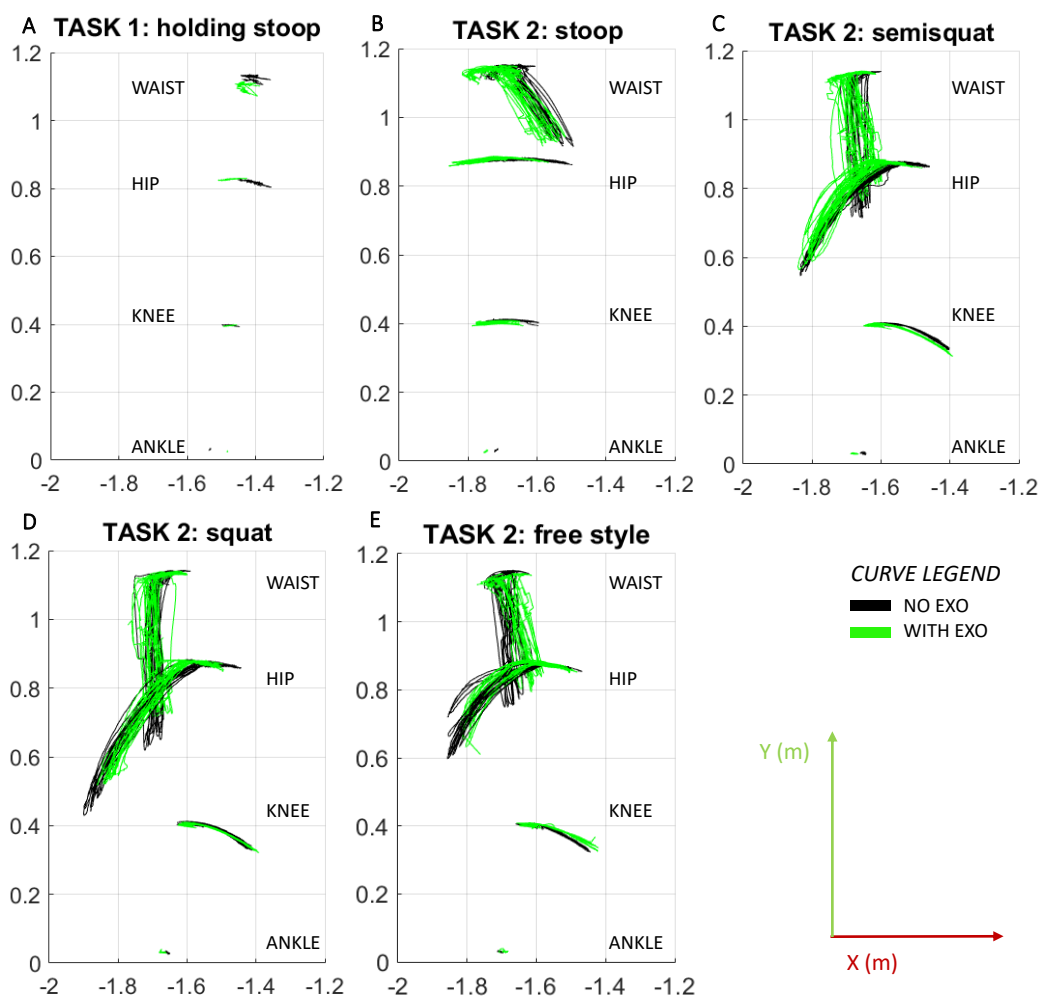


Figure 4.2.8: Lower limbs joints trajectory (waist, hip, knee, ankle) without (black line) and with (green line) exoskeleton, in all performed motions: static holding stoop (A), stoop lifting (B), semisquat lifting (C), squat lifting (D), free lifting (E).

Joints ROM. The range of motion (ROM) is defined as the larger variation of angular displacement and is calculated as the difference between maximum and minimum values. Figure 4.2.9 depicts the histogram comparison of ROMs in case of no wearing and wearing the device, in all the kinematic conditions. From the reported graphs is possible to stress the different angular variations.

The upper body limbs highlight large ROMs values, especially in lifting tasks, but with small differences comparing the exoskeleton conditions (green and black columns). The maximum value for the shoulder joint is registered during stoop lifting task (115° without the exoskeleton, 120° with the exoskeleton), while the elbow joint shows comparable ROMs among lifting strategies (30° without the exoskeleton, 30-40° with the exoskeleton). In squat motion, an increase of elbow ROM if wearing the device is stressed (from 20° to 40°), but no differences can be stressed in other motions.

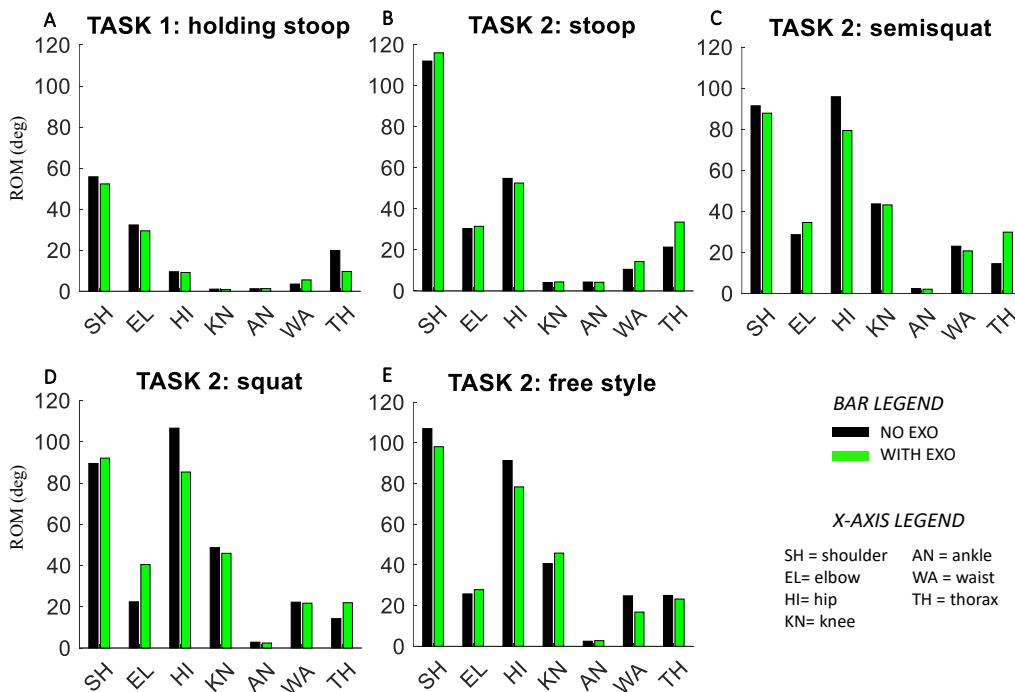


Figure 4.2.9: Joints range of motion without (black bar) and with (green bar) exoskeleton, in all performed motions: static holding stoop (A), stoop lifting (B), semisquat lifting (C), squat lifting (D), free lifting (E).

Considering the lower body, the holding stoop task registers small angular displacement at the lower limbs (< 10°). In dynamic stoop lifting, the greater ROM is registered at the hip joint, but with negligible differences between no exoskeleton and with the exoskeleton (50° ROM). In semisquat and squat motion, the contribution of the legs in performing kinematic motions is stressed by the higher ROMs registered at the knee joints (40°) instead of the value registered in stoop (<10°). The ankle joint depicts small value in all motion conditions (<10°), without any difference due to the presence of the device.

Finally, the waist ROMs indicates the angular displacement between the pelvis and lower trunk, and the thorax, depicting the angular displacement between the lower and upper trunk. In the holding posture the variation of angular displacement resulted small. This result shows a small oscillation of the human trunk during the maintenance of posture, but the thorax oscillation is less when wearing the device ($<10^\circ$). This fact can be interpreted in a more stability in posture due to the exoskeleton assistance. Values around 20° ROM are depicted at the waist joint in all lifting conditions.

Interface pressure. Pressure exchanged at interfaces between the human body and the exoskeleton pad areas is monitored during all the performed movements. Figure 4.2.10 depicts the pressure distribution during the performed movements. The red and blue lines depict the pressure on the trunk pad and on the right thigh pad, respectively.

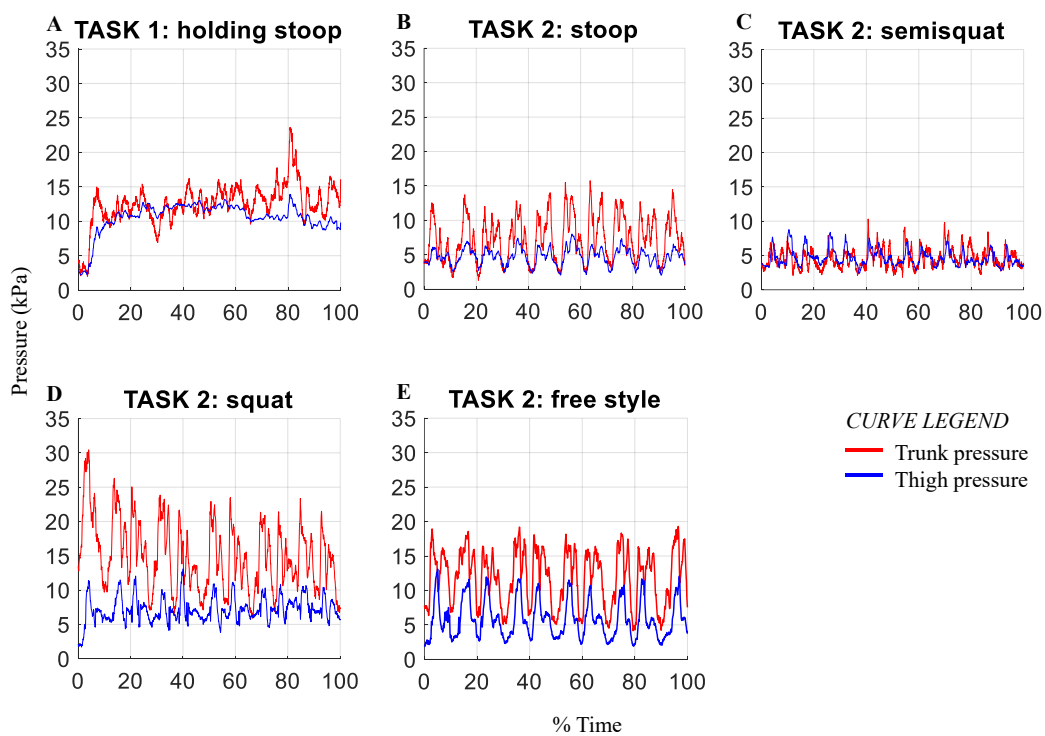


Figure 4.2.10: Pressure distribution on the contact area (trunk, right thigh) in all performed motions: static holding stoop (A), stoop lifting (B), semisquat lifting (C), squat lifting (D), free lifting (E).

On the x-coordinate the percentage with respect to the total lifting cycle is reported, while pressures are expressed in kPa. In each graph, all the five repetitions of each movement are shown. A cyclic trend can be highlighted from the curves. During the first task, the static holding posture involves pressures in the range of 10-20 kPa, with greater distribution on the trunk pad compared to the thigh pad (A). The small oscillation of the trunk can be highlighted by the several oscillations in the trunk pressure curve. The thigh pressure resulted more static and fixed (blue

line). In the dynamic tasks of lifting motions, several pressure peaks can be observed both during the flexion phase and the extension phase. In the stoop (B), the maximum trunk pressure results in the range of 10-15 kPa, that is higher if compared with the maximum thigh pressure (range of 5-10 kPa). The semisquat movement (C) reveals the lowest amount of pressures among the several strategies, with pressure peaks in the range of 5-10 kPa for both trunk and thigh pressures. On the contrary, the squat movement (D) reveals the highest exchanged pressures, with peaks up to 30 kPa for the trunk contact. In the free style motion (E), the trunk pressure registers greater values compared to the thigh pressure, with peaks in the range of 15-20 kPa (10-12 kPa for the thigh contact). In all the performed tasks, compared to the ergonomic guidelines depicted in [109], the pressures can be considered acceptable and lower than critical thresholds of pain tolerance (43 kPa). Moreover, compared to the recent experimental test on the powered ROBOMATE exoskeleton [98], the maximum pressure peaks reveal to be particularly lower both for trunk and thigh contacts. Indeed, in the cited study, the pressure applied to the trunk and thighs was on average 91.6 kPa/93.6 kPa and 69.1kPa/81.2 kPa for the lifting external loads of 7.5kg and 15 kg loads, respectively. Despite the different device structure, the different amount of exoskeleton assistance, the presence of an external lifted load and the different motion kinematics (only free style lifting), the current interface pressures can be considered safer and more acceptable, with lower risk of user's discomfort and pain. Nevertheless, the small dimensions of the current force sensors required the assumption of constant pressure distribution, that is not realistic due to the nonuniform surface stiffness distribution of the interacting bodies. For this reason, deeper investigations might be conducted to validate the measured pressures.

Subjective evaluations. Results can be compared with previous literature researches. Literature studies highlighted the suitability of the Laevo in stoop lifting and holding stoop posture but stressed the perceived difficulty and discomfort in case of semisquat and squat motions. In the current study, subjective assessment of the wearable device is presented both in numerical and graphical evaluations. In Table 4.2.2 the score assigned by the subject for each kinematic (holding stoop, stoop, semisquat, squat, freestyle) and device (without and with) condition is reported. Considering the perceived muscular efforts, the human body areas investigated are the back and the lower limbs (thighs). The modified Borg scale has a range value from 0 to 10. Based on the scores, the participant claims higher efforts at the thighs compared to the back area in all movements. Comparing the motions based on the device (without or with the exoskeleton), small differences can be highlighted at the back area, in particular during the holding stoop task (score 2 without the exoskeleton, score 1 with the exoskeleton) with positive effect of the device, and during squat lifting (score 2 without the exoskeleton, score 3 with the exoskeleton), with negative effects of the device. At the thighs level, during both holding and lifting stoop the subject does not perceive differences due to the exoskeleton (score 3 in all conditions), while discrete negative effects are registered

during semisquat (score 2 without the exoskeleton, score 4 with the exoskeleton) and small negative effects during the freestyle (score 1 without the exoskeleton, score 2 with the exoskeleton) motions. Small positive effects are registered during squat motion (score 4 without the exoskeleton, score 3 with the exoskeleton). The freestyle strategy reveals to be the best motion, with small values (0-1) of perceived efforts both at the back and thighs regions, with and without the exoskeleton. Nevertheless, in that case, the participant does not perceive the additional contribution of the exoskeleton. The worst situation is the squat lifting motion, due to the high value of perceived efforts both without and with the exoskeleton, both at human back and thighs areas.

Table 4.2.2: Subjective evaluation in different tasks of perceived efforts (Borg scale), perceived local discomfort, perceived local pressure, with and without the exo .

<i>Reproduced task</i>		Holding stoop		Stoop lifting		Semisquat lifting		Squat lifting		Free style	
Scale	Human area	No	With	No	With	No	With	No	With	No	With
Borg scale	Back	2	1	1	1	1	1	2	3	0	1
	Thighs	3	3	3	3	2	4	4	3	1	2
Perceived Local Discomfort	Chest	0	4	0	4	0	3	0	3	0	2
	Back	2	0/1	1	0/1	1	0	2	2	0	0
	Thighs	1	2	3	2	2	2	3	3	1	2
Perceived Local Pressure	Shoulder	/	0	/	0	/	0	/	0	/	0
	Chest	/	4	/	4	/	3	/	4	/	3
	Pelvis	/	0	/	0	/	0	/	2	/	0
	Thighs	/	2	/	2	/	3	/	3	/	2

The second subjective variable investigated is the perceived local discomfort and it is evaluated in three different regions: chest, lumbar back and thighs. The local discomfort differs to the perceived muscular efforts. Indeed, it represents the negative perception of fatigue felt by the user in specific body parts, while the perceived efforts indicate the perception of muscles contribution to the motion, without stressing negative or positive aspects. The adopted scale range starts from 0 (minimum score) score and arrives at 5 (maximum score) [108]. The participant claims high scores of discomforts at the chest in case of wearing the exoskeleton. Critical values are pointed out during both static and lifting stoop (4 scores), lower but even critical values during semisquat and squat motions (3 scores). The freestyle motion reveals the lowest registered discomfort score (2 scores). The lumbar back region seems less affected by discomfort, with small values in all kinematic conditions and a small benefit from the device due to the reduced score. A possible reason can be found in the absence of contact points at human back. The squat lifting is the motion with the highest registered lumbar back discomfort, both without and with the device (2 scores), while the freestyle depicts the absence of back discomfort (0 scores). Finally, if considering the thighs area, the squat motion highlights the highest value, both without and with the exoskeleton (3 scores),

followed by the semisquat strategy (2 scores). The stoop lifting registers a small discomfort reduction due to the device (from 3 score to 2 score), but in the holding stoop and the freestyle motion, the presence of exoskeleton seems to supply negative effects, with an increase of perceived discomfort.

The last investigated subjective variable is the perceived local pressure, which can be evaluated only in case of wearing the device, with a scale range from 0 (minimum score) score to 5 (maximum score). Four human body areas are considered: shoulder, chest, pelvis and thighs. These human body parts interface with the user. High pressures are perceived at the chest contact in all kinematic conditions. Smaller values are claimed at the thighs level, but with a critical score (3 scores) during semisquat and squat motion. On the contrary, both pelvis and shoulders contacts do not reveal perceived pressures.

In addition to the singular registered score, a mean value between kinematic conditions has been calculated for each subjective variable of interest. Figure 4.2.11 depicts through graphical representation the assigned score for the different body areas of investigation. The reference color maps are reported in Appendix C.

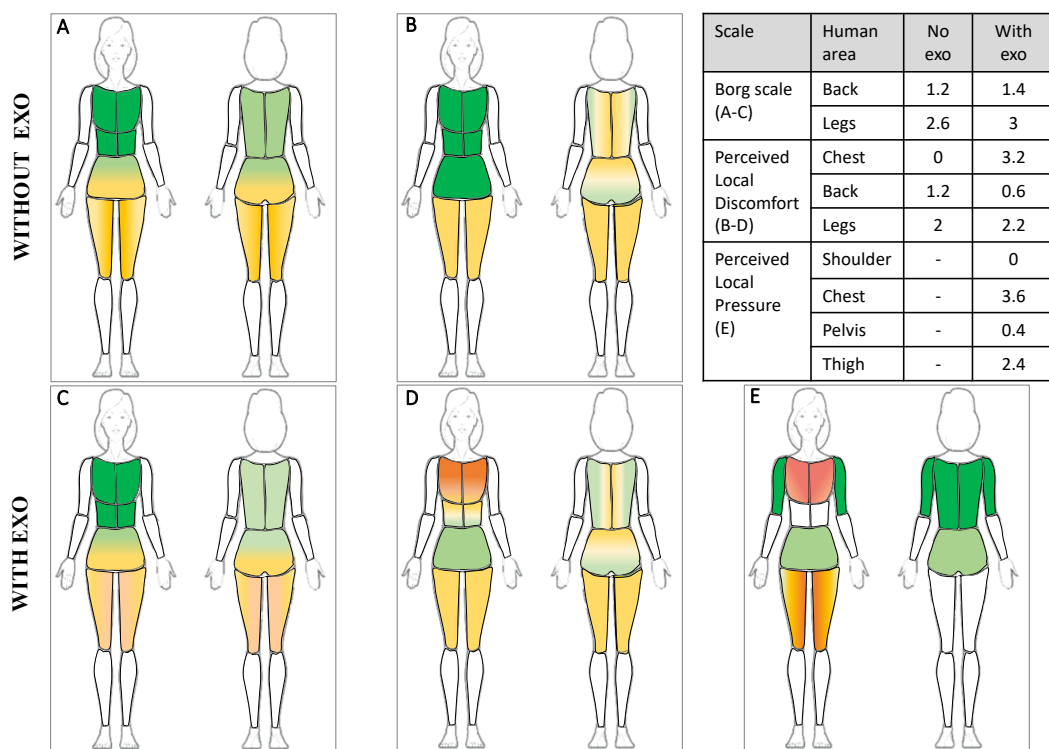


Figure 4.2.11: Mean value of the subjective evaluation among different motion tasks of perceived efforts (Borg scale (A) without exoskeleton, (C) with exoskeleton), perceived local discomfort ((B) without exoskeleton, (D) with exoskeleton) and perceived local pressure ((E) with exoskeleton). Both graphical and numerical values are stressed.

From these maps and the mean numerical values, it is possible to stress the effect of the exoskeleton on the human body in terms of perceived efforts (A-C), perceived local discomfort (B-D) and perceived local pressure. The presence of the device seems to not influence the perceived effort. Indeed, comparable scores have

been registered both at the human back and the human thighs. Comparing the different human body areas, the participant claims higher perceived efforts at legs instead of back.

Different considerations can be pointed out concerning the perceived local discomfort. A smaller score at the human back is registered in case of wearing the device, while a crucial disadvantage can be highlighted at the chest area. Indeed, compared to the nonattendance of discomfort in the absence of exoskeleton, when wearing the device, the subject declares high discomfort (3.2 scores). No differences are pointed out at the thighs.

Finally, concerning the perceived pressure, the chest area reveals a higher value of local pressure (3.6 scores), followed by the thighs area (2.4). Negligible and absent values have been obtained at the pelvis (0.4 scores) and shoulders (0 scores) area, confirming the absence of crucial and uncomfortable contact points.

4.2.4 Conclusion

Joint kinematics. Both from the joints' kinematics and the angular ROM the presence of exoskeleton device seems to be substantially transparent. The subject can perform the task without any obstruction or requirement of kinematic adaptation. In the static holding stoop position, the exoskeleton reduces trunk oscillation. The main differences can be pointed out in the comparison between different lifting strategies. Indeed, the hip and knee joints reveal greater joint displacement and range of motion during squat and semisquat strategy, compared to the stoop lifting. If considering the free style, the subject is more oriented on performing a semisquat lifting motion, even when wearing the exoskeleton.

Interface pressure. All the performed motions depict acceptable maximum pressures and interface pressures are lower than critical ergonomic thresholds, with highest values at the trunk pad compared to the thigh pad. The motion with lowest pressure results the semisquat movement, while the most critical one is the squat motion. Compared to the perceived pressure from the user's point of view, the subjective judgment confirms the trend of monitored values, with highest perceived pressure at the chest area compared to thigh area, and with higher perceived pressure during squat motion and lower during semisquat.

Subjective evaluations. The subjective perception and acceptance of the use of the external wearable device acquire fundamental importance for the assessment of device assistance, wearability and suitability. Moreover, the user's point of view might highlight possible discomfort, limits and drawbacks that have not been considered during the design and development of the mechanical structure. Due to the final aim of the device to supply partial assistance and, consequently, to reduce the human body loads, the perceived muscular efforts of different human body parts results in one of the most important and investigated subjective variables. The chest reveals to be the most critical area both for discomfort and perceived pressure, as previously found by [85, 88, 90]. Some great benefits have been registered for back

efforts, as stressed by [85, 93]. Finally, it must be pointed out the fact that, sometimes, the subject found difficult to determine the score during the interview. A deeper explanation of subjective questionnaire and the difference between the subjective variables may help. In addition, the possible influence of the psychological sphere has not been considered during the test. The subject's evaluation might be affected by the attendance to receive support from the device and the consequent less perception of exertion and fatigue. This point is a current, critical, open challenge in testing exoskeletons in industry.

4.2.5 Future perspectives

The current experimental test could be considered as the starting point for a deeper investigation of passive exoskeleton performance with a larger group of subjects with different gender and age, in order to develop an inter-subject comparison. A greater sample size may allow a statistical analysis of results. In addition to the limited number of participants, the assumption of constant pressure distribution on pad areas may affect the monitoring of interface forces. A proper interface model should be implemented to deeply analyze the exchanged forces. The conducted analysis confirms some literature results and highlights critical effect of the exoskeleton in terms of wearability, discomfort and low perceived assistance. The contact areas with the human body, especially the chest area, are negatively affected by the presence of the exoskeleton. In the summary, considering the different lifting motion, the Laevo exoskeleton results to be unsuitable in case of squat and semisquat strategies, while in holding stoop and stoop lifting it supplies discrete beneficial effects. In future experimental analysis, a proper training process for the use of the exoskeleton could be considered in order to allow the users to increase their confidence to the device. The training could reveal crucial advantages also in the explanation and comprehension of the subjective evaluation. Moreover, the investigation of prolonged periods wearing the exoskeleton similar to workstation conditions may point out different level of user's perception and acceptance, as already highlighted by Hensel and colleague [93] and deeply explained in chapter 2.6. From the previous analysis, indeed, the prolonged use of the wearable device seems to negatively affect the evaluation, with a reduction acceptance and increase of perceived discomfort.

Chapter 5

MODELING APPROACH

5.1. The computational approach

The computational approach has revealed to be a strategical method for the analysis and the evaluation of systems, situations, environments, and concepts in several fields. It mainly consists in the simplified representation of a real study through the development of proper models. The model-based analysis necessarily requires the introduction of some schematizations and assumptions. Nevertheless, model-based strategy allows estimating variables, evaluating several conditions and modifying the setting system, with a final reduction of time and cost.

Model based computational investigation of the interaction between the human body and wearable systems discloses to be a proper methodology for the evaluation of different exoskeleton designs, to test virtual prototyping, to estimate the biomechanical effects on the human body and to analyze the device assistance. The simulation strategy might highlight properties and considerations that are not immediate and cannot be completely evaluated during the project and system development. Despite the numerous and complex biomechanical studies on the development of human body models [110, 111], and the exoskeleton models applications in rehabilitation and clinics [112, 113], only a few researches have been conducted for the development of exoskeleton in the industrial applications. Only the recent studies conducted by Millard and colleagues adopted the computational multibody investigation for the analysis of trunk exoskeleton assistance in lifting tasks [22, 114–116]. The first study presented the design of a two-dimensional human body model constrained to a passive exoskeleton through a kinematic interface. Pairs of agonist-antagonist muscle torque generators actuated all the 15 rotational joints of the human body model [114]. The exoskeleton model consisted in three main parts: upper body support, linked to human body shoulder, lower body support, connected to human thigh and a pelvis belt, rigidly fixed to the

human pelvis. An ideal torsional spring was modeled between the upper and lower supports as the assistance source. The main aim of this first computational approach dealt with the optimization of exoskeleton parameters, in particular, the spring stiffness. Both the human body trajectories and the exoskeleton spring stiffness were solutions of an optimal control problem (OCP), characterized by the main objective function of minimization of the muscle activations over time [117]. Following, the optimal control approach has been combined with registered kinematic experiments [115]. Comparing computational and experimental data, the study confirmed the suitability of the developed 2D human-device model and control optimization. In addition, based on individual object lifting strategies, the support provided by the exoskeleton was varied across the subjects and the joints. In a second step, the exoskeleton has been modeled with two different torsional springs positioned between upper support and pelvis belt (lumbar spring) and lower support and pelvis belt (hip spring). The computational analysis pointed out different optimization values of lumbar and hip springs. The same analysis has been implemented considering a powered exoskeleton with two motors that apply torques to the linkages between the hip and the lumbar spine, during stoop motion [118]. Considering the innovative approach and the obtained design results, Millard and colleagues proposed in future perspectives to increase the models' degrees of freedom, upgrade to a three-dimensional model, consider user's comfort as the objective function. However, the presented analyses did not differentiate the several lifting strategies that could be adopted by the wearer and did not compare results from different exoskeleton structures.

In the current study, in order to develop and design an active trunk support exoskeleton, a computational model was developed. Differently from Millard, a 3D multibody model was developed to focus on the human-exoskeleton interface. Therefore, the present model simulations have three principal aims: the investigation of the influence of different hinge joint positions of the exoskeleton, the comparison between two exoskeleton structures, and the definition of an effective assistance strategy.

5.2. 3D multibody models

The following sub-sections reported the description of the 3D multibody models developed and validated in the current project. All the models have been developed in Matlab Simscape Multibody environment.

5.2.1 Human model

Development. The human body is modeled as a 3D kinematic chain of 15 rigid segments, connected by 14 joints, for a total of 34 degrees of freedom (DOFs). The manikin is scaled on a 50 percentile Italian man with body mass of 75 kg and height of 1.71 m. The manikin scaling and standardization have been implemented based on previous literature researches and defined parameters. ISB standards [119, 120]

have been considered for the joints range of motion and local reference systems characterization, while inertial and mass parameters have been defined according to De Leva's tables [121]. Appendix A deeply describes the definition of local reference system and direction of local axes in accordance to human physiological movements. Moreover, the range of motion of each joint in the 3D space has been defined considering the human body ROMs. Figure 5.2.1 shows a sketch of the human manikin in frontal and sagittal planes, with highlighted center of mass of the single segments. The manikin is assuming the standing posture, that is considered as a reference starting position with all relative angles between segments set to zero value. A solid block is considered to simulate the feet positioning on the floor. The 15 rigid bodies are connecting each other by means of a sequence of revolute joints. Each revolute joint represents 1 DOF and allows the relative rotation between two linked segments in one direction. All the joints present a chain of three revolute joints in order to allow 3D angular movements, excepted the two elbow and the two knee joints, which allow only the rotation in the sagittal plane. Figure 5.2.2 shows a graphical representation of the Simscape model, with solid body element blocks to represent the human body segments and sequence of revolute joint blocks to depict the human DOFs.

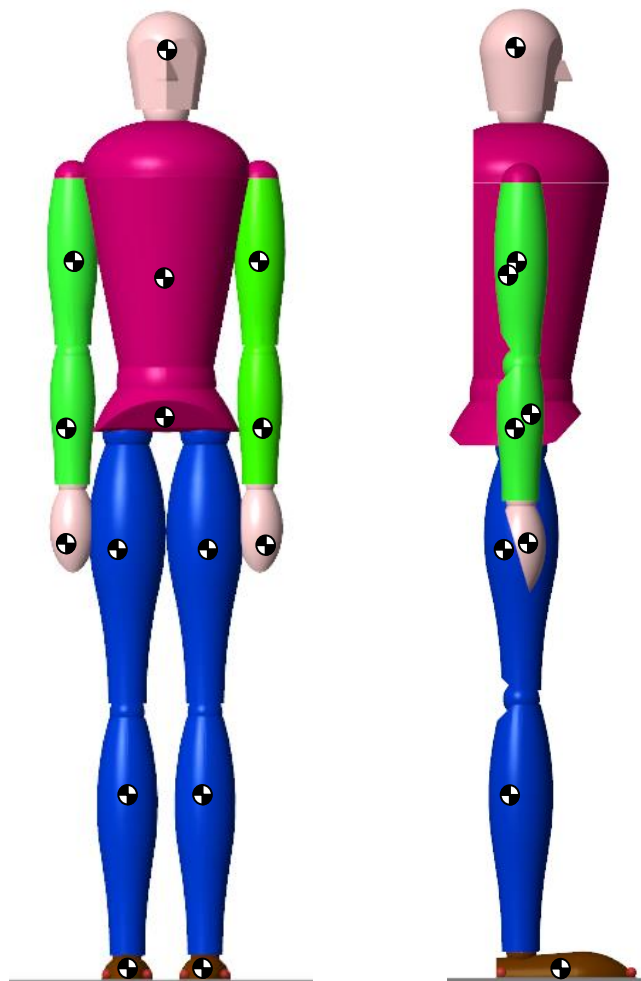


Figure 5.2.1: 3D human body manikin from the frontal and the sagittal planes.

Table 5.2.1: Human body anthropometry and inertial parameters.

Human body 3D model	Segment name	Segment length (m)	Segment breadth (m)	% Distance of COM from proximal end	% Total mass	
50 percentile Italian man body mass= 75 Kg body height= 1.71 m	Head + Neck	0.19	0.15	56	8.4	
	Torso	Lumbar	0.41	0.22	42	22
		Thorax				15
	Pelvis	0.10	0.29	74	13	
	Upperarm	0.32	/	45	2.8	
	Forearm	0.25	/	42	1.7	
	Hand	0.19	0.09	40	0.6	
	Thigh	0.48	0.18	43	10	
	Shank	0.41	0.12	41	4.3	
	Foot	length	0.26	0.10	43	1.4
height		0.05				

Common previous models assume the symmetrical characterization of human left and right sides and prefer to schematize the human body in the sagittal plane, grouping the human legs in one single structure [122, 123]. The human body appears as an open kinematic chain. This solution allows constraining the human foot to a global reference system, simulating the contact with external surface, as the floor. Due to the implementation of a 3D model and the separation between left and right side, the manikin depicts a complex multi-segment closed kinematic chain. A proper contact between the human feet and the reference floor needs to be implemented in order to correctly distribute the loads and to allow the simulation of asymmetrical conditions. With the attempt to release the human feet from any kinematic constraints and to allow the correct evaluation of the multi-segment kinematic chain, a contact force is modelled between the two feet segments and the floor. To implement this type of contact, the Matlab library Simscape Multibody Contact Forces Library is used [124]. This library contains contact force models that can be used both for intermittent contact, both for persistent contact. The block “Face to Plane Force” allows the modeling of contact force between a plane (the floor) and a square face (the foot). Figure 5.2.3 A depicts a graphical scheme of the contact. The plane must be defined significantly larger than the face in order to avoid the contact between edges. The square face is modeled with four spheres, one for each corner, that directly interact with the planar surface (Figure 5.2.3 B). Two frames are defined: one frame positioned at the midpoint of the plane and with the z-axis normal to the surfaces where the force is active and one frame positioned at the midpoint of the element with square face, with the z-axis normal to the surfaces of contact. Dimensions of the faces are necessary as input values and a specific

force and friction laws must be defined. An external reference frame has to be defined for the forces of interaction. This reference frame is aligned with the local reference frame of the plane, with z-axis pointing upward along the direction of penetration and x-axis pointing on lateral direction, as reported in Figure 5.2.3 B.

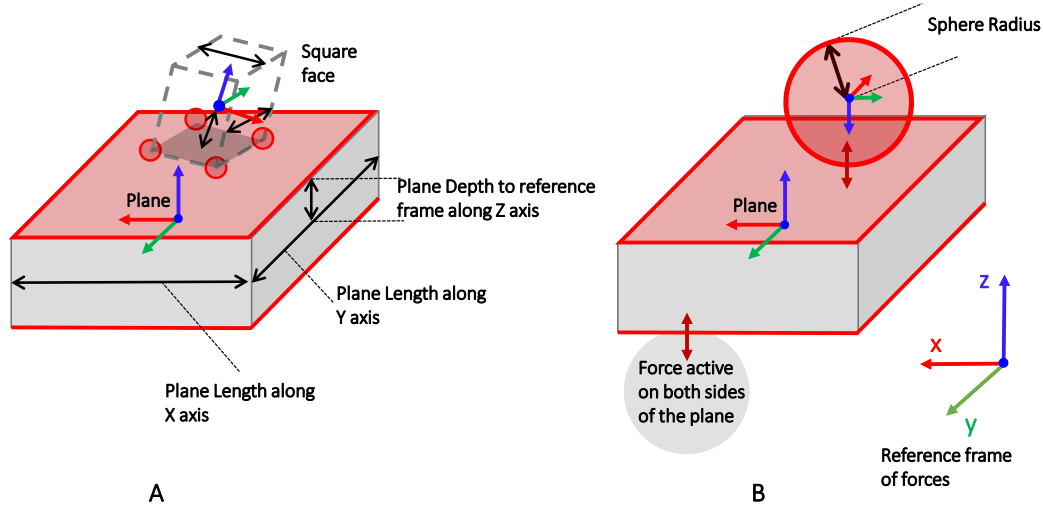


Figure 5.2.3: Matlab Simscape Multibody Contact Forces Library. Graphical representation of the contact model between the floor (Plane) and the human foot (square surface). (A) representation of the two element, relative dimensions and local coordinate system; (B) details of one square face corner modeled with a sphere.

In the present case, a linear force law and stick-slip continuous friction law are supposed for the contact modeling. The linear force law provides a linear spring-damper model that resists penetration (z-axis). The damping force is zero as penetration decreases ($v_{pen} < 0$) and force is applied only along the direction of penetration (z-axis). The following system sums up the mathematical model of the linear force law for the definition of force F_z acting in the penetration direction:

$$F_z = \begin{cases} k * z_{pen} + b * v_{pen} & z_{pen} > 0, v_{pen} > 0 \\ k * z_{pen} & z_{pen} > 0, v_{pen} < 0 \\ 0 & z_{pen} \leq 0 \end{cases}$$

where k is the contact stiffness and b the contact damping. In the current model, the stiffness is imposed pair to 750000 N/m and contact damping pair to 150000 Ns/m. The rolling friction force (F_f) is calculated as the coefficient of friction μ multiplied to the contact force F_z , where the coefficient of friction is a function of the relative velocity at the point of contact:

$$F_f = F_z * \mu$$

$$\mu = \begin{cases} v_{poc} * \mu_s / v_{th} & v_{poc} < v_{th} \\ \mu_s - v_{poc} * \frac{(\mu_s - \mu_k)}{0.5 * v_{th}} & v_{th} \leq v_{poc} \leq 1.5 * v_{th} \\ \mu_k & v_{poc} > v_{th} \end{cases}$$

where the v_{poc} is the relative velocity at the contact point and v_{th} is a threshold velocity. In the present model, the coefficient of kinetic friction μ_k is 0.5, the coefficient of static friction μ_s is 0.7 and the velocity threshold 0.001 m/s. The graphical representation of the force (A) and friction (B-C) laws are reported in Figure 5.2.4.

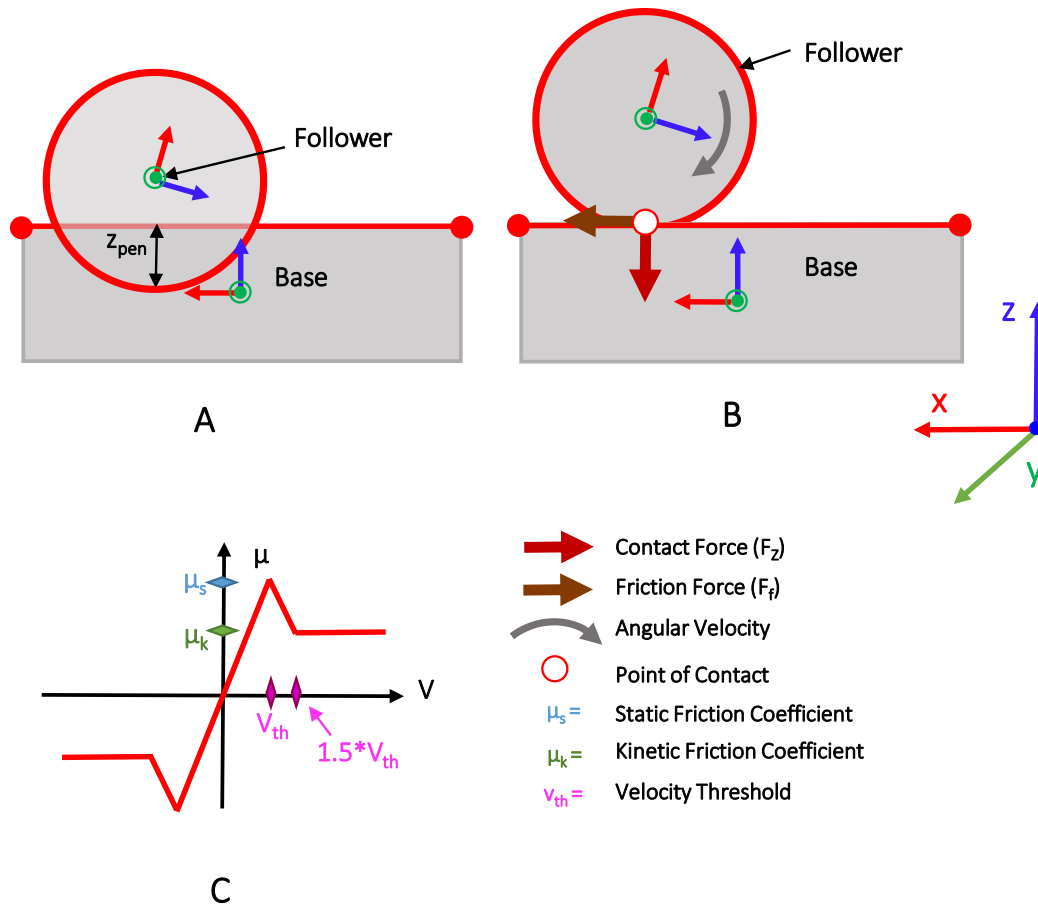


Figure 5.2.4: Matlab Simscape Multibody Contact Forces Library. Linea force law (A) for the definition of contact force in the direction of penetration; (B-C) stick-slip continuous friction law for the calculation of friction force at the contact point.

Validation. Two different analyses are implemented in order to verify the suitability of the developed human body model.

For the verification of the correct development of force contact between the human feet and the floor, three different lifting motions are simulated with the human body model. The force contact distributions under the human feet are compared with previous literature experimental analysis [125]. The literature study proposed a novel and non-invasive method to detect and classify uncomfortable working postures based on the foot plantar pressure distribution measured by an insole pressure system. The subject performed several working tasks including stoop, semisquat and squat lifting. The experimental and simulation results are compared considering the trend of pressure distribution in the different foot subareas, not the net values. Figure 5.2.5 shows the experimental test performed by one subject, in

the different lifting positions of interest. Moreover, the figure depicts the pressure distribution under different feet subareas registered during the experiment with the insole pressure system. Finally, for the comparison with the current study, the simulation results of ground reaction forces exchanged between the right foot segment and the floor are representing. The four curves in the graphs referred to the four corners of the right foot, the right and left rearfoot and the right and left forefoot corners. Due to the lack of information about the detailed kinematics of human joints, the simulation of stoop, semisquat and squat have been implemented with a common initial phase of small trunk flexion (around 15° at the waist joint), then, after a small static holding posture, the manikin reached the position of the specific movements, as depicted in the experimental pictures. Finally, the manikin returned to the starting standing posture with the extension phase. Curves are normalized respect to the percentage of total time. If considering the motion between 40% and 80% of total cycling time, simulations results confirm the pressure distribution obtained during tests. In the stoop movement (A), both the subject and the manikin concentrate the force contact in the rearfoot subareas, while during semisquat (B) and squat (C), the forces are concentrated in the forefoot subareas.

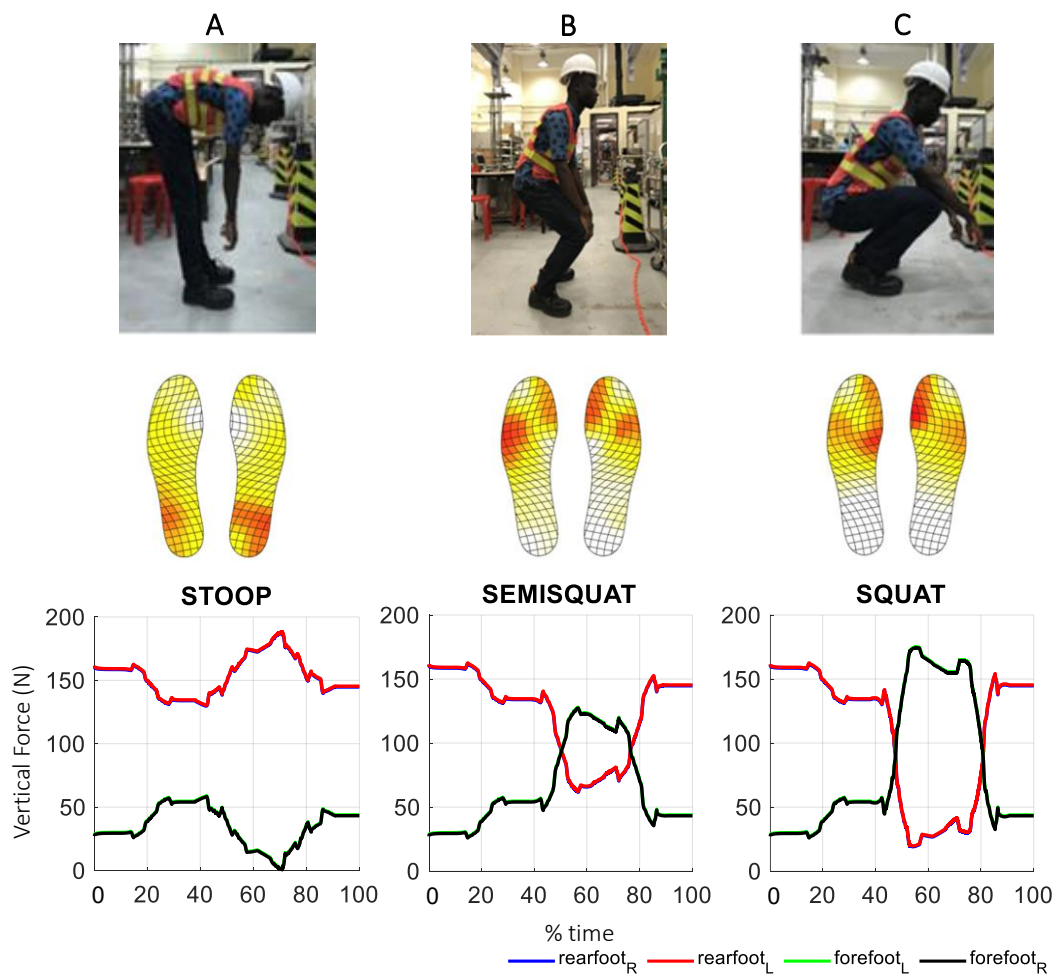


Figure 5.2.5: Comparison of experimental and simulation pressures distribution in different foot subareas during (A) stoop, (B) semisquat and (C) squat lifting motion. Simulation curves are related to the four corners of the right foot model.

The validation of the entire human body model was assessed comparing obtained results with previous experimental literature results [126–128] in which experimental kinematic and dynamic data were collected and analyzed to estimate the joint loads at the lumbar spine during load lifting. In these studies [126–128], the subjects performed a stoop motion (flexion-extension of the trunk at waist joint 100° and with extended legs) and semisquat movement (waist flexion 55° and flexed legs: 80° at hip joints and 110° at knee joints). The subjects lifted different masses (range = 10 - 16 kg) positioned on the floor, starting from a total flexed position and performed extension motion in the sagittal plane. The speed of the motion was selected by the subjects as their comfortable speed (cycle time range = 1 - 3 s). Experimental kinematic and dynamic data were collected with optoelectronic systems and force plates. In the current study 3D model simulations reproducing the same kinematics and performing lifting cycle with durations of 1, 1.5, 2 and 3 seconds and with a 15 kg mass, both in stoop and semisquat movements are considered. During the entire lifting cycle, the extension phase results as the most important in the involvement of human spine muscles and might cause the overload of the human back joint. For these reasons, the validation of the model concentrates on the comparison of waist torques during the extension phase between simulations and literature experimental data. Figure 5.2.6 shows the results of this comparison, both in stoop and semisquat motions.

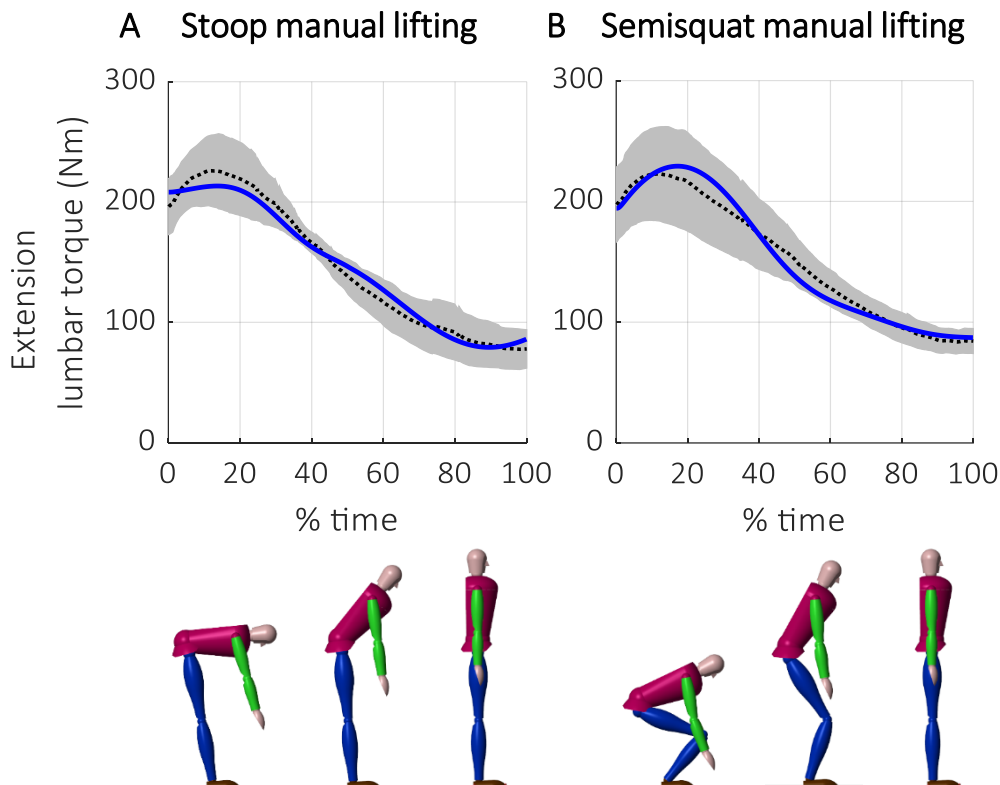


Figure 5.2.6: Extension torque at waist joint in (A) stoop and (B) semisquat: model curves (blue line), experimental reference mean (black dotted line) and experimental range curves (grey area).

For these results the time scale is normalized with respect to the lifting cycle and data from different cycle times are averaged. The black dotted line depicts the mean values and the grey range represents the enveloped area of the different experimental curves reported in [126–128], while the blue line depicts the averaged curve obtained with the simulations. Agreement between simulated results and experimental both in stoop and semisquat lifting strategies is very good. The human model well represents the load distributions and can be used to depict different human movements and conditions.

5.2.2 Exoskeleton model

The modelled exoskeleton consists of four rigid elements as reported in Figure 5.2.7: trunk support, pelvis belt and two thigh supports, one for each human lower limb. Left and right pairs of joints connect the rigid bodies: hinge joints J_1 connect pelvis belt and thigh supports, while hinge joints J_2 connect each thigh support with the trunk support. The nominal configuration of exoskeleton considers joints J_1 and J_2 coaxial with the human hip joint, as depicted in the figure. Moreover, Figure 5.2.7 shows the Simscape multibody model of the exoskeleton structure. This is modeled as a kinematic rigid chain with a total mass of 2.5 kg, equally distributed among the exoskeleton parts.

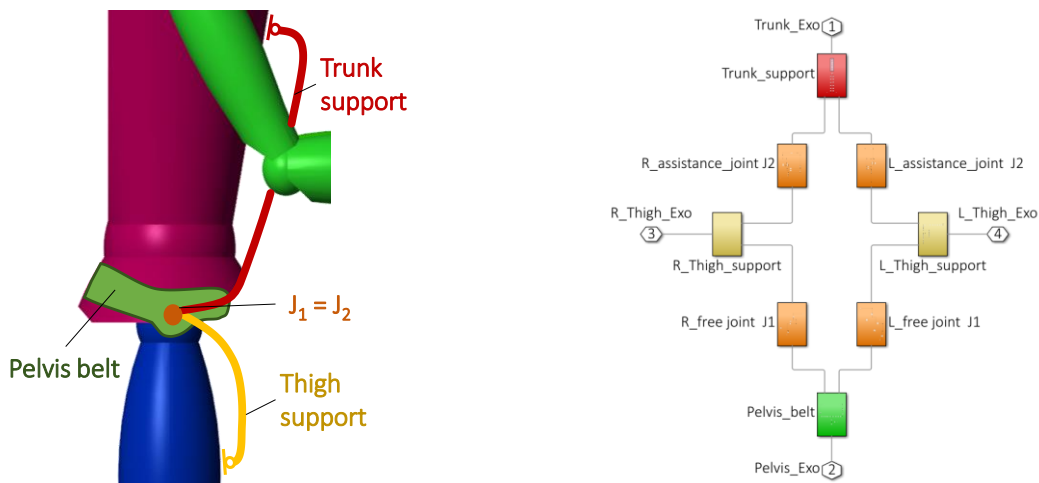


Figure 5.2.7: Sketch of the human body wearing the device. Description of the main parts of the device and Simscape scheme of the exoskeleton model.

The assistance of the exoskeleton is modeled as torques applied in joints J_2 , which represent the passive assistance joints. The free joints connecting the thigh support to the pelvis belt allow the relative rotation between the two parts, but without supplying assistance. The torque assistance supplied by the device can be modeled with different laws, but in these analyses, it will be related to the kinematics of the exoskeleton joints.

The proposed mechanical design of the exoskeleton structure is similar to the commercial passive exoskeleton Laevo [14], but it is different from other commercial products [69, 70], prototypes [22, 129] and designs [114–116], where

the exoskeleton directly interacts with the users at shoulders level. In the current exoskeleton, the upper-body support of the structure interacts with the anterior part of the human torso. This choice of architecture might be a solution to prevent the possibility of shoulder injuries and discomfort due to long-time exoskeleton wearing and a high level of exoskeleton assistance. Indeed, similarly to low back pain, the musculoskeletal disorders at shoulder joints reveal to be widespread among workers [130] and several wearable solutions have been proposed in order to reduce the shoulder loads in working tasks.

5.2.3 Interface model

The human-device interfaces are modeled as kinematic connections at trunk and thighs contact points, while the pelvis belt is rigidly fixed to the posterior part of the human pelvis. Trunk and thighs contacts allow translation along vertical direction and rotation in the sagittal plane, so the forces transmitted by the exoskeleton always result perpendicular to the human body. Figure 5.2.8 depicts the Simscape blocks and the graphical representation of the interface model.

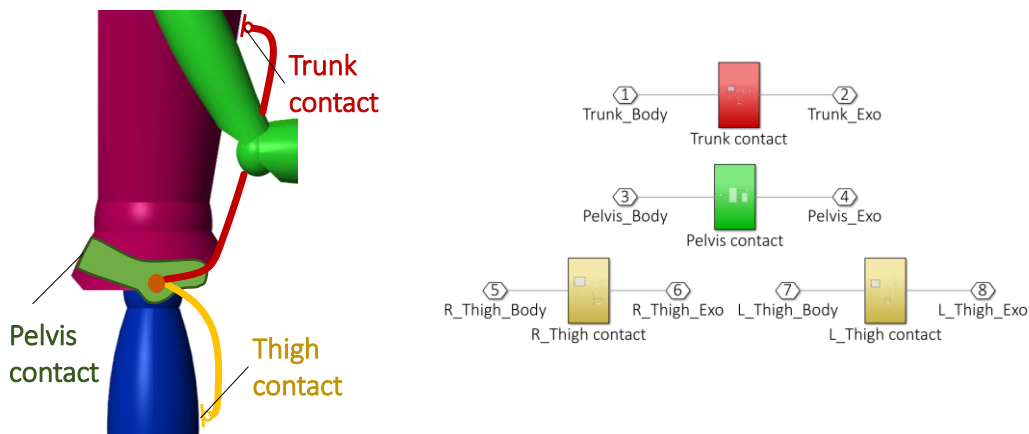


Figure 5.2.8: Sketch of the manikin wearing the device and Simscape scheme of the interface model. Identification of the contact points.

5.2.4 Dynamic simulation

Figure 5.2.9 report a block scheme of the model (human body, interface, exoskeleton) and outlines the whole process (input, simulation, output).

Input. The fundamental aspect of human body motion that needs to be considered in the development of a wearable device entails the analysis of the different kinematics and coordination that can be adopted by the user. Because the lifting motion resulted primarily in the sagittal plane and current ergonomic regulations promote the limitation of human back twisting and lateral flexion because of the augmented risk of injuries [42, 131], the human motion is implemented symmetrically between right and left sides. The other important feature of this analysis is the model of exoskeleton assistance. As previously introduced, the assistance torque may be modeled in several ways, based on the

imposed mathematical law. In the discussed studies, different laws of assistance will be considered and implemented.

Output. Based on the simulation structure, several output variables can be analysed. In particular, since the exoskeleton has to partially support the trunk during specific motion, the principal aim is the evaluation of human back efforts reduction. As already described, the current model simplified the human torso complexity focusing on two joints: waist and hip. For this reason, the waist and hip net moments are considered as output variables. Another important aspect that may contribute to the spine overloads and the occurrence of injuries is the distribution of compression forces along with the intervertebral discs, as previously stressed in chapter 2.2. Numerous studies investigate compression forces, fewer analyses have been conducted on the biomechanical effect of shear forces, however it is important to monitor the range of values in order to prevent intervertebral discs overloads. For this reason, also the intersegmental forces (compression and shear forces) at waist and hip joints are selected as output variables. Finally, to investigate the possible discomfort and drawbacks of the human-device interaction, the interface forces at trunk and thigh contacts are evaluated.

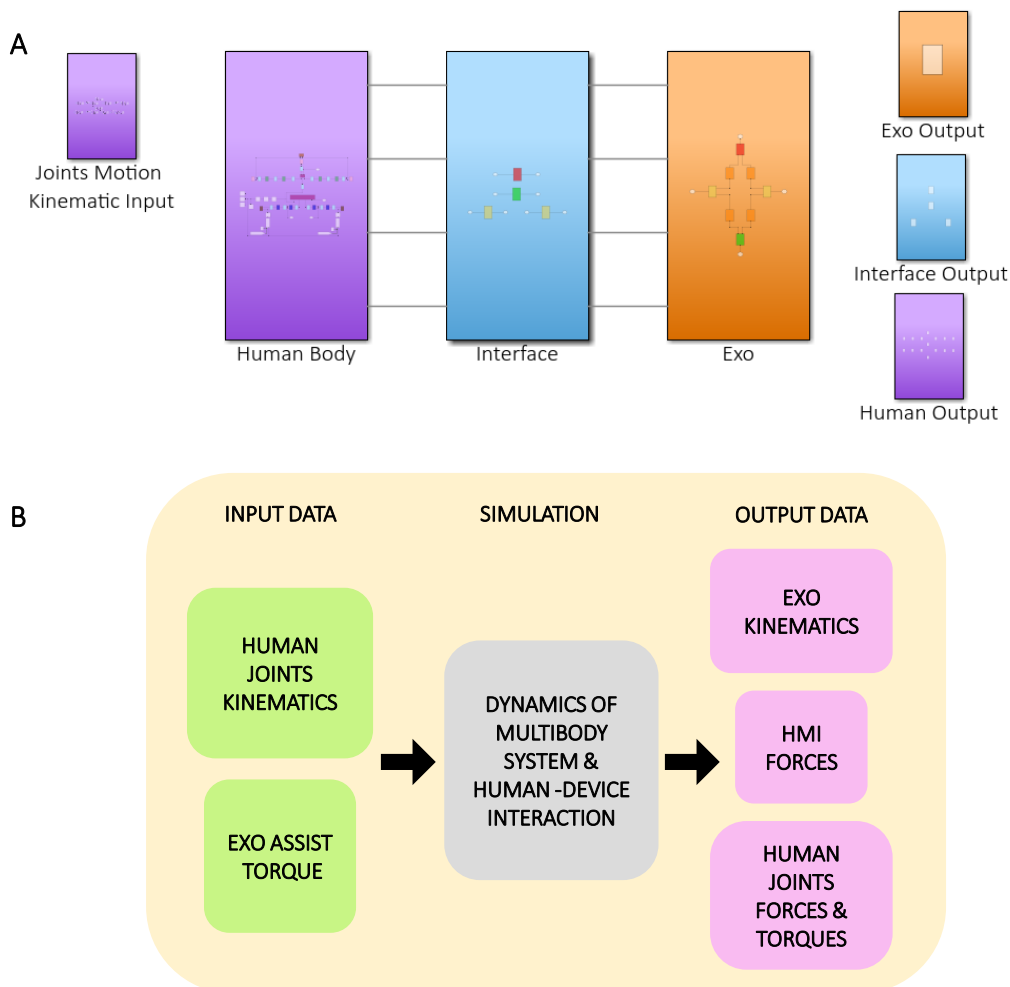


Figure 5.2.9: Simscape scheme of the connection between the three main models (A) and schematic representation of the main passages of the computational process (B).

Chapter 6

SIMULATION ANALYSIS

The current chapter presents the study of the human-exoskeleton interaction when simulating different human body kinematics and modelling different exoskeleton structures. The principal aim of the analyses deals with the comprehension of positive and negative effects of the exoskeleton on human body through the quantification of specific biomechanical variables. The computational approach allows to model and compare several conditions. Results can be compared with previous experimental test. Three main analyses will be described:

- The investigation of exoskeleton effects on human body varying the position of the exoskeleton joints. Both human joints and interface biomechanical parameters are evaluated. The analysis consists in three principal simulation steps that differentiate based on the input assumptions;
- The development of two different passive exoskeleton structures and the analysis of their biomechanical effects on human body when the user is performing several lifting strategies;
- The development, analysis and computational validation of a suitable characterization of the assistance law that must be implemented into the powered exoskeleton. The current law assistance implementation considers the results from the previous two analyses.

6.1. Influence of exoskeleton hinge joint positioning

In this set of simulations, the main aim is to evaluate the influence of the position of the exoskeleton joint on the requested human efforts during manual handling and lifting tasks. Through the evaluation of the net moments at human joints and the interface forces exchanged with the device, it is possible to identify joint positions that allow the reduction of required human efforts. At the same time, the analysis stresses how some exoskeleton configurations have to be discharged and the importance of a suitable development of the interaction surfaces.

Input kinematics. In this first analysis, only the stoop and the semisquat motions are considered. The kinematic inputs are defined based on literature experimental data [126–128] and previous experimental tests described in chapter 4.2. Figure 6.1.1 shows the kinematic inputs for the human body joints as a function of the % of the whole motion cycle. Starting from the reference standing posture, three main phases can be highlighted for stoop and semisquat motion strategies:

- flexion phase, where the body flexes in order to reach the object;
- grasping phase, where the body maintains the flexed posture and lifts an external load, which is modeled as a 15 kg external mass;
- extension phase, the body returns at the reference standing posture, while lifting the external load.

With the attempt to simulate the two lifting strategies, the kinematics of the involved joints should be considered. The standing posture is considered the neutral one, while positive values refer to flexion angles and negative to extension ones. During stoop motion, the human body flexes the trunk with extended legs. The semisquat motion requires lower flexion at the waist joint, but involves large flexion at hip, knee and ankle joints.

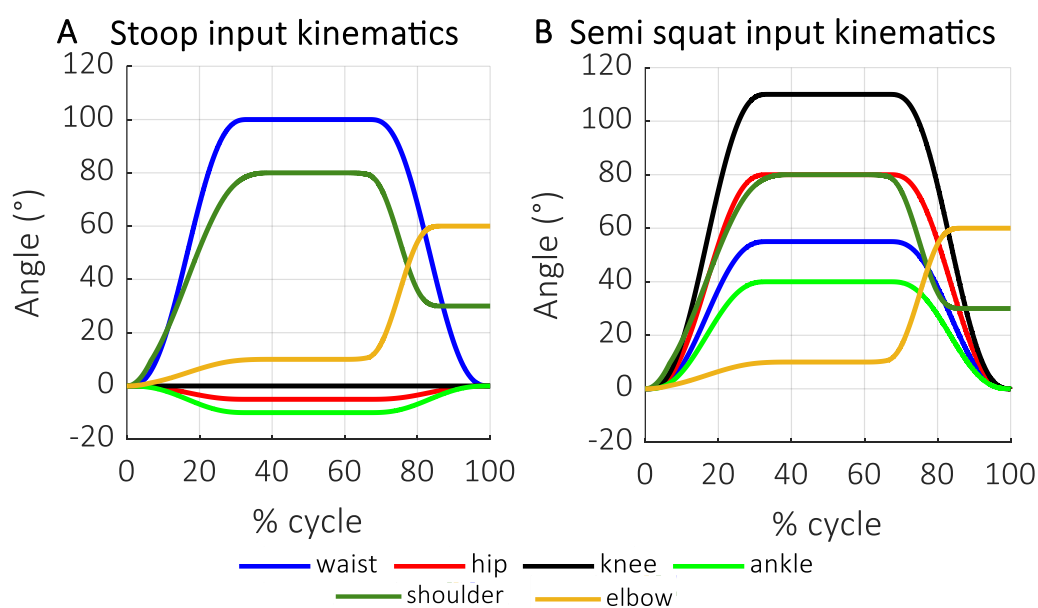


Figure 6.1.1: Human joint angle kinematics in (A) stoop and (B) semisquat lifting.

Concerning the upper body, the kinematic inputs are the same for both motions (from 0° to 80° flexed shoulders during flexion-grasping phase and from 0° to 60° flexed elbows during extension phase). Figure 6.1.2 depicts the graphical representation of the motion and the maximum joints angle reached during the grasping phase at the lower limbs and waist joint.

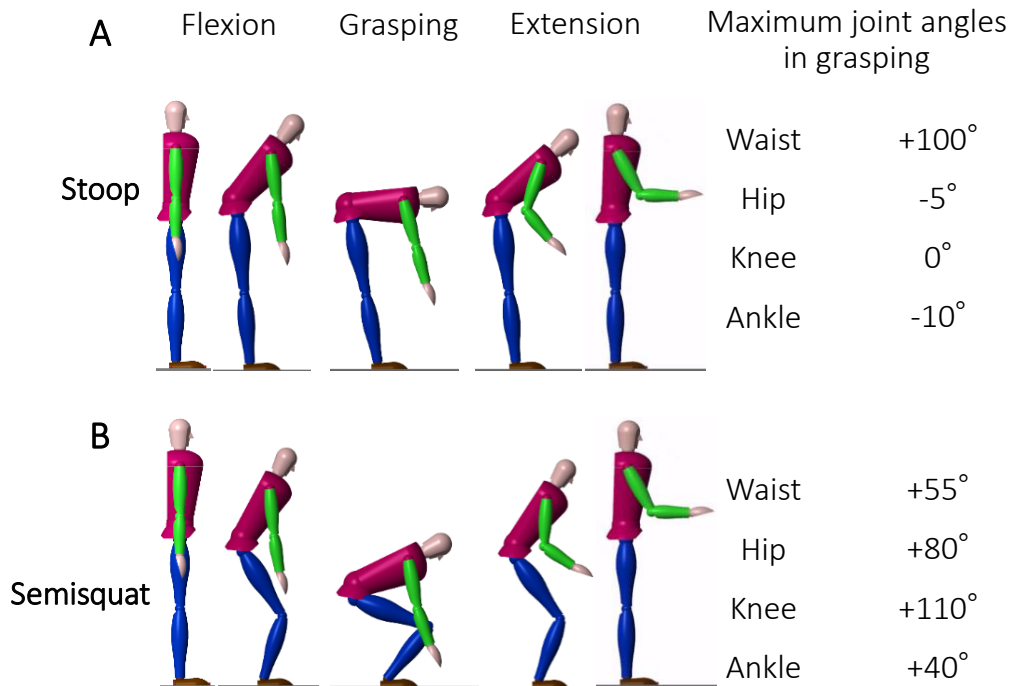


Figure 6.1.2: Graphical representation of the manikin movement and human joint maximum joint angles in (A) stoop and (B) semisquat lifting.

Exoskeleton joint positioning. Concerning the variation of exoskeleton hinge joint position, the study is implemented considering three main simulation conditions. In all the three simulation conditions, the translation of the hinge joints is limited in the XY plane in a circle space around the human hip joint, defined by a radius of 0.2 m. The assistance torque has been implemented as a constant input with the attempt to avoid any effects between simulations caused by the assistance. Figure 6.1.3 graphically depicts the three simulation conditions:

- a set of 100 configuration positions is randomly defined. In this analysis, the translation is applied to the exoskeleton joints J_2 connecting trunk and thigh supports. Indeed, the exoskeleton joints J_1 connecting the pelvis belt and the thigh supports are maintained coaxial with human hip joints. The assistance torque is imposed as a constant value of 20 Nm for each side, for a total of 40 Nm of support [132];
- a parameter set of 200 joints configurations of joint J_2 is defined, while J_1 is maintained fixed and coaxial with human hip joint [133]. The translation of J_2 is mapped with specific and homogeneous order. The simulation starts

from the point in the first circle, with coordinates: $X=0.01$ m, $Y=0$ m and continues in the same circle with a counterclockwise direction. The 21st point has the same Y coordinate as the first point but translated in the second circle ($X=0.03$ m, $Y=0$ m) until the last ones ($X=0.19$ m, $Y=0$ m). Two constant levels of exoskeleton torque assistance are considered as input: 20 Nm and 40 Nm for each side (for total assistance of 40 Nm and 80 Nm, respectively). These values correspond to 20% and 40% waist torque at maximum extension (90°) during stoop motion, when lifting an external load of 15 kg (~ 210 Nm);

- The parameter set of 200 position configurations defined in the second step has been considered for the translation of both J_1 and J_2 hinge joints, which are maintained coaxial during the several simulations. The assistance torques are assumed constant and equal to 20 Nm for each side, for 40 Nm total support [134].

For the analysis of the results, in all the three simulation steps, the waist and hip torques and the interface forces at trunk and thigh contact points are considered. Torque and force impulses and maximum values are considered as parameters of interest.

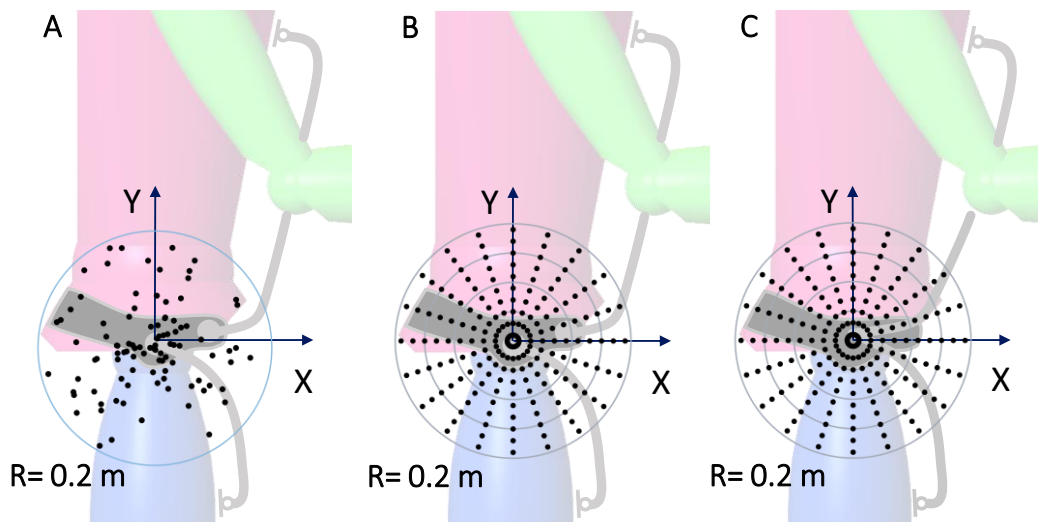


Figure 6.1.3: Maps of exoskeleton configurations in the three analysis: (A) random distribution of 100 hinge joint positions, (B) radial distribution of 200 positions with the displacement of only the assistance exoskeleton joint; (C) radial distribution of 200 positions with the coaxial displacement of both assistance and free exoskeleton joints.

Results and Discussion. All the three simulations consider the comparison of biomechanical variables estimated when the manikin performs the motion without and with the device. The waist and hip joints moments required in case of no exoskeleton are depicted in Figure 6.1.4 and assumed as reference condition. Maximum peak of waist and hip joints moments result around 200-210 Nm and 100-110 Nm respectively.

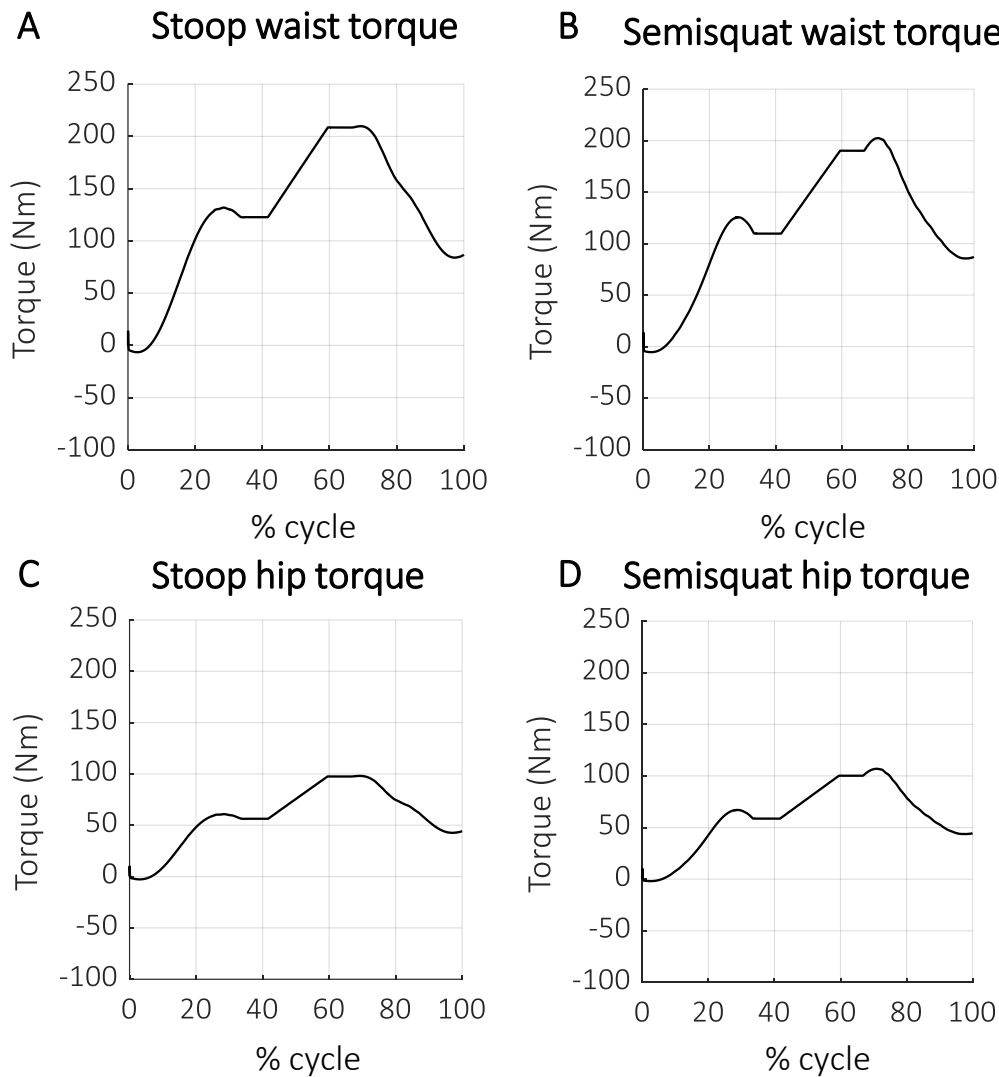


Figure 6.1.4: Net joint moments at the waist and hip joints during (A-C) stoop and (B-D) semisquat lifting motions without wearing the exoskeleton.

In the first set of simulations, considering the random identification of 100 hinge joint positions, the trunk and thigh force impulse (Ns) and waist and hip torque impulse (Nms) have been considered as an overall performance index for each configuration. Although, when considering the impulse, the obtained values are contingent upon the cycle duration, in this case the duration is the same for all the simulation. Figure 6.1.5 shows in a 3D map the relation between force and torque impulses as a function of joint J_2 position in the plane XY during stoop (A) and semisquat (B) movements. Impulse values were linearly interpolated in order to calculate the plane distribution. The different colors depict the investigated variables (trunk and thigh interface force impulses, waist and hip torque impulses). The graphical representations of torques and forces impulse relation can give interesting pieces of advice on how the exoskeleton joint position may affect the interaction with the human body. With the main attempt to reduce the human joint stress, the minimization of hip and waist torques can be considered as principal object function. As attended, the torques minimization involves the maximization

of interface forces, which can be the main drawback if considering the device wearability and discomfort. This problem can be reduced with a proper design of contacts, considering a larger area for a better force distribution. As an alternative, starting from the analysis of the 3D maps, the developer can select a specific force threshold not to be exceeded. The 3D map could be a good starting strategy for the identification of the best position of exoskeleton joints during the design process.

A Stoop impulse distribution B Semisquat impulse distribution

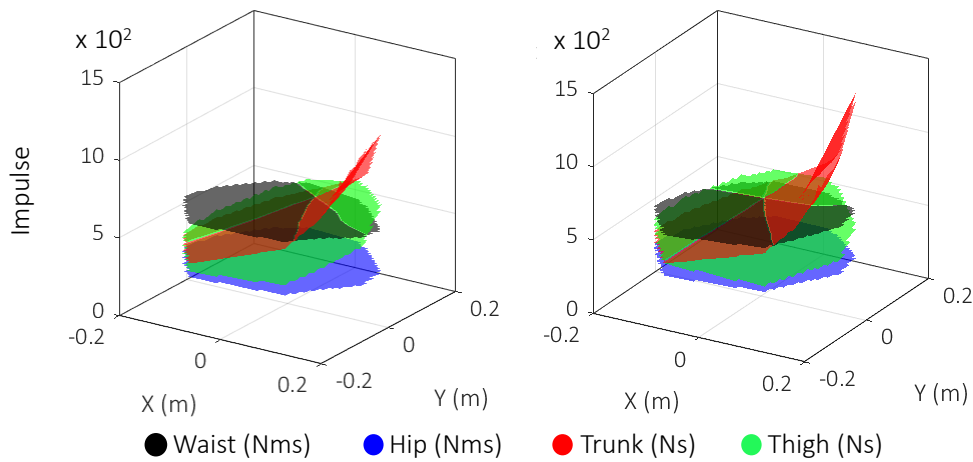


Figure 6.1.5: Distribution of joints torque impulse and interface forces impulse during (A) stoop and (B) semisquat motion with different exoskeleton joint positions.

In the second simulation condition, a larger and more homogeneous position set of J_2 has been simulated. Despite the recent interest in standard guidelines for industrial exoskeleton development, there is not a specific threshold for pressure exerted by the device. Considering the limit of skin capillarity pressure of 32 mmHg (4.5 kPa) established in clinics and more recently updated to 47 mmHg (6 kPa) and the results of a recent study on wearable robotics [135], the maximum pressure value of 15 kPa has been considered to avoid discomfort. A surface of 250 cm² is hypothesized for the trunk and 150 cm² for thigh supports, identifying force thresholds of 350 N and 200 N respectively. Moreover, as overall index, the maximum and minimum peaks of the biomechanical outputs corresponding to each hinge position are analyzed. In this case, considering forces and torques are not directly contingent upon the lifting cycle duration. The term *peaks* refers to the maximum forces and torques along with each single simulation, while *values* refers to global and local maximum and minimum peaks among simulations. Local values refer to comparison among peaks with the same radial distance from the starting reference position, while global values depict the comparison among all the simulations. Figure 6.1.6 shows the maximum peaks of torques (Nm) at the human waist and hip joints, and the maximum peaks of interface forces (N) between the device supports and the human trunk and thighs, as a function of J_2 positions. Hip torques and thigh interface forces refer to the single lower limb. The two lifting strategies and the two assistance levels stress different maximum peaks distribution.

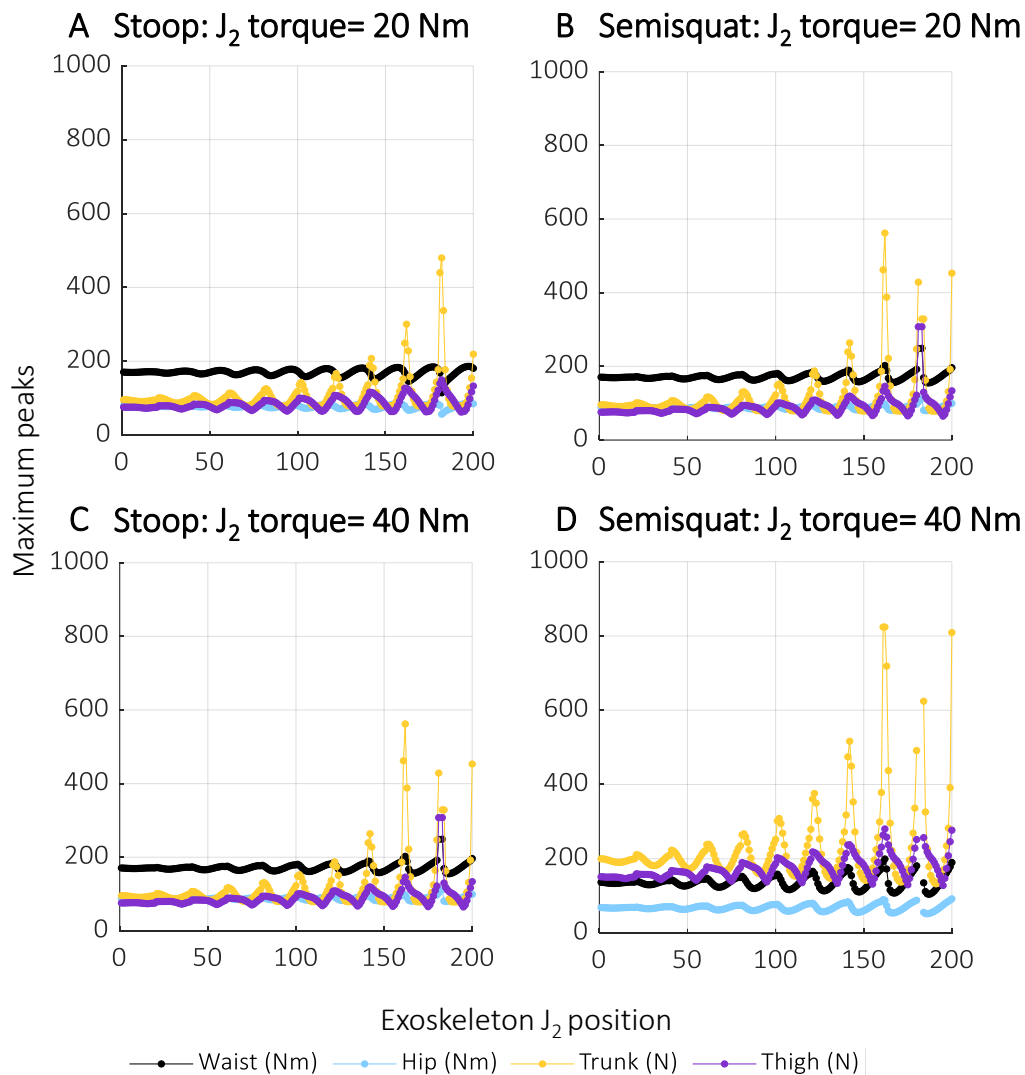


Figure 6.1.6: Interface forces (trunk/thigh) and human joints torques (waist/hip) maximum peaks during (A-C) stoop and (B-D) semisquat motion related to J_2 positions. Graphs A-B refer to 20 Nm exo assistance, graphs C-D to 40 Nm.

Curves have a similar trend among the simulations, showing a succession of local maximum and minimum values. In semisquat, local maximum forces correspond to local maximum torques, while in stoop local maximum forces correspond to local minimum torques. A possible reason could be identified in the different relative motions of human body segments and the different translation of contact points. As expected, lower assistance (20 Nm for side) produces lower interface forces and only a few positions produce pressures with critical values, but also the reduction of human efforts is limited. Analyzing the human torques, in correspondence to specific position of joint J_2 , the value of the maximum peaks is very closed to the maximum values calculated when performing the same motion, but without the exoskeleton. In the case of higher assistance torque (40 Nm for each side), the human net moments are strongly reduced, but interface pressures exceed the selected thresholds in many joint positions. Moreover, even if some external positions reveal greater minimization for both biomechanical variables, the nearest

local maximum results higher. It is necessary to pay attention to this situation. Since actually the device is not rigidly fixed to the human body, but some relative motions may occur, also small sliding of the device during tasks execution may move the joints in critical configurations. For all these reasons, only the internal area of a circle having radius of 0.1 m results suitable for joint positions, as reported in Figure 6.1.7. The figure shows the maps of critical (red) and suitable (green) areas for J_2 translations. The red circles depict where the interface pressure exceeds the limits. Positions that minimize human torques and interface forces are stressed using green dots and green circles, respectively.

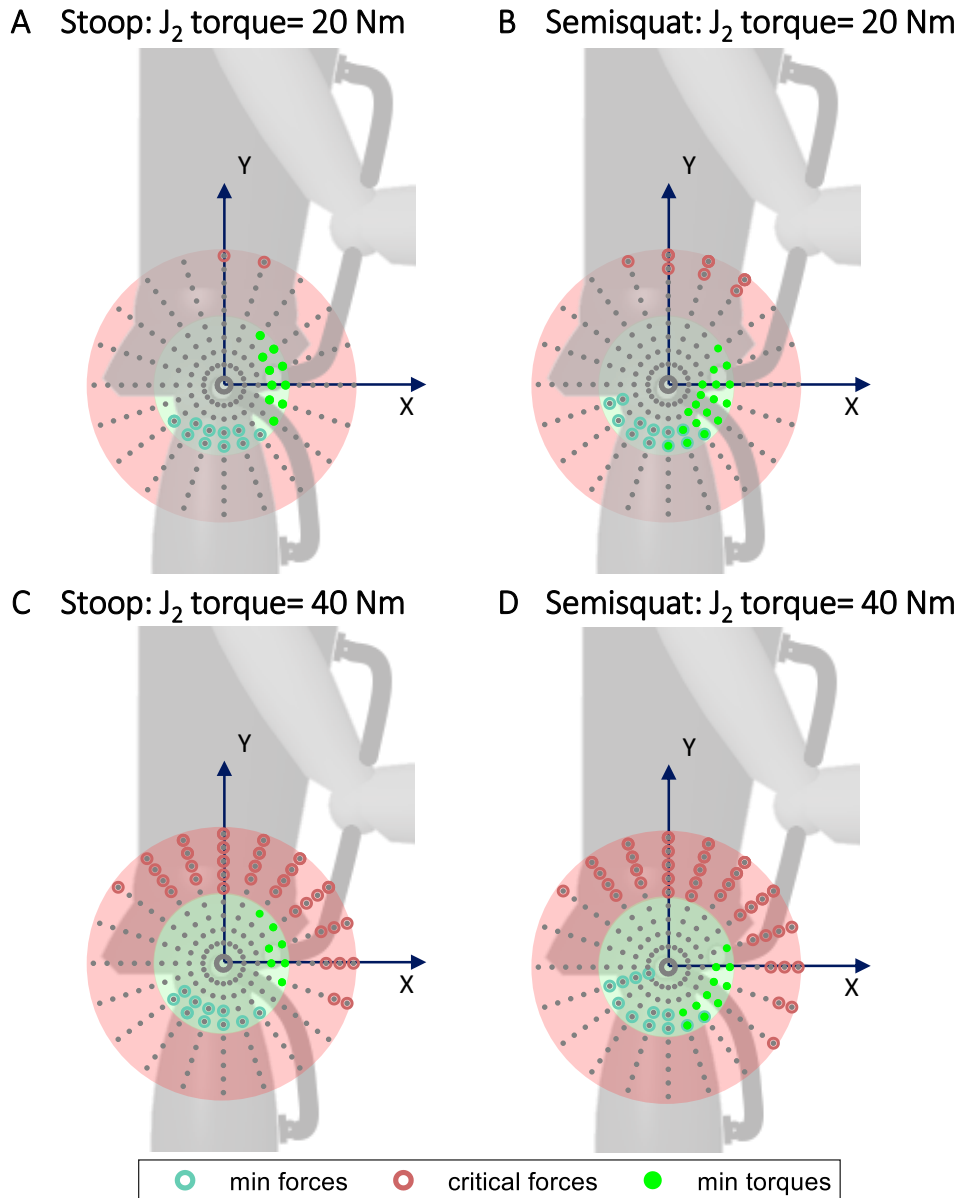


Figure 6.1.7: Maps of optimal and critical zones based on variables in (A-C) stoop and (B-D) semisquat motion. Green areas depict the suitable zone for the exo joint, while the red ones underline the critical areas. Graphs A-B refer to 20 Nm exo assistance, graphs C-D to 40 Nm.

Considering the exoskeleton joints positions inside the green area, all the solutions are suitable because a reduction of the human torque is obtained. Among them, the positions that allow greater global minimization of forces and torques are highlighted as green circles and green dots respectively (global minimum value plus 2.5% of that minimum for lower assistance level, global minimum value plus 5% of that minimum for higher assistance level). In addition, some joint positions are beneficial when considering both stoop and semisquat motion, and for different levels of assistance.

Finally, Figure 6.1.8 shows the net moments results at the waist and hip human joints both during stoop (A-C) and semisquat (B-D) lifting strategies in the last simulation setup. Flexion net joint moments are depicted as positive values, while extension torques as negative ones. Moreover, as in the previous results, hip torque values are related to only one body side. The grey area depicts the range of results obtained with different exoskeleton hinges positions, the blue line the mean value among simulation and the black line the results from case without the exoskeleton.

Concerning the different position of exoskeleton joints, moving only the assistance hinge exoskeleton may require more complex mechanical structure arrangements. The introduction of transmission elements might be necessary to connect exoskeleton parts, causing an increase in the device weight and space encumbrance. For this reason, the study has focused on maintaining J_1 and J_2 coaxial, although testing different position. Moreover, for the exoskeleton assistance torques, a constant value of 40 Nm for each side revealed larger interface forces. Therefore, a constant value of 20 Nm for each assistance joint has been considered. This choice agrees also with the maximal assistive torque provided by other exoskeleton prototypes [136] and commercial products [14]. Considering Figure 5.3.7 waist and hip torques during simulations demonstrates the reduction of human efforts compared with the results obtained without wearing the exoskeleton (black line). The crucial aspect that can be highlighted from the graphs is the required negative torque during the first flexion angles, both in stoop and semisquat motions. The reason can be addressed to the constant contribution of the exoskeleton support. This can cause not only an augmented discomfort perceived by the user but also an additional human back and core muscle activity to drive the exoskeleton during the flexion phase. The present drawback needs to be compensated and appropriate mechanical characteristics for assistance must be defined.

Conclusion. The proposed investigation can be useful for understanding how the exoskeleton mechanical structure may influence the human body joints loads. In the present study, only the position of exoskeleton assistance joint has been considered as the changing parameter, while the exoskeleton assistance has been modeled as a constant value. The computational approach allows depicting suitable and critical areas of exoskeleton hinge joint positions in terms of human joint loads and interface pressures. A deeper investigation about the whole exoskeleton structure, the definition of the mechanical characteristics of the structure and on the law of exoskeleton assistance may be based on the simulation results.

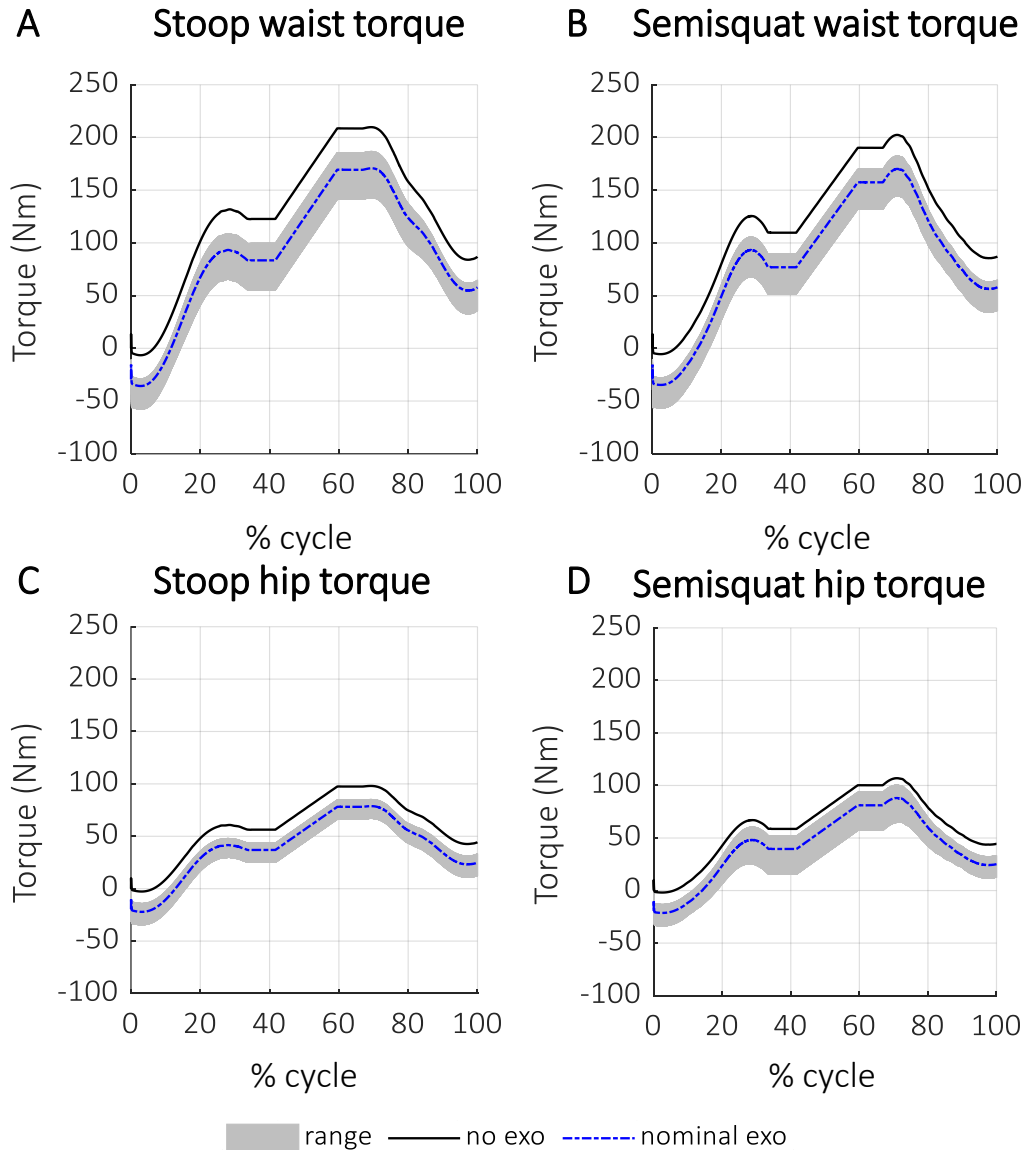


Figure 6.1.8: Net joint moments at the waist and hip joints during (A-C) stoop and (B-D) semisquat lifting motions.

6.2. Comparison of two mechanical designs for a passive exoskeleton

The aim of the current computational analysis is the comparison of two different design solutions of a trunk-support exoskeleton. The multibody simulation intends to evaluate the suitability of mechanical structures to correctly follow the human body movements and to supply assistance. In particular, the study aims both to estimate human joints effort reduction and identify possible crucial drawbacks that might prevent or limit the user's comfort and lack of acceptance. The following sub-chapters presents the differences in the multibody model and simulation process compared to previous analysis and the description and the discussion of the obtained results.

Kinematic inputs. Human body kinematics during lifting motion is considered as input simulation, while human dynamic variables are measured as output results of interest. Three main lifting motions are simulated: stoop, semisquat and squat motion. With the attempt to better reproduce the real human joints coordination during movements, two combined sequences of stoop and squat with inverted order are considered. During all the simulations, the upper limbs are maintained aligned to the human torso. Figure 6.2.1 and Figure 6.2.2 depicts the kinematic curves of human joints considered as input signals of simulations.

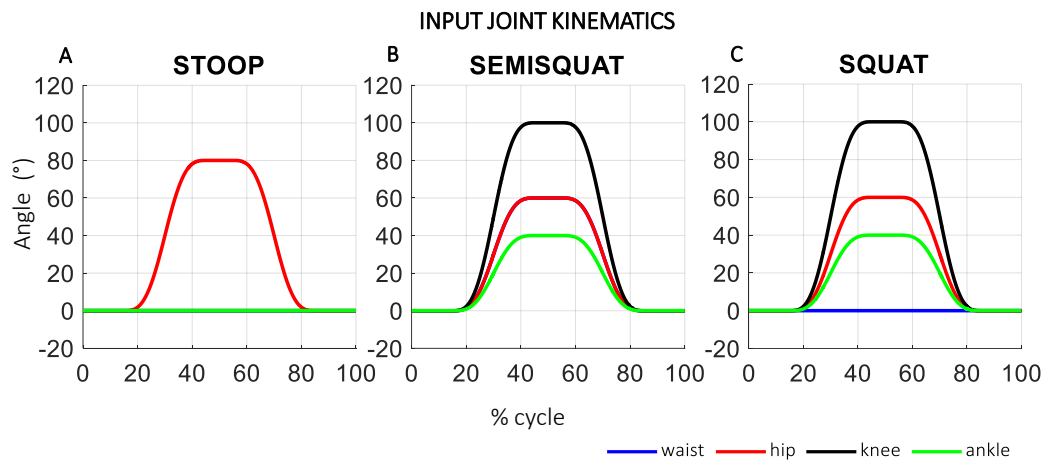


Figure 6.2.1: Human lower limb joint angle kinematics in (A) stoop, (B) semisquat and (C) squat lifting.

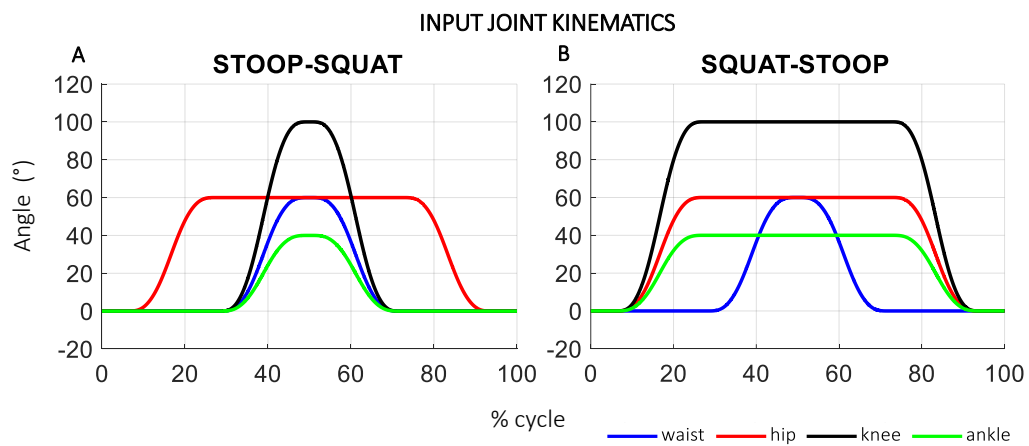






Figure 6.2.2: Human lower limb joint angle kinematics in (A) stoop-squat and (B) squat-stoop lifting.

Table 6.2.1 sums up the sequence of angles at the waist, hip, knee and ankle joints during the performed movements in all the simulations. The values expressed in the table refer to the maximum angles of the specific human joint reached in the lifting phases (flexion, maintenance of the static flexed posture and extension phases).

Table 6.2.1: Kinematic sketches of the several human lifting strategies reproduced in the simulation and detailed angles description for the human trunk and lower body joints.

INPUT KINEMATICS					
Lifting strategies	STOOP	SEMISQUAT	SQUAT	STOOP-SQUAT	SQUAT-STOOP
					
Waist	[0°]	[0°-60°-0°]	[0°]	[0°-0°-60°-0°]	[0°-0°-60°-0°]
Hip	[0°-80°-0°]	[0°-60°-0°]	[0°-60°-0°]	[0°-60°-60°-0°]	[0°-60°-60°-0°]
Knee	[0°]	[0°-100°-0°]	[0°-100°-0°]	[0°-0°-100°-0°]	[0°-100°-100°-0°]
Ankle	[0°]	[0°-40°-0°]	[0°-40°-0°]	[0°-0°-40°-0°]	[0°-40°-40°-0°]

Exoskeleton structures. Figure 6.2.3 shows a graphical scheme of the two proposed mechanical exoskeleton solutions, starting from the exoskeleton model already described.

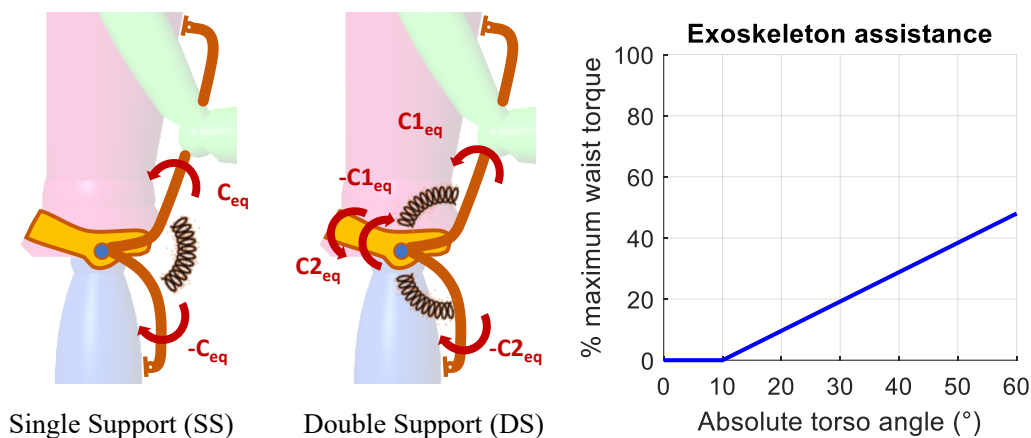


Figure 6.2.3: Graphical description of the two different passive exoskeleton structures and linear input characterization of the exoskeleton assistance expressing the relation between human torso angle and the maximum waist torque required with 60° of flexion.

The first solution, called Single Support (SS), presents, for each side, a free hinge joint connecting pelvis belt and thigh supports, and a hinge joints with passive elastic element connecting trunk and thigh supports. The hinge joint with the elastic element provides a support torque (C_{eq}). The second configuration, named Double Support (DS), presents, for each side, two passive hinge joints connecting the pelvis belt and the trunk support ($C1_{eq}$), and two passive hinge joints connecting the pelvis belt to the thigh supports ($C2_{eq}$). Both solutions show the same characteristics of assistance input that is implemented at the passive hinge joints. The model simulates the mechanical behavior of a torsional spring. The exoskeleton assistance is modeled considering a linear relation between the trunk flexion-extension angle and the trunk torque support provided by the device. In the range 0°-10° of trunk flexion, both the exoskeletons do not provide any assistance. With this strategy, the

user will not perceive any obstacles when starting the flexion motion from the standing posture. Indeed, as outlined by previous sets of simulations, a constant assistance contribution from the exoskeleton, a negative effect at the first flexion degrees may occur. This negative effect could be translated as a demand of a higher efforts from the human body muscles to drive the exoskeleton during the flexion phase. The stiffness of exoskeleton support is defined in order to obtain a 50% assistance value of physiological maximum waist torque when reaching 60° of flexion (48 Nm). This angular value is selected as reference threshold for the development of assistance law because it is assumed in numerous flexion activities and tasks. Due to the symmetrical design of the structure, the total amount of the exoskeleton torque contribution is divided between the two sides. The graph in Figure 6.2.3 depicts the linear relation between exoskeleton torque and kinematics.

For each kinematic sequence, the simulation is repeated for three configurations: no exoskeleton, Single Support and Double Support exoskeleton. Figure 6.2.4 shows a simplified representation of the whole simulation. For the analysis of the results, in all the kinematic sequence and exoskeleton conditions, the waist and hip torques (T_W and T_H), the waist and hip compression (F_{cW} and F_{cH}) and shear (F_{sW} and F_{sH}) forces, and the interface forces at trunk ($F_{i_{tr}}$) and thigh ($F_{i_{th}}$) contact points are considered. Torque and force impulses and maximum values are considered as parameters of interest.

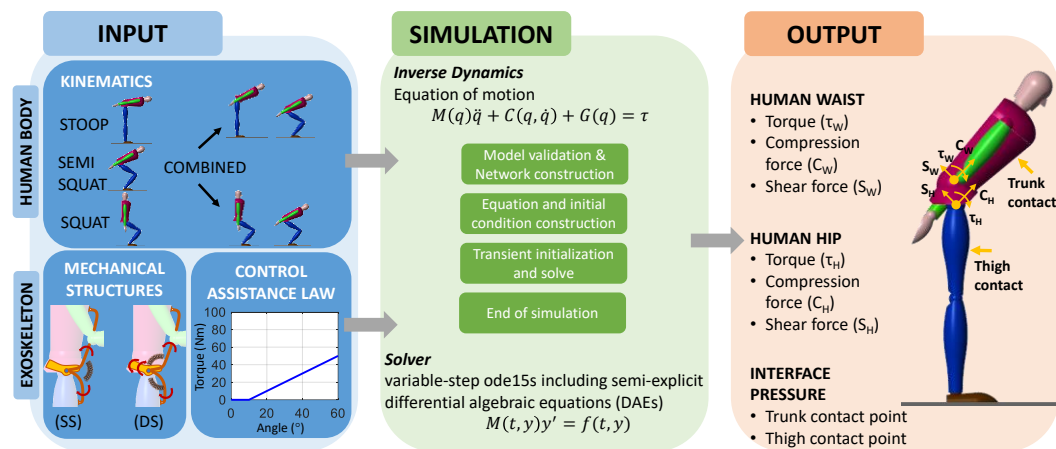


Figure 6.2.4: Simulation map of the current analysis with the two exoskeletons.

Results and Discussion. Two different mechanical designs of the exoskeleton were considered. Interaction with the human body during several lifting motions, biomechanical effects in terms of human joints loads and exchanged interface pressures are analyzed. In Figure 6.2.5, Figure 6.2.6, and Figure 6.2.7 the difference of maximum values when wearing the exoskeletons compared to the physiological condition (no exoskeleton) is calculated for stoop, semisquat and squat motion separately.

Graphs help to visualize the calculated results and to stress the increase and the decrease of the values related to the physiological condition. The numbers reported on each bar are the absolute value.

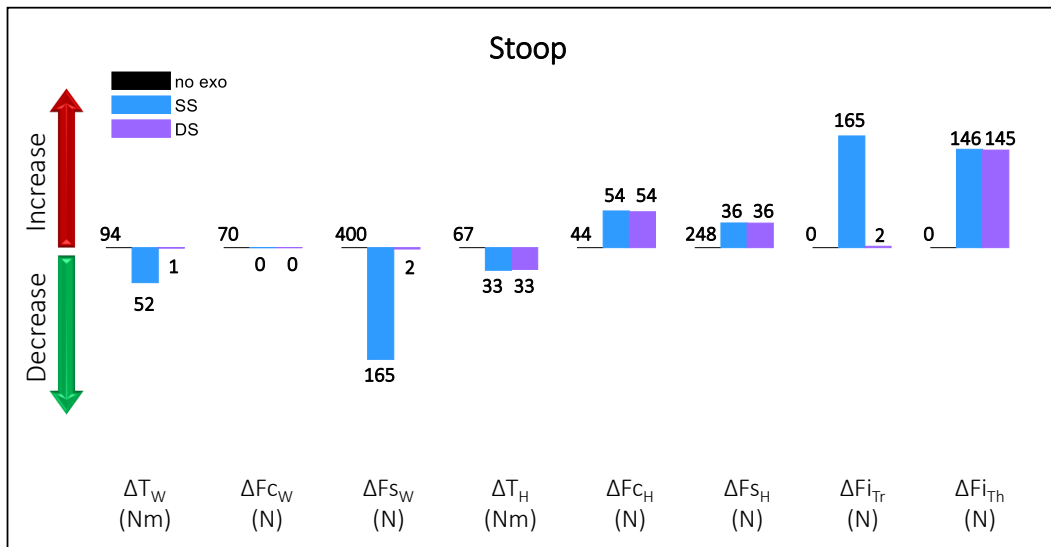


Figure 6.2.5: Relative variation of biomechanical variables during the stoop motion when wearing the two different exoskeleton structures (blue and purple columns) compared to the physiological condition without the exoskeleton (black reference line).

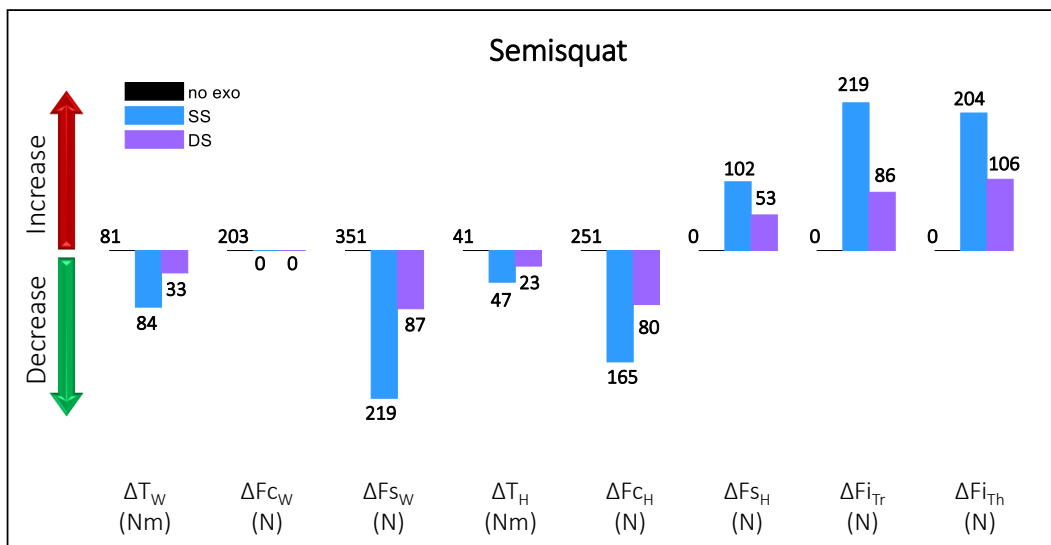


Figure 6.2.6: Relative variation of biomechanical variables during the semisquat motion when wearing the two different exoskeleton structures (blue and purple columns) compared to the physiological condition without the exoskeleton (black reference line).

In order to avoid influence by the masses and required torques of the human body and by the exoskeleton assistance law, the results are normalized. The output variables are related to a reference value:

- hip and waist torques are normalized with respect to the waist and hip torques in 90° torso flexion in static position (96 and 68 Nm respectively);
- intersegmental compression forces at the waist and hip joints are related to a maximum reference value in standing posture (405 N and 251 N for waist and hip respectively);

- intersegmental shear forces at the waist and hip joints are related to a maximum reference value when reaching 90° flexion (405 N and 251 N for waist and hip respectively);
- for the contact pressure, the maximum pressure of 15 kPa has been considered as a threshold to avoid discomfort and pain to human body parts involved in the contact with the device [135]. To direct refer the interface forces from the calculation to the reference threshold of the maximum pressure, a circular trunk pad area with 150 mm diameter and a circular thigh pad area with 100 mm diameter have been hypothesized.

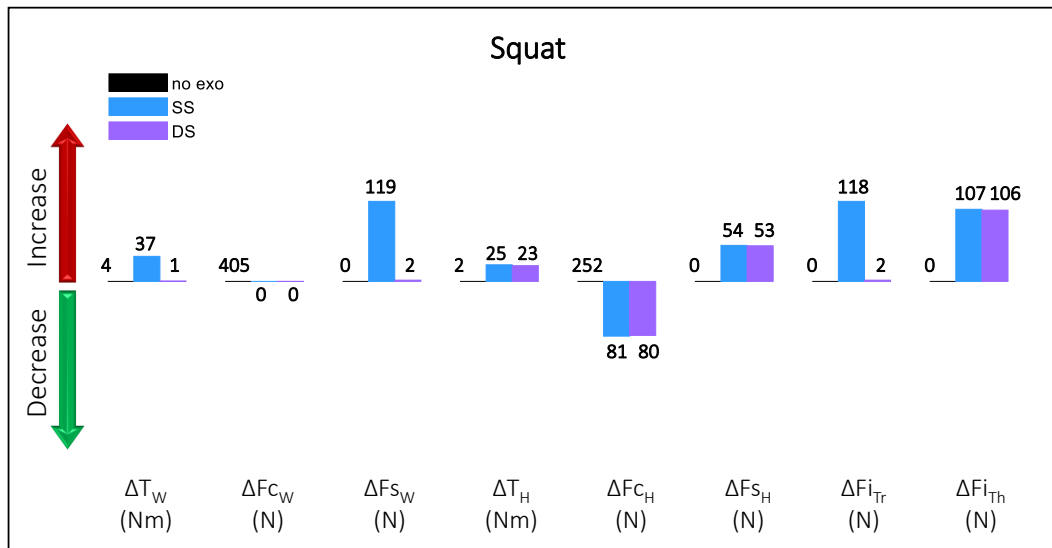


Figure 6.2.7: Relative variation of biomechanical variables during the squat motion when wearing the two different exoskeleton structures (blue and purple columns) compared to the physiological condition without the exoskeleton (black reference line).

The following figures sum up the biomechanical results. The graph background allows the interpretation of values, stressing the suitable (green area) and negative (red area) percentages. Figure 6.2.8 A and Figure 6.2.9 A show respectively the human waist and hip joint moments developed during the motion in the three different lifting strategies (stoop, semisquat and squat) and with the three human-device configurations (without the exoskeleton, with SS exoskeleton and with DS exoskeleton). The movements are expressed as a percentage of the total cycle simulation. The different lifting strategy strongly affects the results. In the stoop strategy (Figure 6.2.8 A - Figure 6.2.9 A), both exoskeleton solutions partially reduce the hip torques with a positive effect on the human body, while only the SS configuration contributes to reduce the waist torque (around 45% of reference value). In the DS exoskeleton, since there is no relative motion between trunk support and pelvis belt, the spring does not supply any assistance and the device reveals to be unsuitable to reduce human waist torque.

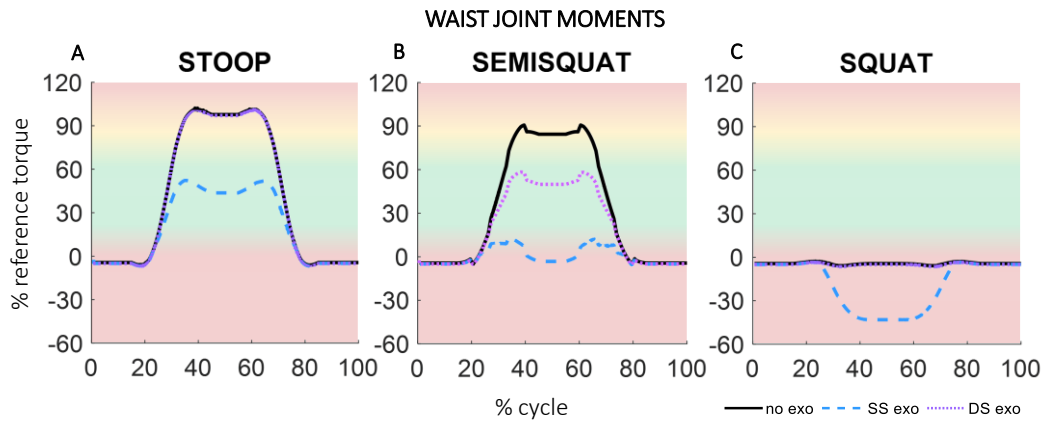


Figure 6.2.8: Torques results at the human waist joint in (A) stoop, (B) semisquat and (C) squat. Graphs compared the 3 conditions: without (no exo), with single (SS exo) and with double (DS exo) support exoskeleton. The background highlights suitable values.

In the semisquat motion (Figure 6.2.8 B - Figure 6.2.9 B), both exoskeleton configurations reduce the physiological required waist and hip torques. However, the SS configuration reduces the loads up to zeroing it. This might result in a perceived negative aspect by the user. Since the user is a healthy worker and the device must partially contribute to the human efforts, the strong and excessive reduction of human joints loads results to be a critical outcome. The user might perceive the lack of control in performing the task. The total absence of muscular contribution may be a risk of injury comparable with overloads. In the SS configuration, the exoskeleton supplies assistance with the variation of the relative motion between trunk and thigh supports that, in the semisquat simulation, reveals to be higher compared to the kinematics of the human waist joint. The DS configuration avoids that problem thanks to the splitting of support. Finally, in squat (Figure 6.2.8 C - Figure 6.2.9 C), both SS and DS configurations are unsuitable for the assistance of the user. Indeed, due to the maintenance of human trunk in an upright posture (flexion angle = 0°), the human body joints do not require any assistance during squat. The DS does not supply torque assistance to the waist joint, while the hip torque is negative. Similarly, the SS configuration records a relative motion between trunk and thigh supports and assists both waist (-40%) and hip (-35%) joints, causing the over-reduction of torques. The inversion of the curves can be translated as the requiring of greater core and lumbar muscle activations in order to contrast the exoskeleton action and to pull down the device. During squat, the external device might cause discomfort, require a torque opposite to the physiological one and encumbrance. These results strongly agree with experimental tests conducted in [88, 93], which assessed a passive commercial exoskeleton in human daily and working activities. During squat, the perceived difficulty and discomfort resulted higher than without exoskeleton. In this case, the exoskeleton contribution did not provide support in performing motion.

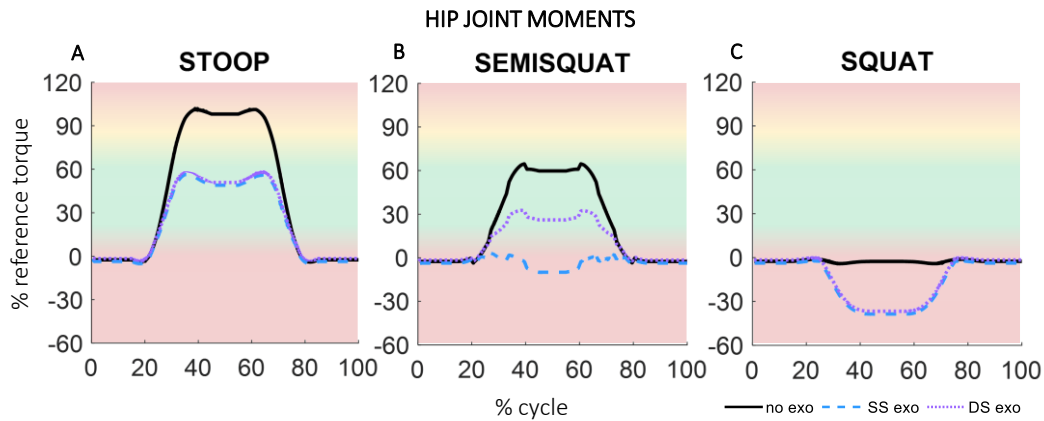


Figure 6.2.9: Torques results at the human hip in stoop (A), semisquat (B) and squat (C). Graphs compared the three conditions: without (no exo), with single support (SS exo) and with double support (DS exo). The graph background highlights the range of suitable values.

Intersegmental forces are also evaluated. Figure 6.2.10 shows the maximum peak of intersegmental forces at the waist (compression forces C_W and shear forces S_W) and hip (compression forces C_H and shear forces S_H) in the three lifting motions. The peak values of compression and shear forces has been normalized with reference values, corresponding to the maximum compression force registered during standing position and the maximum shear force developed with a 90° trunk flexion respectively.

The stoop motion (Figure 6.2.10 A) shows a limited peak value of C_W and C_H in the absence of the exoskeleton (20% of reference value). The presence of SS or DS exoskeleton does not entail a variation of C_W , while C_H increases in both cases, reaching 40% of the reference value.

S_W and S_H reach values near to 90% reference value without the exoskeleton. With the SS configuration S_W is reduced to 60%, while with DS exoskeleton there is no change and the value 90% is reached. Concerning S_H , with both exoskeleton configuration the force increases and reaches the 115% of the reference value.

In the semisquat motion (Figure 6.2.10 B), the C_W does not underline any differences between exoskeleton conditions, for a total of 50% of the reference value.

Both the SS and DS configurations register a C_H reduction (30% and 70%) compared to the no exoskeleton condition (100%). The exoskeleton solutions reduce the S_W , while they have a negative consequence on the S_H .

In squat (Figure 6.2.10 C), despite the absence of exoskeleton effects on the C_W and the reduction of the C_H (from 100% to 70% of reference value), it is possible to stress the increase of S_W and S_H with the SS exoskeleton and the increase of S_H with DS configuration.

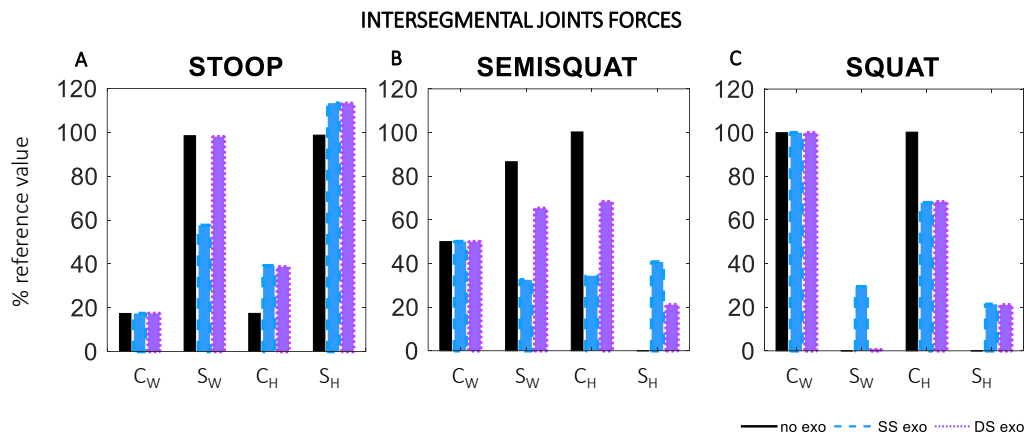


Figure 6.2.10: Compression and shear forces at the waist ($C_W - S_W$) and hip ($C_H - S_H$) in stoop (A), semisquat (B) and squat (C). Bar graphs compared the three conditions: without (no exo), with a single (SS exo) and with double support (DS exo) exo.

Considering the results, it is possible to conclude that C_W in anycase is not affected by the presence of the exoskeleton. Some considerations can be pointed out concerning S_W , C_H and S_H . Both SS and DS configurations impose an increase of S_H in all motions; this increase is linked with the intensity of the external applied torque. Hence, a particular attention should be payed when setting the maximum assistance torque supplied by the exoskeleton, to prevent any injuries, overloads and discomfort to user. About the S_W and C_H , it is not possible to generalize their trend, since they strictly depend on the lifting motion.

Figure 6.2.11 and Figure 6.2.12 describe respectively the human trunk and thigh interface pressures developed during the motion in the three different lifting strategies (stoop, semisquat and squat) and with the two exoskeleton configurations (with SS and DS exoskeleton). On the x-axis the percentage of the total cycle is reported, as in the previous graphs.

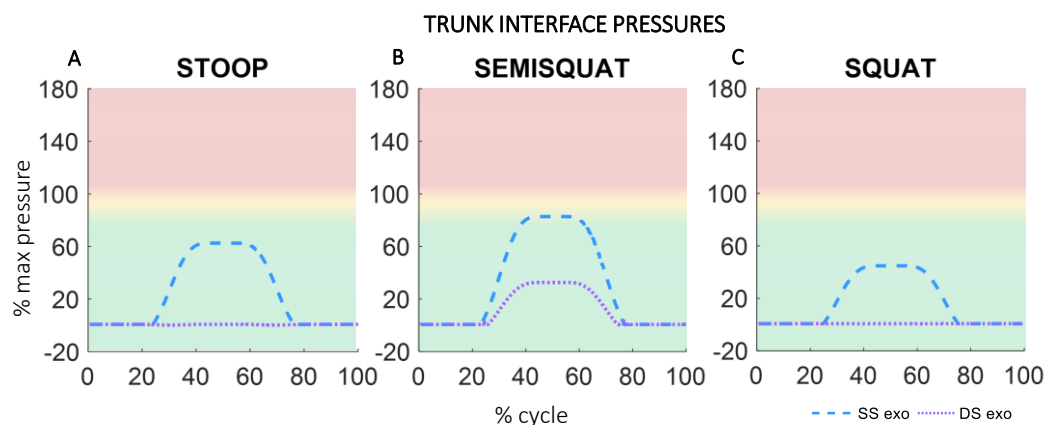


Figure 6.2.11: Interface pressures results at the human trunk in stoop (A), semisquat (B) and squat (C). Graphs compared the two-exoskeleton conditions: with single support (SS exo) and with double support (DS exo). The graph background highlights the range of suitable values.

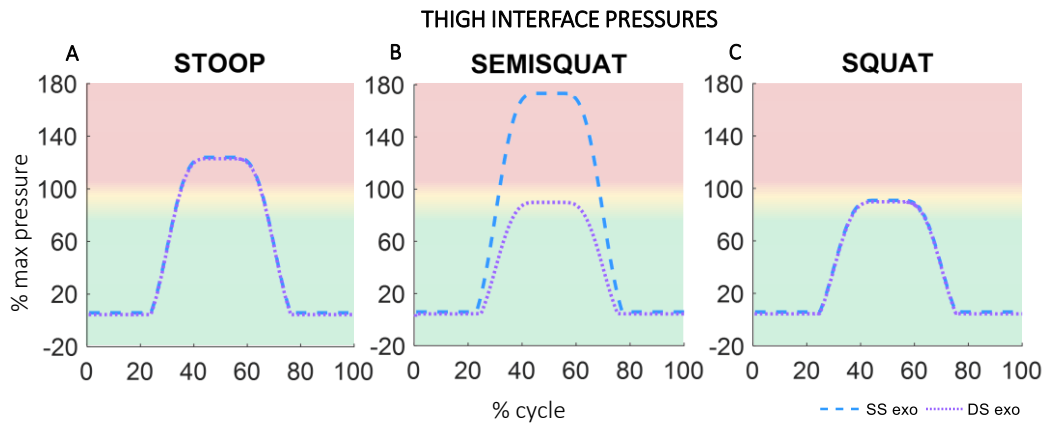


Figure 6.2.12: Interface pressures results at the human thigh in stoop (A), semisquat (B) and squat (C). Graphs compared the two-exoskeleton conditions: with single support (SS exo) and with double support (DS exo). The graph background highlights the range of suitable values.

Curves are stated as a percentage of a reference value of maximum pressure (15 kPa) that can be endured by the human body without feeling discomfort. As already mentioned, to direct refer the interface forces, a circular trunk pad area with 150 mm diameter and a circular thigh pad area with 100 mm diameter have been hypothesized.

For the trunk contact (Figure 6.2.11), both SS and DS exoskeleton do not exceed a critical value of interface pressures in all motions, with a maximum of 80% and 30% respectively during the semisquat (Figure 6.2.11 B). Considering the thigh interface (Figure 6.2.12), both configurations exceed the pressure threshold of tolerance in stoop motion (Figure 6.2.12 A) for a maximum peak of 120% of reference pressure.

In the semisquat (Figure 6.2.12 B) only the SS configuration shows critical values near to 170% of reference pressure.

In the squat movement (Figure 6.2.12 C), both configurations involve a large value of interface pressure (around 90% of reference value), but without overcoming the discomfort threshold.

These results are strongly affected by the design of the exoskeleton pads area. Moreover, the pressure threshold has been defined based on previous literature results [135], but it must consider the different subjective perception of discomfort and pain. In addition, trunk and thigh segments show different tissues and muscular composition, so they might perceive and tolerate different pressure levels, while in that case it has been considered the same value. Nevertheless, the present study highlights the importance of interface quantification in order to limit the perceived discomfort and pain. At the same time, the analysis shows the possibility to design the contact area of exoskeleton pads based on the simulation approach.

In conclusion, when simulating the three lifting strategies, the summary in Table 6.2.2 allows comparing the effect of the two device configurations on several biomechanical variables. It should be a helpful instrument to point out the

advantages and the drawbacks of the two design solutions, to characterize the exoskeleton assistance, related to the motion required by specific industrial tasks. The simulation highlights the relationship between the adopted lifting kinematics and the support provided by the wearable device.

Both the analyzed exoskeleton configurations reveal positive effects in specific conditions, but without completely avoiding drawbacks and possible discomfort. Based on the simulation, the SS configuration reveals greater advantages in the stoop motion, and it can be suitable for industrial tasks that require holding a static trunk-flexed posture, even for a long time. Both the semisquat and the squat motion might be negatively affected by the exoskeleton assistance.

Thanks to the separation of assistance joints at two different levels, the DS configuration can differentiate the pelvis-trunk and pelvis-thigh relative motion. It reveals some fundamental advantages in the case of semisquat, which can be considered the most adopted strategy for lifting external objects during industrial activities [26, 41]. However also the DS configuration exhibits inaccurate adaptation in the case of squat motion, and it reveals no effects during the stoop. The principal reason for the exoskeletons' ineffectiveness or even worse encumbrance could be explained by the fact that the spring supplies a passive force whenever a relative rotation between the links takes place, without differentiating the trunk and leg flexion. This behavior can be avoided with the introduction of active joints and customized exoskeleton assistance laws.

Table 6.2.2: Comparison of the two passive exoskeleton structure (Single and Double Support) in terms of biomechanical effects on human variables.

EFFECTIVENESS OF EXOSKELETON ASSISTANCE						
<i>Exoskeleton configurations</i>	Single Support			Double Support		
<i>Lifting strategies</i>	STOOP	SEMISQUAT	SQUAT	STOOP	SEMISQUAT	SQUAT
Waist torque	✓	✗	✗	○	✓	○
Waist compression force	○	○	○	○	○	○
Waist shear force	✓	✓	✗	○	✓	○
Hip torque	✓	✗	✗	✓	✓	✗
Hip compression force	✗	✓	✓	✗	✓	✓
Hip shear force	✗	✗	✗	✗	✗	✗
Trunk interface force	✓	✓	✓	○	✓	○
Thigh interface force	✗	✗	✗	✗	✗	✗




 Negative effect
 No effect
 Positive effect

Figure 6.2.13 and Figure 6.2.14 report the biomechanical effects on the human waist and hip due to the two kinematic combinations of stoop and squat and the two exoskeleton configurations. In the stoop-squat motion (A) the DS configuration is more suitable than the SS configuration because it could partially assist the user (up to 50% and 30% of reference value respectively for waist and hip joints).

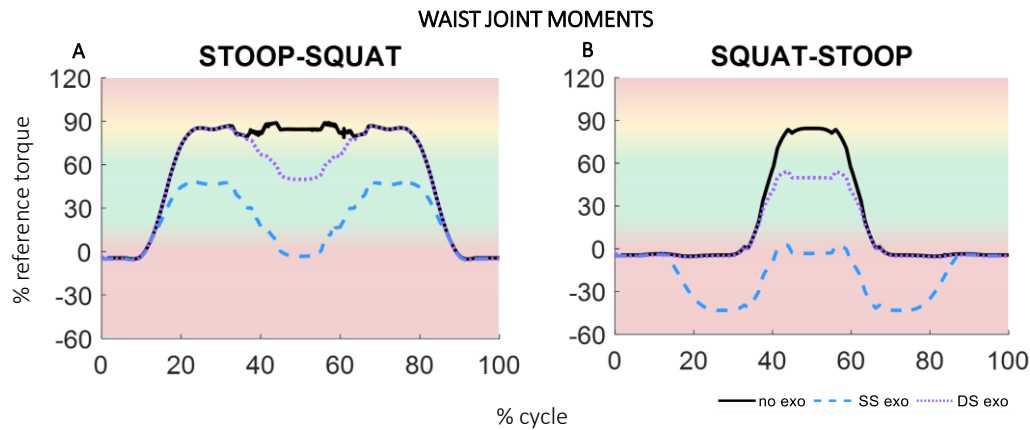


Figure 6.2.13: Torques results at the human waist joint in combined motion stoop-squat (A) and squat-stoop (B). Graphs compared the three conditions: without (no exo), with single support (SS exo) and with double support (DS exo) exoskeleton. The graph background highlights the range of suitable values.

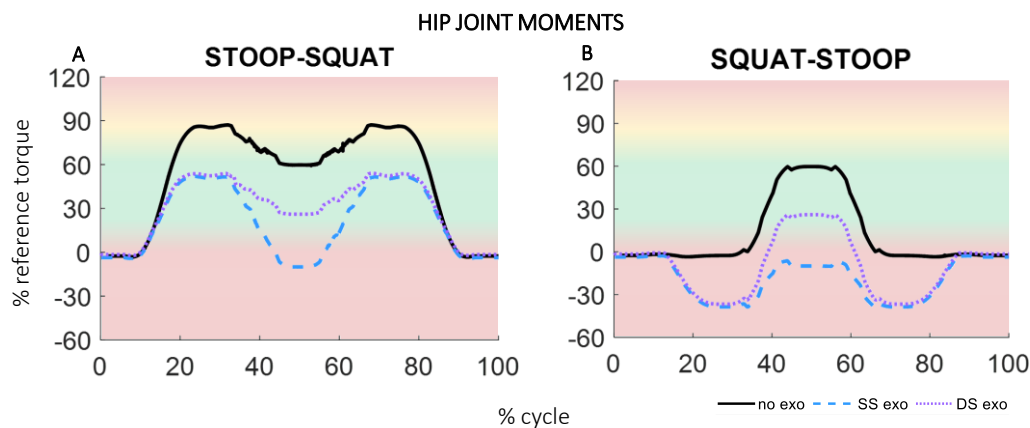


Figure 6.2.14: Torques results at the human hip joint in combined motion stoop-squat (A) and squat-stoop (B). Graphs compared the three conditions: without (no exo), with single support (SS exo) and with double support (DS exo) exoskeleton. The graph background highlights the range of suitable values.

Even though the positive effect of the SS configuration during the stoop flexion and extension phase, the exoskeleton supplies additional assistance when the human body started the lower limb flexion (squat phase), causing an excessive torque reduction both at waist and hip.

Considering the squat-stoop movement combination (B) the SS exoskeleton reveals to be unsuitable for both joints, requiring additional human muscle activation (up to 50% and 30% of reference value respectively for waist and hip

joints) in order to flex the trunk with the exoskeleton. The DS configuration reduces waist joint effort from 80% to 50% with respect to the reference value, while it supplies too much assistance torque at the hip joint, with an additional request of muscle effort (up to 30% of reference value).

Conclusion. The current study presents a computational approach to investigate two trunk-support device configurations through the evaluation of the effects on human body biomechanics and human efforts reduction. Both exoskeleton configurations show advantages and partial support to the user in specific tasks. Some discomfort and disadvantages due to the mechanical structure and assistance characteristics may occur. Passive solutions with elastic elements limit the encumbrance and the weight of the structure, but they reveal to be suitable only for some specific tasks. The adaptation of the passive system to a specific user kinematic law requires different architecture of the device and different levels of assistance. These drawbacks could be overcome by the introduction of an active joint and a suitable mechanical structure. The powered exoskeleton might be able to recognize the human body motion and consequently adapt the assistance as needed, based on the human body joint kinematics. A deeper investigation designing different laws needs to be investigated.

6.3. Simulation maps for differentiating lifting strategies

Based on previous experimental and simulation results, some limitations and drawbacks concerning the passive exoskeleton can be summed up. Indeed, the passive exoskeleton assists the user in lifting tasks with flexed trunk and extended lower limbs, but it is not suitable when the user maintains the trunk aligned to the vertical position and bends the knees, as in semisquat and squat motions. Moreover, despite the restrained weight and encumbrance, the device may cause an increase of perceived discomfort to the user in specific tasks and body positions. A powered solution modulating a proper law of assistance might compensate the previous reported limitations, by modifying the assistance torque based on the adopted lifting strategy, or more in general on the user's joint kinematics. Moreover, the assistance can be customized on the user's anthropometry and personal preferences. For the development of the powered exoskeleton and the identification of components and sensors that must be integrated, the definition of the assistance law is fundamental. For these reasons also in this case the computational approach is employed.

As depicted in Figure 6.3.1, different human body poses can be assumed by the user without changing the absolute flexion angle of the trunk (α angle), while the angles of the lower limb joints is different.

Figure 6.3.2 shows the three main lifting strategies and a simple stick-diagram of the human body, distinguishing an upper and a lower segment, is superimposed to the photos.

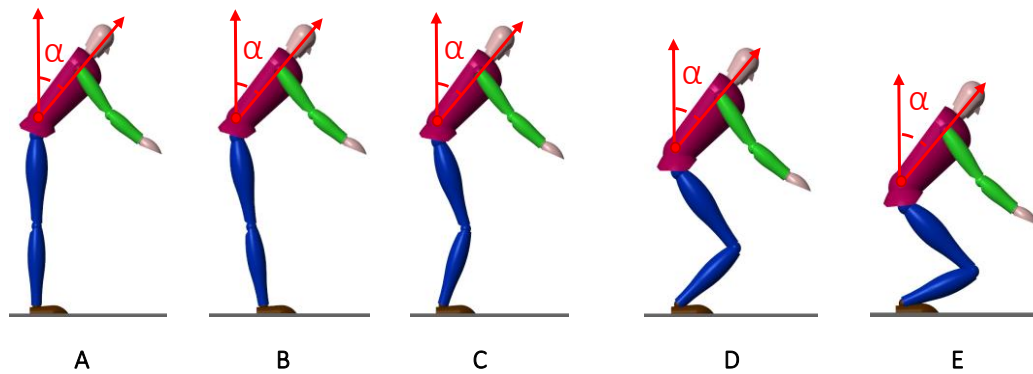


Figure 6.3.1: Different human body poses assumed by the user without changing the absolute flexion angle of the trunk: (A) stoop, (B) stoop with extended hips, (C) semisquat; (D) squat; (E) deep squat.

The body stick diagram outlines the principal angles involved during the lifting motions that need to be considered for the development of a suitable assistance strategy. Starting from the standing posture (Figure 6.3.2 A), the body segments are aligned with the vertical direction. In particular, the angle between the upper and lower segments (β angle) can be assumed as 180° . When performing a stoop motion, even if the subject may extend the lower limb with negligible hip iper-extension and anterior pelvic tilt (Figure 6.3.2 B), the variation of β angle corresponds to the trunk flexion with respect to the standing posture (α angle).

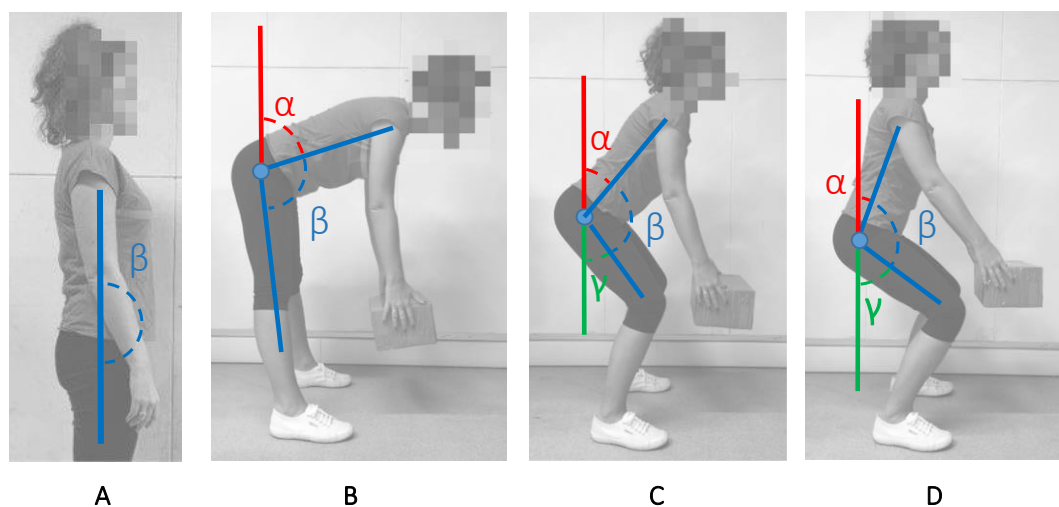


Figure 6.3.2: Starting from the standing posture (A), a description of principal angles involved during the three main lifting strategies: (B) stoop, (C) semisquat, (D) squat.

When also the lower limbs are involved in the motion, as in semisquat and squat movements, the stick diagram depicts a relative movement between the two segments and an absolute rotation of both upper and lower segments respect to the vertical direction. Three main angles can be underlined: α angle (trunk flexion), β angle (between upper and thigh segment) and γ angle (thigh flexion from the vertical direction) (Figure 6.3.2 C-D), where $\alpha + \beta + \gamma = 180^\circ$. The exoskeleton device that presents the single support configuration considers the relative motion between

upper and lower body. In stoop strategy, the exoskeleton monitors the β angle and correctly provides the required amount of assistance. Nevertheless, in case of squat and semisquat motion, the exoskeleton provides the assistance independently to α and γ values, without considering the whole posture performed by the user. Due to the different combinations of α and γ angles, the monitoring of β angle only is not adequate to differentiate lifting strategies and one other angle (α or γ) needs to be measured.

As already stressed in the previous analysis, the passive mechanism of Laevo exoskeleton modifies the assistance torque based on the β angle, without recognizing if it is caused by a trunk flexion (α angle) or hips-knees-ankles flexion (γ angle). This characteristic may reveal perceived discomfort and augmented obstacle to human movement during semisquat and squat lifting, as confirmed by literature and current experimental and simulation tests. When the user tries to perform a squat lifting with the maintenance of trunk aligned to the vertical direction, the exoskeleton increases the assistance with the increased flexion of lower limbs. Instead of supporting, the exoskeleton contribution may push the user's trunk in iper-extension position and additional muscular forces are required from the human back to contrast this action.

Considering the biomechanics of the lifting strategies it will be suitable to supply assistance during static flexed posture and during the extension phase, without or reduced support during the flexion phase. Finally, in passive exoskeleton, the stiffness of the spring is fixed, without the possibility to adapt it to different anthropometric, mass and needs of the user. The powered prototype integrated with a proper actuator system and control law might overcome all these limits. Figure 6.3.3 depicts a scheme of the exoskeleton considering the previous reported angles. The evaluation of a suitable support law for the active exoskeleton is defined using the previous presented multibody models.

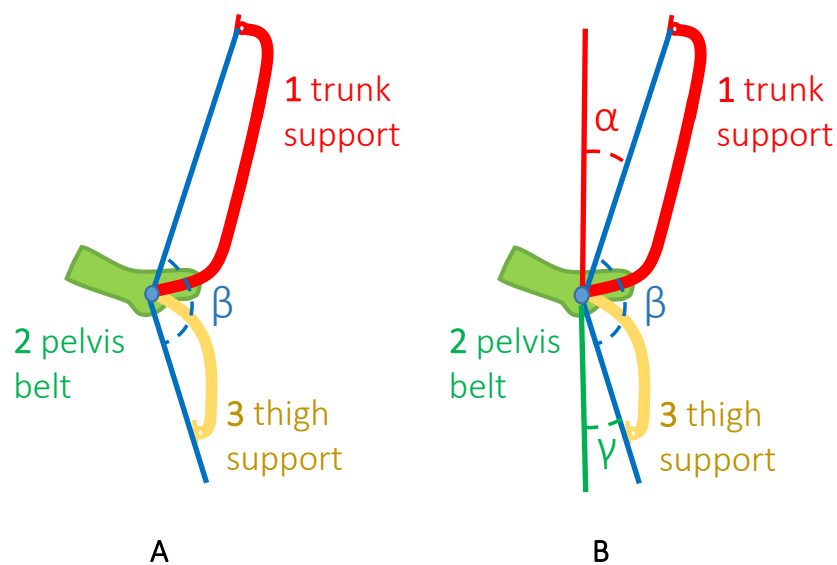


Figure 6.3.3: Graphical schematization of the angles involved in the definition of mechanical assistance in the passive (A) and powered exoskeleton (B).

Simulation Design. The human body and the exoskeleton model used for the analysis are the same presented in the previous chapters. Three different conditions are simulated: without wearing the exoskeleton, with the passive exoskeleton and with the powered exoskeleton. In particular, in the passive system the law of assistance is fixed and is a function of the angle between trunk and thigh supports (β), while in the active solution might provide different torques of support according also to the capacity to differentiate β , α and γ angles. For this reason, the assistance law of the active device has been defined taking into account the drawbacks that emerged from the previous simulations.

The assistance torque is still applied between upper and lower exoskeleton structures, connected to the human trunk and thighs respectively. During the flexion phase (positive angular velocity), the assistance is set lower compared to the values provided in the extension phase (negative angular velocity). In this way, the exoskeleton can partially support the torque required to maintain the posture against the gravity force, but without any obstacles or the necessity for the user to provide additional muscle activity. Figure 6.3.4 depicts a graphical representation of the assistance law implemented in the model. The 3D map shows the variation of torque assistance (z-axis) based on the value of the trunk angle (x-axis) and the trunk angular velocity (y-axis). The map refers to a single joint, since considering also the contralateral one the values of the torque are double.

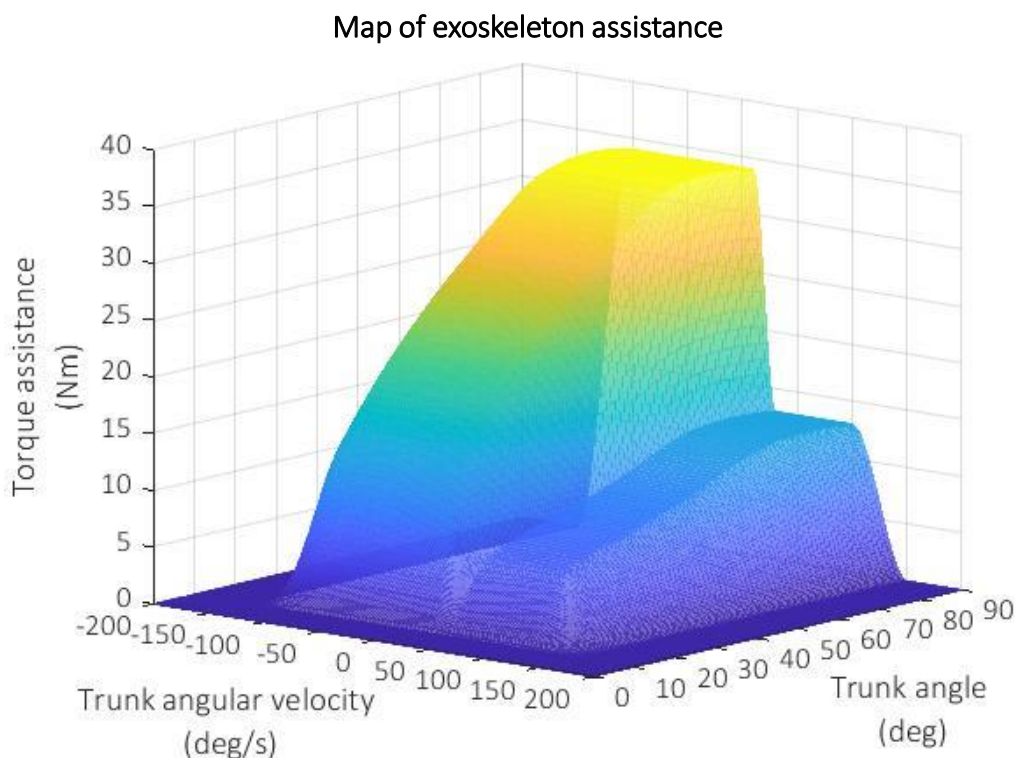


Figure 6.3.4: Example of assistance map based on the manikin parameters and joint loads calculation. The map represents the assistance law which must be implemented for each exoskeleton motorized joint, for the final support of 50% at the human waist.

The value of the assistance is scaled based on the anthropometric parameters of the manikin and provides maximum support of 50% of the waist torque required during 90° of trunk flexion with extended upper limbs and without external loads (around 130 Nm). Due to the considerations highlighted in the previous analysis, in the range of small trunk angles (0°-10°) the exoskeleton does not provide assistance, both during flexion and extension phase. This choice avoids the activation of core and back muscles to flex the device and does not activate the support in case of trunk oscillations in standing posture. Moreover, the range can be regulated based on the user's needs.

Based on the previous considerations, if the developed function is named *assistance*, the relation between torque and angle can be summed up. If

$$\gamma = 0$$

the exoskeleton torque is modeled as:

$$\tau_{exo} = f(\beta, \dot{\beta})$$

where $f(\beta, \dot{\beta})$ depicts the variation of the angle measured between the upper and lower supports starting from a reference position β_0 , while the sign of $\dot{\beta}$ is used for the discrimination between flexion and extension motion.

While, if

$$\gamma \neq 0$$

the exoskeleton torque is modeled as:

$$\tau_{exo} = f(\beta, \dot{\beta}, \alpha)$$

or

$$\tau_{exo} = f(\beta, \dot{\beta}, \gamma)$$

based on the monitoring of trunk support-pelvis belt angle (α) or thigh support-pelvis belt ones (γ). The recognition of lifting strategies allows the possibility of introducing an additional condition for the variation of assistance contribution.

Indeed, during squat and semisquat motion the user may require lower assistance compared to static and dynamic stoop posture with equal trunk flexion angle. Due to the flexion of hip and knee joints, the human body activates the muscles of lower limbs. In particular, the quadriceps femoris (vastus lateralis, vastus medialis, vastus intermedius and rectus femoris) carry out concentric knee extension, as well as eccentrically resisting knee flexion [137]. The exoskeleton push on the lower limbs through the thigh pads might create an additional discomfort during the holding flexed position and the extension phase. In addition, the discomfort can proportionally increase with the augmented degree of knees flexion. For this reason, the introduction of factor that can monitor the range of lower limb flexion and

reduce the assistance from the device might be a strategical solution to overcome discomfort and encumbrance perception.

For this reason, the previous equations are modified. If

$$\gamma \neq 0$$

the exoskeleton torque is modeled as:

$$\tau_{exo} = f(\beta, \dot{\beta}, a) * \cos \gamma$$

or

$$\tau_{exo} = f(\beta, \dot{\beta}, \gamma) * \cos \gamma$$

with $\gamma > \gamma_{threshold}$, where $\gamma_{threshold}$ represents a minimum thigh angle that must be reached in order to discriminate against the squat motion and to overcome. It considers possible misalignment of thighs with respects to the vertical direction due to the different user's anatomy, possible thighs oscillations during motion or comfortable posture chosen by the user with slight hip flexion. In the current computational analysis, $\gamma_{threshold} = 20^\circ$. The compensating factor is modeled as a cosine function of the γ angle. In that way, the assistance reduction will start from small values of γ angle and will be reset for γ angle near to 90° . Flexion and extension need to be differentiated. Indeed, during the flexion phase, in order to avoid any obstacles to human motion, the assistance torque must be lower. The monitoring of trunk angular velocities allows that differentiation, based on the sign of the parameter (positive for flexion, negative for extension). Finally, in order to avoid undesired discontinuities on the implemented curve, a 5th order polynomial function is used to interpolate boundary values. Figure 6.3.5 describes the assistance torque defined in the 3D map in relation to the trunk angular velocity (A) and trunk angle (B).

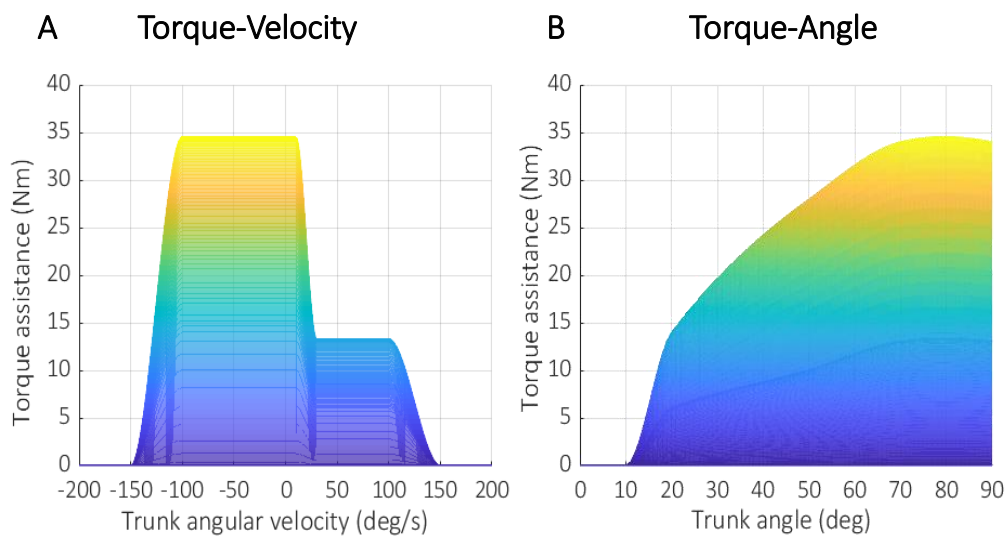


Figure 6.3.5: (A) Torque-Velocity and (B) Torque-Angle relation describing the assistance map.

The three conditions that characterized the type of exoskeleton (no exo, passive, powered) are implemented for two human lifting strategies with the attempt to verify the assistance both during stoop and squat movements. Both motions start with a small trunk flexion (15° at the waist joint and 15° at the hip joints), stop into a flexed position and restart the motion with different joints angles coordination. In the first case, the manikin flexes the trunk reaching 45° of flexion at waist joint and 15° of flexion at the hip joints, while the knees and ankles maintain the extended posture. In the second motion, the manikin flexes all the lower limb joints, performing the squat motion. In both kinematic strategies, the upper limbs perform the same range of motion, with a maximum angular flexion of 85° for the shoulder motion and 60° for the elbow motion. Figure 6.3.6 depicts the kinematic inputs during stoop and squat motion strategies of both upper and lower limb joints. Moreover, Table 6.3.1 depicts the curves and the maximum joints angle reached during the cycle at the lower limb. No external load is added in this simulation.

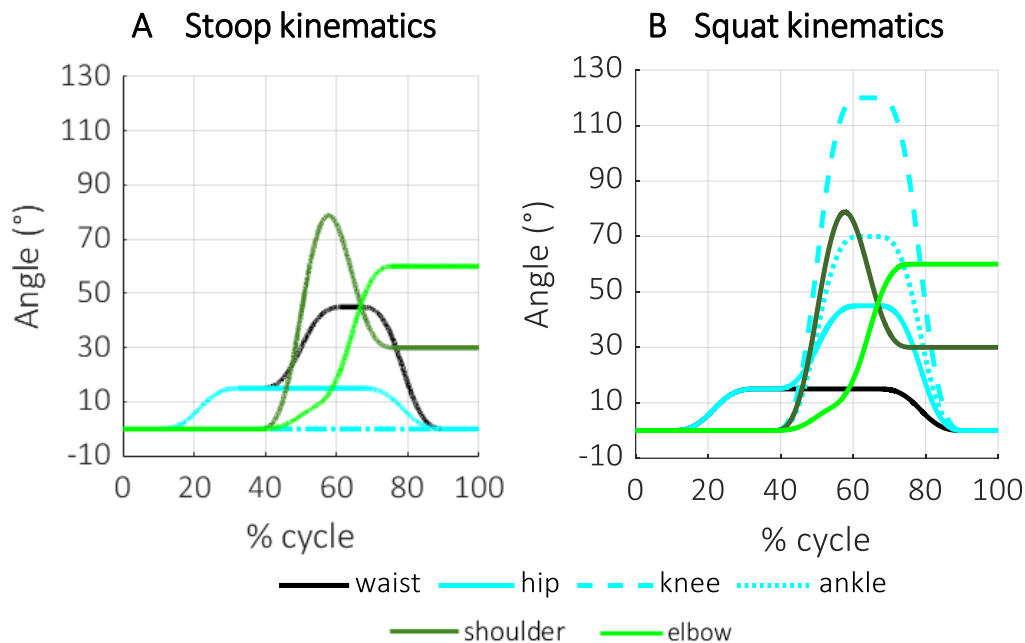


Figure 6.3.6: Graphical curves of the kinematic inputs for upper and lower human limbs in (A) stoop and (B) squat.

Results and Discussion. Figure 6.3.7 displays the comparison of the human joint kinematics (model inputs) during the two lifting movements, the angular trajectory of the human trunk respect to the vertical direction and the exoskeleton angles β between trunk and thigh support, α between trunk support and pelvis belt. Human and exoskeleton kinematics evaluating the trunk flexion differ because the different alignment of exoskeleton joint respect to human waist joint. From the kinematic curves, it is possible to stress the differences between stoop and squat movements, as to compare the human and exoskeleton joint angles. In the stoop (Figure 6.3.7 A) all human motion is concentrated at the waist and hip joints. The total trunk flexion reaches 60° as the maximum value. The relative angle between trunk and thigh supports (β) well approximates the human kinematics, with small

differences compared to trunk flexion (50° instead of 60°). Moreover, the relative angle between pelvis belt and trunk support (α) registers the same amount of β . In the squat motion (Figure 6.3.7 B) the graph stresses the large contribution of lower limb joints to perform the movement, while the human trunk reveals small degrees of flexion. In addition, considering the exoskeleton joint kinematics, a discrepancy between β and α is pointed out. The great disagreement between β and human trunk flexion depicts the misalignment in exoskeleton and human joints.

Table 6.3.1: Manikin motion schematization and maximum human joint angles.

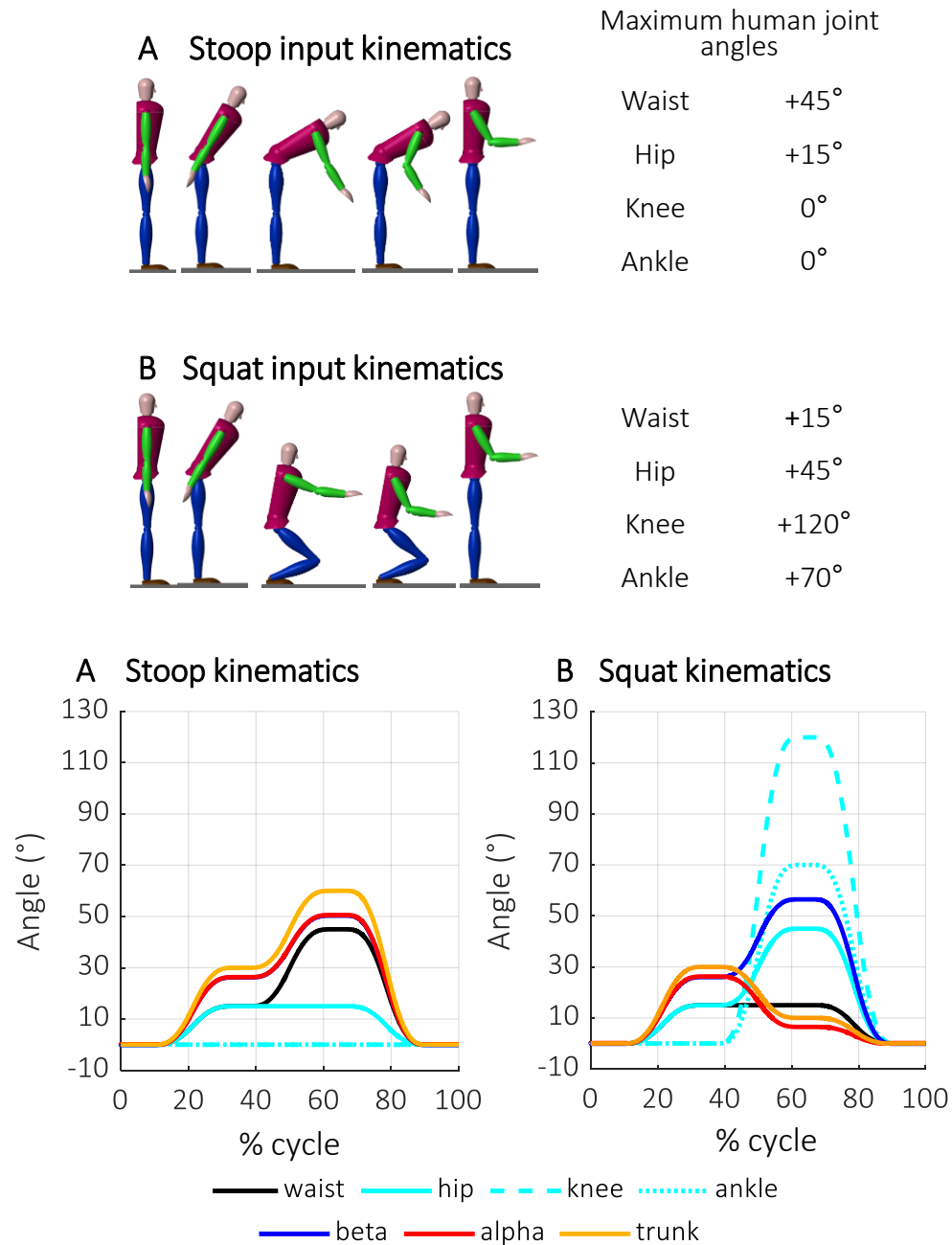


Figure 6.3.7: Kinematics of (A) stoop and (B) squat motions for the waist (black line) and lower limb (light blue line) joints of the human body manikin, the absolute trunk angle (orange line) and the exoskeleton β (blue line) and α (red line) angles.

Figure 6.3.8 shows the net moments results in stoop (A) and squat (B) simulations at the waist joint during the three exoskeleton conditions: without exo, with passive exo and with powered exo. The graphs depict also the exoskeleton assistance (T_{ass}) provided by the passive and powered structures. In the last case the torque map of assistance reported in Figure 6.3.4 is implemented.

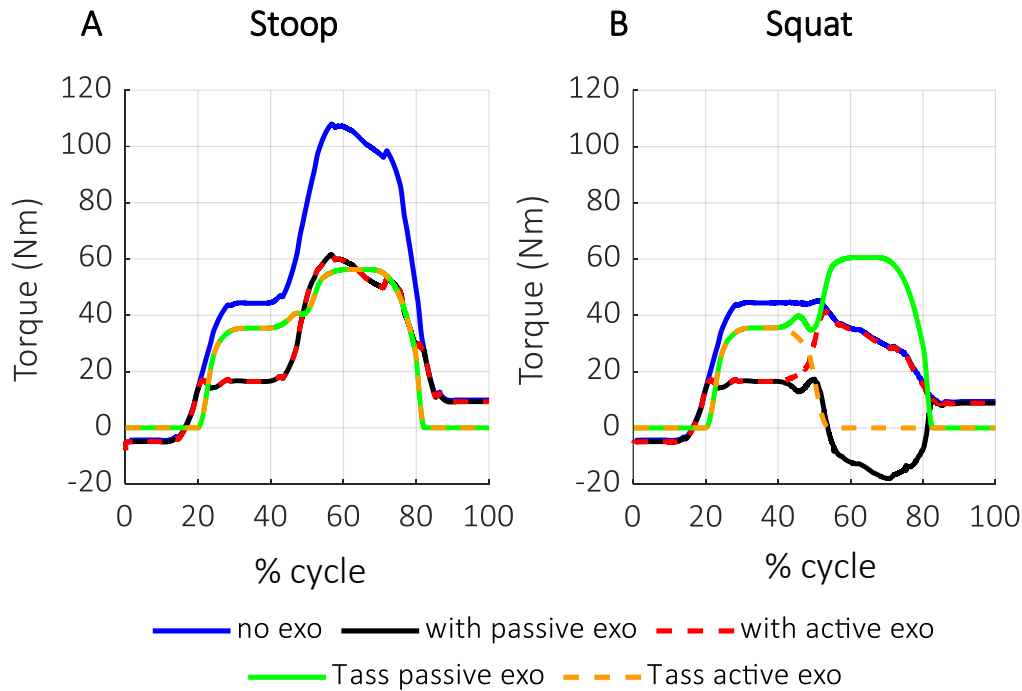


Figure 6.3.8: Comparison results of waist torques in the three simulated conditions (without exoskeleton, with a passive exoskeleton, with a powered exoskeleton) and exoskeletons assistance torque during (A) stoop and (B) squat motion.

The figure points out the level of support and human body reduction obtained in the two different cases, but also any possible exoskeleton drawbacks and limitations. In the first case, the assistance of an external device partially reduces the human body loads at the waist joint. The use of passive and powered exoskeleton reveals the same amount of exoskeleton assistance and, consequently, the same reduction of waist torques. No difference is highlighted between flexion and extension phases because the motion has been simulated slowly and the joint angular velocities are reduced. In the squat representation, the two exoskeleton conditions reveal similar behavior at the beginning and end of the cycle, with a partial reduction of human waist efforts. In this part, indeed, the γ angle results lower than imposed threshold of 20° . During the second part of the cycle, the passive exoskeleton increases the assistance (green line) causing the inversion of the waist torque. This fact can be translated as an additional requirement of back and core muscle activation in order to contrast the excessive exoskeleton push. The powered solution, instead, thanks to the recognition and differentiation of joints coordination, reduces the exoskeleton assistance until the zero value. For this reason, the waist torque overlaps the waist torque registered without the

exoskeleton. Finally, it must be noted that the negative torque registered at the beginning of simulation cycle is due to the human body center of masses positions.

Conclusion. The simulation results pointed out the effectiveness of the proposed assistance law and the possibility to properly modify the support based on the monitoring of human body kinematics. The powered exoskeleton well answers to the needs of motion differentiation and assistance adaptation, overcoming the limits of the passive solution. The definition of several maps of assistance as motor input may satisfy the different user's requirements of the higher or lower amount of support, also based on the anthropometric characteristics. The recognition of the trunk and leg flexion seems to be a suitable strategy to reduce the number of components required for the development of the powered solution. It guarantees at the same time lower weight and encumbrance from the mechanical point of view and the simplicity in assistance law regulation from the control side.

Chapter 7

POWERED PROTOTYPE: the actuation and control scheme

7.1. Introduction

The present analysis deals with the identification of a suitable actuator system, the design of the control architecture and the description of the assistive strategy that will be implemented for the estimation and providing of assistance torque. After a proper literature analysis and investigation of actuator solutions adopted for exoskeletons, the electric system and a two-level control scheme are identified as the best suitable proposal for the current application. This is a fundamental passage for the definition and selection of mechanical and electric components of the powered joint. Due to the crucial aspect of compliance at the human-device interface, the simulation modeling, design and development of a serial elastic actuator with a proper customized elastic element is presented as possible alternative solution or future perspective.

The chapter is organized as following:

- Analysis of the actuator solutions for wearable robotic devices;
- Selection of the suitable actuator system for the current study;
- Description of assistance strategy and implementation of the control architecture;
- Selection of electric components;
- Introduction to serial elastic actuator and literature analysis;
- Modelling, design and computational validation of customized elastic element and description of a suitable control architecture.

7.2. Actuation solutions for wearable robotics

For many years, “*the stiffer the better*” has been the reference statement for the development of robotic systems in traditional applications. Stiff actuators have been adopted in several classical robotic systems, both in the industry (pick and place operations) and rehabilitation (posture support and muscular training of human body parts) [138]. This can be explained because stiff actuators contribute to improve precision, stability and control of position movements and trajectory tracking. These types of actuators reveal to be fast-response systems with high bandwidth, the perfect choice for precise open-loop position control. Indeed, the increase of interface stiffness decreases the end-point position error in case of load disturbances.

In wearable technologies, such as orthoses, prostheses and exoskeletons, the robotic system is in direct contact with the human body. This interaction requires compliance and the capability of adaptation to unpredictable situation and variable environment. A perfect example of compliant actuators are the human muscles, that, in combination with a sophisticated neuromechanical control system, allow adaptation, modulation and tuning of parameters. Moreover, an ideal actuation system should provide zero stiction, zero impedance and infinite bandwidth. Among the real actuators, the human muscles represent the best type to satisfy these requests, due to the low impedance, low stiction and moderate bandwidth. The main characteristic that differentiates the biological system from the common mechanical actuation system can be identified in the like-spring behavior. A compliant actuator allows deviation from a position, depending on the applied external force. The equilibrium position is defined where the resultant of forces and/or torques results to be null. As a consequence, instead of the position control, the technological system has to supply the desired torque/force (τ_{des} / F_{des}) in response to the applied external load, with a proper ideal force/torque controlled actuator [139]. The ideal force-controllable actuator supplies exactly the required force independent of external environment movement and disturbance. Moreover, a low impedance allows also backdrivability. Hence, the use of a low impedance system might provide safety and stability in human-robot direct interaction.

Among the several types of actuators, the electric, hydraulic and pneumatic systems are the commonly adopted solutions both in traditional and wearable robotic systems. All actuators present both pro and cons due to their intrinsic limits (bandwidth dimension, stiction, impedance), avoiding the possibility to identify the ideal system. Considering the powered exoskeletons development, several commercial and research prototypes have been proposed with all these three actuator solutions.

The actuation system needs to be prompt to generate the appropriate force/torque, which can be translated in high bandwidth capabilities. The safety is one other fundamental aspect that must be considered due to the direct contact between the user and the device. Unfortunately, all the expected requirements are

often in conflict and difficult to achieve, hence it is necessary to look for compromises.

Electrical motors. Electric motors are the preferred solution for most of the robotic applications because they are relatively easy to install, to integrate with the mechanical structure and to control in case of pre-defined position. They reveal good stability in position control. Nevertheless, the electric motors have large mass with low power to weight and volume ratio. Moreover, in many applications, the electric motors need to be coupled with gear-boxes reducers to increase the output torque, which introduces additional weight, backlash and friction. Concerning the reflected inertia, the introduction of reducer with N ratio contributes to positive effects if considering the motor side, while it could reveal some problems and crucial increases if seen from the load. Finally, heat dissipation is another problem to be solved with electric motors [140].

Hydraulic actuator. Hydraulic actuators use fluid to transmit power to the actuated joint. Hydraulic system presents a high bandwidth, they can provide very high force/torques and stiffness compared to any other solutions. However, hydraulic solutions are rather complex, the power supply is problematic and cumbersome. The structure might be unsuitable for many robotic applications requiring reduced weight and encumbrance. It results difficult to backdrive and with high level of stiction. Cause by the presence of liquid, the efficiency might be lower than other solutions [141].

Pneumatic actuator. Pneumatic actuators use air to generate output forces. Compared to hydraulic systems, pneumatic actuators have a lighter and simpler construction. These characteristics depict lower weight and encumbrance, but also reduced cost. Pneumatic actuators have a higher power to weight ratio if compared with electric motors, but it is less than hydraulics. However, these solutions have lower positional stiffness than other common actuators cause by the compressibility of the gas. The external gas source might reveal increased discomfort, risk and encumbrance when the robotic system is applied in specific applications with reduced workspace. Moreover, a relatively low bandwidth capability and static friction problems might cause the unsuitability of the system [141].

Table 7.2.1 sums up advantages and drawbacks of the most common actuators (electric, hydraulic and pneumatic) adopted for powered exoskeletons.

Table 7.2.1: Description of the most common actuators solution for the development of powered exoskeleton, stressing the advantages and the drawbacks.

Actuators for exoskeletons			
	Electric system	Hydraulic system	Pneumatic system
✓	<ul style="list-style-type: none"> • Optimal position control • Easy integration with the system 	<ul style="list-style-type: none"> • Force / Torque >> • Bandwidth capability >> 	<ul style="list-style-type: none"> • Good compliance • Light and simple structure

×	<ul style="list-style-type: none"> • Stiction >> • Force / Torque << • Reflected inertia >> ($J_{eq} = J_m N^2$) • Difficult to backdrive • Heat dissipation 	<ul style="list-style-type: none"> • Stiction >> • No backdrive • High encumbrance due to structure • Low efficiency due to liquid 	<ul style="list-style-type: none"> • Efficiency in position control << • Bandwidth << • External gas source
---	--	--	--

7.3. Exoskeleton actuator selection

Among the three main solutions presented in the previous section (electric, hydraulic and pneumatic), the electric system is considered for the current exoskeleton prototype. Indeed, the easier integration to the structure due to the compact geometry, the smaller and lighter structure, and the possibility to obtain larger assistance torque with the motor-reducer coupling are considered as primary requirements. Recent technologies provide compact electric systems that can be easily integrated in a wearable structure in correspondence of the actuated joint, with restrained encumbrance and weight. Moreover, the electric actuation results as the most common solution adopted in powered exoskeletons in current researches [76, 142].

Smaller and lighter actuator might provide small torque, particularly if compared with the human joint torques required in performing motion. In addition, the human body motion is characterized by smaller angular joint velocities. Due to the specific application and the interaction with human body, the motors need to be coupled with a gear reduction system, with the main attempt to increase the supplied torque and reduce the velocities. Figure 7.3.1 describes the interaction between the powered wearable device, that is represents by the motor-reducer coupling, and the human body, represented by the load.

Exoskeleton – Human Interaction

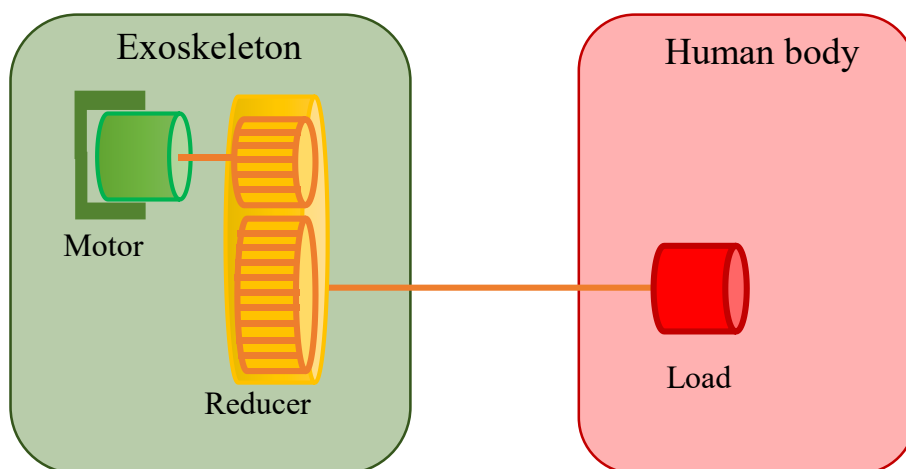


Figure 7.3.1: Description of powered exoskeleton (motor-reducer) and human body (load) interaction.

Current control can then be applied to the geared actuator to control force output. The increasing of reflected inertia seen from the load caused by the gear reduction might result in poor force fidelity and the actuator's impedance might become extremely large. A closed loop control with integrated force sensor might mitigate the undesired effects of friction and inertia.

Nevertheless, the closed loop control might enhance instability problems due to the stiffness characteristics of the load cell. Indeed, in case of small movements due for example to human physiological oscillations, the load sensor may register large force readings. With the attempt to reduce the mechanical impedance, the high-gain feedback controller would promptly act on the actuator, in order to reduce interaction force. Nevertheless, the result would be chatter between the actuator and the user. A low-gain feedback controller might overcome the instability problem, but it will result in slow and inappropriate control system [138].

The positioning of elastic element in series to the motor-reducer system has revealed to be a possible solution. The monitoring of elastic element deformation transforms the force-control into a positioning-control. In addition, the elastic element might provide the required compliance to filter motion oscillations and tremors that need to be neglected by the actuator side. The positioning of elastic element (torsional/linear spring) in series to the actuator system depicts the implementation of a serial elastic actuator (SEA).

Nevertheless, the implementation of SEA depicts some disadvantages and difficulties in terms of customized spring design, spring stiffness selection, experimental validation tests, cost and time.

During the last years, some innovative researches have tried to overcome the limits and the difficulties of SEA. Indeed, even though in rehabilitation the compliance of the serial elastic actuator revealed to be fundamental for exoskeletons for the safety of the patient and for filtering any tremors or disturbances, some clinic [143, 144] and industrial [142] exoskeleton solutions proposed the electric actuator without the spring. The ergonomic requirements, the inherent human compliance due to the human soft tissues and the additional exoskeleton compliance due to the soft materials used for contact pads reduce the need for series-elastic actuation. Moreover, the industrial exoskeleton must interact with healthy users, which rarely present tremors and shocks that must be filtered. The spring can be omitted thanks to a proper design of interface contacts areas, the implementation of stable torque control and the integration of mechanical safety mechanisms. The presented idea has been adopted for the development of the current first prototype and a proper control architecture based on torque control is proposed.

7.4. Control Architecture: model-based strategy and torque control

Considering the previous studies on exoskeletons and wearable technologies, several control strategies have been proposed and implemented. Yan and colleagues review the most common assistant strategies implemented in power lower limbs wearable devices [145].

The control system presents a hierarchical architecture, with several level of control loops. The number of levels defines the complexity of the control scheme and each level must be correctly defined and implemented. The high-level control depicts the desired torque that must be applied by the device as assistance to the human body. Different methodologies can be applied, and several sensors can be adopted in order to calculate the desired torque from the measured biological signals. As previously mentioned, some clinic [143, 144] and industrial [142] exoskeleton solutions proposed control architecture base on torque control. The inherent human compliance provided by soft tissues and the additional exoskeleton compliance provided by the soft materials used for contact pads contribute to overcome limitations of the stiff electric motor.

In the current study, a two-level control strategy is adopted. The high-level control imposes the desired torque to the device. The human motion is described by the angular displacement between human body parts (trunk, pelvis, thighs). Through the model-based analysis and the 3D maps of assistance, the desired torque assistance can be supplied to the user. The low-level control consists in the direct manage of the actuators in a closed-loop control. In the current study this is a classical proportional-integral (PI) regulator. The PI regulator calculates the current error between the desired current imposed as input and the measured feedback motor current. Based on the error, the electrical current provided to the motor will be modulated. The regulation of the current is directly linked to the motor torque by means of the torque constant. The tuning procedure of the motor driver allows to define the control parameters. At this starting solution, the power supply and the master control are thought external to the structure. This strategy reduces the total weight of the device and allows the improving of the system in following steps. Acquisition data system and communication interface device are necessary to register the sensors data and to provide connection between the control master and the motor drivers.

Figure 7.4.1 sums up the proposed control architecture of the device, the two levels of control and the several components needed for the implementation.

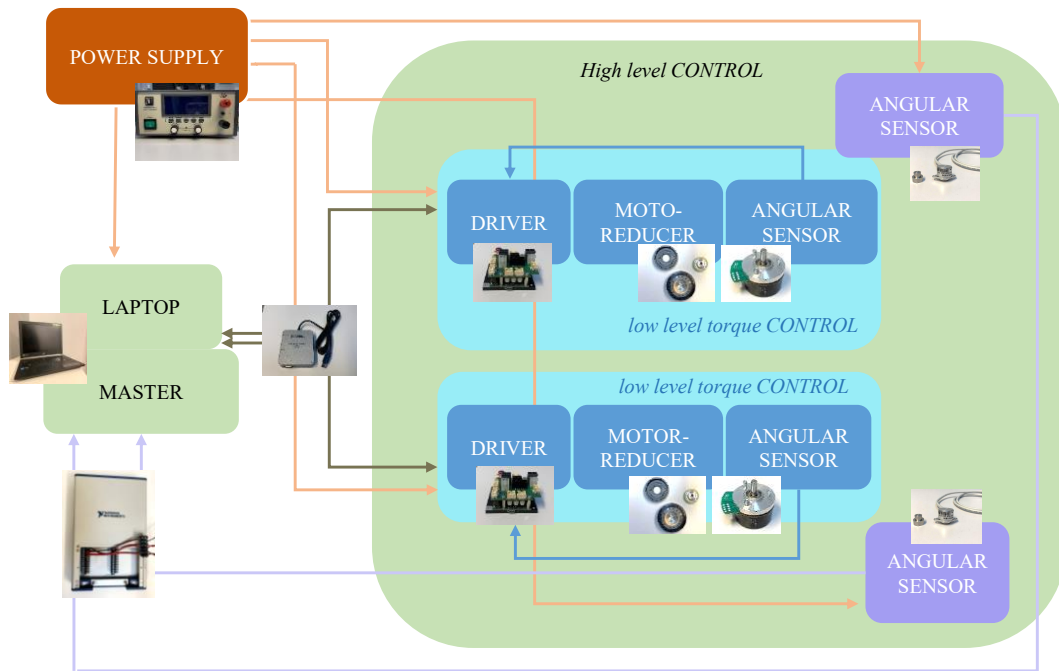


Figure 7.4.1: Concept of the torque control scheme of powered exoskeleton without the elastic element. Two main levels of control: high-level control and low-level control.

7.5. Electronic components

The control hardware of the powered exoskeleton consists of:

- Driver EPOS4 Compact 50/15 CAN by Maxon Motor for the communication with actuators;
- CAN (Controller Area Network) communication interface device USB-8502 by National Instruments for the connection between drivers (slave nodes) and master control unit;
- DAQ system USB-6341 by National Instruments for the acquisition of kinematic sensors data;
- Personal laptop with Microsoft Windows operating systems and Labview software for developing input desired torque.

The EPOS4 driver is a small-size, full digital motion controller able to operate in position, velocity and current control modes. The high-power density allows flexible use for brushed DC and EC motors up to 750 Watts. The device is specially designed to be commanded and controlled as a slave node. If the motor is provided with an integrated encoder, the driver can also register the kinematic data from the sensor. Only one motor can be connected to the driver, so, for the current application, two drivers must be considered, one for each motor. Since the motor will be considered as torque source, a proper current control mode needs to be imposed to the driver. The EPOS4 sends the measured actual position, speed and current values to the master. The auto-tuning procedure by Maxon motor system allows the definition of control parameters. In Figure 7.5.1 the main characteristics

of the driver are summed up, with a front (A) and lateral (B) view of the system. The driver board presents numerous connector ports, in order to connect motor, encoder, power supply and CAN interface. The presence of two CAN ports allows the series connection for the communication of the drivers to one master system through the CAN interface device.

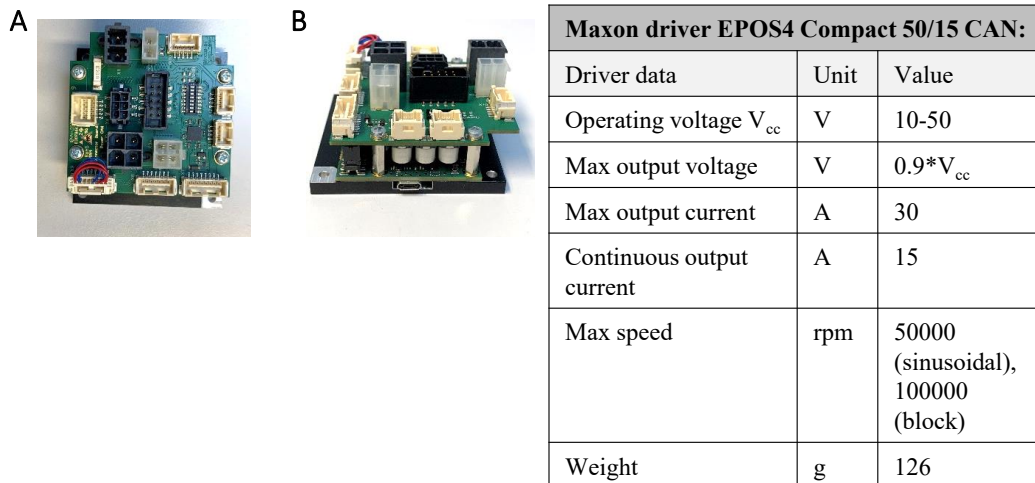


Figure 7.5.1: Front (A) and lateral (B) view of the motor driver with the summary of the main characteristics.

Figure 7.5.2 depicts the two interface communication devices from National Instruments. The USB 6341 device allows the acquisition of analogical and digital data from additional sensors. The Figure 7.5.2 A shows a graphical representation of the board and a summary table of the device characteristics. It must be stressed that the device is firstly used for the data acquisition from the secondary encoder for the calculation of the desired torque and the control implementation. Moreover, it can be used for the data registration from external sensors during the experimental test (as the interface force sensors). The USB 8502 CAN communication device allows the interface between slave nodes (motor drivers) and the master node (the personal laptop) for the regulation of whole control scheme. The Figure 7.5.2 B depicts the graphical representation of the device and the summary table of main characteristics. The CAN communication represents a standardized application layer and communication profile. It is a high-integrity networking system based on communication bus, commonly used in automotive and industrial systems. CAN devices send data across the CAN Network by means of packets called frames. A typical CAN frame contains a Start of Frame for hard synchronization of all nodes, arbitration ID determining the priority of messages, a Control field for the specification of total bytes of data in the message, a Data field with the actual data needed to be transmitted, an error frame and an overload frame to detect possible transmission errors and the End of Frame to close the data frame. The translation of the data field into usable data can be applied with a specific database that describes the channels contained in the message. The use of an Object Dictionary allows the translation of input and output information. Finally, the personal laptop

with Microsoft Windows operating system and Labview software is considered as the master node for the implementation of the high-level control and the imposition of the desired assistance torque. All the interface communication devices are directly connected to the master laptop by the USB ports connection.

All the electronic components are maintained external to the exoskeleton device. The integration of a proper control unit to the structure will be considered as future improvements of the prototype.



USB 6341 DAQ system:			USB 8502 CAN interface device:		
DAQ data	Unit	Value	Device data	Unit	Value
BUS connector	-	USB high speed	BUS connector	-	USB high speed
N analog channel	-	16	Max baud rate	Mbps	1
Max sample rate	kS/s	500	N port	-	1
analogical output	-	2	Input base freq	MHz	1
Analog accuracy	μ V	2190	Input voltage	V	4.5-5.25
N digital input	-	24	Working current	mA	500 max, 250 typical
N counter	-	4	Weight	g	207
Measured signal	V	Tension			

Figure 7.5.2: (A) National Instruments USB 6341 DAQ system interface and (B) National Instruments USB 8502 CAN interface communication device presentation. Graphical picture of the devices and tables summing up the main characteristics.

7.6. Serial elastic actuator

As already mentioned, another possible solution when considering exoskeleton is the positioning of elastic element in series to the actuation system. Several SEAs (Series Elastic Actuator) have been proposed in recent studies for the development of powered orthoses [146], prostheses [147] and exoskeletons, particularly for rehabilitation applications [148]. Through the monitoring of elastic displacement, the interface force can be derived using the Hooke's law and considered in closed-loop control to diminish the friction and inertia of the system. A proper impedance/admittance control loop must be considered to calculate the force/torque error and adjust the current of the motor. The use of passive elastic element could be adopted both with electric and hydraulic solutions, with the final implementation of a serial elastic actuator (SEA). Compared with the stiff actuator, the benefits of serial elastic actuator in exoskeletons can be following summed up:

- increased transparency of the system and reduced inertia;
- increased tolerance to external disturbance, for example foot contact and patient tremors, that will be overcome with low-pass filtering;
- augmented safety for the user;
- non-linearity filtering;
- increased backdrivability due to the lower mechanical impedance;
- improvements in control loop design and higher control gains;
- filtering of the actuator response at the high frequency, with the only effect of spring stiffness (K_s).

As final results, the SEA contributes to lower stiction, lower impedance and moderate bandwidth of the whole structure. Several serial elastic actuators have been implemented and adopted in robot arms [149], legged robots [150], exoskeletons [151, 152] and industrial applications [153]. Figure 7.6.1 schematizes the human-exoskeleton interaction by means of the serial elastic actuator and the closed-loop control of spring displacement for the monitoring of interface force.

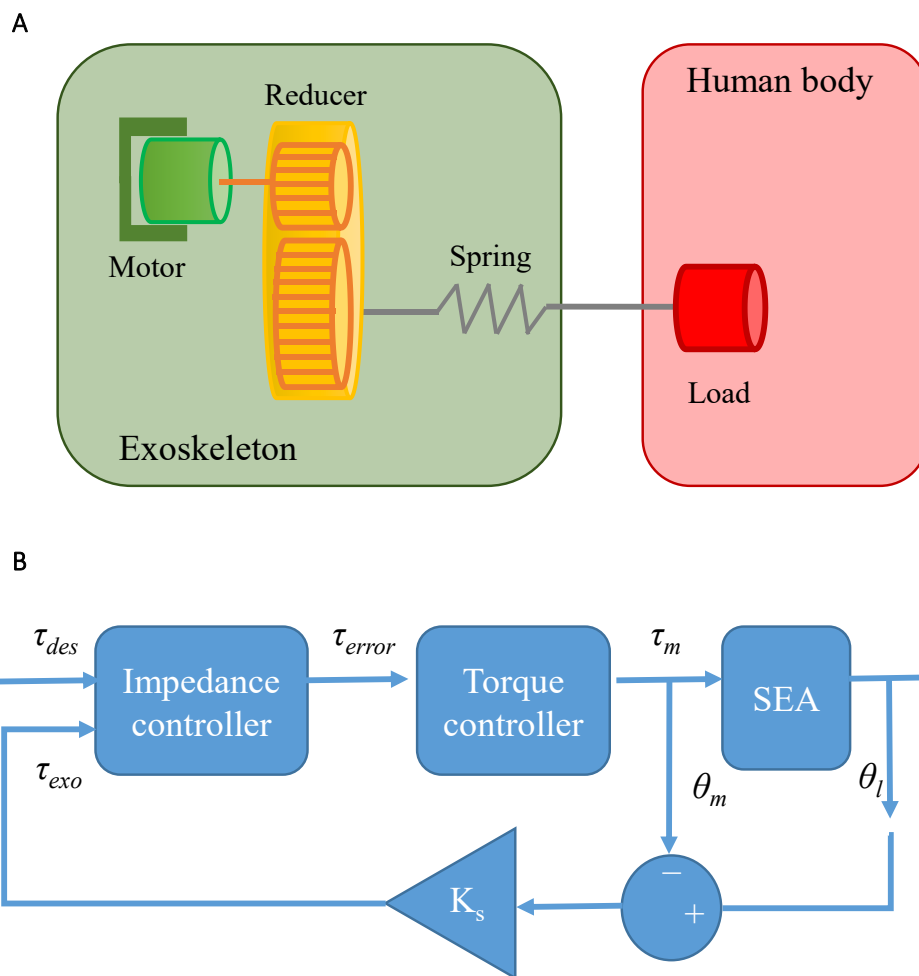


Figure 7.6.1: Serial elastic actuator schematization implemented in exoskeleton-human body interaction (A); example of control loop for the regulation of SEA (B).

Despite the numerous advantages of SEA, a proper and correct dimension of the spring stiffness is required. Moreover, different applications may require different spring stiffness dimensions and design, and different range of compliance. A high value of K_s could entail a fundamental lack of resolution in the evaluation of spring deformation and a too high mechanical impedance of the whole actuation system. On the contrary, a low value of K_s will reduce the actuator bandwidth, limiting the range of effectiveness of the actuator. For these reasons, a minimum spring stiffness to guarantee a suitable frequency bandwidth and a maximum spring stiffness to guarantee low impedance must be defined as reference thresholds. Moreover, it is difficult to identify commercial elastic spring with high stiffness and strongly compact geometry. The customization of the spring requires additional time and cost for the development and the experimental verification of mechanical properties, linearity and stiffness. The validation of the elastic element is a fundamental procedure before the integration into the structure. In addition, the spring increases the total weight of the device and the encumbrance of the powered assistance joint. For the monitoring of spring deformation, an additional angular sensor needs to be integrated to the structure and properly monitored. Finally, the elastic element adds complexity to the control architecture due to the needed additional control level, that must be correctly connected to the other levels.

7.6.1 Spring design

The elastic element must be carefully designed based on the specific application, considering both the human frequency bandwidth, the required assistance torque and the assisted human joint. A proper design of customized torsional spring must be considered. The present section presents the estimation of design requirements, the dynamic analysis and the geometrical project of a customized torsion spring configuration for the modeling of SEA that can be integrated in the powered trunk-support exoskeleton for industrial lifting tasks.

Design Assumptions. Due to the final role of the exoskeleton in assisting the worker during industrial lifting task, it is necessary to define a maximum value of torque that must be applied by the actuator and, therefore, to select a suitable motor that can provide that torque. If considering the simulation of human body 50thile Italian man manikin with 90° trunk flexion and with extended upper limbs, as previously calculated for the assistance map development in chapter 6.3, the human body torque required at the waist joint is around 130 Nm. This value is considered as reference value for the calculation of ideal maximum torque provided by the exoskeleton, neglecting the real efficiency of the actuator, that might reduce the effective supplied torque. The human motion results in a frequency range 0 - 10 Hz, with a reference value of 4-8 Hz in case of gait motion. During repetitive lifting tasks in industrial works, the frequency of trunk motion results lower than the gait motion, with value lower than 2 Hz. In this design process, a minimum reference

bandwidth of 5 Hz is defined as a requirement to the torque control. That value will be used for the calculation of control gains.

Stiffness Modeling. For the selection of the spring stiffness value, the methodology proposed by Robinson and colleagues and used in many previous researches in SEA development is considered [154]. Among previous research, a similar approach has been presented by [146]. The selected approach deals with the identification of lower and upper bounds for the definition of suitable range of stiffness values, assuring the large bandwidth and low impedance at the same time. In order to define the equivalent inertia and damping of the actuator system and then proceed with the dynamic analysis, it is necessary to identify a suitable motor+reducer that can satisfy the required maximum torque. For this simulation process, the DC brushless Maxon motor EC60 flat is considered, coupled with a reducer system with reduction ratio 160:1. Table 7.6.1 sums up the main characteristics of the selected motor that must be considered for the dynamic analysis of the system and the dimensioning of spring stiffness.

The Figure 7.6.2 A shows a schematic representation of the system composed by the control, the serial elastic actuator and the load.

Table 7.6.1 Mechanical description of main characteristics of the selected motor for the simulation of serial elastic actuator.

MECHANICAL CHARACTERISTICS OF THE MOTOR		
Variable	Unit	Value
Nominal torque	mNm	401
No load speed	rpm	4300
No load current	mA	497
Torque constant	Nm/A	0.053
Rotor inertia	gcm ²	810
Reduction ratio	-	160

The schematic model depicted in Figure 7.6.2 B points out the principal parameters that will be considered for the calculation, in particular the equivalent inertia J_{eq} and the equivalent damping B_{eq} seen through the transmission, that are calculated as:

$$J_{eq} = J_m N^2$$

$$B_m = K_t i_{NOload} / \omega_{NOload}$$

$$B_{eq} = B_m N^2$$

where J_m is the motor inertia, B_m is the motor damping, K_t is the torque constant, i_{NOload} and ω_{NOload} are respectively the no load current and speed of the motor, and N is the reduction ratio. For the determination of the torque applied to the external load, that represents the human side, the following relations describing the τ_l torque applied to the load and τ_m torque generated by the motor can be obtained from the free body diagrams reported in Figure 7.6.2 C:

$$\tau_l = K_s(\theta_m - \theta_l)$$

$$\tau_m = \tau_l + I_{eq}\ddot{\theta}_m + B_{eq}\dot{\theta}_m$$

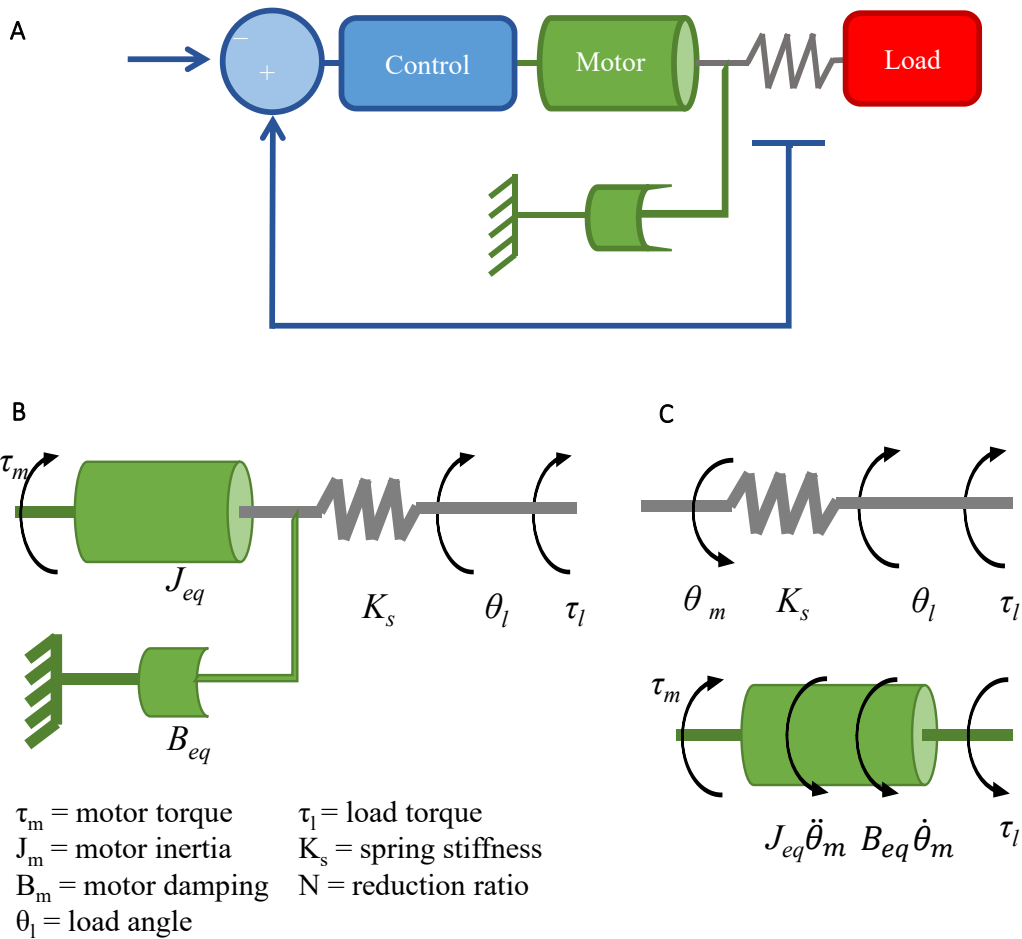


Figure 7.6.2: Graphical schematization of the complete system with control-SEA-load (A), rotary serial elastic actuator (B) and passages for the evaluation of stiffness (C).

The torque applied to the external load solved the frequency domain is expressed as:

$$\tau_l(s) = \frac{K_s}{I_{eq}s^2 + B_{eq}s + K_s} \tau_m(s) - \frac{K_s[I_{eq}s^2 + B_{eq}s]}{I_{eq}s^2 + B_{eq}s + K_s} \theta_l(s)$$

where K_s is the spring constant stiffness and θ_l is the load position. Starting from this equation, two different conditions must be analyzed in order to define the range of suitable spring stiffness: fixed load and free load with desired torque.

For the definition of the large torque bandwidth, the load position is considered fixed and the maximum motor torque is applied. The transfer function from the maximum torque τ_{max} to the maximum output torque τ_{lmax} can be derived from the following relation:

$$\tau_l(s) = \frac{K_s}{I_{eq}s^2 + B_{eq}s + K_s} \tau_m(s)$$

and the saturation frequency ω_c results:

$$\omega_c = \omega_n = \sqrt{\frac{K_s}{I_{eq}}}$$

From the last relation, it is possible to underline the direct proportion between the spring constant stiffness and the frequency bandwidth. The higher spring stiffness results in higher frequency bandwidth. This relation is used to define the lower threshold of the range of suitable spring stiffness. Considering the parameters of the selected Maxon motor EC60 flat and four values of spring stiffness (100, 200, 300 and 800 Nm/rad), the Bode plot representation of the underdamped frequency responses is shown in Figure 7.6.3. From the current analysis, it is important to stress the only influence of the motor inertia for the determination of saturation frequency, while the control system does not influence the value.

When the external load is free to move, considering a simple proportional controller, the analysis of the output impedance is necessary to define the gain K_P :

$$\tau_m = K_P (\tau_{des} - \tau_l)$$

And the output impedance can be derived from the relation:

$$\tau_l(s) = -\frac{K_s[I_{eq}s^2 + B_{eq}s]}{I_{eq}s^2 + B_{eq}s + K_s(K_P + 1)}\theta_l(s)$$

assuming a constant motor output torque. The controller gain K_P is calculated with the imposition of 5 Hz as natural frequency:

$$\omega_c = \omega_n = \sqrt{\frac{K_s(K_P + 1)}{I_{eq}}}$$

At the high frequencies, the actuator will be decoupled from the load, that will perceive the compliant behavior of the spring (K_s). It must be stressed that with the decreasing of spring stiffness also the impedance at high frequencies will be reduced. This is in contrast with the fixed load analysis, and, for this reason, a compromised spring stiffness value must be selected. Figure 7.6.4 depicts the impedance analysis with proportional controller and different supposed values of spring stiffness (100, 200, 300, 800 Hz).

Considering the obtained results and the range of spring stiffness of 100-300 Nm/rad commonly used in SEA for wearable devices in interaction with the human body [146, 155, 156], the spring constant of 200 Nm/rad is defined as the reference value for the design. It allows torque bandwidth of 1.5 Hz, low impedance at low frequencies, and amplitude of spring constant value for frequencies > 5 Hz.

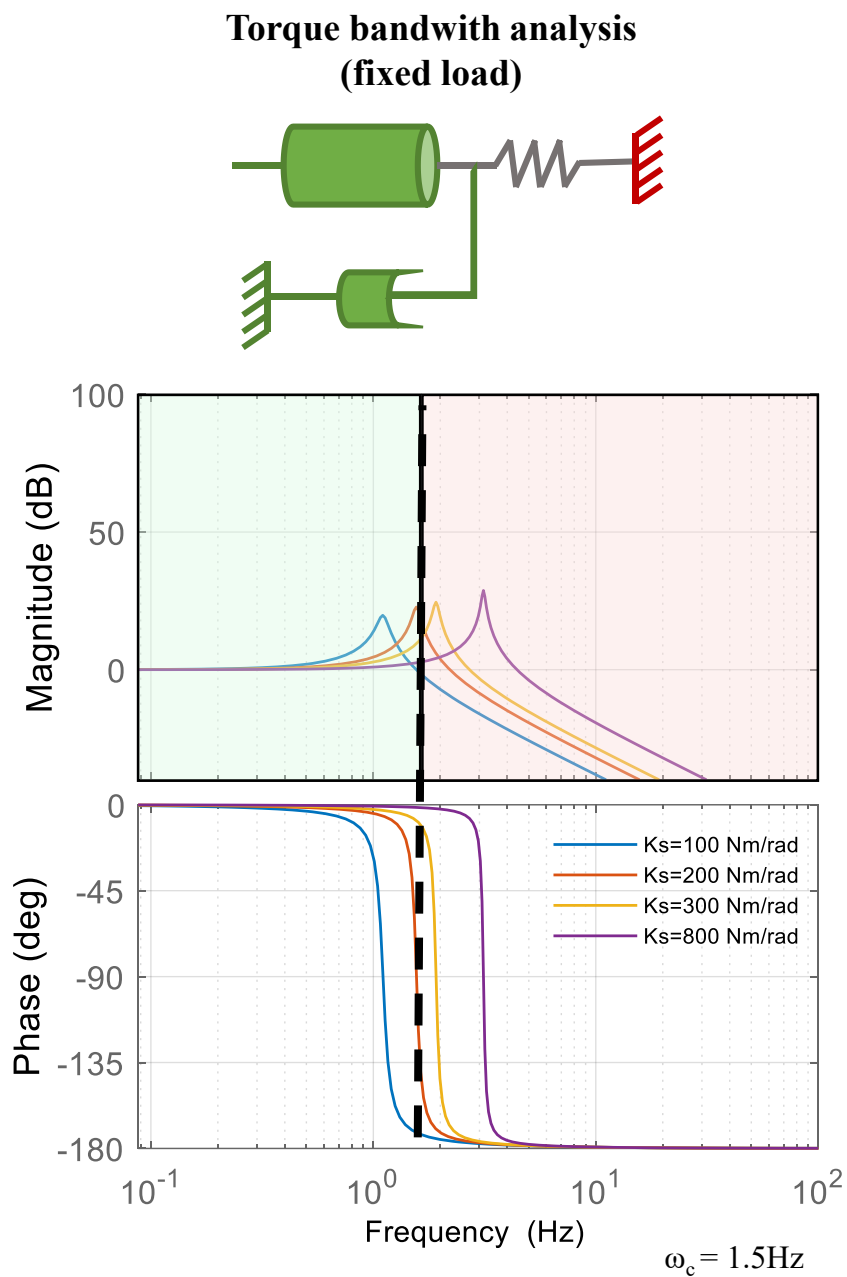


Figure 7.6.3: Bandwidth analysis simulation with different value of spring stiffness (100, 200, 300, 800 Nm/rad) in case of fixed load: the bode diagram. In the magnitude plot, the green and the red areas stress the range of torque frequencies if considering a spring stiffness of 200 Nm/rad.

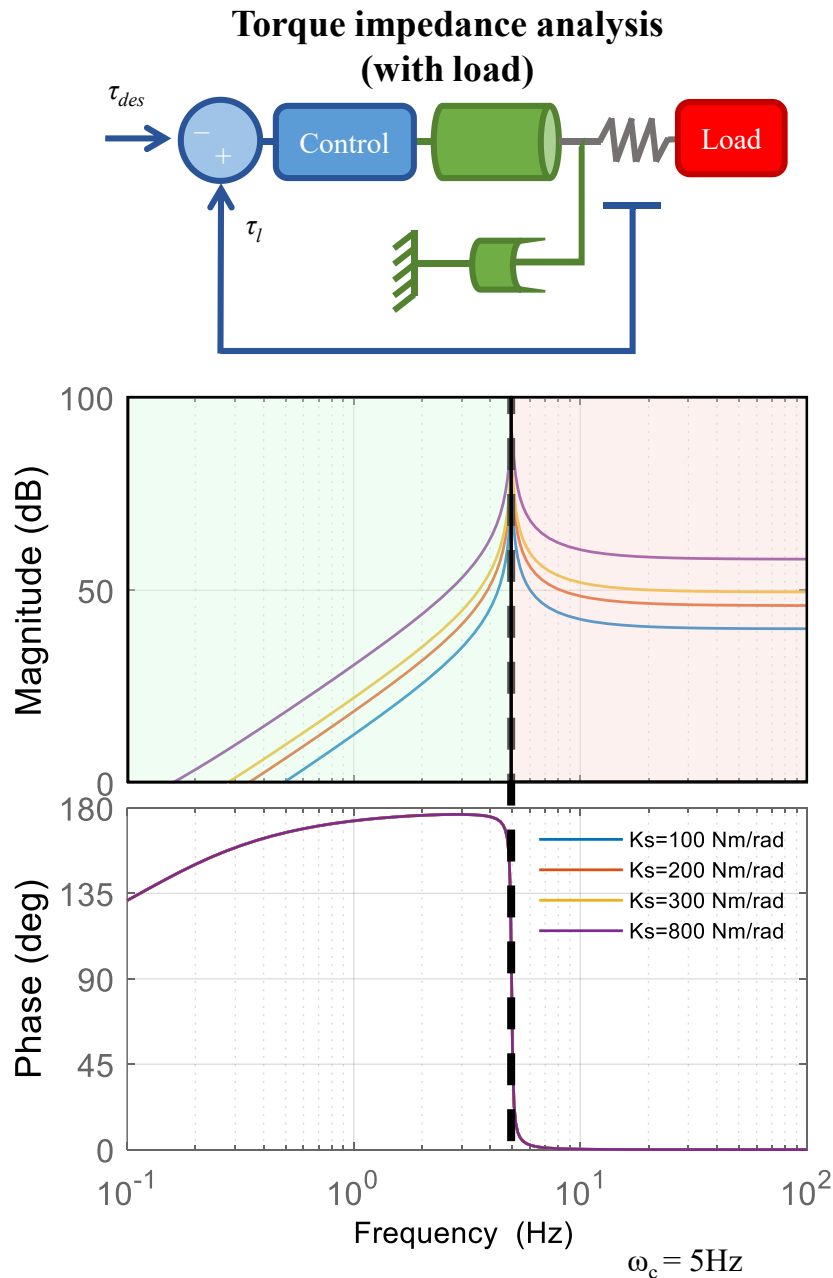


Figure 7.6.4: Impedance analysis simulation with different value of spring stiffness (100, 200, 300, 800 Nm/rad) with applied external load: the bode diagram. The natural frequency of 5 Hz is selected in order to calculate the gain of the proportional controller.

Mechanical Spring Design. Once defined the expected value of the spring stiffness, it is necessary to proceed with the mechanical design and implementation of the elastic element. Due to final aim of use into a wearable device, the spring must be thought lightweight, compact, with reduced encumbrance, easy integration onto the powered joint and direct assembling with the actuator. The spring must be able to endure the high torque applied by the actuator. Caused by the difficulty to find available commercial spring products with the required geometrical and stiffness proprieties, a customized solution is designed and virtually tested using the software Solidworks. The spring is composed by one inner ring and one outer

ring, connected by a spiral flexible system. The geometric characterization of the spring is depicted in Figure 7.6.5 A-B. The proposed geometry and dimensions try to limit the total encumbrance of the element, maintaining a proper adaptation for the connection with the motor+reducer by means of inner and outer rings. The spiral design contributes to obtain higher stiffness of the element. The inner ring has a diameter of 18 mm, the outer ring a diameter of 100 mm. Four semicircles define the spiral system of connection between rings. The total thickness results of 20 mm. This last value represents the amount of encumbrance that the integration of the spring will add to the total encumbrance of the actuation system.

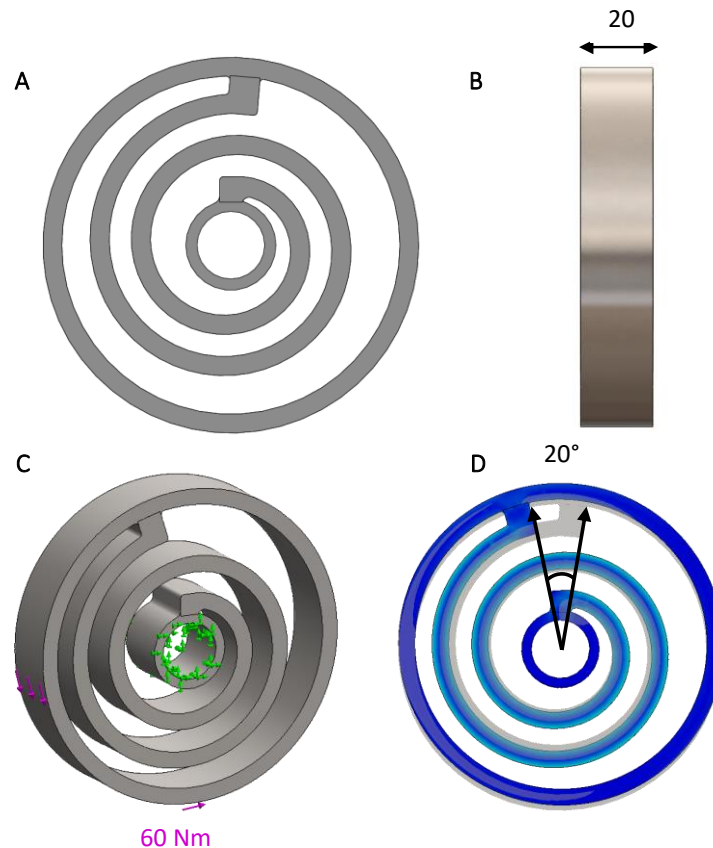


Figure 7.6.5: Design of custom spring: (A) front view with inner (18 mm) and outer (100 mm) diameters, (B) lateral view with thickness (20 mm), (C) simulation design of the maximum expected load (torsional moment of 60 Nm on the external ring) with constrained inner ring, (D) Von Mises results with stressed angular displacement (20°).

The material selected for the analysis is chrome-molybdenum-vanadium steel DIN 1.2367 (X38CrMoV5-3). The main mechanical characteristics of the selected material are highlighted in Table 7.6.2. Previous studies on torsional spring development considered the chromium-vanadium steel AISI 6150 [146], maraging steel VACO 180 T [155], 17-4P H900 steel [157], maraging steel Böhler W720 [158] as suitable materials.

After the design implementation, it is necessary to verify the stress distribution and the deformation of the spring in case of applied maximum load, in order to avoid yield strength in extreme conditions and to test the suitability of the proposed

model. The finite element method (FEM) simulation is conducted in Solidworks environment. The static analysis entails the inner ring fixed with a geometrical constraint and the application of a torsional moment of 60 Nm on the external ring, as graphically depicted in Figure 7.6.5 C. An alternative load condition may be implemented with the application of correspondent tangential maximum forces on the outer ring, obtaining the same final results. For the simulation, a high-quality mesh with Jacobian check applied on nodes is selected. The theoretical spring stiffness is evaluated considering the maximum applied torque of 60 Nm and the maximum angular deformation, that was set of 20° , as reported in Figure 7.6.5 D.

Table 7.6.2: Mechanical description of the main characteristics of the designed spring. The material is chrome-molybdenum-vanadium steel DIN 1.2367 (X38CrMoV5-3).

MECHANICAL CHARACTERISTICS OF THE SPRING (steel X38CrMoV5-3)		
Variable	Unit	Value
Young modulus	N/m^2	$2.15 \cdot 10^{11}$
Poisson's ratio	N/A	0.28
Shear modulus	N/m^2	$7.90 \cdot 10^{10}$
Mass density	kg/m^3	7850
Yield strength	N/m^2	$2.12 \cdot 10^9$

Considering the ratio between these two values, the computational spring stiffness is 172 Nm/rad, near to the supposed 200 Nm/rad. Figure 7.6.6 shows the results from the simulation. Von Mises stress distribution σ_{VM} is considered. From the results, a trivial stress concentration in correspondence of link between the spiral element and the two rings (Figure 7.6.6 A) is present. As expected, due the applied loads and constraints characteristics, the results highlight higher resultant displacement of the spring at the outer ring, while the value appears reduced if moving closed to the inner ring (Figure 7.6.6 B). The strain evaluation pointed out the geometric response and the change in shape due to the applied forces (Figure 7.6.6 C). The factor of safety (FOS) is calculated as the ratio of the maximum allowed spring stress and the maximum spring stress during the operation (Figure 7.6.6 D). In this case the FOS is around 3, hence any parts of the element are critical.

Control architecture. If considering the integration of the spring, an additional closed-loop control level, the low-level impedance control, needs to be added to the previous proposed control scheme, as depicted in Figure 7.6.7. The additional control loop consists in the monitoring of the impedance between the human and the device interface through the measurement of spring displacement. Two encoders must be positioned before and after the spring to allow the estimation of spring deformation. The effective measured torque could be calculated considering the spring stiffness K_s . The difference between the desired torque and the applied torque depicts the torque error, that must be assumed as the motor torque input.

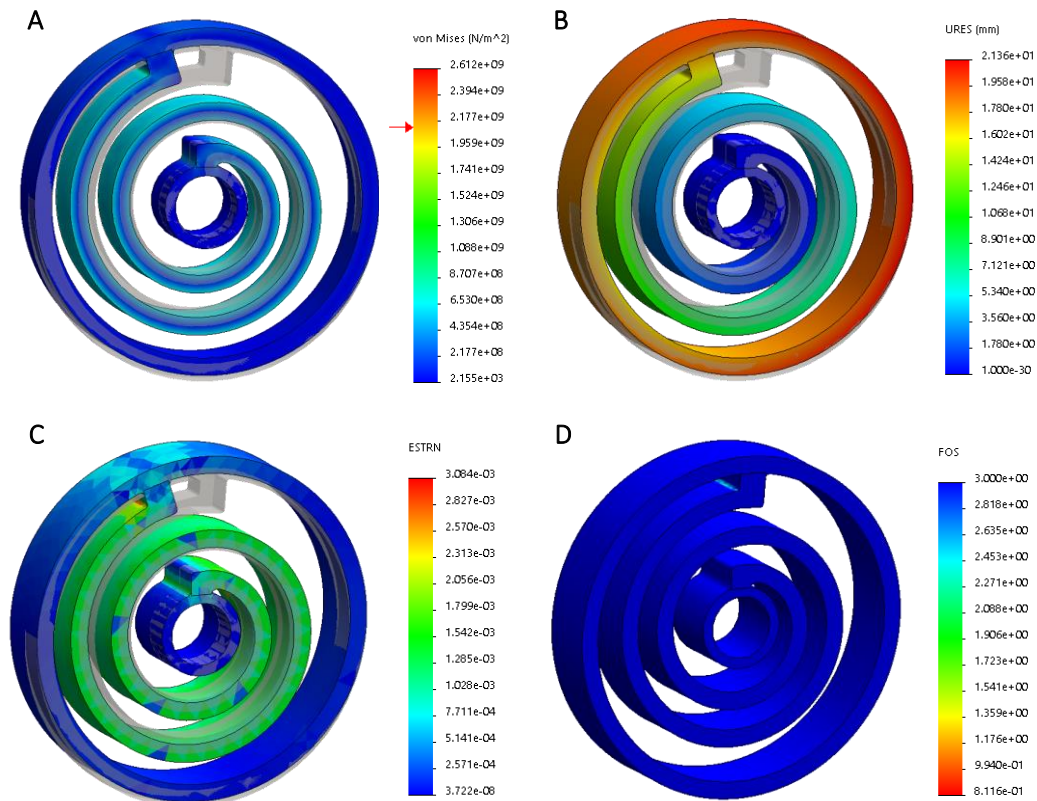


Figure 7.6.6: Simulation results of the static analysis with imposed torsional moment on the external ring and constraints on the inner ring: (A) Von Mises stress results, (B) displacement results, (C) strain results and (D) safety factor evaluation.

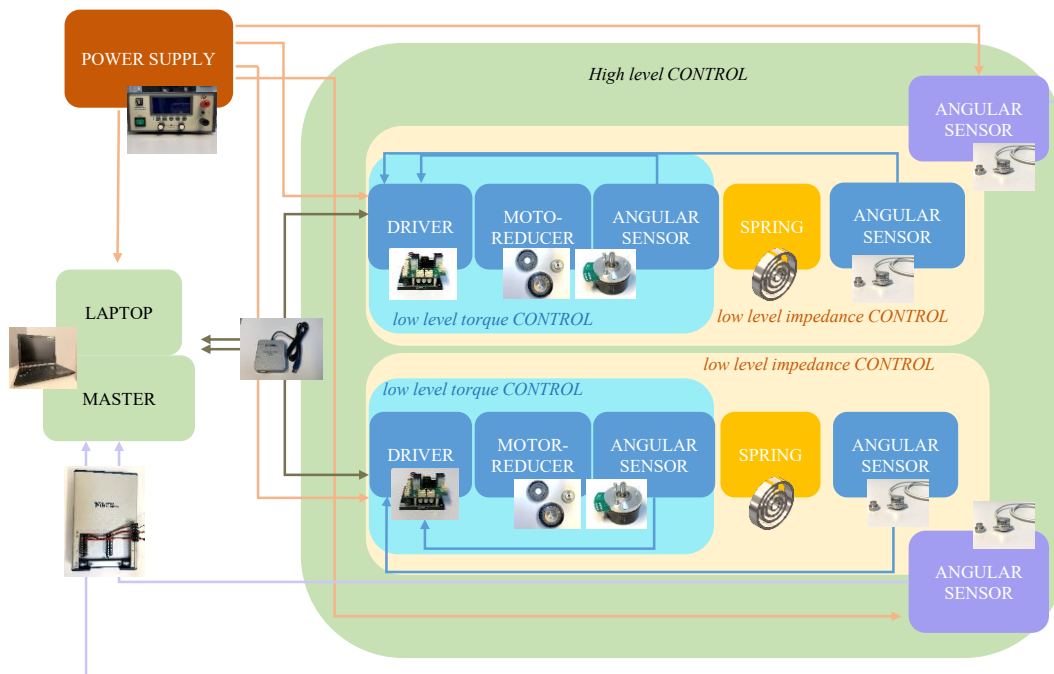


Figure 7.6.7: Concept of the control scheme of powered exoskeleton with SEA. Three main levels of control: high level control, impedance control and low-level control.

7.7. Conclusion

In the presented analysis, a suitable assistance strategy and control architecture has been proposed, based on literature analysis, comparison between actuator solutions and common assistance strategies implemented in powered exoskeletons. The main advantage of avoiding the elastic element from the actuation system is the simplicity of both the mechanical and the control structure. Indeed, the whole structure will appear lighter and less encumbering. Nevertheless, if necessary, in order to provide more compliance to the system and enhance the backdrivability, the modeled customized spring might be integrated into the powered structure for a serial elastic actuator implementation.

Chapter 8

POWERED PROTOTYPE: the mechanical concept

8.1. From Passive to Powered Exoskeleton

Based on the previous results and considerations, a powered exoskeleton structure is developed.

The following sections describe:

- the dimensioning of the actuation system based on allowed pressure thresholds and required maximum torque;
- the selection of mechanical components and the description of their main characteristics;
- the several phases of the mechanical design of the structure;
- the final solution of the prototype.

The design and selection of the mechanical components and sensors are conducted with the attempt to limit the total encumbrance and additional weight of the structure, that are two crucial aspects for a wearable robotic system. The soft components and the connection bars of the Laevo exoskeleton will be maintained. For this reason, the contact points with the human body will not be modified. Due to the length of the trunk support bars, also the powered prototype will be suitable for user with total height less than 1.71 m. The mechanical design and implementation of the powered joint is conducted with the attempt to obtain a reversible structure with the passive Laevo exoskeleton.

8.2. Actuation system

8.2.1 Pressure thresholds

The first step is the dimensioning of the actuation system. The selection of the mechanical components is based on the analysis of the torque that must be provided in order to support the wearer. Results from the computational approach obtained with the multibody model are used to identify the required support-torque.

Before selecting the torque, it is important to consider the relation between external mechanical load and the duration of loading, and the relation between the intensity of the physical activity and the risk of low back pain.

Due to the direct contact between the wearable device and the human body, it is important to analyze the pressure exerted by the exoskeleton on human body. In the past, several attempts to define safe thresholds for the external mechanical loading of human soft tissues have been based on the interface pressure. The first threshold has been defined by Landis in 1930 and it corresponds to the skin capillarity pressure of 32 mmHg (4.3 kPa), but later researched have defined the threshold to 47 mmHg (6.3 kPa). More recent studies have depicted the possibility of soft tissues to support interface pressures above the capillarity pressures. For example, during sitting posture, pressures up to 165 mmHg (22 kPa) may occur. Moreover, in a recent analysis of interface pressure at thigh contact between exoskeleton and human body, the maximum average pressure of 220 mmHg (29.3 kPa) has been recorded. One other important aspect that must be stressed is the non-linear relation between interface pressure and internal stress, due to the nature and characteristics of the soft tissues.

Two main parameters that relate pressure to pain and discomfort can be quantified: the pressure magnitude at which the pain occurs, that is called the Pain Detection Threshold (PDT), and the pressure magnitude that cause intolerable pain, that is called Pain Tolerance Threshold (PTT). O'Sullivan and colleagues [135] presented in a recent review study the investigation of pressure with the attempt to depict a guideline for acceptable levels of mechanical tissue compression in humans. In addition, they suggested the probability of deep tissue injury when loaded with pressure-induced pain thresholds. The risk curve depicted in Figure 8.2.1 A shows the relation between the external load and the time duration. Two fields define the level of tissue damage: high risk and low risk.

The PTT and PDT thresholds results inside this range of values, but they are located near the two extreme limits respectively. From the reported curve, it is possible to highlight the higher risk of pain with higher mechanical loads also for short time duration, while, for reduced loads, the pain resulted lower independently from the loading duration. These two limits are stressed in the reported graph of Figure 8.2.1 A (red and green dashed lines). To define the safety standard of external loading, the value of the pressure lower limit must be identified. Sullivan et al. [135] analyzed 13 previous studies where the computerized cuff pressure

algometry was performed on healthy adults at lower and upper limbs. The PDT level ranged from 16 to 34 kPa at the lower limb, from 19 to 34 kPa at upper limb. The PTT level ranged from 42 to 90 kPa at the lower limb, from 69 to 99 kPa at the upper limb [135]. There are no previous investigations concerning the pressure threshold applied on human trunk related to pain perception. When considering the development of a wearable exoskeleton, it is essential not to exceed the PDT level.

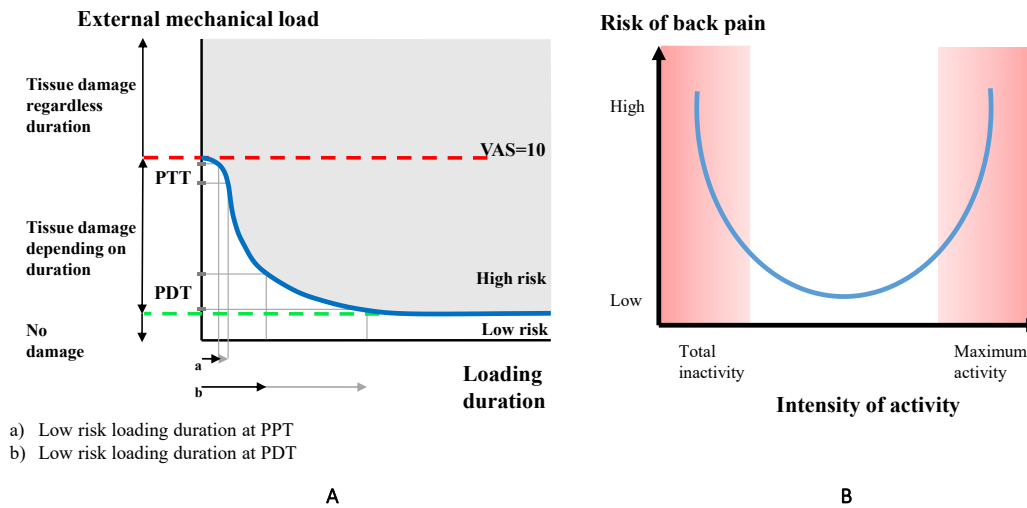


Figure 8.2.1: Theoretical description of the relation between the external load applied and the duration for the definition of tissue damage (A); theoretical relation between physical activity and risk of low back pain (B).

In addition to the level of pressure that can be applied to human tissue, it is important to define the level of assistance that the exoskeleton can provide. Indeed, the main role of an industrial exoskeleton, due to the interaction with healthy users, is to partially support and reduce the human muscular efforts. The device does not substitute the human body in performing the task, neither it enhances the human capability of working. The assistance of external wearable device allows the prevention of injuries, accidents and risk. In the current study, the exoskeleton must reduce the risk of low back pain. Heneweer and colleagues proposed a U shape relation between the physical activity and the risk of low back pain [159]. The graphical representation of low back pain risk versus intensity of activity is reported in Figure 8.2.1 B. Both inactivity and excessive activities may increase the risk of pain. For this reason, the exoskeleton should provide partial assistance to avoid excessive loads, but a complete assistance has to be avoided due to negative effect on low back pain.

The required human body efforts, the involved muscular activities and the biomechanical joint loads are strongly affected by the gender, the age, the health, the physical preparation, the anthropometry of the user. For this reason, it is important to have the possibility to control the value of assistance. On the other hand, in order to identify a suitable motor that can be integrated in the actuation structure, a maximum supplied torque must be defined.

8.2.2 Evaluation of the demanded torque

The multibody model of the human body is used to design the assistance torque during lifting motion. In the current study, a 50thile Italian man has been considered as reference model. With a different scaling of the manikin it is possible to investigate loads and solutions for other %ile of population. One other important element that influences the required effort is the weight of external object and the duration of cyclic lifting, which depend to the specific industrial task performed by the worker and can change based on necessity. For the dimensioning of the maximum torque, the first relation investigated is between the area of contact and the applied force. The relation is shown in Figure 8.2.2 A.

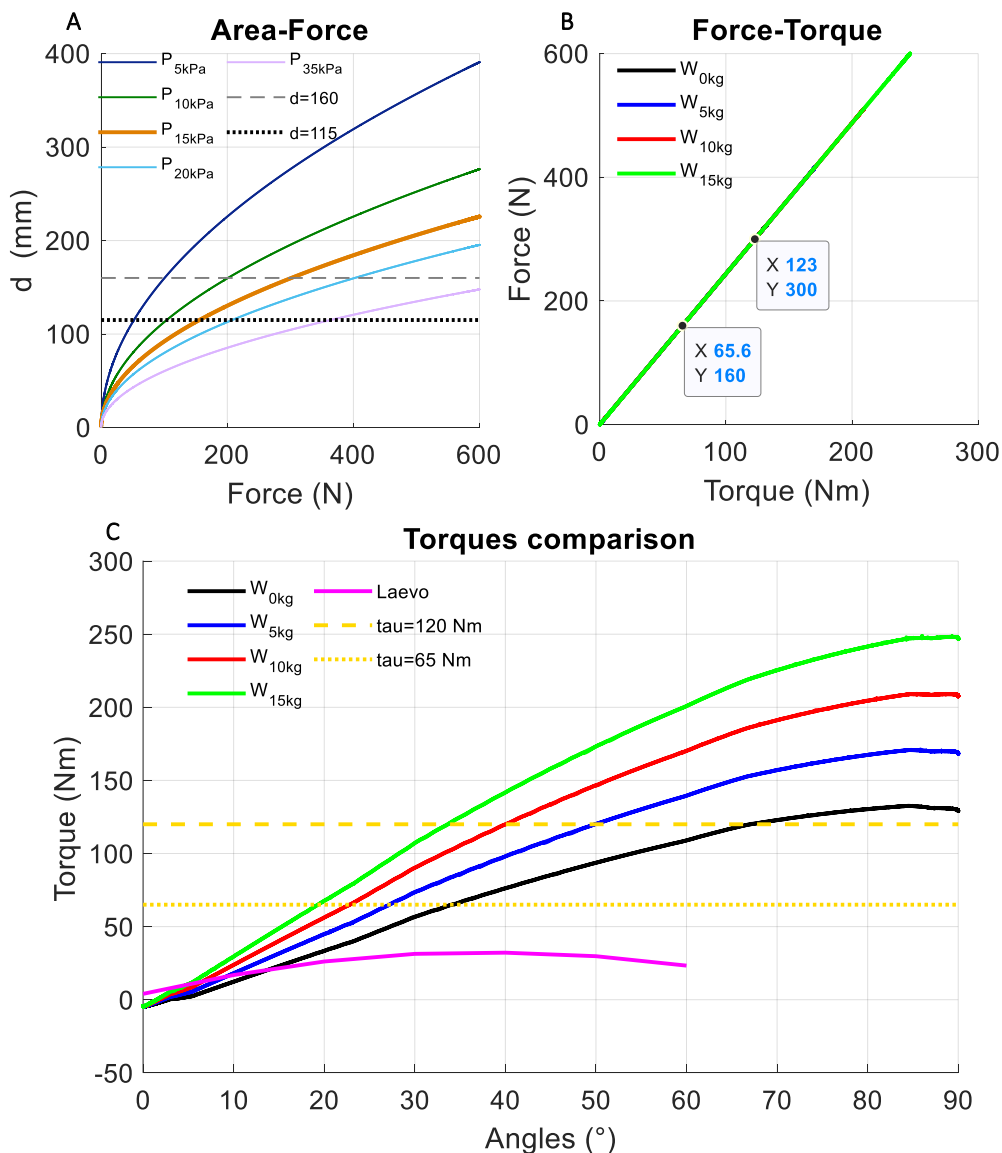


Figure 8.2.2: Simulation and design of the max assistance torque: (A) relation between contact area and applied force considering maximum pressure, (B) force-torque relation considering the Laevo's dimensions, (C) comparison among waist joint moments required in lifting conditions and the dimensioned max assistance torque.

Different pressure thresholds from 5 to 35 kPa are taken into account, but the value of 15 kPa is considered as the PDT for the current study. Over that limit, the user might start perceiving discomfort and pain. Considering the area of exoskeleton pads, that has been schematized as circular area, two different equivalent diameters are evaluated: 160 and 115 mm. With the identification of pressure and diameter parameters, two levels of force are calculated: 300 N and 160 N respectively. Considering the length of trunk bars (0.41 m), the relation between force and torque can be expressed, as reported in Figure 8.2.2 B. This relation highlights two values of torque: 123 Nm and 65.6 Nm corresponding to the 300 N and 160 N forces respectively. Finally, as shown in Figure 8.2.2 C, the two maximum torques are related to the waist moments required at the human body when lifting several weights (0-15 kg). The graph shows the relation between torques (Nm) and trunk flexion angles ($^{\circ}$). In addition, the torque curves are compared to the assistance torque supplied by the passive Laevo, as described in the chapter 4.1. Both the selected thresholds overcome the assistance supplied by the passive exoskeleton, in all trunk flexion conditions. This is an important aspect for the possibility to supply more assistance with the powered exoskeleton.

Secondly, considering the different waist torque required during trunk flexion from 0° to 90° with several external weights (from 0 kg to 15 kg), some considerations can be pointed out in relation to the two selected thresholds.

The lower selected torque (65 Nm) allows to reach near to the total support in all cases for a trunk flexion angle lower than 20° , while, if considering the case of no external load (0 Kg), the total support can be supplied for trunk angle $< 30^{\circ}$. At higher trunk flexion, the selected threshold could contribute to 50% of torque reduction in case of no load, and 25% of torque reduction if lifting a 15 kg load.

The second selected threshold (120 Nm), allows a large amount of support (up to 100% support) for angles under 35° for all weight conditions, while allows total support up to 70° of trunk flexion in case of no load. At maximum flexion degrees, when lifting a 15 kg load the exoskeleton can provide 50% of assistance.

Considering the previous analysis of physical activity and low back pain [159], it must be stressed that at lower angles of flexion the torque provided by the exoskeleton must be modulated in order to not provide the 100% of the required torque. Based on the present relations and on the assistance maps developed in chapter 6.3, the torque value of 120 Nm is selected as the maximum torque for the actuation system. With this value, based on anthropometry of 50%ile Italian man, it is possible to provide 50% of assistance when lifting 15 kg object with all trunk flexion conditions. Obviously, it allows greater level of support in case when lifting a lower mass. In any case, in order to assure the partial assistance, a maximum level of 80% of support is allowed.

8.2.3 Selection of the mechanical components

Once defined the amount of maximum required torque (120 Nm), the actuation system can be identified. It must be noted that the exoskeleton will be made of two

powered joints, one for each body side. For this reason, the total torque required for one actuation unit is 60 Nm. As already described in chapter 7.1, an electric solution was chosen for the actuation of the exoskeleton. Nevertheless, in order to maintain the small dimensions and the lightweight of the motor, it is necessary to select a suitable reducer that must be coupled with the motor, for the reduction of velocity and the augmentation of the output torque. The harmonic reducer reveals to be a suitable solution for the expected requirements. Indeed, the system presents high ratio of reduction, up to 320:1, in small and flat dimensions and reduced weight.

After a bench marketing, Maxon motor EC60 flat and Harmonic drive CPU-20A are selected for the system. The Figure 8.2.3 shows the selected electric motor.

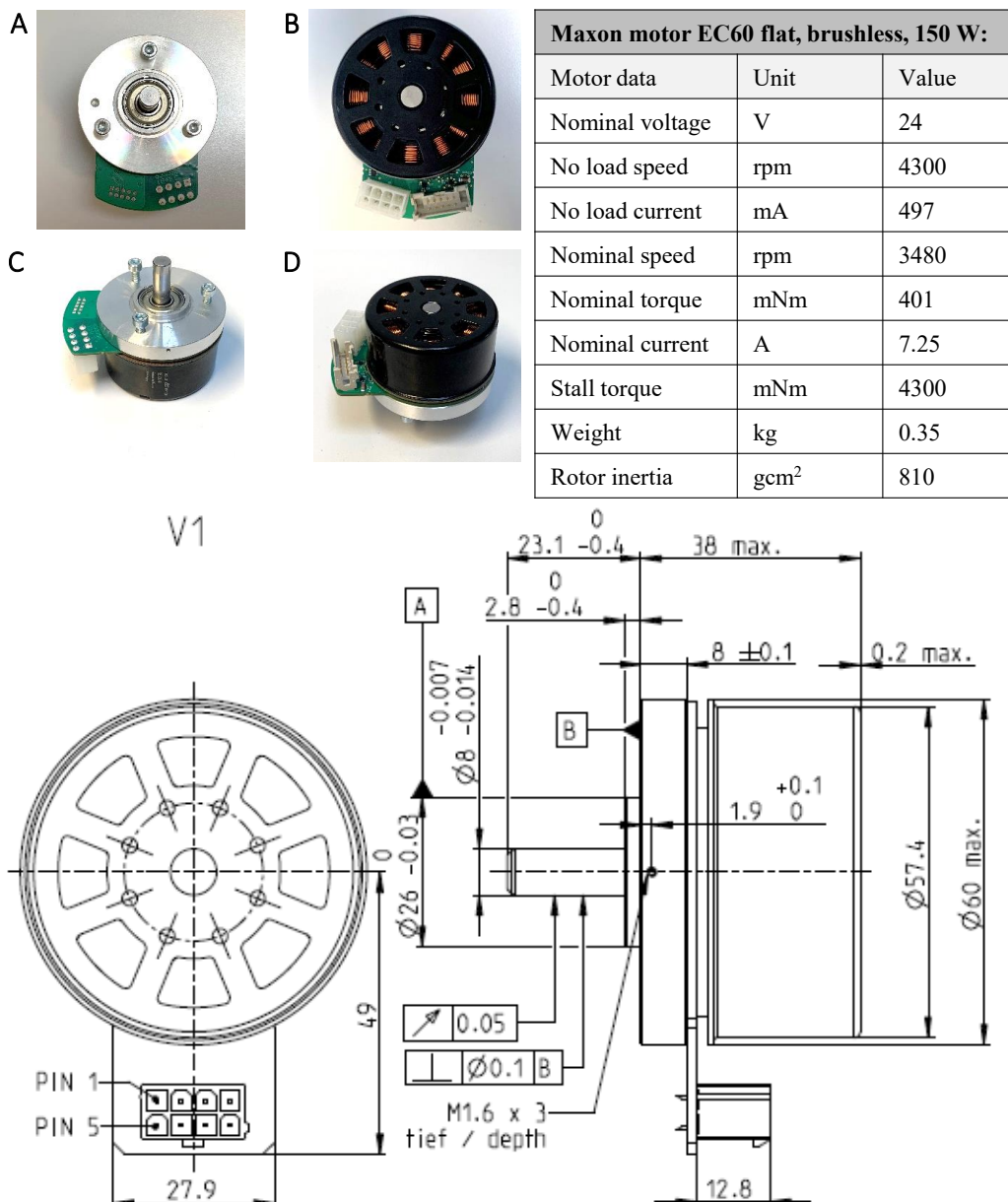


Figure 8.2.3: Front (A), back (B) and lateral (C-D) view of the selected Maxon motor EC60 flat. Description of the main mechanical, electric and technical characteristics.

It is a Maxon motor DC brushless, with flat and open rotor properties. The open rotor supports cooling during operations, so a greater continuous torques can be allowed. The figure shows different views of the motor: front view (A), back view (B) and lateral view (C-D). In addition, a table describing the main mechanical and electric characteristics, and the design with detailed geometrical dimensions is reported. The same motor has been previously considered for the implementation of the serial elastic actuator and for the design of the elastic element in chapter 7.6.1. For this reason, if necessary, in the future it will be possible to integrate the spring into the structure. Compared to other similar Maxon motor, the rotor inertia results lower and acceptable.

The nominal torque of the selected motor is 401 mNm. With the attempt to obtain a maximum reference torque of 60 Nm, a ratio reduction of 160:1 is necessary. For this reason, the Harmonic Drive reducer CPU-20A is considered for the coupling with Maxon Motor. It is presented in Figure 8.2.4.

Harmonic Drive (HD) is a special gearbox system which allows a large reduction ratio in just one stage, thanks to an elastic deformation of thin walled gearing. The harmonic drive has been applied in several applications, starting from the actuator of robot, driving parts of measurement system, semiconductor manufacturing system, and also powered wearable devices. The main difference from the conventional speed reducer is the operation by elastic theory instead of the concept of rigid bodies. Harmonic drive has several advantageous characteristics, for instance, a high precision, compactness, lightweight property and high reduction ratio when compared to the conventional ones [160]. For these reasons, the harmonic drive is chosen to satisfy design and performance requirements of the exoskeleton active joint. Despite the numerous advantages, some problems still exist, as the backdrivability and the dynamics of HD, with a compromised control performance. Indeed, it is note that harmonic drive systems are affected by the so called “kinematic error” (deviation between expected and actual output), dominant vibrations at high speeds and nonlinear friction. The integration of dynamic or adaptive based controls are common solutions to overcome harmonic drive limitations. Moreover, in exoskeletons application, the serial elastic component may contribute in increasing backdrivability.

Three principal components characterize the harmonic drive system, as reported in Figure 8.2.4: Circular spline (blue), Flexspline (red) and Wave Generator (yellow). The Circular spline presents internal teeth that interact with the external teeth of the Flexspline. The Flexspline has fewer teeth compared to the Circular spline, and, consequently, it presents a smaller effective diameter. The Wave Generator is a link with two rollers that rotates within the Flexspline, causing it to interact with the Circular spline progressively. When the Wave Generator rotates clockwise and the Circular spline is fixed, the Flexspline will rotate at a much slower rate in a counterclockwise direction. The ratio of input and output speed depends on the difference in the number of teeth of the Circular spline and of the Flexspline. Either the Circular spline, the Flexspline, or the Wave generator may be fixed while the other two elements can be connected to the input and or the

output. In the current study, the Wave Generator is fixed to the motor shaft with a clamping element, while the Flexspline is linked to the flange connected to the thigh support, and the Circular Spline to the flange connected with the trunk support.

The Figure 8.2.4 shows both graphical representation of the disassembled system: front (A) and back (B) views of the circular spline with the Flexspline, and front (C) and back (D) view of the wave generator.

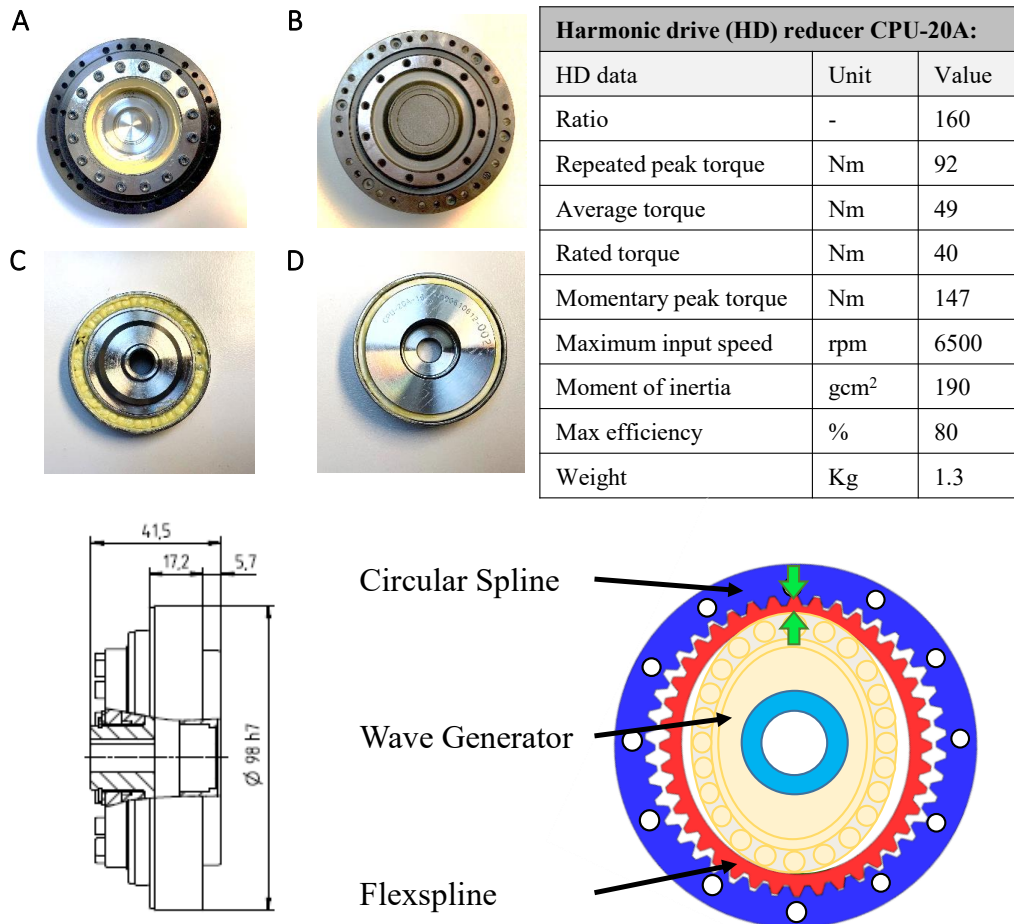


Figure 8.2.4: Front (A) and back (B) view of the Circular Spline and Flexspline, front (C) and back (D) view the Wave Generator of the selected Harmonic Drive CPU-20A. Description of the main mechanical and technical characteristics and graphical representation of harmonic reducer operation.

Moreover, a summary table of the main mechanical characteristics is reported. The maximum input speed of 6500 rpm is higher than the maximum output speed of the motor (3480 rpm). The selected model allows the imposition of 160:1 ratio of reduction, as expected. With the selected motor, the ideal output maximum torque that the actuation system could provide is 64 Nm. The efficiency for HD gears varies depending on the output torque. The efficiency may be determined using the efficiency graph or using a compensation curve and equation supply by the producer. From the efficiency graph, the higher efficiency η results 80%, the

lower 70%. If considering the efficiency, a maximum output torque of 45-51 Nm can be obtained. With a final output torque of 50 Nm from each actuator a total amount of 100 Nm could be obtained as assistance. Despite these considerations, additional experimental tests may be conducted on the motor+reducer system in order to verify the real efficiency of the system and the maximum output torque of the actuator. The total mass of the actuation system is 1.65 kg (1.30 kg from the reducer and 0.35 kg from the motor). Some additional mass will be due to the interface flanges and mechanical components that need to be adopted to link all the elements. As pointed out a mechanical interface flange must be designed for the connection of motor and reducer. In Figure 8.2.5 graphical pictures and dimensioning design of the developed flange are reported.

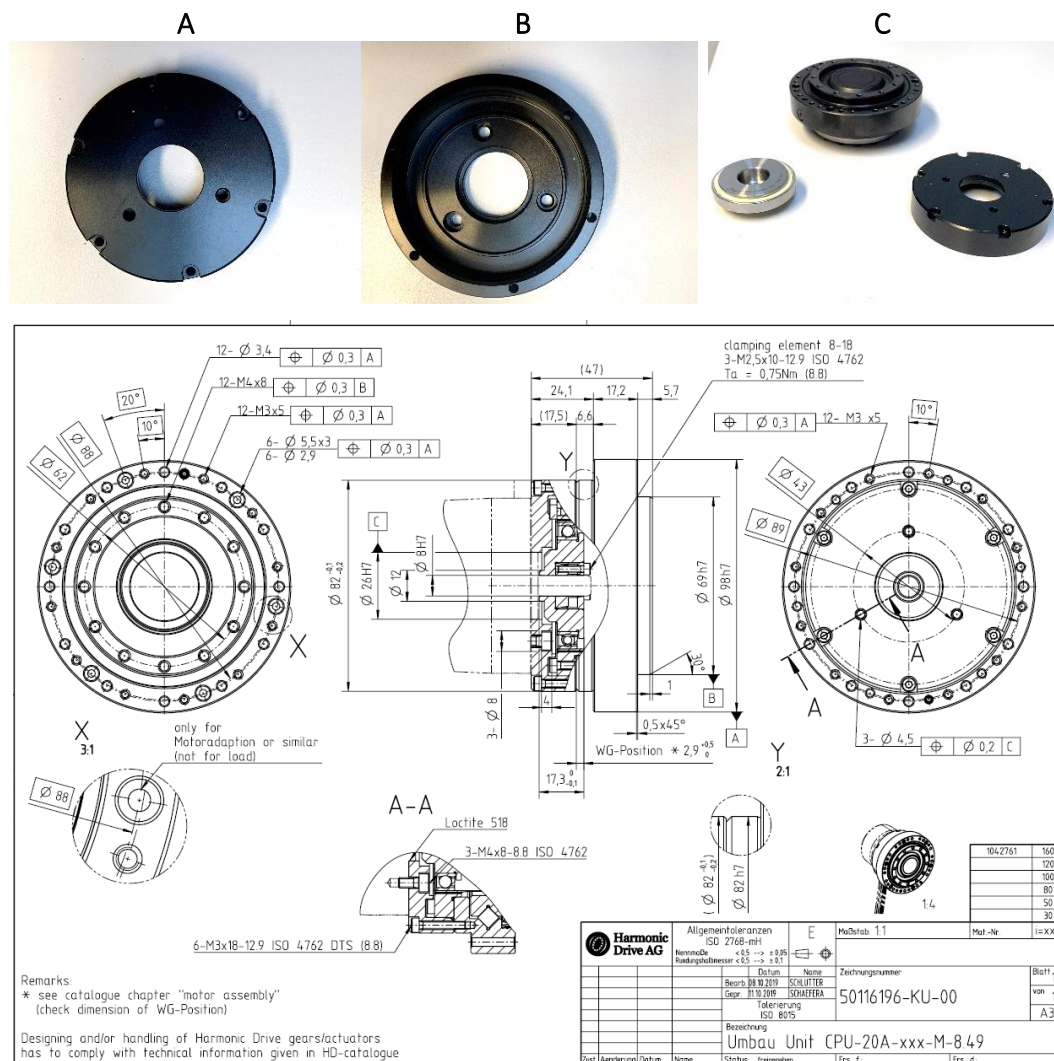


Figure 8.2.5: Dimensioning data of the flange for the interface adaptation of the harmonic reducer to the maxon motor. Back (A) and front (B) view of the realized flange, graphical representation of the Harmonic Drive components and the designed flange (C).

The internal ring considers the diameter of motor flange (26 mm), while the external diameter of 88 mm allows the connection with the harmonic drive circular spline. Three holes with 60° open angle let the fixation of the motor to the flange.

The Wave Generator must be directly mounted on the motor shaft by means of a clamping element. In Figure 8.2.5 A the external view of the flange is reported, while the internal view is depicted in Figure 8.2.5 B.

The assembly of the whole actuator parts must be conducted in a precise sequence and with a final verification of the absence of eccentric tooth mesh. The first step deals with the mounting of the adaptor flange to the motor. Secondly, the Wave Generator must be fixed on the motor shaft, avoiding any axial movements of the clamping element. The last step considers the installation of the flange including the motor and the Wave Generator onto the Unit of the Harmonic Drive. It is important that the teeth of each components mesh symmetrically with the other, for proper functioning.

8.3. Angular sensors

As already mentioned in chapter 6.3, the input torque required to the motor must be calculated based on the assistance maps developed by the model approach. The assistance torque implemented by the high level of control is a function of the user's kinematics. In details, the relative angles between trunk, pelvis and thigh segments must be monitored to recognize the lifting strategy and to understand the direction of motion (flexion or extension). The sensors are embedded in the powered joint of the exoskeleton. This choice entails attention in the definition of the correlation between the user's and exoskeleton's kinematics due to angles offset, but it avoids any sensors positioning on the user.

8.3.1 Inertial sensors analysis

Previous powered exoskeletons proposed the positioning of one inertial sensor in correspondence to the human trunk [71, 161]. The inertial sensor allows the monitoring of trunk angular velocity for the identification of direction of motion (flexion and extension) and the evaluation of the absolute trunk angle relative to a global coordinate system. The inertial sensor is a suitable sensor in terms of reduced cost and dimensions, but it has several disadvantages concerning the drift in angular estimation and the correct positioning along the human trunk. Indeed, with the attempt to estimate the angular position, an integration must be conducted starting from the registration of angular velocity of gyroscope. Moreover, the human back is often approximated as one single rigid body, even if it presents several DOFs due to the interaction between vertebrae. For this reason, based on the alignment of the sensor along the human trunk, different values of flexion can be measured.

An experimental test is implemented using the passive Laevo exoskeleton for the analysis of angles measured by two inertial sensors positioned in two different points of the human trunk: the thorax and the pelvis. In details, the two sensors are positioned in correspondence of suitable points that will be in contact with the exoskeleton, as depicted in Figure 8.3.1.

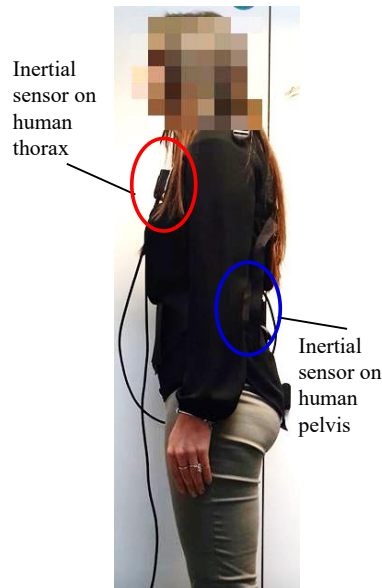


Figure 8.3.1: Configuration of two inertial sensors in suitable positions for the contact with exoskeleton components: human thorax (blue circle) and human pelvis (red circle).

The first sensor is positioned in correspondence of the chest pad, the second one in correspondence of the pelvis belt. One female subject performs different flexion-extension movements, varying the lifting strategy. The measured angles from the inertial sensors are compared during the motions. The Figure 8.3.2 depicts the signals registered by the sensor on the thorax (red line) and on the pelvis (blue line) and represents sequence of pictures of the corresponding position. The subject started from a standing posture, flexed the trunk in a stoop position, extended the trunk in a quasi-standing posture and performed a deeper stoop flexion movement, until the total flexed position. The subject performed a sequence of squat motion, then a sequence of semisquat motion. At the end, the subject concluded the movement with the holding of a stoop posture. Considering the comparison between the two curves, it is possible to stress the different angles measured by the sensors in all the lifting positions. During the stoop motion, the difference between pelvis and thorax angles reaches more than 20° . In the total trunk flexion position, the pelvis sensor registered a maximum of 80° , while the thorax a maximum of 60° . The pelvis sensor resulted better for the monitoring of stoop posture. During the squat motion, the thorax sensor correctly recognized the movement and registered a small angle oscillation around 0° , while the pelvis sensor registered angles up to 30° . In this task, the thorax position reveals better performance. In the semisquat motion, the difference among the two curves recorded values of 30° . One other crucial aspect will be the necessity of the inertial sensor to work in real time for the description of the angular position. This required elaboration data may introduce some delay in supplying the torque assistance. Considering these results, both sensors reveal to be unsuitable for the powered exoskeleton and the differentiation of the lifting tasks.

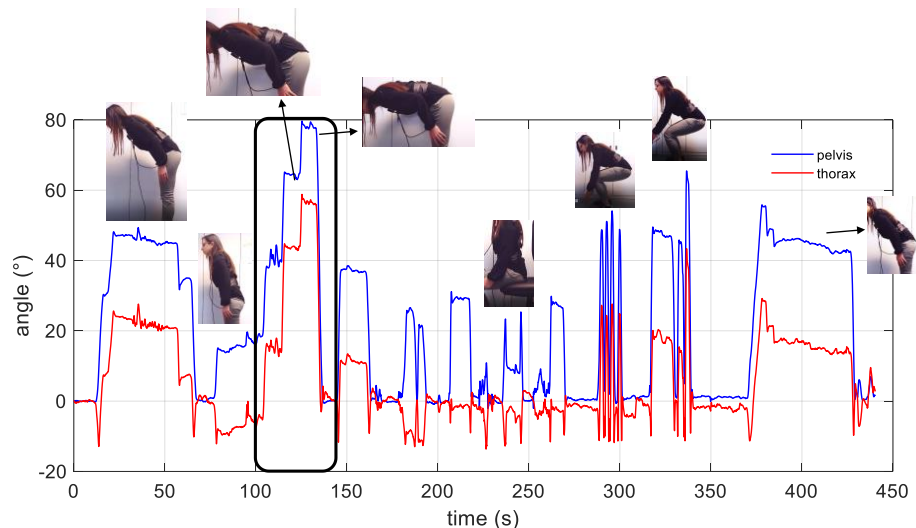


Figure 8.3.2: Experimental comparison of angular kinematics registered with inertial sensors positioned on the human thorax and human pelvis during several performed lifting simulations.

8.3.2 Measurement of trunk-thigh angle

Maintaining the idea of integrating the sensors into the device structure, the first angular sensor can be positioned between the trunk and the thigh support, assembled with the motor system. The sensor measures the variation of the angle between the upper and the lower body parts, so it corresponds to the β angle described in 6.3. The Maxon incremental encoder MILE is selected for the monitoring of β angle. The selected Maxon motor EC60 flat has the possibility to integrate the rotational incremental encoder. Due to the robustness of the proposed MILE technology in terms of magnetic interference, it is possible to integrate an encoder into the flat motor with minimal change of dimensions compared to the same motor without the encoder. This solution contributes to the limitation of space encumbrance and weight of the structure. The Maxon encoder MILE is presented in Figure 8.3.3. A summary table depicts the main characteristics of the sensors and a schematization of the output digital signal is reported into a graph. The resolution of the sensor is 4096 impulse for turn, corresponding to angular resolution of 0.09° . The MILE encoder adopts an inductive angle measurement system to generate incremental quadrature output signals. Two channels (A, B) with differential electrical signals are available as output. The signals are registered and elaborated by the driver EPOS4, that could send to the control master both angular velocity and angle position of the motor as output information.

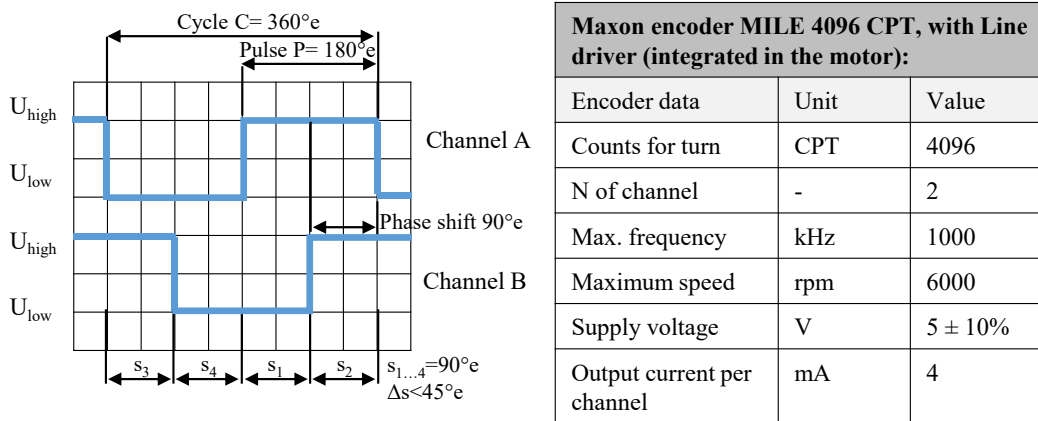


Figure 8.3.3: Maxon encoder Mile integrated in the Maxon motor EC60 flat for the measuring of relative angular position between trunk and thigh support. Description of the main characteristics and the output digital signal for the calculation of kinematics.

8.3.3 Measurement of the thigh flexion

In addition to the present encoder, a second angular sensor must be integrated into the powered joint to measure the angle between thigh or trunk support and pelvis belt, as suggested in 6.3. Several solutions have been investigated for the identification of the second angular sensor.

The second angle could be measured between pelvis belt and trunk support (α angle), or between pelvis belt and thigh support (γ angle). The angle between the pelvis belt and the thigh support is selected as the second monitored angle. This choice is supported by the different complexity and coordination of the involved human body joints and range of motions. Indeed, considering the sagittal plane, the approximation to one single hinge joint results more appropriate for the hip joint, connecting the human pelvis to the lower limb, instead of the spinal cord, defining the relative motion between the human trunk and the pelvis. The monitored human motion has a maximum range of 150° (-30° hip iper-extension, $+120^\circ$ hip flexion). For the current application, the registration of $\pm 1^\circ$ for the angular variation detection is required.

Starting from the idea of a through-hole absolute encoder, several solutions have been identified on commercial market. Among them, the best identified solutions are depicted in Figure 8.3.4.

A



HEIDENHAIN Optical Incremental ERA 4000:		
Encoder data	Unit	Value
Inner ring diameter	mm	40-512
Outer ring diameter	mm	76.5-560.46
Thickness	mm	12
Accuracy	°	2
Max speed	rpm	10000

B



RENISHAW magnetic absolute encoder AksIM2:		
Encoder data	Unit	Value
Inner ring diameter	mm	55
Outer ring diameter	mm	80
Thickness	mm	5
Accuracy	°	0.05
Max speed	rpm	10000

C



ZETTLEX inductive rotary encoder INC-3-75:		
Encoder data	Unit	Value
Inner ring diameter	mm	25
Outer ring diameter	mm	75
Thickness	mm	16.5
Accuracy	°	0.05
Max speed	rpm	6000

Figure 8.3.4: Three commercial angular solutions with through-hole configuration: (A) optical, (B) magnetic, (C) inductive encoders.

The commercially available encoders presented geometrical dimensions unsuitable for the current device, with substantial encumbrance and requiring specific mechanical integrations for the adaptation with the structure. In addition, the sensor's cost was too high for the required function. The through-hole solution has been discharged after the several researches and products' comparison.

Common potentiometer with stator-rotor-shaft configuration is considered. Nevertheless, due to the geometry, the sensor cannot be positioned aligned with the axis of the powered joint. For this reason, a proper transmission mechanism needs to be implemented and integrated into the structure. Figure 8.3.5 depicts a schematic representation of the transmission mechanism (blue) between the motor-reducer system (green+yellow) and the misaligned secondary encoder (red). Instead of a co-axial solution, this alternative design allows a better distribution of the mechanism

and contributes to the compactness of the joint, avoiding an excessive and unsuitable size on the lateral side. This choice could reveal fundamental advantages in case of exoskeleton application in reduced working space.

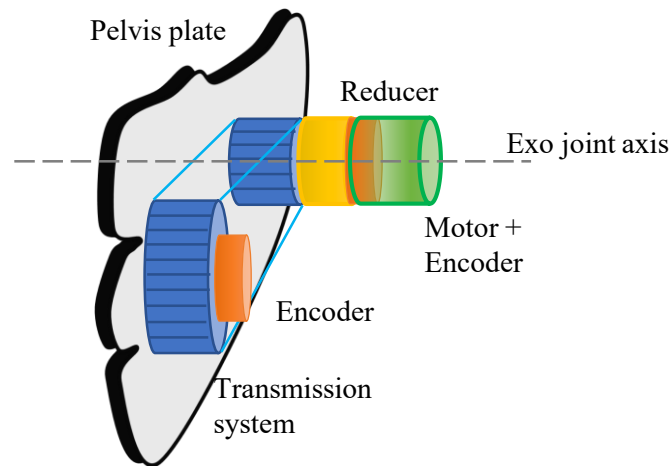


Figure 8.3.5: Schematization concept of the transmission system between the exoskeleton assistance joint and the secondary encoder.

The ELAP magnetic sensor RM22Vx is selected for the measuring of the second angle. The Figure 8.3.6 depicts a graphical picture of the device (A-B), a summary table of the main characteristics, a graphical representation of the output signal and the geometrical dimensions of the system. The digital relative angular position is converted into linear voltage with a built-in 10 bit digital/analog (D/A) converter. The linear output voltage has a range from 0 V to 5 V. The number of periods within one revolution (N_{period}) of the selected model is 2, representing one full swing over an angle of 180° (φ_{period}). The output signal is composed by steps which represent the angular movement required to register a change in the position ($\varphi_{\text{step}}=0.18^\circ$ resolution of the measure) and the resulting change in the output voltage (V_{step}). The number of steps in one period is 1024 (N_{step}). The sensor reveals a good resolution for the current application. For clockwise rotation of the magnetic actuator, the output voltage increases, while, for counterclockwise rotation, the output voltage decreases. The encoder presents non-contact, friction-less and compact characteristics. The total spatial encumbrance of the sensor in the axial direction is 27 mm.

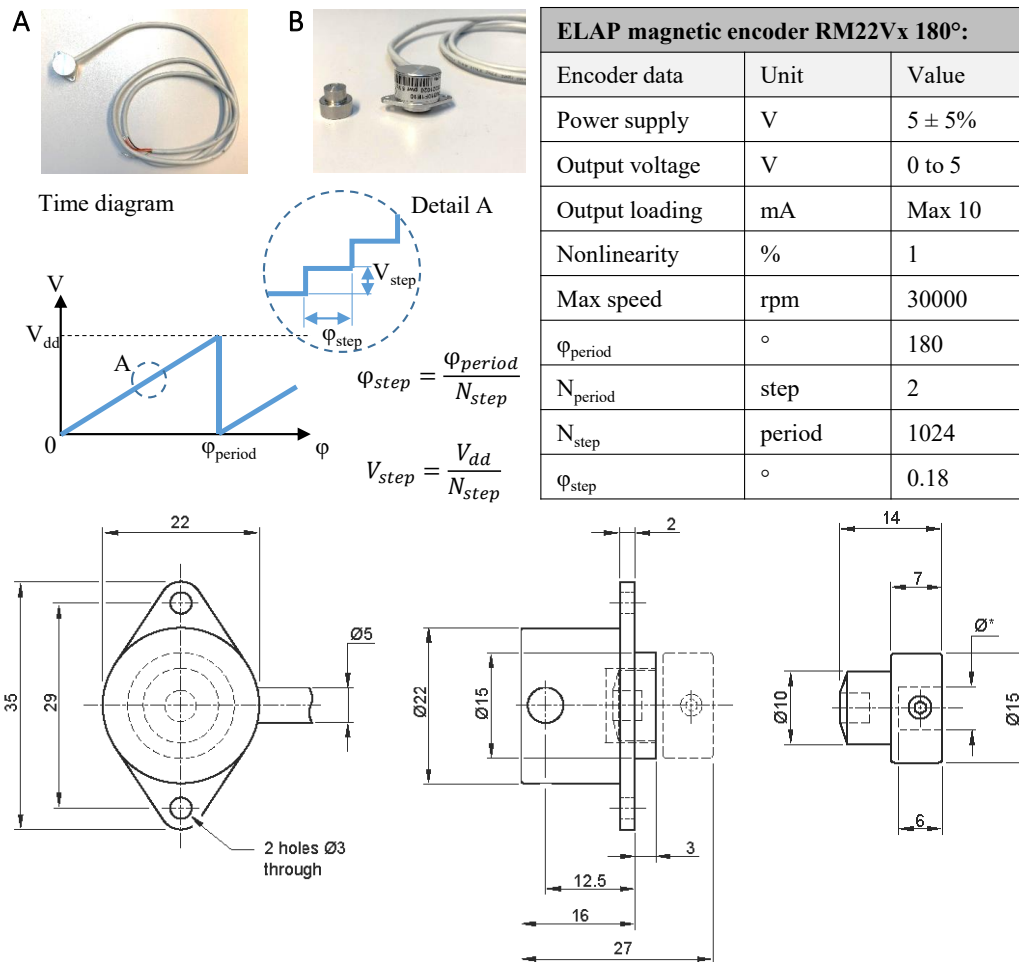


Figure 8.3.6: ELAP encoder RM22Vx used for the monitoring of relative angular displacement between thigh support and pelvis belt. Graphical representation of the encoder (A-B), description of the main characteristics, technical data of dimensions and graphical report of the output analogical signal for the calculation of kinematics.

8.4. Powered joint design

8.4.1 From the first to the final solution

The developing of the powered system must consider the integration of the powered joint into the passive structure of the Laevo exoskeleton. Indeed, the new mechanical components will be designed and dimensioned in order to allow the interaction with the trunk and thigh rigid bars of the passive system. The actuation mechanism will provide assistance between the trunk support and the thigh support, so the assistance will act between the trunk and thigh human body parts. Figure 8.4.1 depicts a graphical representation of the powered joint (A) and the several mechanical components that are present in the mechanism (B).

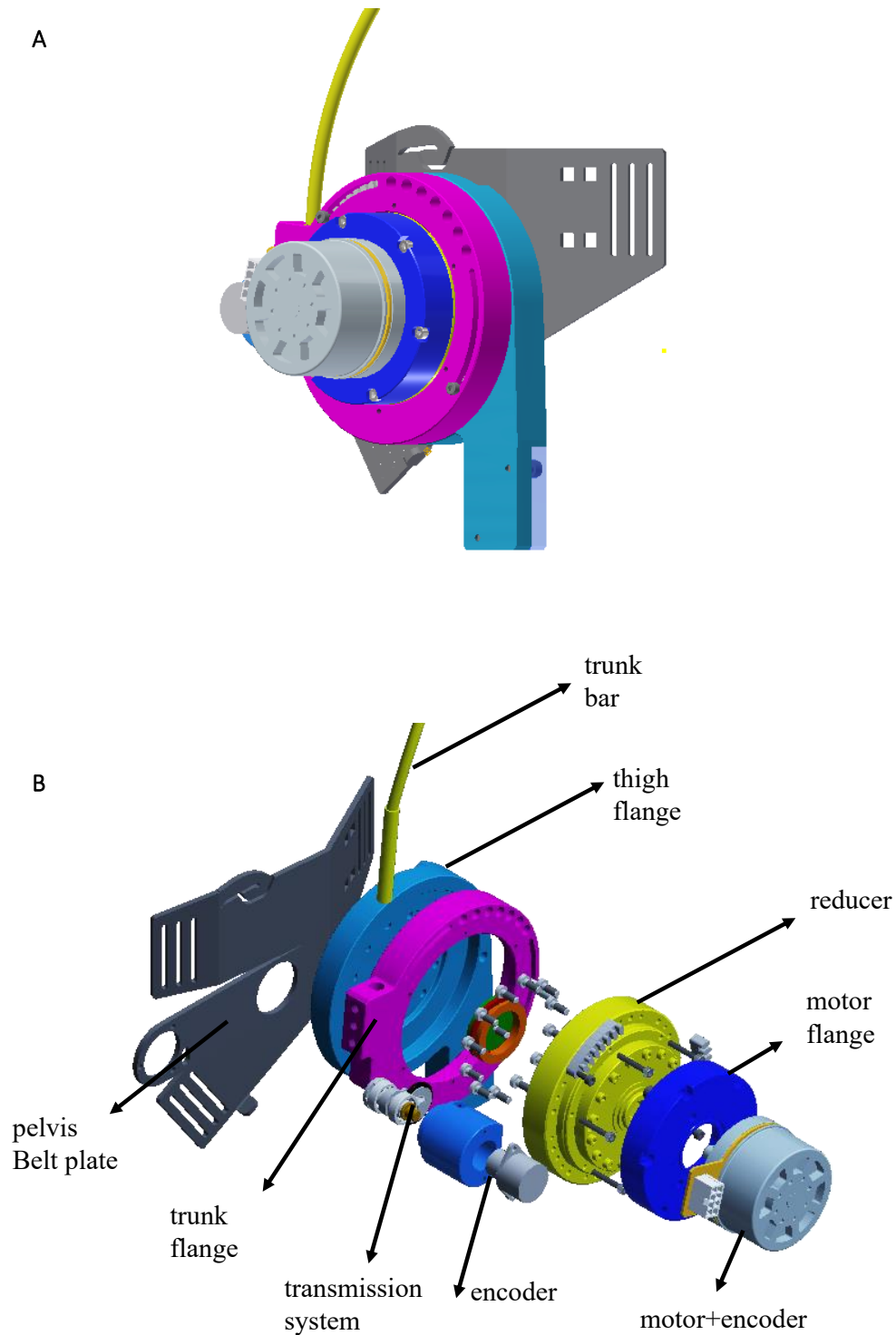


Figure 8.4.1: Graphical representation of the powered joint of the exoskeleton (A) and description of the components (B).

The magenta flange connects the trunk support bar to the circular spline of the harmonic drive and allows the connection between the actuation system with the trunk support. The cyan element connects the thigh support bar to the Flexspline of the harmonic drive, depicted in yellow color. The thigh flange has the role to connect the actuation system to the lower support part. The blue flange is the

adaptor to properly connect the Maxon motor with integrated incremental encoder to the harmonic drive reducer. The integrated encoder allows the monitoring of the relative angle between the trunk and the thigh support bars. Thanks to a properly designed transmission system, the relative rotational motion between the thigh support and the pelvis belt plate is transmitted and registered by the secondary angular sensor. This encoder is positioned in the backside part of the pelvis plate. By means of a combination of these two relative angles, the desired torque assistance can be calculated.

8.4.2 Design solutions

Four different exoskeleton powered joint solutions are designed. The proposals differ for the adopted transmission mechanism, the integration of the second encoder, the limitation of range of motion by means of mechanical end-strokes, and some geometrical arrangements of the connecting flanges. The four proposals are depicted in Figure 8.4.2 in the frontal view (sagittal plane of the exoskeleton), in Figure 8.4.3 in the lateral view (45° back-lateral side of the exoskeleton) and in Figure 8.4.4 as the exploded view drawing. In all the solutions, the actuation system (motor, adaptor flange, harmonic drive reducer) is fixed to the structure by means of connection flanges. All the solutions present the implementation of a new pelvis belt plate in order to provide a suitable integration of the secondary encoder. The first solution (A) presents the O-ring drive belt transmission of rotary motion and the integration of the encoder by means of the one double row deep groove ball bearing. Moreover, compared to the passive solution, the geometry of the magenta element is designed for the connection to the trunk bar with a vertical translation of 40 mm of the insertion. This translation results in a different position of the contact point with the human chest. The new design will modify the wearability and the size of the device. For this reason, a proper new design must be implemented. In addition, the dimensions of the cyan element result too bulky and can be improved with simpler and slimmer geometry.

Based on the considerations stressed on the first solution, a second design is developed (B). The new exoskeleton powered joint presents a modified geometrical shape of the magenta flange, with the attempt to preserve the same exoskeleton size and length of the passive system. The thickness of the cyan element has been reduced. Despite the modified geometry, the transmission element has been maintained. The O-ring drive belt transmission presents some constructive limitations. Indeed, in order to protect the user and to avoid any undesirable interactions between the transmission components and some human body parts (hands, fingers, limbs), the transmission structure might require to be covered and occluded. Moreover, in case of an unexpected O-ring's damage, the whole encoder mechanism may need to be disassembled for the replacement of the drive belt. Finally, the model presents the introduction of a holes' sequence on the magenta flange for the positioning of an external mechanical pin. This mechanism has the role of defining the starting flexed position of the trunk bar for any adaptations to

human chest anthropometry and dimensions. Instead of this first approach, proper mechanical end-stroke definition must be considered for the ROM limitation.

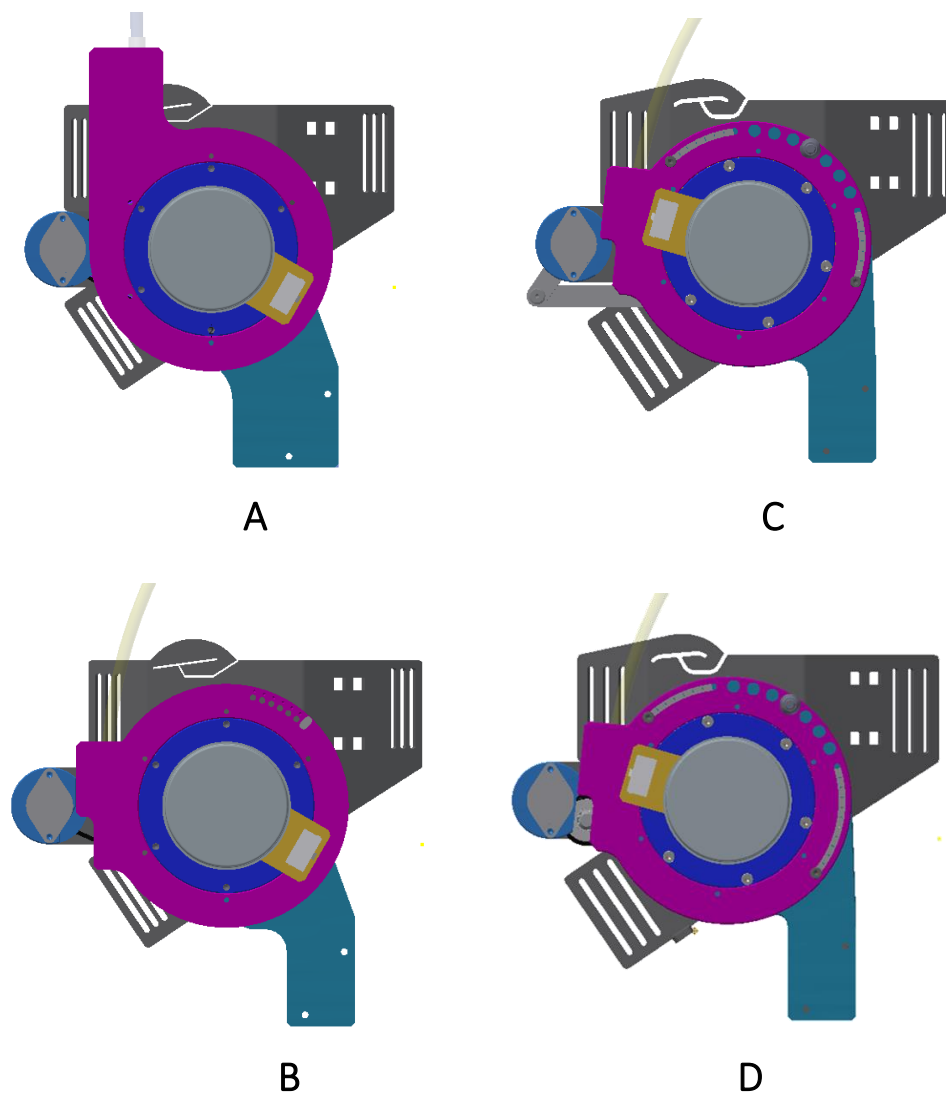


Figure 8.4.2: Front view of the powered joint (sagittal plane of the exoskeleton) in the four different solutions: (A) powered joint with O-ring drive belt transmission, (B) powered solution with O-ring drive belt transmission and modified flanges of connection, (C) powered solution with four-bar linkage mechanism for the motion transmission, (D) final powered solution with a freewheel mechanism for the motion transmission.

A third model is developed (C). The new version presents an improvement for the definition of the mechanical end strokes, considering limitations both to the opening both to the closing phase. A buttonhole with several holes for the pin positioning is implemented for both the end-strokes in the magenta flange. The system avoids the iper-extension of the human trunk and the excessive reduction of the relative angle between upper and lower body. An additional sequence of seven holes is depicted between the two buttonholes. This part could be used to fix a static flexed position in case of holding static trunk-flexion posture. A deeper explanation of the end-strokes definition will be presented in the following sub-chapter. The transmission mechanical system has been modified with a four-bar linkage mechanism and the

encoder fixation to the pelvis belt plate has been improved with the substitution of the one double row deep groove ball bearing with two single row deep groove ball bearings.

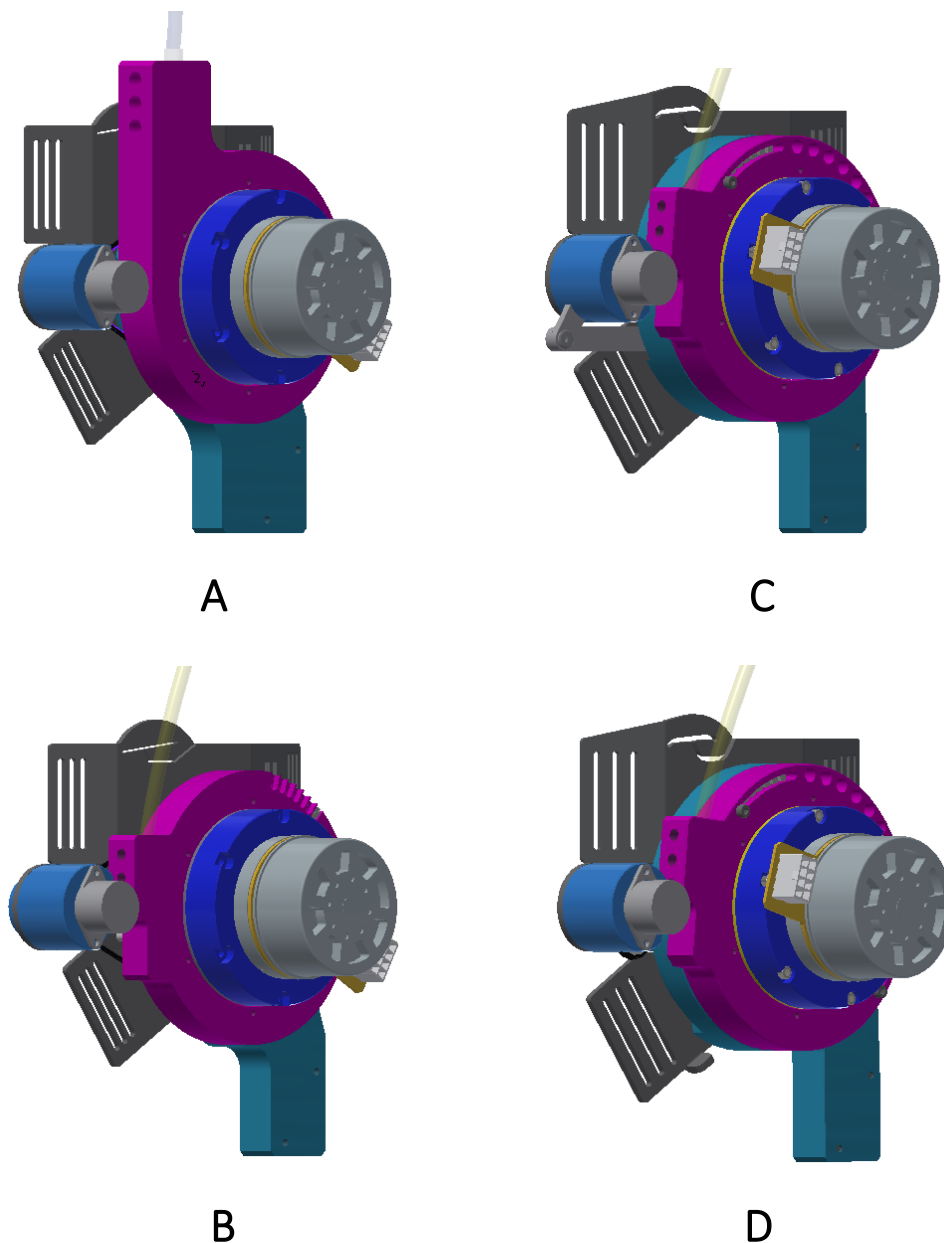


Figure 8.4.3: Lateral view of the powered joint in the four different solutions: (A) powered joint with O-ring drive belt transmission, (B) powered solution with O-ring drive belt transmission and modified flanges of connection, (C) powered solution with four-bar linkage mechanism for the motion transmission, (D) final powered solution with a freewheel mechanism for the motion transmission.

A fourth design solution is proposed (D). The new exoskeleton powered joint presents some improvements based on the previous highlighted limitations. First, the transmission mechanism has been substituted with a freewheel system. The closing end-stroke buttonhole has been modified and enlarged, guaranteeing the human hip iper-extension during the stance phase of gait motion. Finally, a small

mechanical lever has been added to the pelvis belt plate to limit the clockwise rotation of the thigh support bar. This lever improves the wearability of the device but does not restrict user's motion.

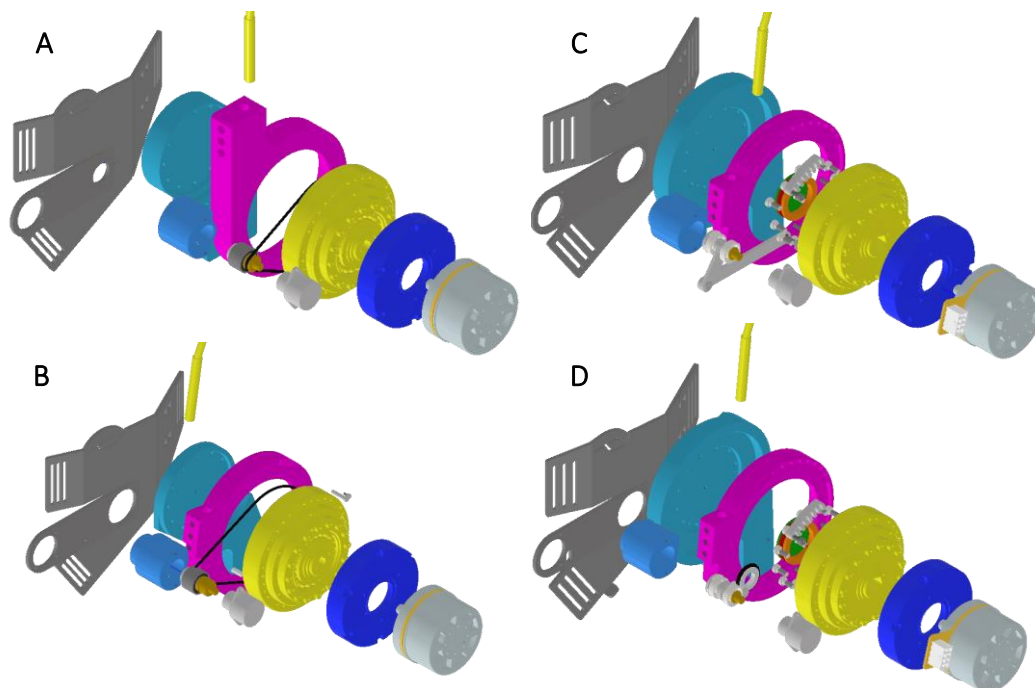


Figure 8.4.4: Exploded view drawing of the four proposed solutions: (A) powered joint with O-ring drive belt transmission, (B) powered solution with O-ring drive belt transmission and modified flanges of connection, (C) powered solution with four-bar linkage mechanism for the motion transmission, (D) final powered solution with a freewheel mechanism for the motion transmission.

8.4.3 The transmission mechanism

A defined transmission mechanism must be implemented in order to transmit the relative rotational motion between the pelvis belt and the thigh support bar around the powered exoskeleton joint to the misaligned encoder sensor. As already mentioned, the integration of a transmission mechanism results necessary due to the geometrical shape of the selected encoder. Three different solutions are proposed and investigated. All the three systems are schematized in Figure 8.4.5.

The driver pulley corresponds to the external diameter of the flange connecting the thigh support (depicted with a transparent view in the picture) to the Flexspine of the reducer.

The first solution consists in the transmission of rotational motion by means of O-ring drive belt system (A). The driven pulley is fixed to the shaft integral to the ELAP encoder. The transmission ratio is 7:1. The O-ring choice allows a simple transmission solution with low cost, easy maintenance, protection from overloads, high mechanical efficiency (95%) and easy disengagements. Nevertheless, some limitations may occur, as ease of stretching and slippage and the restriction to transmit moderate speeds.

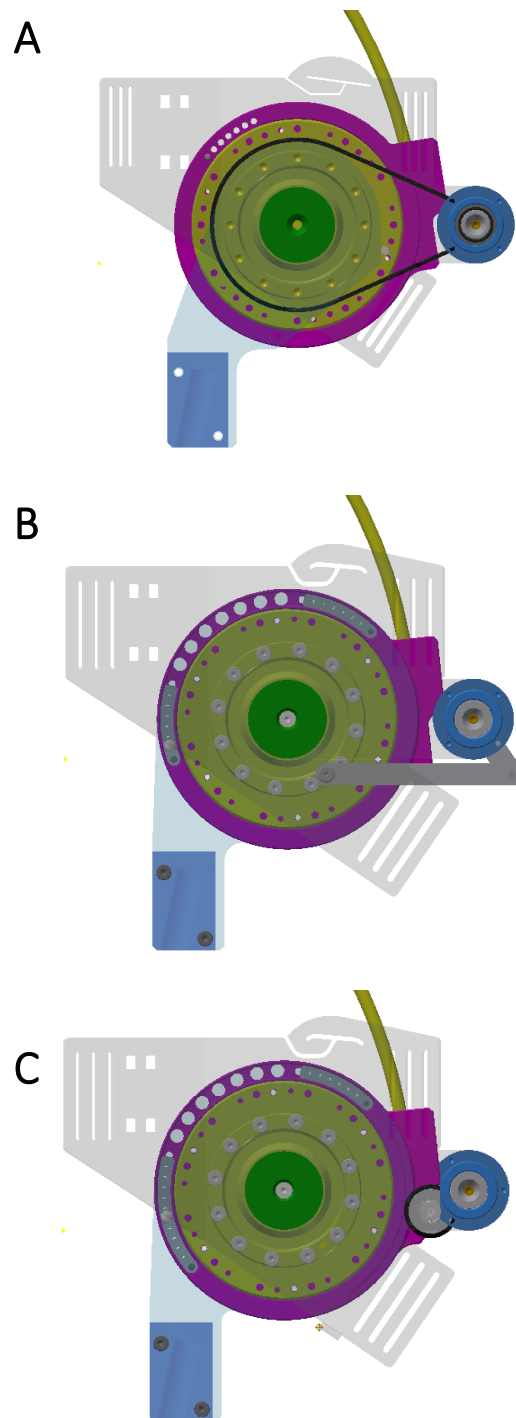


Figure 8.4.5: Back view of the powered joint stressing the three proposed solutions for the transmission of rotary motion from the motor to the misaligned encoder: (A) O-ring drive belt transmission, (B) four-bar linkage mechanism, (C) freewheel mechanism.

The second solution consists in the transmission of rotational motion by means of a four-bar linkage mechanism (B). Compared to the previous solution, the main advantage can be identified in the absence of slippage between components, contributing in the robustness of the connection. The mechanism needs a precise design in order to cover all the range of motion of interest, without causing

unexpected restrictions. The design results more cumbersome, with spatial occupation of the back zone of the human pelvis and possible discomfort to the user. Moreover, an undesirable contact and involvement with the mechanical links may occur both with human body parts (fingers and hands), both with external objects.

The third solution consists in the transmission of rotational motion by means of a free wheel mechanism (C). A small aluminum wheel with 20 mm diameter is positioned between the driving and the driven pulleys in order to transmit the rotation. An O-ring is fixed on the wheel to improve the contact between the pulleys. The rotational motion is transmitted by means of contact forces. The transmission ratio is the same of the first solution (7:1). This configuration, compared with the previous two proposals, contributes to the compactness of the mechanism and reduces the risk of any unexpected contacts with human body parts. This choice presents reduced spatial dimensions and improves the compactness of the system. For the user's safety, the limited space between the components prevent the contact of human body parts with the mechanical elements. In addition, it is a simple and cheap implementation.

In addition to the rotational motion transmission, the encoder must be fixed to the structure. The new implementation of the pelvis belt plate allows the geometrical modification required for the integration. Indeed, a 26 mm diameter hole is realized in the back-lateral side of the plate for the encoder's housing. The rotor part of the encoder is linked to the transmission by means of a shaft-pulley system for an integral rotation. The stator of the encoder is fixed to a cylindrical external coupling, the latter being rigidly fixed to the pelvis belt plate. Two different solutions are developed for the connection between the shaft-pulley system and the external coupling, in order to support the axial and radial loads from the encoder. Figure 8.4.6 depicts the two implemented proposals.

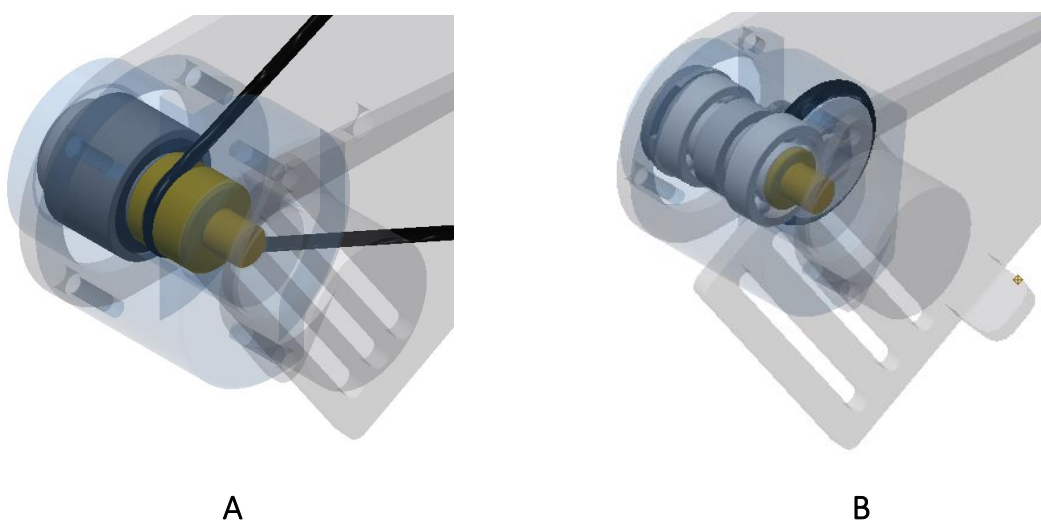


Figure 8.4.6: Two different solutions for the integration of the misaligned encoder with the plate of the pelvis belt: one double row deep groove ball bearing (A) and two single row deep groove ball bearings (B).

As a first step, the proposal considers a one double row deep groove ball bearing (A), while the second solution proposed two single row deep groove ball bearings (B). The latter improves the load distribution and the stability of the whole mechanism. Figure 8.4.7 a semi-section of the two solutions. From the depicted view it is possible to highlight the several linkages between elements.

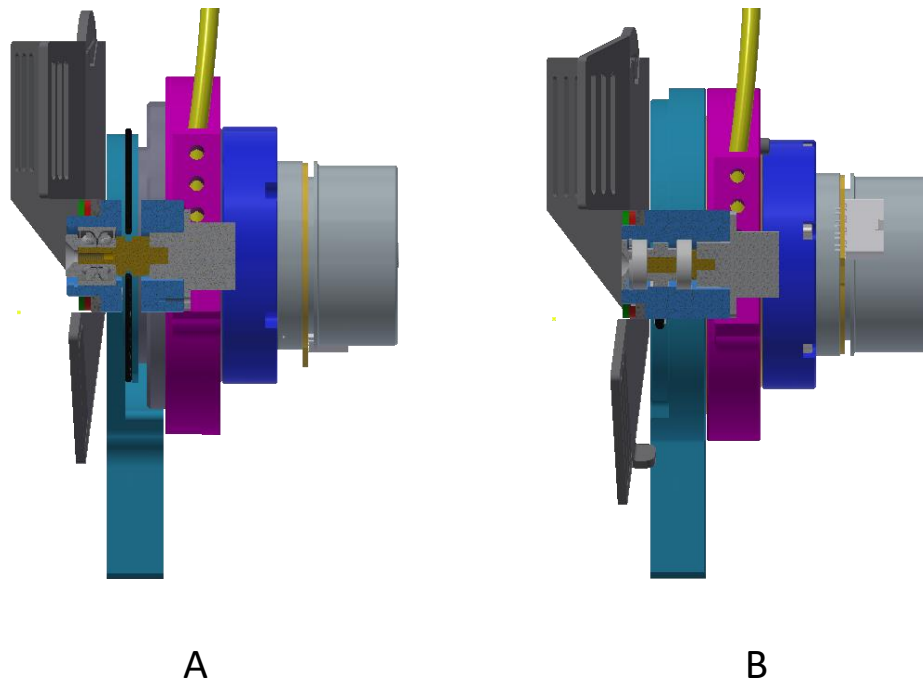


Figure 8.4.7: Semi-section view of the two solutions for the encoder integration: one double row deep groove ball bearing (A), two single row deep groove ball bearings (B).

8.4.4 Mechanical end-strokes definition

Due to the direct interaction between the wearable device and the user and the intended industrial application, the safety of the subject acquires a central role. The integration of the actuation system into the device imposes additional safety requirements in order to avoid any risks of accidents, breakdown of the system and malfunctions. In addition to stop and alarm conditions implemented in the control system, the exoskeleton must present some mechanical end-strokes. The mechanisms must prevent undesirable human kinematic postures in case of motor problems and unexpected control errors. The challenge consists in defining the correct range of motion available for the upper and the lower exoskeleton parts that could be modulated based on the anthropometry of the user.

The current Laevo passive exoskeleton allows the definition of the trunk angle at which the passive support element starts to be effective. The mechanism presents an adjustable range of motion from 0° to 35° , as already described in 4.1. For the powered prototype, it is necessary to define end-strokes for both trunk and thigh support bars. The main function of these end-strokes consists in the prevention of rotation of the exoskeleton bars beyond the physiological human range of motion. The mechanical end-strokes are independent to the actuation system, so they can

work in case of unexpected errors and/or failure of the control system. Moreover, with the attempt to satisfy different users characterized by different anthropometric dimensions, angular ranges are defined for trunk and thigh end-strokes.

Figure 8.4.8 depicts the graphical scheme of the three exoskeleton components, the trunk support, the pelvis belt and the thigh support (A) already described in previous chapters, the mechanisms of trunk support regulation available in the passive Laevo exoskeleton (B), and the mechanical end-strokes that must be implemented in the powered system (C).

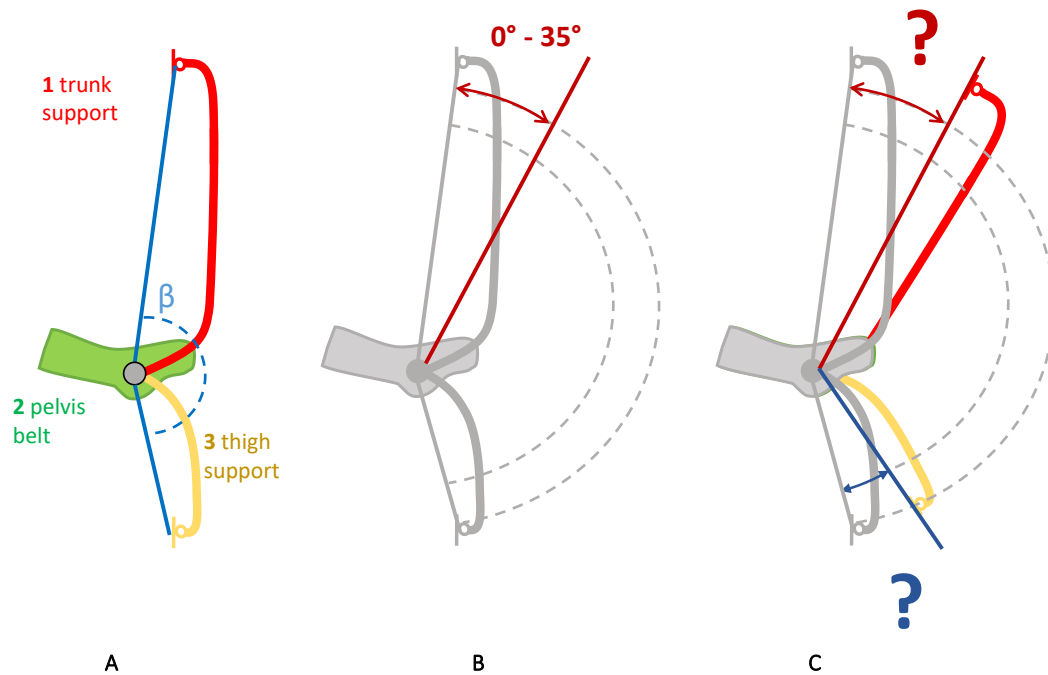


Figure 8.4.8: Graphical representation of the main exoskeleton components (A), range of the end-stroke in the passive Laevo solution that can be regulated (B), identification of the two end-stroke ranges that need to be defined in the powered prototype (C).

In addition to the safety end-strokes, a “*holding posture*” function can be added to the powered device. The working principle is the same of the two mechanical end-strokes. A specific angle range of trunk flexion is considered for the holding static posture. The user can define the angle of flexion, can fix the trunk support bar in the selected position with a mechanical pin and can hold the static stoop posture even for a long time. The exoskeleton maintains the position and the user can lean the trunk on the chest pad. This function can substitute the actuation in case of prolonged task, preventing the overload and the heating of the motors.

Starting from the dimensions of the exoskeleton, a map is developed for the definition of angular ranges. As shown in Figure 8.4.9, the β angle depicts the relative angle between the segment HT (link between the exoskeleton joint center and the trunk pad position) and the segment HL (link between the exoskeleton joint center and the thigh pad position). These two segments (yellow bar in Figure 8.4.9) define the starting zero configuration of the device. The map is defined starting

from the segment HL and describing rotational motion in counterclockwise direction. Three main areas are depicted by the map, covering all the angular range between the two bars. Figure 8.4.9 shows the schematization of the exoskeleton with the overlapping of the developed map.

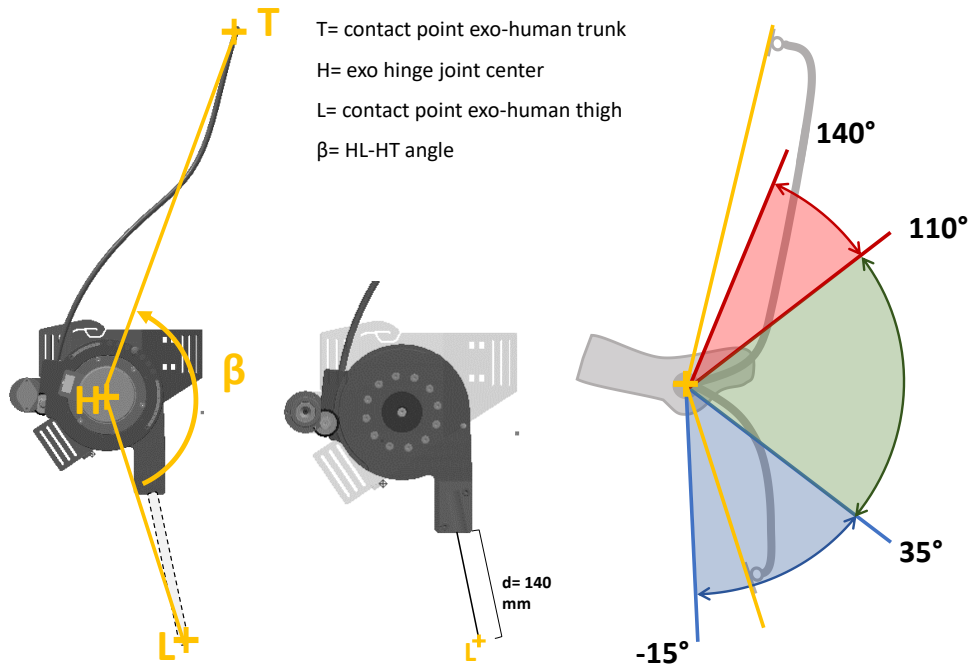


Figure 8.4.9: Exoskeleton map of the different angular ranges implemented in the powered system.

- The blue area depicts the angular interval that defines a safety lock to limit the minimum angle of the trunk and thigh bars, in case of trunk and/or thigh flexion. It describes a range from -15° to 35° respect to the zero-starting posture. The negative range of angles allows the user to perform an iper-extension of the hip joint. It is necessary in order to avoid any restrictions in a standing position or in the stance phase during gait.

- The red area depicts the safety lock to limit human trunk iper-extension in opening phase. It is necessary in case of motors error and undesirable push of the trunk support bar in counterclockwise direction. Moreover, it allows the adjustable starting flexion of the bar based on the anthropometric measure of the user's chest. The red area covers a range from 110° to 140° .

- The green area, covering the range from 35° to 110° , represents the lock for the holding static stoop posture. This lock can be fixed and removed during the task, based on the user's motion and requirement.

All the safety blocks must be defined by the user during the wearing process. Both the blue and red safety areas allow a 5° step for the pin positioning, while the green area allows a 10° step. Table 8.4.1 sums up the function, the range and the pin positions of the three areas. The experimental verification of functionality of the safety block has been conducted with the same four subjects that tested Laevo wereability.

The validation consists in the overlapping of the exoskeleton range map on the pictures of subjects wearing the exoskeleton and performing different motion positions. The first movement describes the static standing posture and it is reported in Figure 8.4.10.

Table 8.4.1: Numerical definition of the end-stroke angular range implemented in the powered prototype.

END STROKE RANGE		
Function	PIN Positioning	PIN Positioning details
OPEN (Safety lock to limit human trunk iper-extension)	Range 110°-140° with 5° step	140° 135° 130° 125° 110°
CLOSE (Lock to maintain static stoop posture)	Range 35°-110° 7 pins	
CLOSE (Safety lock to limit the closing range of exoskeleton)	Range -15°-35° with 5° step	35° 30° 25° 20° -15°

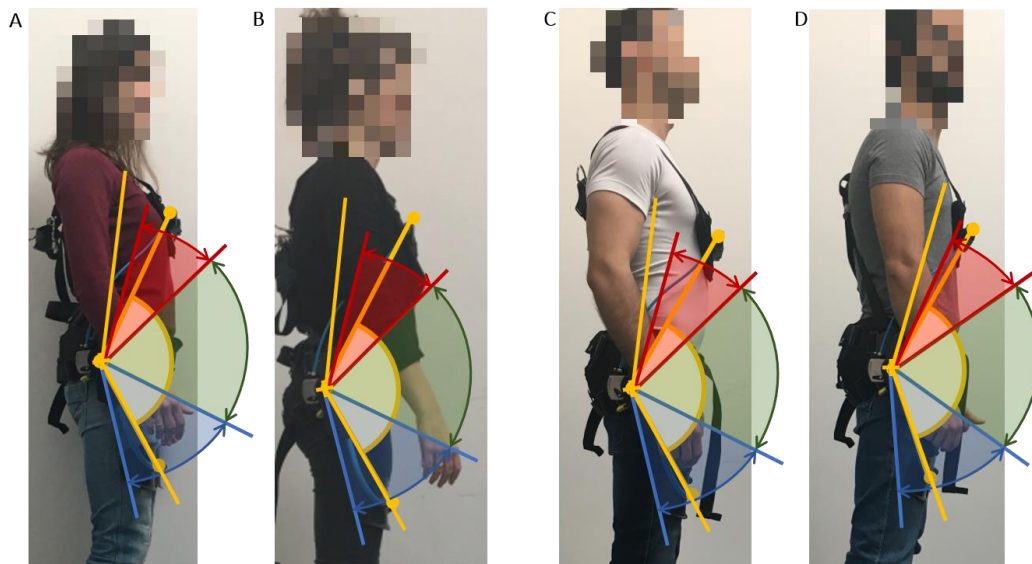


Figure 8.4.10: Validation of the exoskeleton end-stroke map during standing posture with four different subjects, two females (A-B) and two males (C-D).

The two females (A-B) and one male (C) shows good results. Indeed, the trunk-support bar correctly falls on the red area. It means that, the red area can be used for the definition of the starting trunk flexion posture and satisfy the wearability

requirements of different subjects. For the second male (D), the trunk bar results inside the red area, but in a border position. Nevertheless, it must be stressed that based on this height the subject is not suitable for the present size of the exoskeleton. For these reasons, he could be considered as a borderline case. The β angle between the two bars results 127° (A), 122° (B), 126° (C) and 135° (D) respectively.

Figure 8.4.11 depicts the four subjects performing the holding stoop posture. In all cases the trunk support bar falls on the green area. The two females (A-B) perform a lower trunk flexion because they are just leaning the hands on the table, but they are not working on it, as the two males are doing (C-D). The β angle results 95° (A), 94° (B), 82° (C) and 85° (D) respectively.

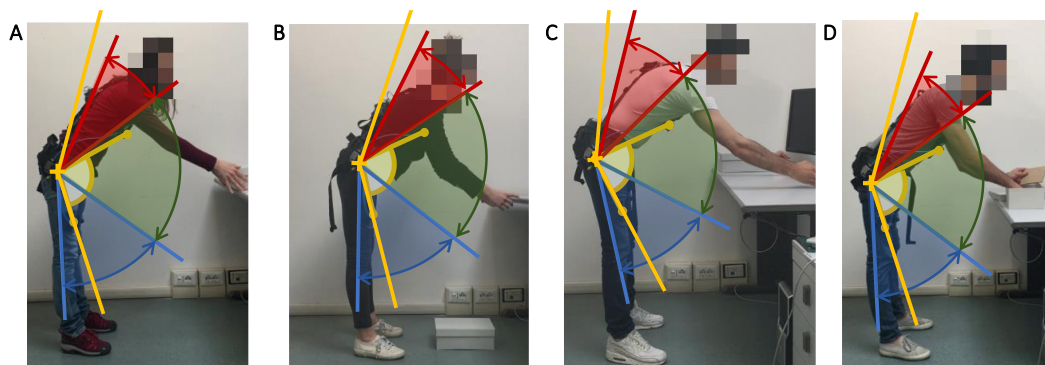


Figure 8.4.11: Validation of the exoskeleton end-stroke map during static holding stoop posture with four different subjects, two females (A-B) and two males (C-D).

Figure 8.4.12 depicts the first female subject performing three lifting strategies: stoop (A), semisquat (B), and squat (C). In stoop and semisquat, both trunk and thigh support bars fall on the blue area, while, in the squat, the thigh support bar falls on the blue area, the trunk support bar on the green area. The β angle results 30° in stoop, 26° in semisquat and 40° in squat.

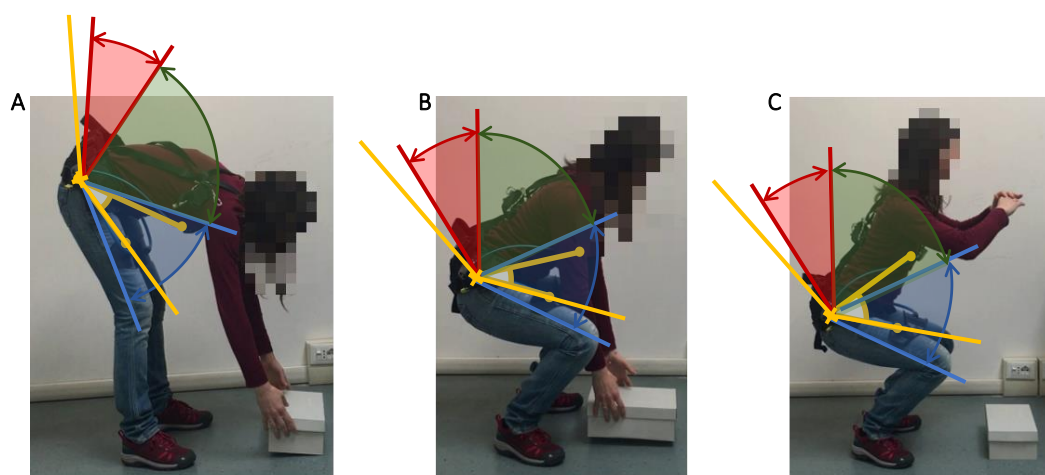


Figure 8.4.12: Validation of the exoskeleton end-stroke map with the first female subject during three lifting dynamic motion: stoop (A), semisquat (B), squat (C).

Figure 8.4.13 depicts the second female subject during stoop (A), semisquat (B), and squat (C). In semisquat motion, both trunk and thigh support bars fall on the blue area, while in the stoop and squat, the thigh support bar falls on the blue area, the trunk support bar on the green area. The β angle between the two bars results 45° in stoop posture, 27° in semisquat posture and 90° in squat posture.

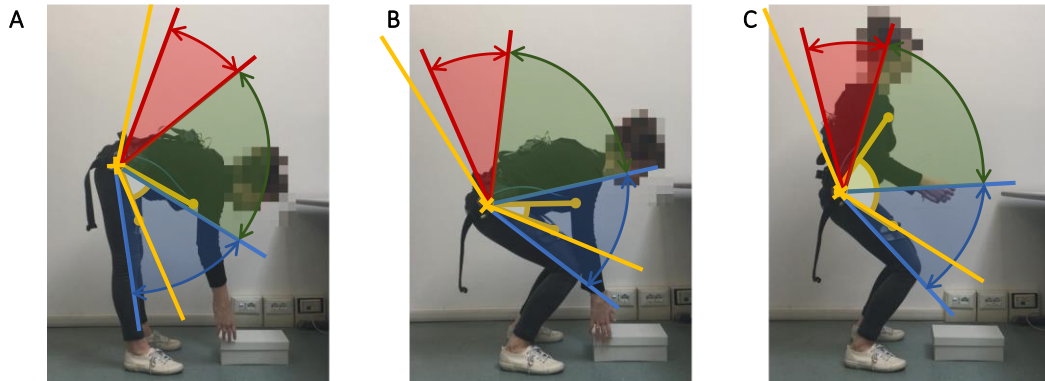


Figure 8.4.13: Validation of the exoskeleton end-stroke map with the second female subject during three lifting dynamic motion: stoop (A), semisquat (B), squat (C).

Figure 8.4.14 depicts the first male subject during stoop (A), semisquat (B), and squat (C). In all the three motions both trunk and thigh support bars fall on the blue area. The β angle between the two bars results 25° in stoop posture, 10° in semisquat posture and 45° in squat posture. Figure 8.4.15 depicts the second male subject during stoop (A), semisquat (B), and squat (C). In all the three motions both trunk and thigh support bars fall on the blue area. The β angle between the two bars results 45° in stoop, 13° in semisquat and 27° in squat posture. The results stress the validity and suitability of the designed exoskeleton range map both with different anthropometric measures, with different performed angular range and in all lifting strategies (stoop, semisquat, squat). Indeed, the exoskeleton bars never fall outside the depicted areas. The semisquat reveals to be the movement with closest relative angle, while the squat is performed with different depth due to the subject's ability.

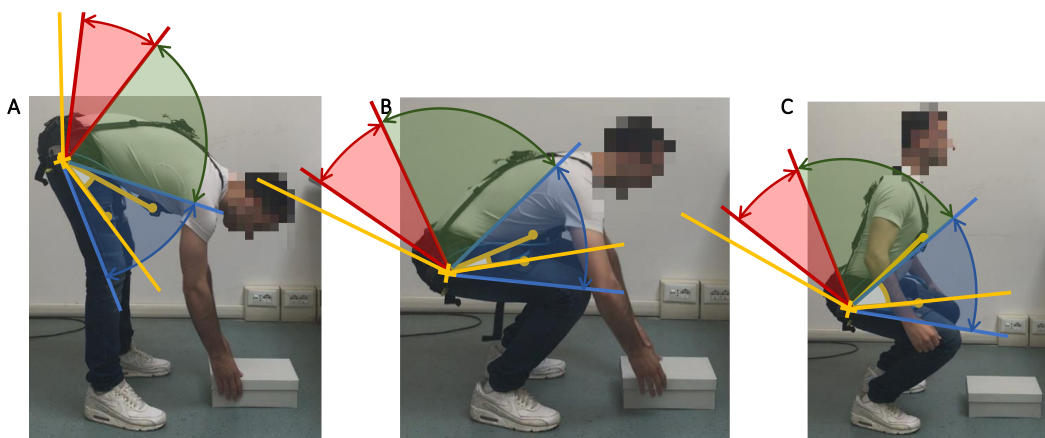


Figure 8.4.14: Validation of the exoskeleton end-stroke map with the first male subject during three lifting dynamic motion: stoop (A), semisquat (B), squat (C).

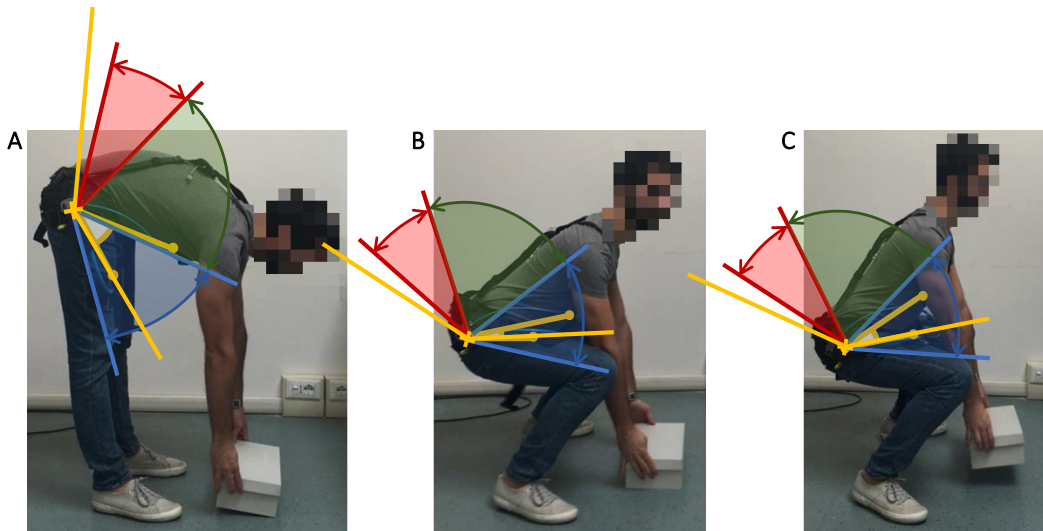


Figure 8.4.15: Validation of the exoskeleton end-stroke map with the second male subject during three lifting dynamic motion: stoop (A), semisquat (B), squat (C).

8.4.5 Mechanical description of the final proposal

From the previously described mechanical considerations, biomechanical analyses and the several proposals, the final solution of the powered exoskeleton joint can be summed up.

The implemented solution allows the maintenance of Laevo support bars, without the modification of the exoskeleton size. The contact points between the human body and the exoskeleton are maintained. The powered joint provides a new pelvis belt plate for the integration of all the kinematic sensors. The powered joint must be positioned in correspondence of the human hip joint. Two independent assistance systems are developed, one for each side. The separation of the actuation system in two parts allows to consider the whole assistance torque provided by two motor units, reducing the maximum torque required to the motor system. More compact, smaller and more lightweight actuation system can be implemented. Additional advantages can be stressed in terms of the distribution of the total weight of the device. Indeed, the user can perceive the added weight on different lateral parts of the human body. This solution avoids the overloads of the human back and the reduction of human body balance which may occur in case of positioning the actuation on the backside of the human body. The additional weight results 2 kg for each side, for a total weight of 6.5 kg of the whole powered system. Figure 8.4.16 A shows the Laevo exoskeleton and the zoom view of the device component with the powered component. The implemented solution can be considered with a small encumbrance. Indeed, as reported in Figure 8.4.16 B, the overall dimension is 115 mm for the diameter of the joint and 101 mm for the lateral involved space. Figure 8.4.17 and Figure 8.4.18 depict the exploded view of the CAD design from 45° view and lateral view respectively. The several mechanical elements are labeled and stressed with different colors.

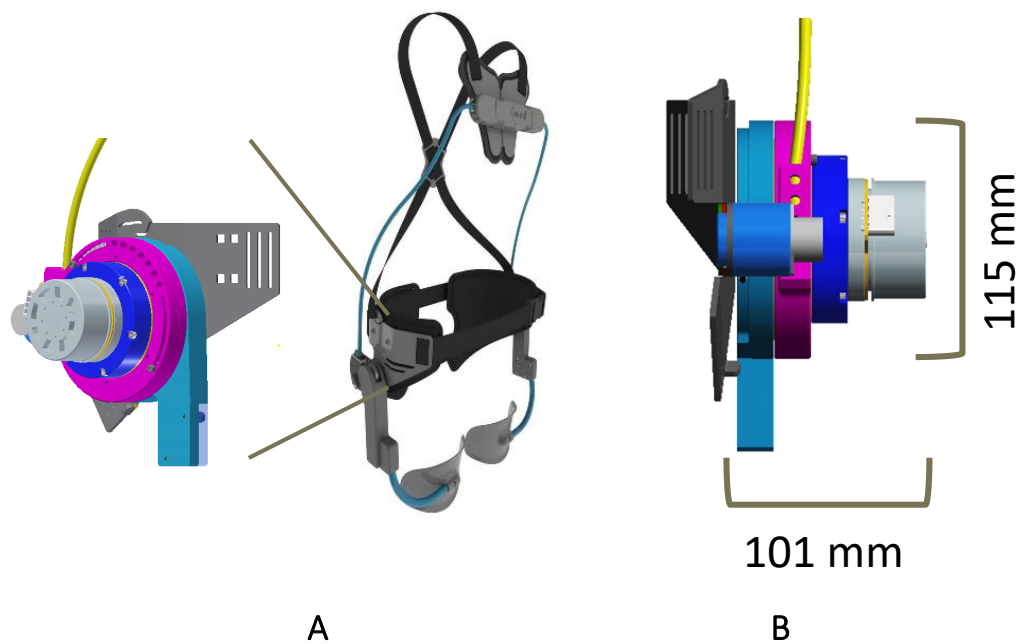


Figure 8.4.16: Powered exoskeleton joint solution proposed: (A) graphical representation of the integration of the powered joint into the Laevo exoskeleton, (B) lateral view of the powered joint stressing the height and lateral encumbrance.

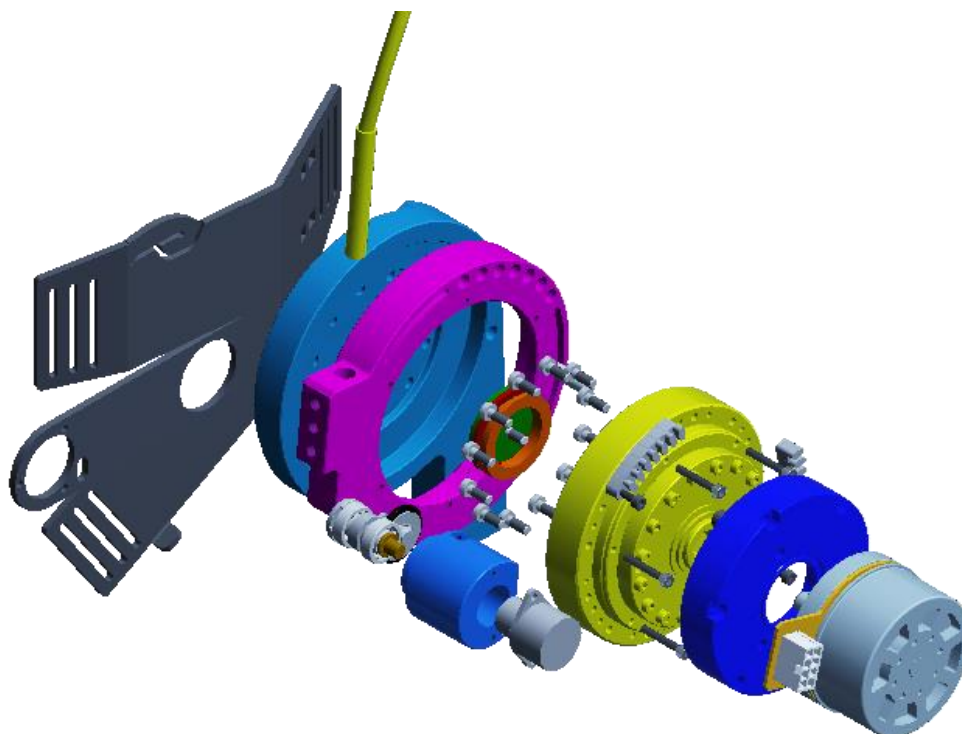


Figure 8.4.17: Exploded view drawing of the powered joint: the final solution.

Based on the previous discussions, the solution presents:

- the freewheel transmission system to transmit the rotational motion of the thigh bar support relative to the pelvis belt plate to the misaligned secondary encoder (ELAP encoder);

- draft-pulley system to connect the rotary encoder to the freewheel;
- the two single row deep groove ball bearings to fix the secondary encoder to the pelvis belt plate by means of coupling element;
- optimization of the geometrical shape of the mechanical components in order to limit the encumbrance and spatial dimensions;
- proper definition of the mechanical end-strokes ranges based on the biomechanical analysis of human movements both during lifting and gait tasks.

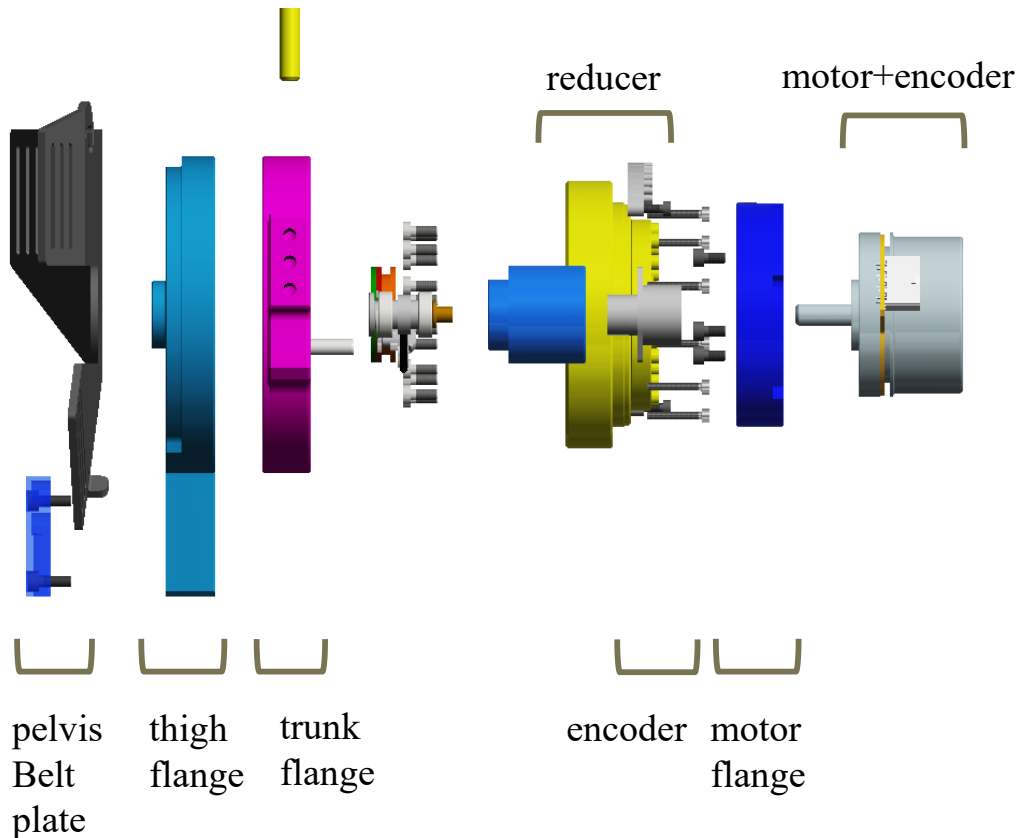


Figure 8.4.18: Exploded lateral view drawing of the powered joint: the final solution. Labeling of the several components.

8.5. Mechanical components connection

Once defined all the mechanical and electrical components, it is necessary to realize a proper connection between them and the integration to the Laevo passive exoskeleton. As already mentioned, in this first prototype only the actuation system and the sensors will be added to the structure, while the control and powering systems will be remote. Suitable cables must be considered for the linkage between elements. The CAN-CAN cable allows the series connection between the two drivers, while the CAN-COM cable is necessary to link the second driver to the can interface device. A shield cable with proper connectors lined the motor to driver, and a ribbon cable with connector links the integrated encoder to the driver. Finally,

two power cables allow the connection with the two power supply devices, one for each exoskeleton joint. Figure 8.5.1 depicts the simulation of connection with the motor-reducer. The secondary encoder and the connection by means of the DAQ system is not reported in the present picture.

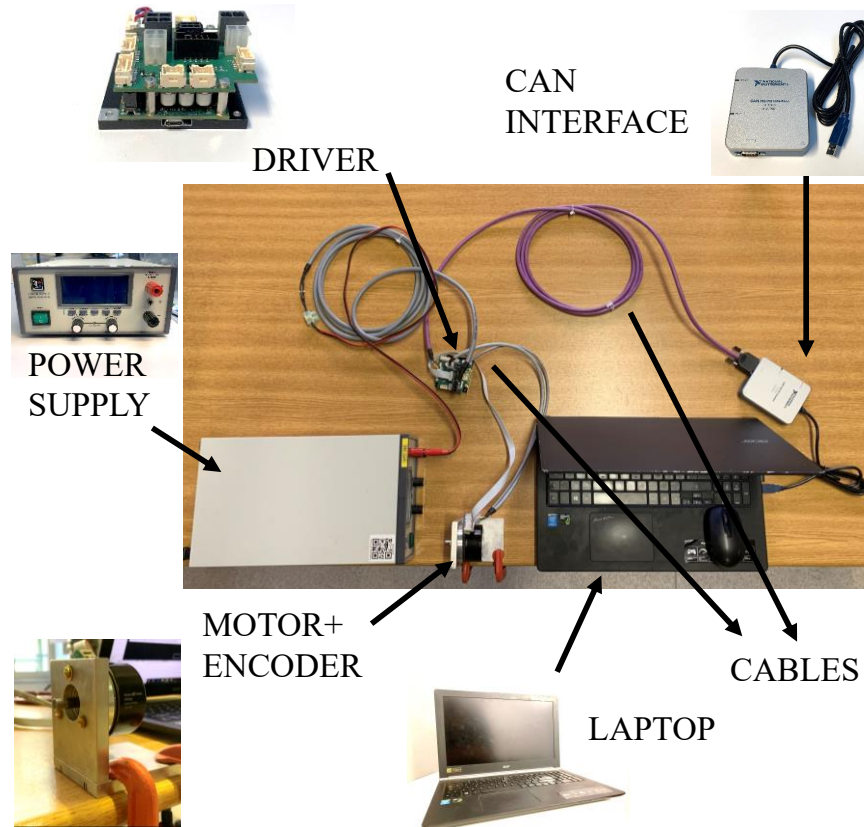


Figure 8.5.1: Bench simulation of the mechanical components (motor and integrated encoder) and electronic devices (laptop, driver, can interface device and power supply) connections.

8.6. Exoskeleton assembly

Once defined the final design of the structure, the several mechanical elements of connections have been realized and assembled. All the several components are made of Aluminium 6082, expected the pelvis plate, that is made of stainless steel AISI 304. Figure 8.6.1 depicts the pelvis plate from frontal (A), behind (B) and perspective (C) view. Figure 8.6.1 D-E represents a detailed view of the housing for the secondary angular sensor and the free wheel for the transmission of the rotational movement. The first step of the assembly consists in the connection between the pelvis plate and the flange for the thigh connection, depicted in Figure 8.6.2 from the front (A) and behind (B) side. Figure 8.6.2 shows the two components with the washers and spacer for the connection.

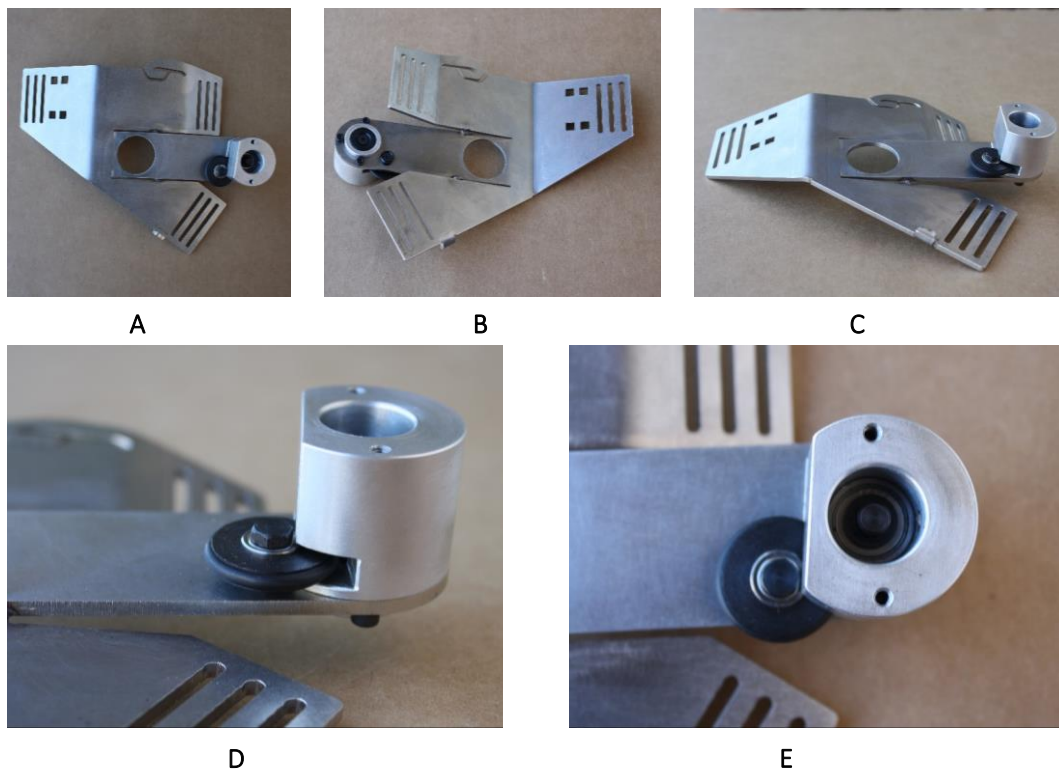


Figure 8.6.1: Pelvis plate of the powered exoskeleton realized in stainless steel AISI 304. Front (A), behind (B), perspective (C) view of the plate. Zoom view (D-E) on the support for the secondary angular sensor and the free wheel.

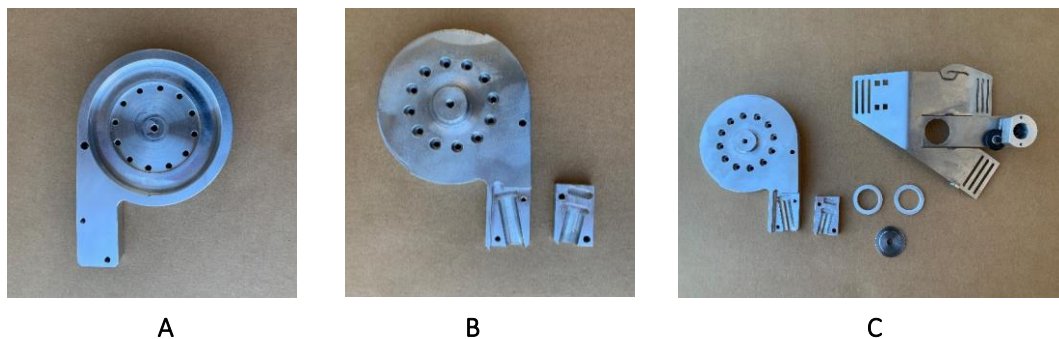


Figure 8.6.2: Flange for the connection with leg pad from front (A) and behind (B) view, made in Aluminium 6082. Thigh flange, pelvis belt, washers and spacer (C).

The second step consists in fixing the harmonic drive reducer to the thigh flange, followed by the positioning of trunk flange connected to the harmonic drive. In particular, in the current configuration, for a correct torque transmission between the thigh and trunk flanges, the Flexspline is connected to the thigh flange, while the trunk flange is fixed to the Circular Spline. Moreover, considering the motor, the rotor results linked to the reducer by means of the Wave Generator, and the stator to the Circular Spline by means of the motor flange. Figure 8.6.3 depicts the flange for the connection with the trunk support from several views (front, behind and lateral). In the picture, a zoom view on the buttonhole for the end-stroke range definition is reported.

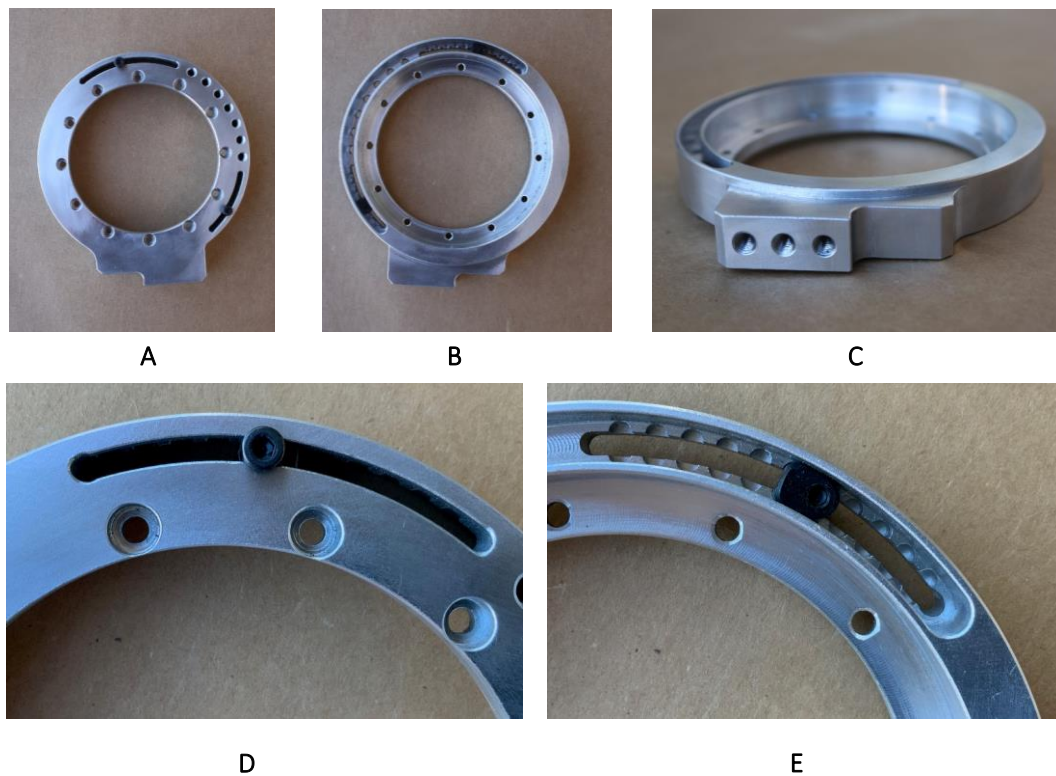


Figure 8.6.3: Exoskeleton flange for the connection with the trunk support from frontal (A), behind (B) and lateral (C) view. Zoom view of the buttonhole for the end-stroke range implementation (D-E).

Figure 8.6.4 shows the two passages for the connection of harmonic drive (A) and the trunk flange (B), as the representation of motor assembled with the flange (C) for motor-reducer connection. Finally, once positioned the motor fixed to the reducer, the powered joint results assembled. The last step consists in the positioning of the ELAP angular sensor.

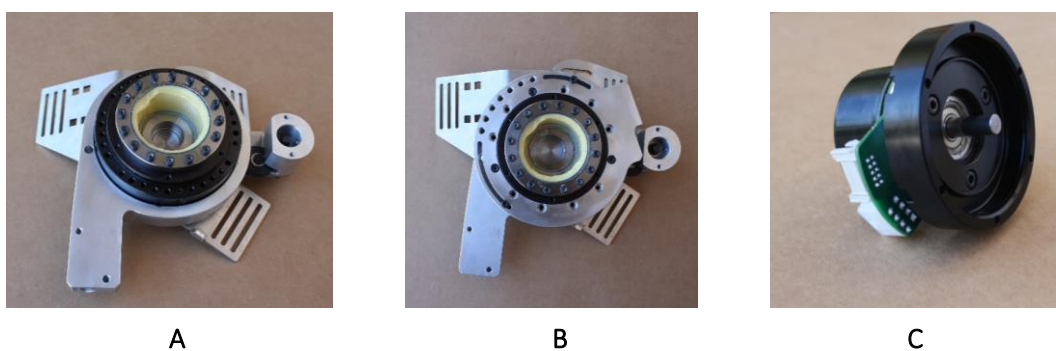


Figure 8.6.4: Positioning of the harmonic drive reducer (A), of the trunk flange (B) and particular view of motor+flange assembly (C).

Figure 8.6.5 depicts several views of the final two powered joints. The total weight of each powered joints is 2.8 Kg. Once connected all the rigid components of the powered joints, the trunk and thigh bars can be connected in order to fix the interface pads to the structure. Soft pelvis belt and shoulder suspenders are

integrated into the structure for the flexible connection. The final assembly of the entire exoskeleton is depicted in Figure 8.6.6. The total weight of the structure is 7 Kg.

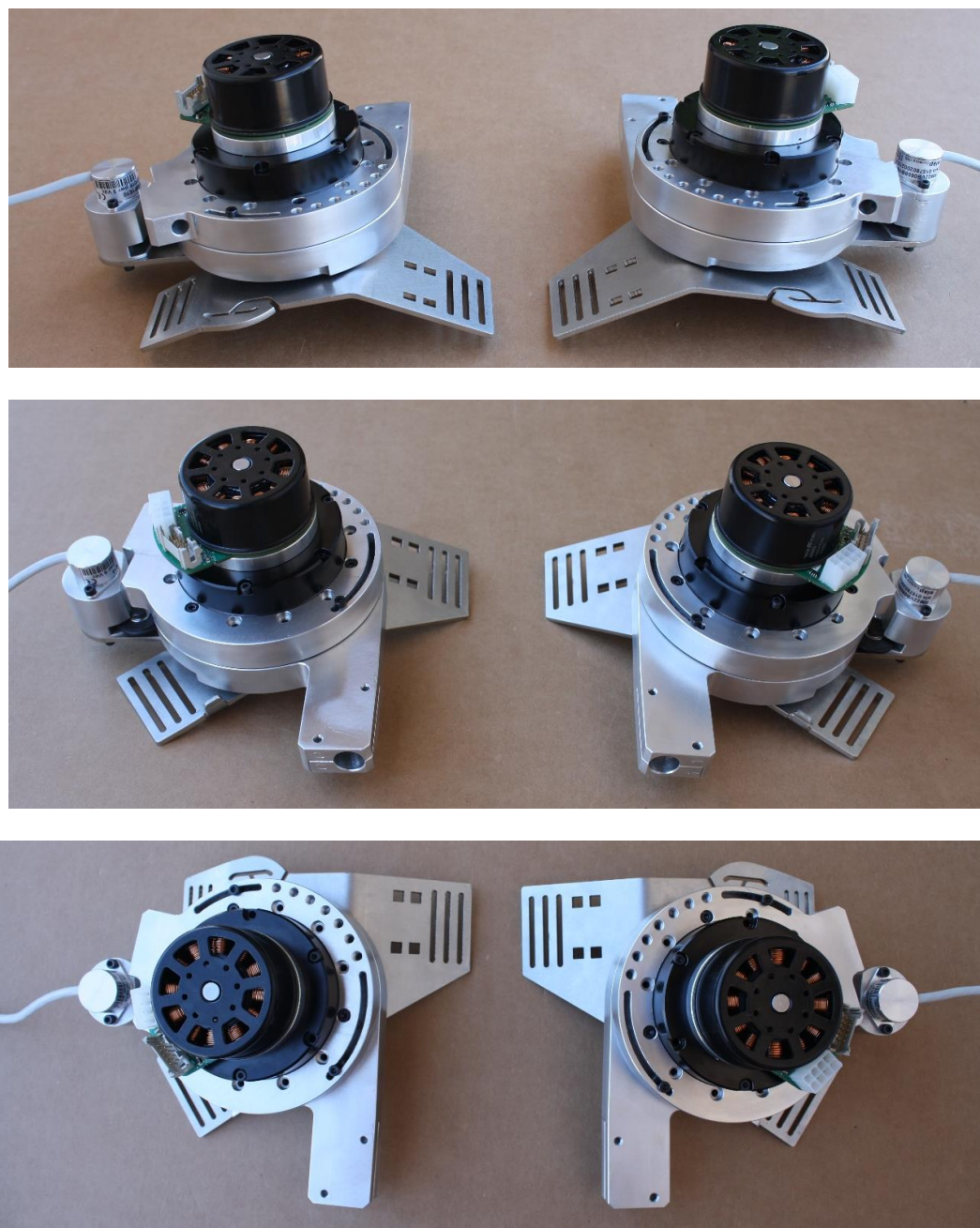


Figure 8.6.5: Perspective views of the two powered joints assembled.



Figure 8.6.6: Final assembly of the powered exoskeleton.

8.7. First wearability assessment

The powered exoskeleton has been worn in a preliminary step by one female subject, in order to verify the wearability of the structure, the perception and the distribution of the total weight of the structure and the possibility to perform the different lifting strategies. Figure 8.7.1 shows the subject in standing posture from different views (lateral, frontal and behind sides). The subject is wearing the powered exoskeleton without the cable connections. From the current pictures, it is possible to highlight good wearability and limited lateral encumbrance of the structure. Figure 8.7.2 shows a detailed view of the standing posture from frontal and lateral sides. Figure 8.7.3 depicts the subject during dynamic lifting motion of an external mass performing stoop (A), semisquat (B) and squat (C) strategy. Both in static and dynamic movements, the subject declared a positive perception of the device, with a good weight distribution around the pelvis.

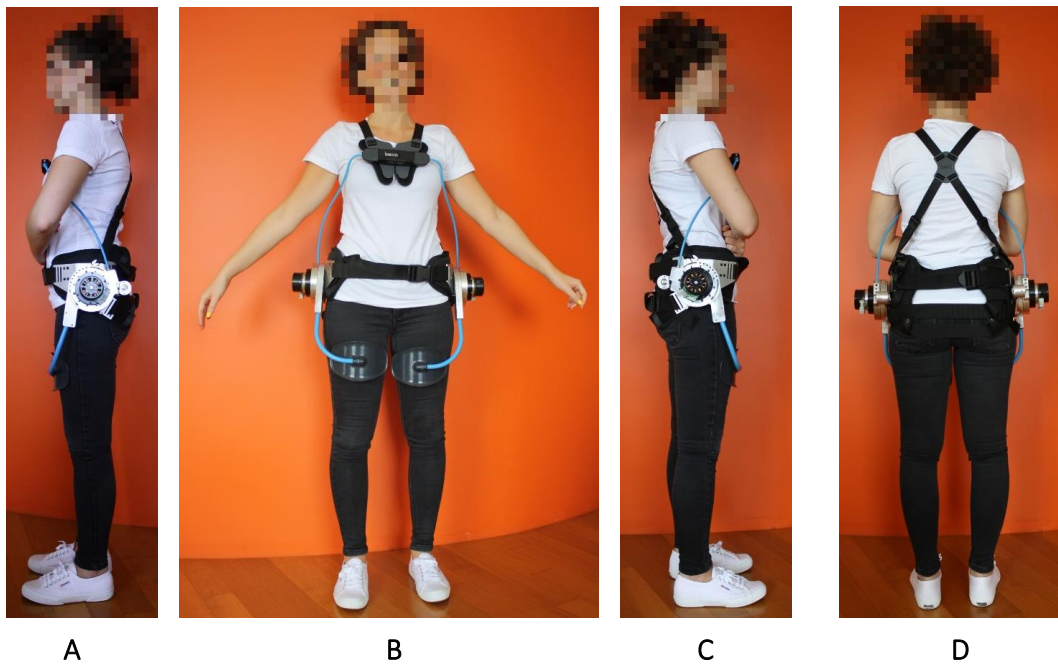


Figure 8.7.1: One female subject with a height < 1.72 m wearing the powered exoskeleton from lateral view (A-C), front view (B) and behind view (D).

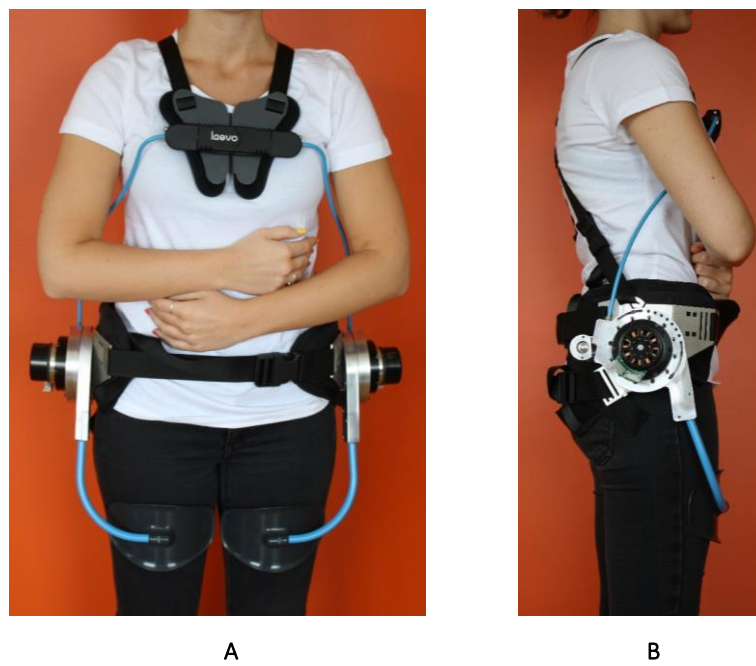


Figure 8.7.2: Detailed view of frontal (A) and lateral (B) sides during standing.

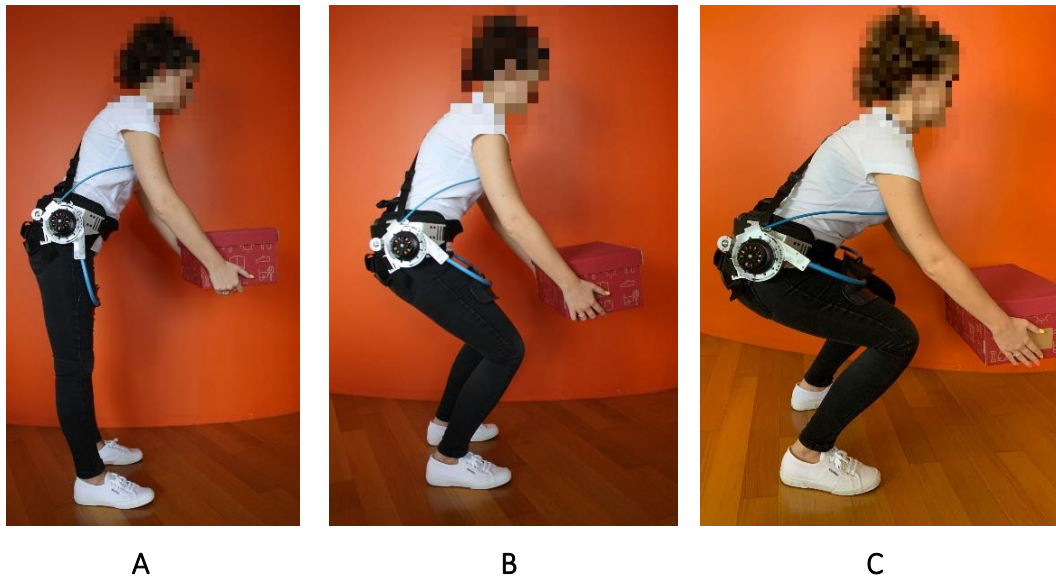


Figure 8.7.3: One female subject wearing the powered prototype exoskeleton and performing stoop (A), semisquat (B) and squat (C) lifting.

Chapter 9

CONCLUSIONS

9.1. Study results

The current study has presented the analysis, design, development of a trunk-support exoskeleton prototype for the worker's assistance in lifting and handling tasks in a manufacturing environment. The proposed device is characterized by powered joints that supply assistance to the user acting between the trunk and the thigh supports. Electric motors coupling with harmonic drive reducers are integrated in the powered joint for providing the needed torque.

The support torque is modulated based on the kinematics of the movements and the user's requirements. Incremental encoder integrated into the motor systems monitors the angles between trunk and thigh supports, while the secondary encoder with a proper transmission system monitors the angle between the thigh support and the pelvis plate.

The structure was developed based on a careful and profound investigation on the human-device interaction, both with experimental and computational approach. The biomechanical evaluation allowed to assess the architecture of the exoskeleton, the position of its joints, the intensity of the assistive torque and the necessity to distinguish between the different lifting strategies, since the assistance required to the powered exoskeleton depends on the user's kinematics.

The mechanical device and control system were designed to be suitable for the required assistance and to assure a good interaction with the human body. A final assembly of the structure is presented and preliminary tests of wearability have been conducted.

The use of wearable devices in industrial and manufacturing environments promises to be a suitable solution for the prevention of musculoskeletal diseases, for supporting the workers in repetitive and heavy tasks and to reduce the human

body efforts. Deeper investigations and experimental tests might be necessary in order to improve the current proposed solutions.

9.2. Future perspectives

Once assembled the whole structure, it is important to test it. For this reason, the first future step will consider the validation of the control law according to the assistance map. A test bench might be implemented with the attempt to verify the supplied torque, the stability and the backdrivability of the system, the transparency in case of no required input torque and the effectiveness of the high-level control. Due to the remote master control, it is possible to investigate several assistive strategies. One important aspect that needs deeper investigation is the effectiveness of the device in case of motion asymmetry. Due to the powered system and the possibility to differentiate the required assistance torque from left and right side, a proper assistance law may be implemented. Also, in this case, the 3D multibody models might be a beneficial support for the analysis of human motion asymmetry.

Experimental tests can be conducted in laboratory setting in order to simulate the lifting and handling industrial task of interest. Due to the reversible structure from passive to powered solution, the same exoskeleton with the two mechanisms can be worn by the same users in short interval time. The direct comparison of the two solutions can be one fundamental test verification for future perspectives. The presented preliminary test could be the starting point for the implementation of an experimental protocol. Larger sample size with participants of different gender and age might be considered. Additional setup conditions and biomechanical variables can be integrated in the experimental study.

Finally, some structural improvements might interest the adaptation of interface pads to additional comfort. A larger contact area could be useful for the reduction of perceived pressure. The pelvis belt and the shoulder suspenders might be revised in order to improve the wearability of the exoskeleton. Moreover, some free degrees of freedom at the hip joint level can be integrated to reduce the obstruction of 3D motion.

References

1. Alonso V, De La Puente P (2018) System transparency in shared autonomy: A mini review. *Front. Neurobot.* 12
2. <http://www.botmag.com/the-rise-and-fall-of-unimation-inc-story-of-robotics-innovation-triumph-that-changed-the-world/>, accessed 2019/09/04
3. <https://new.abb.com/products/robotics/>, accessed on 2019/09/04
4. <https://www.kuka.com/en-gb>, accessed on 2019/09/04
5. Parent-Thirion A et al. (2016) Sixth European Working Conditions Survey: Overview Report. Eurofound (European Foundation for the Improvement of Living and Working Conditions).
6. De Looze MP, Bosch T, Krause F, et al (2016) Exoskeletons for industrial application and their potential effects on physical work load. *Ergonomics* 59:671–681. <https://doi.org/10.1080/00140139.2015.1081988>
7. <https://www.osha.gov/laws-regs/oshact/completeoshact>, accessed 2019/08/28
8. <http://www.niosh.com.my/>, accessed on 2019/09/04
9. Toxiri S, Näf MB, Lazzaroni M, et al (2019) Back-Support Exoskeletons for Occupational Use: An Overview of Technological Advances and Trends. *IISE Trans Occup Ergon Hum Factors* 1–13. <https://doi.org/10.1080/24725838.2019.1626303>
10. <https://www.comau.com/it/mate>, accessed 2019-08-20
11. <https://www.levitatetech.com/>, accessed 2019/08/20
12. Kadota K, Akai M, Kawashima K, Kagawa T (2009) Development of power-assist robot arm using pneumatic rubber muscles with a balloon sensor. In: *Proceedings - IEEE International Workshop on Robot and Human Interactive Communication*. pp 546–551
13. <https://www.suitx.com/backx>, accessed 2019/08/20.
14. <http://en.laevo.nl/>, accessed 2018/11/21
15. Stadler KS, Altenburger R, Schmidhauser E, et al (2017) Robo-Mate an Exoskeleton for Industrial Use—Concept and Mechanical Design. *Adv Coop Robot* 806–813
16. <https://www.noonee.com/en/>, accessed 2019/08/20.
17. <https://www.lexbyastride.com/>, accessed on 2020/03/04
18. <https://www.archelis.com/>, accessed on 2020/03/04
19. Taal SR, Sankai Y (2011) Exoskeletal spine and shoulder girdle for full body exoskeletons with human versatility. In: *Proceedings - IEEE International Conference on Robotics and Automation*. pp 2217–2222
20. Marcheschi S, Salsedo F, Fontana M, Bergamasco M (2011) Body extender: Whole body exoskeleton for human power augmentation. In: *Proceedings - IEEE International Conference on Robotics and Automation*. pp 611–616
21. Christensen S, Bai S, Rafique S, et al (2019) AXO-SUIT - a modular full-body exoskeleton for physical assistance. In: *Mechanisms and Machine Science*. Springer Netherlands, pp 443–450

22. Näf MB, Koopman AS, Baltrusch S, et al (2018) Passive Back Support Exoskeleton Improves Range of Motion Using Flexible Beams. *Front Robot AI* 5:1–16. <https://doi.org/10.3389/frobt.2018.00072>
23. Herkowitz, H. N., Garfin, S. R., Eismont, F. J., Bell, G. R., & Balderston RA (2011) *Rothman-Simeone The spine- sixth edition*, Expert Con. ELSEVIER, SAUNDERS
24. Smith LJ, Fazzalari NL (2009) The elastic fibre network of the human lumbar annulus fibrosus: Architecture, mechanical function and potential role in the progression of intervertebral disc degeneration. *Eur. Spine J.* 18:439–448
25. Augustus A White MMP (1990) *Clinical Biomechanics of the Spine*. JB Lippincott
26. Vecchio L Del (2017) Choosing a Lifting Posture: Squat, Semi-Squat or Stoop. *MOJ Yoga Phys Ther* 2:1–7. <https://doi.org/10.15406/mojypt.2017.02.00019>
27. Oxland TR (2016) Fundamental biomechanics of the spine—What we have learned in the past 25 years and future directions. *J Biomech* 49:817–832. <https://doi.org/10.1016/J.JBIOMECH.2015.10.035>
28. Nachemson A (1966) Electromyographic studies on the vertebral portion of the psoas muscle: With special reference to its stabilizing function of the lumbar spine. *Acta Orthop* 37:177–190. <https://doi.org/10.3109/17453676608993277>
29. Nachemson A (1974) Lumbar intradiscal pressure Results from in vitro and in vivo experiments with some clinical implications. In: *Biopolymere und Biomechanik von Bindegewebsystemen*. Springer Berlin Heidelberg, Berlin, Heidelberg, pp 61–76
30. Wilke H-J, Neef P, Hinz B, et al (2001) Intradiscal pressure together with anthropometric data – a data set for the validation of models. *Clin Biomech* 16:S111–S126. [https://doi.org/10.1016/S0268-0033\(00\)00103-0](https://doi.org/10.1016/S0268-0033(00)00103-0)
31. Wilke HJ, Neef P, Caimi M, et al (1999) New in vivo measurements of pressures in the intervertebral disc in daily life. *Spine (Phila Pa 1976)* 24:755–762. <https://doi.org/10.1097/00007632-199904150-00005>
32. Nachemson A (1965) In vivo discometry in lumbar discs with irregular nucleograms some differences in stress distribution between normal and moderately degenerated discs. *Acta Orthop* 36:418–434. <https://doi.org/10.3109/17453676508988651>
33. Rohlmann A, Pohl D, Bender A, et al (2014) Activities of Everyday Life with High Spinal Loads. *PLoS One* 9:e98510. <https://doi.org/10.1371/journal.pone.0098510>
34. Polga DJ, Beaubien BP, Kallemeier PM, et al (2004) Measurement of In Vivo Intradiscal Pressure in Healthy Thoracic Intervertebral Discs. *Spine (Phila Pa 1976)* 29:1320–1324. <https://doi.org/10.1097/01.BRS.0000127179.13271.78>
35. Dreischarf M, Shirazi-Adl A, Arjmand N, et al (2016) Estimation of loads on human lumbar spine: A review of in vivo and computational model studies. *J Biomech* 49:833–845. <https://doi.org/10.1016/J.JBIOMECH.2015.12.038>
36. Burgess-Limerick R (2003) Squat, stoop, or something in between? In: *International Journal of Industrial Ergonomics*. pp 143–148
37. Videman T, Rauhala H, Asp S, et al (1989) Patient-handling skill, back

- injuries, and back pain: An intervention study in nursing. *Spine (Phila Pa 1976)* 14:148–156. <https://doi.org/10.1097/00007632-198902000-00002>
38. Nygård CH, Merisalo T, Arola H, et al (1998) Effects of work changes and training in lifting technique on physical strain: A pilot study among female workers of different ages. *Int J Ind Ergon* 21:91–98. [https://doi.org/10.1016/S0169-8141\(97\)00028-0](https://doi.org/10.1016/S0169-8141(97)00028-0)
39. Potvin JR, McGill SM, Norman RW (1991) Trunk muscle and lumbar ligament contributions to dynamic lifts with varying degrees of trunk flexion. *Spine (Phila Pa 1976)* 16:1099–1107. <https://doi.org/10.1097/00007632-199109000-00015>
40. Van Dieën JH, Van Der Burg P, Raaijmakers TAJ, Toussaint HM (1998) Effects of repetitive lifting on kinematics: Inadequate anticipatory control or adaptive changes? *J Mot Behav* 30:20–32. <https://doi.org/10.1080/00222899809601319>
41. Van Dieën JH, Hoozemans MJM, Toussaint HM (1999) Stoop or squat: A review of biomechanical studies on lifting technique. *Clin Biomech* 14:685–696. [https://doi.org/10.1016/S0268-0033\(99\)00031-5](https://doi.org/10.1016/S0268-0033(99)00031-5)
42. <https://www.osha.gov>, accessed 2020/01/15
43. <https://www.iso.org/obp/ui/#iso:std:iso:11228:-1:ed-1:v1:en>, accessed 2019/08/28
44. <https://www.iso.org/obp/ui/#iso:std:iso:11228:-2:ed-1:v1:en>, accessed 2019/08/28
45. <https://www.iso.org/obp/ui/#iso:std:iso:11228:-3:ed-1:v2:en>, accessed 2019/08/28
46. Abdoli-E M, Agnew MJ, Stevenson JM (2006) An on-body personal lift augmentation device (PLAD) reduces EMG amplitude of erector spinae during lifting tasks. *Clin Biomech* 21:456–465. <https://doi.org/10.1016/j.clinbiomech.2005.12.021>
47. Frost DM, Abdoli-E M, Stevenson JM (2009) PLAD (personal lift assistive device) stiffness affects the lumbar flexion/extension moment and the posterior chain EMG during symmetrical lifting tasks. *J Electromyogr Kinesiol* 19:. <https://doi.org/10.1016/j.jelekin.2008.12.002>
48. Lotz CA, Agnew MJ, Godwin AA, Stevenson JM (2009) The effect of an on-body personal lift assist device (PLAD) on fatigue during a repetitive lifting task. *J Electromyogr Kinesiol* 19:331–340. <https://doi.org/10.1016/j.jelekin.2007.08.006>
49. Sadler EM, Graham RB, Stevenson JM (2011) The personal lift-assist device and lifting technique: a principal component analysis. *Ergonomics* 54:392–402. <https://doi.org/10.1080/00140139.2011.556259>
50. Abdoli-E M, Stevenson JM (2008) The effect of on-body lift assistive device on the lumbar 3D dynamic moments and EMG during asymmetric freestyle lifting. *Clin Biomech* 23:372–380. <https://doi.org/10.1016/j.clinbiomech.2007.10.012>
51. Godwin AA, Stevenson JM, Agnew MJ, et al (2009) Testing the efficacy of an ergonomic lifting aid at diminishing muscular fatigue in women over a prolonged period of lifting. *Int J Ind Ergon* 39:121–126. <https://doi.org/10.1016/j.ergon.2008.05.008>
52. Collaboration HR, Ortiz JJ, Sreenivasa M, et al (2018) Optimizing wearable assistive devices with neuromuscular models and optimal control. *Appl Ergon* 49:2–4. <https://doi.org/10.1016/j.apergo.2017.11.004>

53. Heydari H, Hoviattalab M, Azghani MR, et al (2013) Investigation on a developed wearable assistive device (WAD) in reduction lumbar muscles activity. *Biomed Eng - Appl Basis Commun* 25:. <https://doi.org/10.4015/S101623721350035X>
54. Hadi Heydari, Mohamad Parnianpour, Maryam Hoviattalab, Mahmood Reza Azghani MR (2010) The Effect of a Developed Wearable Assistive Device (WAD) on Decreasing Lumbar and Erector spine Muscle Activities During *ESDA2010-24568*
55. Imamura Y, Tanaka T, Suzuki Y, et al (2011) Motion-based design of elastic belts for passive assistive device using musculoskeletal model. In: 2011 IEEE International Conference on Robotics and Biomimetics. IEEE, pp 1343–1348
56. Lamers EP, Yang AJ, Zelik KE (2018) Feasibility of a biomechanically-assistive garment to reduce low back loading during leaning and lifting. *IEEE Trans Biomed Eng* 65:1674–1680. <https://doi.org/10.1109/TBME.2017.2761455>
57. Wehner M, Rempel D, Kazerooni H (2010) Lower extremity exoskeleton reduces back forces in lifting. In: Proceedings of the ASME Dynamic Systems and Control Conference 2009, DSCC2009. American Society of Mechanical Engineers (ASME), pp 961–968
58. Alemi MM, Geissinger J, Simon AA, et al (2019) A passive exoskeleton reduces peak and mean EMG during symmetric and asymmetric lifting. *J Electromyogr Kinesiol* 47:25–34. <https://doi.org/10.1016/J.JELEKIN.2019.05.003>
59. <https://www.strongarmtech.com/>, accessed on 2019/08/28
60. Naruse K, Kawai S, Yokoi H, Kakazu Y (2003) Development of wearable exoskeleton power assist system for lower back support. *Proc 2003 IEEE/RSJ Int Conf Intell Robot Syst (IROS 2003) (Cat No03CH37453)* 3:3630–3635. <https://doi.org/10.1109/IROS.2003.1249719>
61. Kawai S, Naruse K, Yokoi H, Kakazu Y (2004) An Analysis of Human Motion for Control of a Wearable Power Assist System. *J Robot Mechatronics* 16:237–244. <https://doi.org/10.1299/jsmermd.2003.82>
62. Hara H, Sankai Y (2010) Development of HAL for lumbar support. *SCIS ISIS 2010 - Jt 5th Int Conf Soft Comput Intell Syst 11th Int Symp Adv Intell Syst* 416–421
63. Miura K, Kadone H, Koda M, et al (2018) The hybrid assistive limb (HAL) for Care Support successfully reduced lumbar load in repetitive lifting movements. *J Clin Neurosci* 53:276–279. <https://doi.org/10.1016/J.JOCN.2018.04.057>
64. Miura K, Kadone H, Koda M, et al (2018) The hybrid assisted limb (HAL) for Care Support, a motion assisting robot providing exoskeletal lumbar support, can potentially reduce lumbar load in repetitive snow-shoveling movements. *J Clin Neurosci* 49:83–86. <https://doi.org/10.1016/J.JOCN.2017.11.020>
65. Naruse K, Kawai S, Kukichi T (2005) Three-dimensional lifting-up motion analysis for wearable power assist device of lower back support. *2005 IEEE/RSJ Int Conf Intell Robot Syst IROS* 3443–3448. <https://doi.org/10.1109/IROS.2005.1545503>
66. Luo Z, Yu Y (2013) Wearable stooping-assist device in reducing risk of low back disorders during stooped work. In: 2013 IEEE International Conference

- on Mechatronics and Automation, IEEE ICMA 2013. pp 230–236
67. Toxiri S, Masood J, Fern J, et al (2015) A Wearable Device for Reducing Spinal Loads during Lifting Tasks : Biomechanics and Design Concepts. In: IEEE (ed). pp 2295–2300
 68. Toxiri S, Verstraten T, Calanca A, et al (2019) Using parallel elasticity in back-support exoskeletons: a study on energy consumption during industrial lifting tasks. In: 2019 Wearable Robotics Association Conference (WearRAcon). IEEE, pp 1–6
 69. <http://atoun.co.jp/products/atoun-model-y>, accessed 2019/08/30
 70. <https://www.germanbionic.com/crayx/>, accessed on 2019/09/05
 71. Ko HK, Lee SW, Koo DH, et al (2018) Waist-assistive exoskeleton powered by a singular actuation mechanism for prevention of back-injury. *Rob Auton Syst* 107:1–9. <https://doi.org/10.1016/j.robot.2018.05.008>
 72. Hyun DJ, Lim HS, Park SI, Nam S (2020) Singular Wire-Driven Series Elastic Actuation with Force Control for a Waist Assistive Exoskeleton, H-WEXv2. *IEEE/ASME Trans Mechatronics* 25:1026–1035. <https://doi.org/10.1109/TMECH.2020.2970448>
 73. Hassan M, Kennard M, Yagi K, et al (2019) MRLift: a Semi-active Lower Back Support Exoskeleton based on MR Fluid and Force Retention Technology. In: 2019 IEEE/RSJ International Conference on Intelligent Robots and Systems (IROS). IEEE, pp 7349–7354
 74. Ting Zhang HH (2018) A lower-back robotic exoskeleton: industrial handling augmentation used to provide spinal support. *IEEE Robot Autom Mag* 25.2:95–106
 75. Lee J won, Kim G (2019) Design and Control of a Lifting Assist Device for Preventing Lower Back Injuries in Industrial Athletes. *Int J Precis Eng Manuf*. <https://doi.org/10.1007/s12541-019-00183-0>
 76. Yong X, Wang C, Wang C, et al (2017) Development of a low-power wearable powered waist exoskeleton with mechanical clutch. 2017 IEEE Int Conf Inf Autom ICIA 2017 177–182. <https://doi.org/10.1109/ICInfA.2017.8078902>
 77. Yong X, Yan Z, Wang C, et al (2019) Ergonomic Mechanical Design and Assessment of a Waist Assist Exoskeleton for Reducing Lumbar Loads During Lifting Task. *Micromachines* 10:463. <https://doi.org/10.3390/mi10070463>
 78. Kobayashi H, Nozaki H (2007) Development of muscle suit for supporting manual worker. *IEEE Int Conf Intell Robot Syst* 1769–1774. <https://doi.org/10.1109/IROS.2007.4399412>
 79. Aida T, Nozaki H, Kobayashi H (2009) Development of muscle suit and application to factory laborers. 2009 IEEE Int Conf Mechatronics Autom ICMA 2009 1027–1032. <https://doi.org/10.1109/ICMA.2009.5246279>
 80. <https://innophys.jp/>, accessed on 2019/08/30
 81. Hirotsugu S, Cho F, Noritsugu T (2017) Improvement of Wearable Power Assist Wear for Low Back Support. *Proc - 2016 Int Conf Multimed Syst Signal Process ICMSSP 2016* 12:90–94. <https://doi.org/10.1109/ICMSSP.2016.028>
 82. Näf MB, De Rijcke L, Guerrero CR, et al (2017) Towards low back support with a passive biomimetic exo-spine. *IEEE Int Conf Rehabil Robot* 1165–1170. <https://doi.org/10.1109/ICORR.2017.8009407>
 83. Agnew MJ (2008) Kinetic and Kinematic Adaptations To Use of a Personal

- Lift Assist Device. Sch Kinesiol Heal Stud Doctor of:
84. Picchiotti MT, Weston EB, Knapik GG, et al (2019) Impact of two postural assist exoskeletons on biomechanical loading of the lumbar spine. *Appl Ergon* 75:1–7. <https://doi.org/10.1016/J.APERGO.2018.09.006>
 85. Bosch T, van Eck J, Knitel K, de Looze M (2016) The effects of a passive exoskeleton on muscle activity, discomfort and endurance time in forward bending work. *Appl Ergon* 54:212–217. <https://doi.org/10.1016/J.APERGO.2015.12.003>
 86. Baltrusch SJ, van Dieën JH, Bruijn SM, et al (2019) The effect of a passive trunk exoskeleton on metabolic costs during lifting and walking. *Ergonomics* 62:903–916. <https://doi.org/10.1080/00140139.2019.1602288>
 87. Koopman AS, Kingma I, Faber GS, et al (2019) Effects of a passive exoskeleton on the mechanical loading of the low back in static holding tasks. *J Biomech* 83:97–103. <https://doi.org/10.1016/J.JBIOMECH.2018.11.033>
 88. Baltrusch SJ, van Dieën JH, van Bennekom CAM, Houdijk H (2018) The effect of a passive trunk exoskeleton on functional performance in healthy individuals. *Appl Ergon* 72:94–106. <https://doi.org/10.1016/j.apergo.2018.04.007>
 89. Baltrusch SJ, van Dieën JH, Bruijn SM, et al (2018) The Effect of a Passive Trunk Exoskeleton on Functional Performance and Metabolic Costs. In: *Int. Symp. on Wearable Robotics*. Springer, Cham, pp 229–233
 90. Alemi MM, Madinei S, Kim S, et al (2020) Effects of Two Passive Back-Support Exoskeletons on Muscle Activity, Energy Expenditure, and Subjective Assessments During Repetitive Lifting. *Hum Factors J Hum Factors Ergon Soc* 001872081989766. <https://doi.org/10.1177/0018720819897669>
 91. Madinei S, Alemi MM, Kim S, et al (2020) Biomechanical Evaluation of Passive Back-Support Exoskeletons in a Precision Manual Assembly Task: “Expected” Effects on Trunk Muscle Activity, Perceived Exertion, and Task Performance. *Hum Factors J Hum Factors Ergon Soc* 001872081989096. <https://doi.org/10.1177/0018720819890966>
 92. Poon N, van Engelhoven L, Kazerooni H, Harris C (2019) Evaluation of a Trunk Supporting Exoskeleton for reducing Muscle Fatigue. *Proc Hum Factors Ergon Soc Annu Meet* 63:980–983. <https://doi.org/10.1177/1071181319631491>
 93. Hensel R, Keil M (2019) Subjective Evaluation of a Passive Industrial Exoskeleton for Lower-back Support: A Field Study in the Automotive Sector. *IISE Trans Occup Ergon Hum Factors* 5838:1–9. <https://doi.org/10.1080/24725838.2019.1573770>
 94. Baltrusch SJ, Houdijk H, van Dieën JH, et al (2020) Perspectives of End Users on the Potential Use of Trunk Exoskeletons for People With Low-Back Pain: A Focus Group Study. *Hum Factors* 62:365–376. <https://doi.org/10.1177/0018720819885788>
 95. Hara H, Sankai Y (2012) HAL equipped with passive mechanism. 2012 *IEEE/SICE Int Symp Syst Integr SII* 2012 1–6. <https://doi.org/10.1109/SII.2012.6427323>
 96. Durante F, Antonelli MG, Zobel PB (2018) Development of an Active Exoskeleton for Assisting Back Movements in Lifting Weights. *Int J Mech Eng Robot Res* 7:353–360. <https://doi.org/10.18178/ijmerr.7.4.353-360>

97. Muramatsu Y, Umehara H, Kobayashi H (2013) Improvement and quantitative performance estimation of the back support muscle suit. *Conf Proc . Annu Int Conf IEEE Eng Med Biol Soc IEEE Eng Med Biol Soc Annu Conf 2013*:2844–2849. <https://doi.org/10.1109/EMBC.2013.6610133>
98. Huysamen K, de Looze M, Bosch T, et al (2018) Assessment of an active industrial exoskeleton to aid dynamic lifting and lowering manual handling tasks. *Appl Ergon* 68:125–131. <https://doi.org/10.1016/j.apergo.2017.11.004>
99. Toxiri S, Koopman AS, Lazzaroni M, et al (2018) Rationale, Implementation and Evaluation of Assistive Strategies for an Active Back-Support Exoskeleton. *Front Robot AI* (in Press). <https://doi.org/10.3389/frobt.2018.00053>
100. Tsuneyasu K, Ohno A, Fukuda Y, et al (2018) A soft exoskeleton suit to reduce muscle fatigue with pneumatic artificial muscles
101. Tan CK, Kadone H, Miura K, et al (2019) Muscle Synergies During Repetitive Stoop Lifting With a Bioelectrically-Controlled Lumbar Support Exoskeleton. *Front Hum Neurosci* 13:142. <https://doi.org/10.3389/fnhum.2019.00142>
102. von Gliniski A, Yilmaz E, Mrotzek S, et al (2019) Effectiveness of an on-body lifting aid (HAL® for care support) to reduce lower back muscle activity during repetitive lifting tasks. *J Clin Neurosci* 63:249–255. <https://doi.org/10.1016/J.JOCN.2019.01.038>
103. Miura K, Kadone H, Abe T, et al (2020) Successful Use of the Hybrid Assistive Limb for Care Support to Reduce Lumbar Load in a Simulated Patient Transfer. *Asian Spine J*. <https://doi.org/10.31616/asj.2019.0111>
104. Baltrusch SJ, van Dieën JH, Koopman AS, et al (2019) SPEXOR passive spinal exoskeleton decreases metabolic cost during symmetric repetitive lifting. *Eur J Appl Physiol*. <https://doi.org/10.1007/s00421-019-04284-6>
105. Baltrusch SJ, Van Dieën JH, Van Bennekom CAM, Houdijk H (2020) Testing an exoskeleton that helps workers with low-back pain: Less discomfort with the passive spexor trunk device. *IEEE Robot Autom Mag* 27:66–76. <https://doi.org/10.1109/MRA.2019.2954160>
106. Kozinc Ž, Baltrusch S, Houdijk H, Šarabon N (2020) Short-Term Effects of a Passive Spinal Exoskeleton on Functional Performance, Discomfort and User Satisfaction in Patients with Low Back Pain. *J Occup Rehabil*. <https://doi.org/10.1007/s10926-020-09899-7>
107. Borg GAV (1982) Psychophysical bases of perceived exertion. *Med Sci Sport Exerc* 14:377–381. <https://doi.org/10.1249/00005768-198205000-00012>
108. Corlett EN, Bishop RP (1976) A technique for assessing postural discomfort. *Ergonomics* 19:175–182. <https://doi.org/10.1080/00140137608931530>
109. Jespersen A, Dreyer L, Kendall S, et al (2007) Computerized cuff pressure algometry: A new method to assess deep-tissue hypersensitivity in fibromyalgia. *Pain* 131:57–62. <https://doi.org/10.1016/j.pain.2006.12.012>
110. Keren R, Or Y (2018) Theoretical Analysis and Numerical Optimization of a Wearable Spring-Clutch Mechanism for Reducing Metabolic Energy Cost During Human Walking. *J Mech Robot* 10:. <https://doi.org/10.1115/1.4041262>
111. Sartori M, Reggiani M, Mezzato C, Pagello E (2009) A lower limb EMG-driven biomechanical model for applications in rehabilitation robotics. In:

- 2009 International Conference on Advanced Robotics, ICAR 2009. IEEE, pp 1–7
112. Refour EM, Sebastian B, Chauhan RJ, Ben-Tzvi P (2019) A General Purpose Robotic Hand Exoskeleton With Series Elastic Actuation. *J Mech Robot* 11:. <https://doi.org/10.1115/1.4044543>
113. Manna SK, Dubey VN (2019) A Portable Elbow Exoskeleton for Three Stages of Rehabilitation. *J Mech Robot* 11:. <https://doi.org/10.1115/1.4044535>
114. Manns P, Sreenivasa M, Millard M, Mombaur K (2017) Motion Optimization and Parameter Identification for a Human and Lower Back Exoskeleton Model. *IEEE Robot Autom Lett* 2:1564–1570. <https://doi.org/10.1109/LRA.2017.2676355>
115. Harant M, Sreenivasa M, Millard M, et al (2017) Parameter optimization for passive spinal exoskeletons based on experimental data and optimal control. In: *IEEE-RAS International Conference on Humanoid Robots*. IEEE Computer Society, pp 535–540
116. Millard M, Sreenivasa M, Mombaur K (2017) Predicting the Motions and Forces of Wearable Robotic Systems Using Optimal Control. *Front Robot AI* 4:. <https://doi.org/10.3389/frobt.2017.00041>
117. Manns P, Mombaur K (2017) Towards Discrete Mechanics and Optimal Control for Complex Models. *IFAC-PapersOnLine* 50:4812–4818. <https://doi.org/10.1016/j.ifacol.2017.08.966>
118. Millard M, Sreenivasa M, Mombaur K (2017) Predicting the Motions and Forces of Wearable Robotic Systems Using Optimal Control. In: *Frontiers in Robotics and AI*. pp 1–12
119. Wu G, Siegler S, Allard P, et al (2002) ISB recommendation on definitions of joint coordinate system of various joints for the reporting of human joint motion - Part I: Ankle, hip, and spine. *J. Biomech.* 35:543–548
120. Wu G, Van Der Helm FCT, Veeger HEJ, et al (2005) ISB recommendation on definitions of joint coordinate systems of various joints for the reporting of human joint motion - Part II: Shoulder, elbow, wrist and hand. *J Biomech* 38:981–992. <https://doi.org/10.1016/j.jbiomech.2004.05.042>
121. De Leva P (1996) Adjustments to zatsiorsky-seluyanov's segment inertia parameters. *J Biomech* 29:1223–1230. [https://doi.org/10.1016/0021-9290\(95\)00178-6](https://doi.org/10.1016/0021-9290(95)00178-6)
122. Sreenivasa M, Harant M (2018) ModelFactory: A Matlab/Octave based toolbox to create human body models. 1–17. <https://doi.org/10.5281/zenodo.1137656>
123. Manns P, Sreenivasa M, Millard M, Mombaur K (2017) Motion optimization and parameter identification for a human and lower-back exoskeleton model. *IEEE Robot Autom Lett* 1–1. <https://doi.org/10.1109/LRA.2017.2676355>
124. Steve Miller (2020) Simscape Multibody Contact Forces Library, MATLAB Central File Exchange. <https://www.mathworks.com/matlabcentral/fileexchange/47417-simscape-multibody-contact-forces-library>. Accessed 7 Feb 2020
125. Antwi-Afari MF, Li H, Yu Y, Kong L (2018) Wearable insole pressure system for automated detection and classification of awkward working postures in construction workers. *Autom Constr* 96:433–441. <https://doi.org/10.1016/j.autcon.2018.10.004>
126. Faber GS, Kingma I, van Dieën JH (2010) Bottom-up estimation of joint

- moments during manual lifting using orientation sensors instead of position sensors. *J Biomech* 43:1432–1436. <https://doi.org/10.1016/j.jbiomech.2010.01.019>
127. Hwang S, Kim Y, Kim Y (2009) Lower extremity joint kinetics and lumbar curvature during squat and stoop lifting. *BMC Musculoskelet Disord* 10:15. <https://doi.org/10.1186/1471-2474-10-15>
128. Kingma I, Baten CTM, Dolan P, et al (2001) Lumbar loading during lifting: a comparative study of three measurement techniques. *J Electromyogr Kinesiol* 11:337–345. [https://doi.org/10.1016/S1050-6411\(01\)00011-6](https://doi.org/10.1016/S1050-6411(01)00011-6)
129. Toxiri S, Ortiz J, Masood J, et al (2015) A wearable device for reducing spinal loads during lifting tasks: Biomechanics and design concepts. 2015 IEEE Int Conf Robot Biomimetics, IEEE-ROBIO 2015 2295–2300. <https://doi.org/10.1109/ROBIO.2015.7419116>
130. Schneider SP (2001) Musculoskeletal injuries in construction: A review of the literature. *Appl. Occup. Environ. Hyg.* 16:1056–1064
131. Bernold LE, Guler N (1993) Analysis of Back Injuries in Construction. *J Constr Eng Manag* 119:607–621. [https://doi.org/10.1061/\(ASCE\)0733-9364\(1993\)119:3\(607\)](https://doi.org/10.1061/(ASCE)0733-9364(1993)119:3(607))
132. Panero E, Muscolo GG, Pastorelli S, Gastaldi L (2019) Influence of hinge positioning on human joint torque in industrial trunk exoskeleton. In: *Mechanisms and Machine Science*. Springer Netherlands, pp 133–142
133. Panero E, Muscolo GG, Gastaldi L, Pastorelli S (2020) Multibody Analysis of a 3D Human Model with Trunk Exoskeleton for Industrial Applications. In: *Computational Methods in Applied Sciences*. Springer, pp 43–51
134. Panero E, Muscolo GG, Pastorelli S, Gastaldi L (2020) Model Based Analysis of Trunk Exoskeleton for Human Efforts Reduction. In: *Advances in Intelligent Systems and Computing*. Springer Verlag, pp 410–418
135. Kermavnar T, Power V, de Eyto A, O’Sullivan LW (2018) Computerized Cuff Pressure Algometry as Guidance for Circumferential Tissue Compression for Wearable Soft Robotic Applications: A Systematic Review. *Soft Robot* 5:1–16. <https://doi.org/10.1089/soro.2017.0046>
136. Toxiri S, Sposito M, Lazzaroni M, et al (2019) Towards standard specifications for back-support exoskeletons. In: *Biosystems and Biorobotics*
137. Schoenfeld BJ (2010) Squatting Kinematics and Kinetics and Their Application to Exercise Performance. *J Strength Cond Res* 24:3497–3506. <https://doi.org/10.1519/JSC.0b013e3181bac2d7>
138. Pratt J, Krupp B, Morse C (2002) Series elastic actuators for high fidelity force control. *Ind Rob* 29:234–241. <https://doi.org/10.1108/01439910210425522>
139. Ham VR, Sugar TG, Vanderborght B, et al (2009) Compliant actuator designs: Review of actuators with passive adjustable compliance/controllable stiffness for robotic applications. *IEEE Robot Autom Mag* 16:81–94. <https://doi.org/10.1109/MRA.2009.933629>
140. Pratt GA, Williamson MM (1995) Series elastic actuators. In: *IEEE International Conference on Intelligent Robots and Systems*. IEEE, pp 399–406
141. Brown M, Tsagarakis N, Caldwell DG (2003) Exoskeletons for human force augmentation. *Ind Rob* 30:592–602. <https://doi.org/10.1108/01439910310506864>

142. Toxiri S, Calanca A, Fiorini P, Caldwell DG (2018) A Parallel-Elastic Actuator for a Torque-Controlled. *IEEE Robot Autom Lett* 3:492–499. <https://doi.org/10.1109/LRA.2017.2768120>
143. Witte KA, Fatschel AM, Collins SH (2017) Design of a lightweight, tethered, torque-controlled knee exoskeleton. In: *IEEE International Conference on Rehabilitation Robotics*. IEEE Computer Society, pp 1646–1653
144. Wang J, Li X, Huang TH, et al (2018) Comfort-Centered Design of a Lightweight and Backdrivable Knee Exoskeleton. *IEEE Robot Autom Lett* 3:4265–4272. <https://doi.org/10.1109/LRA.2018.2864352>
145. Yan T, Cempini M, Oddo CM, Vitiello N (2015) Review of assistive strategies in powered lower-limb orthoses and exoskeletons. *Rob Auton Syst* 64:120–136. <https://doi.org/10.1016/j.robot.2014.09.032>
146. dos Santos WM, Caurin GAP, Siqueira AAG (2017) Design and control of an active knee orthosis driven by a rotary Series Elastic Actuator. *Control Eng Pract* 58:307–318. <https://doi.org/10.1016/j.conengprac.2015.09.008>
147. Rouse EJ, Mooney LM, Martinez-Villalpando EC, Herr HM (2013) Clutchable series-elastic actuator: Design of a robotic knee prosthesis for minimum energy consumption. In: *IEEE International Conference on Rehabilitation Robotics*
148. Giovacchini F, Fantozzi M, Peroni M, et al (2013) A Light-weight Exoskeleton for Hip Flexion-extension Assistance. In: *Proceedings of the International Congress on Neurotechnology, Electronics and Informatics (RoboAssist-2013)*. SCITEPRESS, Vilamoura, Portugal, pp 194–198
149. Campbell E, Kong ZC, Hered W, et al (2011) Design of a low-cost series elastic actuator for multi-robot manipulation. In: *Proceedings - IEEE International Conference on Robotics and Automation*. pp 5395–5400
150. Pratt JE, Krupp BT (2004) Series Elastic Actuators for legged robots. In: Gerhart GR, Shoemaker CM, Gage DW (eds) *Unmanned Ground Vehicle Technology VI*. SPIE, pp 135–144
151. Zhu Y, Yang J, Jin H, et al (2014) Design and evaluation of a parallel-series elastic actuator for lower limb exoskeletons. In: *Proceedings - IEEE International Conference on Robotics and Automation*. Institute of Electrical and Electronics Engineers Inc., pp 1335–1340
152. Ragonesi D, Agrawal S, Sample W, Rahman T (2011) Series elastic actuator control of a powered exoskeleton. In: *Proceedings of the Annual International Conference of the IEEE Engineering in Medicine and Biology Society, EMBS*. pp 3515–3518
153. Isik K, He S, Ho J, Sentis L (2017) Re-Engineering a High Performance Electrical Series Elastic Actuator for Low-Cost Industrial Applications. *Actuators* 6:5. <https://doi.org/10.3390/act6010005>
154. Robinson DW (2000) Design and Analysis of Series Elasticity in Closed-loop Actuator Force Control. PhD thesis, MIT. <https://doi.org/10.1016/j.sedgeo.2010.04.008>
155. Sergi F, Accoto D, Carpino G, et al (2012) Design and characterization of a compact rotary Series Elastic Actuator for knee assistance during overground walking. In: *Proceedings of the IEEE RAS and EMBS International Conference on Biomedical Robotics and Biomechatronics*. pp 1931–1936
156. Giovacchini F, Vannetti F, Fantozzi M, et al (2015) A light-weight active orthosis for hip movement assistance. *Rob Auton Syst* 73:123–134. <https://doi.org/10.1016/j.robot.2014.08.015>

157. Cummings JP, Ruiken D, Wilkinson EL, et al (2016) A compact, modular series elastic actuator. *J Mech Robot* 8: <https://doi.org/10.1115/1.4032975>
158. Cempini M, Giovacchini F, Vitiello N, et al (2013) NEUROExos: A powered elbow orthosis for post-stroke early neurorehabilitation. In: *Proceedings of the Annual International Conference of the IEEE Engineering in Medicine and Biology Society, EMBS*. Institute of Electrical and Electronics Engineers Inc., pp 342–345
159. Heneweer H, Vanhees L, Picavet HSJ (2009) Physical activity and low back pain: A U-shaped relation? *Pain* 143:21–25. <https://doi.org/10.1016/j.pain.2008.12.033>
160. Awasthi, S. K. and RKS (2014) Analysis of flexspline in the harmonic drive system. *Int J Eng Sci Technol* 3:
161. Toxiri S, Koopman AS, Lazzaroni M, et al (2018) Rationale, Implementation and Evaluation of Assistive Strategies for an Active Back-Support Exoskeleton. *Front Robot AI*. <https://doi.org/10.3389/frobt.2018.00053>
162. Norkin, Cynthia C. DJW (2016) *Measurement of joint motion: a guide to goniometry*, Fourth Edi

A. Appendix: Anatomical reference position

With the main attempt to describe the kinematics, the range of motion and the direction of movements of human body segments and joints, several studies and investigations have been conducted in the past. Due to the complexity of the human body, many human joints connecting bones, and the possibility to coordinate and combine the relative movements between human body parts, some simplifications and approximations need to be considered. Starting from the anatomical and physiological analysis of human body motions in several activities, standardized and repetitive methods for the definition of global and local coordinate systems have been implemented. Among them, The International Society of Biomechanics (ISB) has depicted a common guideline for the biomechanical reporting of human body movements [119, 120]. The use of an approved and shared method allows the comparison among various studies, in addition to the increased relevance and easier interpretation of biomechanical results in clinics, rehabilitation, and sports environments. The ISB developed the biomechanical recommendations for the description of human motions starting from the procedure proposed by Grood and Suntay in 1983. The procedure considers two adjacent body segments and defines a Cartesian coordinate system (CCS) for each segment. The axes in these CCSs are defined based on bony landmarks that are visible and palpable. The common origin of both axis systems is the point of reference for the linear translation occurring in the joint, at its initial neutral position. Secondly, the joint coordinate system (JCS) is established based on the two CCSs. Two of the JCS axes are body fixed, and one is “floating”.

Considering the whole human body, a reference starting point has to be defined in order to identify the zero-reference condition. In the biomechanical analysis, the anatomical reference position refers to a person standing erect with the following characteristics:

- all human joints extended
- upper body limbs closed to the body
- hand palms facing forward
- fingers closed together
- feet parallel on the ground

Figure A.1 depicts a female human body in the reference position in front and lateral view. This position can be considered as the starting point for the characterization of human body segments descriptions and orientations. Moreover, the figure shows the nomenclature used to describe in the 3D space the relative position and the motion direction between human segments. The identification of a standardized nomenclature allows referring to local human body parts without misunderstanding and difficulty. The reference position is fundamental not only for the inter-subject relations. Indeed, in numerous studies and experimental tests, the standing posture has been assumed as the zero-starting point before the motions and

all kinematic data have been referred to the zero condition, in order to let intra-subject comparison during difference performances.

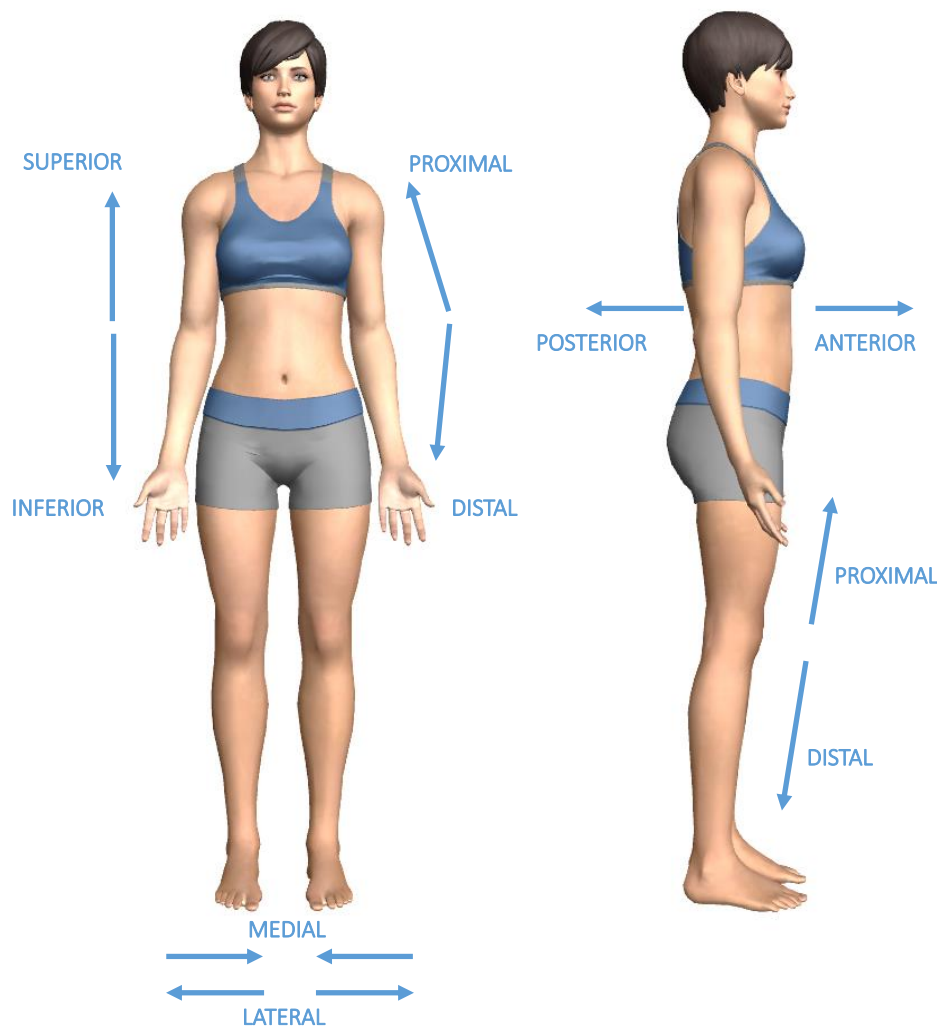


Figure A.1: Front and sagittal view of the anatomical reference position. Graphical explanation of anatomical reference direction used to describe the relative position of a specific human body part.

Another important aspect deals with the definition of standardized anatomical reference planes and axes for the description of movements in the 3D environment, graphically summed up in Figure A.2. The sagittal plane (also called median or anteroposterior) is the vertical plane and it divides the body in half along the midline, into right and left masses. It runs superior to inferior and anterior to posterior. The frontal plane (also called coronal or lateral) is another vertical plane, but it divides the body in half along the midline into anterior and posterior masses. It runs superior to inferior and side-to-side. Finally, the transverse plane (also called horizontal) passes through the body horizontally and divides it into superior and inferior masses. The transverse plane passes through anterior to posterior and side-to-side. Considering the reference axes, the mediolateral axis (also called bilateral, frontal, and transverse) crosses horizontally side-to-side, perpendicular to the sagittal plane. Anteroposterior axis (also called sagittal, sagittal-horizontal, and

sagittal-transverse) runs horizontally from front to back and is perpendicular to the frontal plane. Finally, the superoinferior axis (also called frontal-sagittal, longitudinal, and vertical) crosses up and down and is perpendicular to the transverse plane.

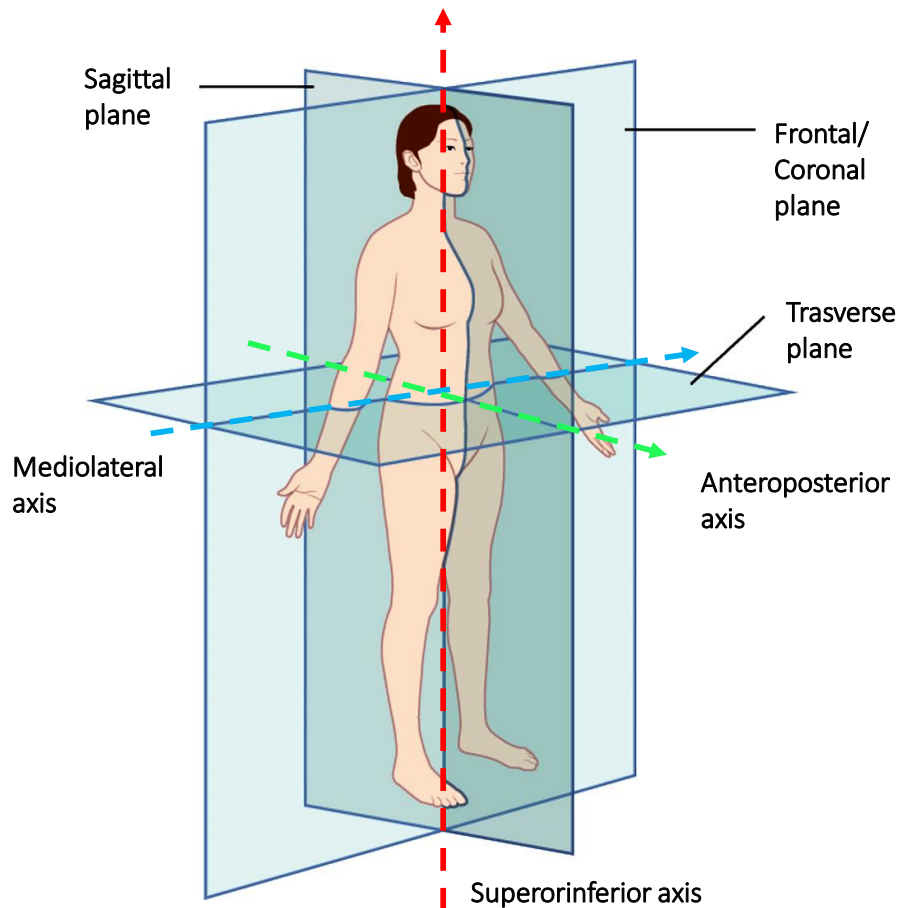


Figure A.2: Graphical representation of anatomical reference planes and anatomical reference axes in the 3D space.

The human body could be divided into several human body segments, with the attempt to identify and describe specific human body parts. There is not a standardized number of human segments, but the complexity of the identification is defined based on the necessity and the precision that occurs in the study. Each human body parts that have been identified is connected to the adjacent segments by means of human joints, that regulate and approximate the relative motion between segments. Both human segments and joints could be described with labels, as reported in Table A.1. The table depicts the division of human body considered in the current study and shows a graphical representation of the whole female manikin with the several human body segments and joints of interest.

The following passage deals with the definition of local reference systems of each human body segment and the description of human joints degrees of freedom, considering the physiological and natural range of motion. In the present study, the limits of movement for each joints has been imposed considering the range of motion described in [162]. Table A.2 shows the human joints identified for the

description of human body 3D model in the multibody approach, the body segments linked by the joints, the description of the physiological degrees of freedom in each plane and the nomenclature of reference indicating the movement of interest. Finally, Figure A.3 shows the graphical representation of local coordinate systems in the front, sagittal and lateral views. It must be noted that in the current multibody model, the elbow and the knee joints have been approximated as hinge joints.

SEGMENT		LABEL	
HEAD	HE		
UPPERARM	UA		
FOREARM	FA		
HAND	HA		
TRUNK	TR		
PELVIS	PE		
THIGH	TH		
SHANK	SH		
FOOT	FO		
JOINT	LABEL		
NECK	NE		
WAIST	WA		
SHOULDER	SL		
ELBOW	EL		
WRIST	WR		
HIP	HI		
KNEE	KN		
ANKLE	AN		

LEFT SIDE: _L		RIGHT SIDE: _R	
HE	NE	SL_R	SL_L
UA_R	UA_L	EL_R	EL_L
FA_R	FA_L	WR_R	WR_L
HA_R	HA_L	TH_R	TH_L
TH_R	TH_L	KN_R	KN_L
SH_R	SH_L	AN_R	AN_L
FO_R	FO_L		

Table A.2: Definition of relative motion between human segments and description of physiological ranges of motion.

JOINT	BODY SEGMENT INVOLVED		JOINT RANGE OF MOTION (<i>deg</i>)		MOTION (Physiological Reference)
			DESCRIPTION		
	PROXIMAL	DISTAL	RIGHT	LEFT	
NECK	Trunk	Head	(+45) Head moves ANTERIORLY (-45) Head moves POSTERIORLY		FLEXION - EXTENSION
			(+45) Head moves LATERALLY RIGHT (-45) Head moves LATERALLY LEFT		LATERAL FLEXION
			(+70) Eyes to LEFT SIDE (-70) Eyes to RIGHT SIDE		ROTATION
WAIST	Pelvis	Trunk	(+80) Trunk moves ANTERIORLY (-25) Trunk moves POSTERIORLY		FLEXION - EXTENSION
			(+30) Trunk moves LATERALLY RIGHT (-30) Trunk moves LATERALLY LEFT		LATERAL FLEXION
			(+45) Right shoulder ANTERIORLY (-45) Left shoulder ANTERIORLY		ROTATION
SHOULDER	Trunk	UpperArm	(+180) Arm moves ANTERIORLY (-60) Arm moves POSTERIORLY	(+180) Arm moves ANTERIORLY (-60) Arm moves POSTERIORLY	FLEXION - EXTENSION
			(+180) Arm moves LATERALLY (-30) Arm moves MEDIALY	(+180) Arm moves LATERALLY (-30) Arm moves MEDIALY	ABDUCTION - ADDUCTION

			(+80) Hand moves INTERNALLY (-90) Hand moves EXTERNALLY	(+80) Hand moves INTERNALLY (*) (-90) Hand moves EXTERNALLY (*)	INT- EXT ROTATION
ELBOW	UpperArm	ForeArm	(+150) Forearm moves ANTERIORLY (0) Forearm moves POSTERIORLY	(+150) Forearm moves ANTERIORLY (0) Forearm moves POSTERIORLY	FLEXION - EXTENSION
			(+10) Forearm moves LATERALLY (-10) Forearm moves MEDIALY	(+10) Forearm moves LATERALLY (-10) Forearm moves MEDIALY	VALGUS – VARUS (**)
			(+150) Thumb moves INTERNALLY (-10) Thumb moves EXTERNALLY	(+150) Thumb moves INTERNALLY (-10) Thumb moves EXTERNALLY	PRONATION – SUPINATION (**)
WRIST	ForeArm	Hand	(+80) Hand moves ANTERIORLY (-70) Hand moves POSTERIORLY	(+80) Hand moves ANTERIORLY (-70) Hand moves POSTERIORLY	PALMAR – DORSAL FLEXION
			(+20) Hand moves LATERALLY (-30) Hand moves MEDIALY	(+20) Hand moves LATERALLY (-30) Hand moves MEDIALY	ABDUCTION - ADDUCTION
			(+150) Thumb moves INTERNALLY (-10) Thumb moves EXTERNALLY	(+150) Thumb moves INTERNALLY	PRONATION – SUPINATION

				(-10) Thumb moves EXTERNALLY	
HIP	Pelvis	Thigh	(+120) Thigh moves ANTERIORLY (-30) Thigh moves POSTERIORLY	(+120) Thigh moves ANTERIORLY (-30) Thigh moves POSTERIORLY	FLEXION - EXTENSION
			(+45) Knee moves LATERALLY (-30) Knee moves MEDIALY	(+45) Knee moves LATERALLY (-30) Knee moves MEDIALY	ABDUCTION - ADDUCTION
			(+45) Toe moves INTERNALLY (-45) Toe moves EXTERNALLY	(+45) Toe moves INTERNALLY (-45) Toe moves EXTERNALLY	INT- EXT ROTATION
KNEE	Thigh	Shank	(+150) Shank moves POSTERIORLY (0) Shank moves ANTERIORLY	(+150) Shank moves POSTERIORLY (0) Shank moves ANTERIORLY	FLEXION - EXTENSION
			(+30) Shank moves LATERALLY (-30) Shank moves MEDIALY	(+30) Shank moves LATERALLY (-30) Shank moves MEDIALY	VALGUS - VARUS (**)
			(+20) Toe moves INTERNALLY (-20) Toe moves EXTERNALLY	(+20) Toe moves INTERNALLY (-20) Toe moves EXTERNALLY	INT- EXT ROTATION (**)

ANKLE	Shank	Foot	(+20) Toe moves UP (-50) Toe moves DOWN	(+20) Toe moves UP (-50) Toe moves DOWN	DORSI – PLANTAR FLEXION
			(+20) Foot moves MEDIALY (-35) Foot moves LATERALLY	(+20) Foot moves MEDIALY (-35) Foot moves LATERALLY	EVERSION - INVERSION
			(+25) Toe moves INTERNALLY (-35) Toe moves EXTERNALLY	(+25) Toe moves INTERNALLY (-35) Toe moves EXTERNALLY	ADDUCTION - ABDUCTION

(*) with elbow 90° flexed

(**) not recognized in the manikin description

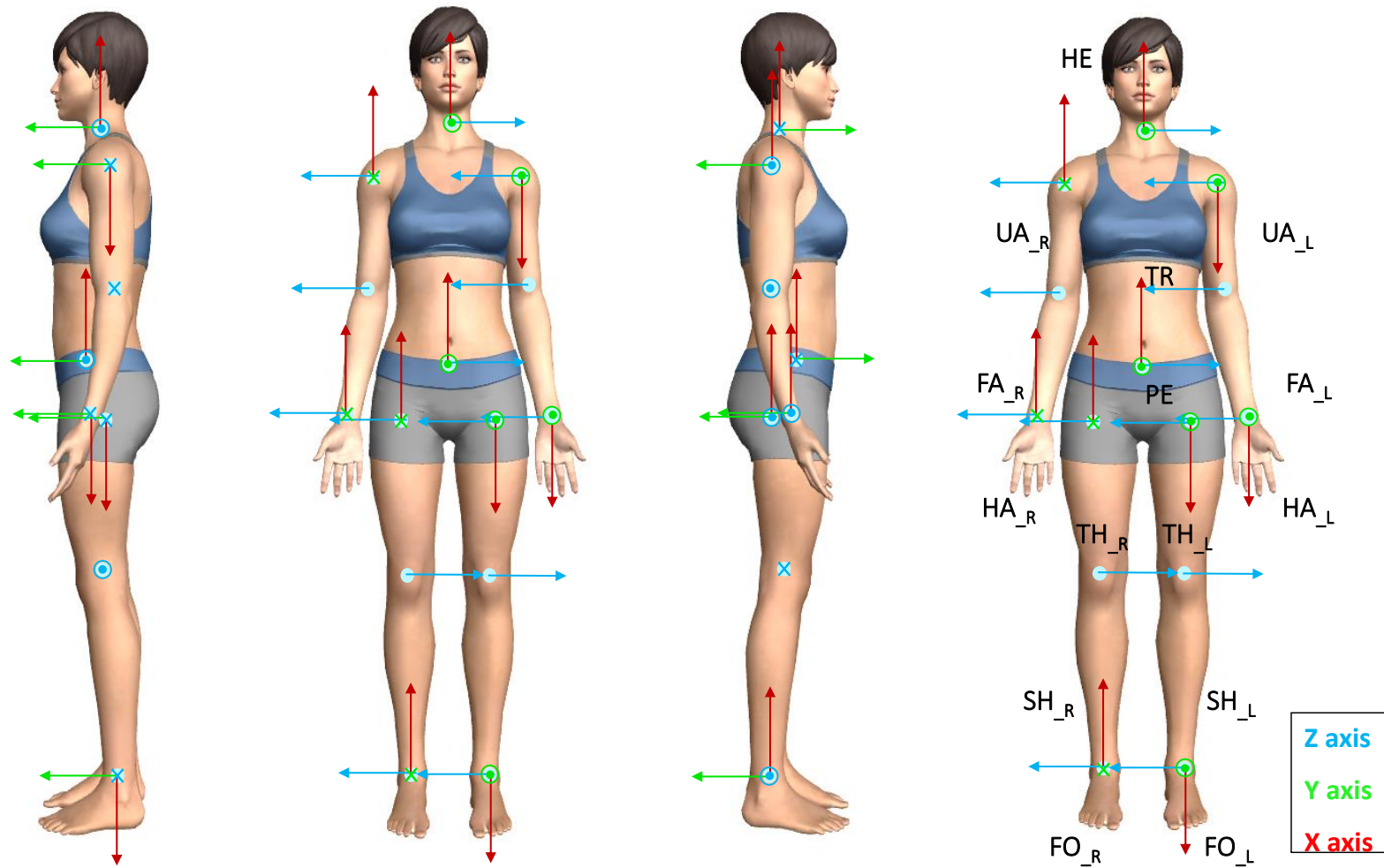


Figure A.3: Representation of local reference systems of several human body parts with corresponding labels in the front and lateral (right and left) views.

B. Appendix: ISO reference guidelines

During the last decades, numerous experimental tests and statistical studies have been conducted in order to highlight the working risk factors that contribute to the outbreak of neuro-muscular pathologies caused by biomechanical overloads of human joints and body parts. Considering the manual handling tasks in industry, several risk factors, that can act singularly or in synergy, may contribute to the overload of the human back and upper limbs. Figure B.1 sums up the main factor risks that must be considered in the evaluation of manual handling tasks with the attempt to limit the occurrence of injuries and pain.

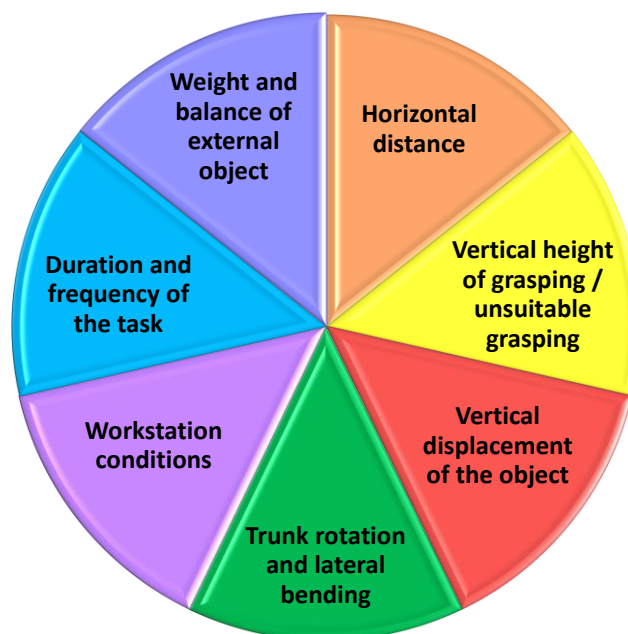


Figure B.1: Graphical list of common and crucial risk factors that must be considered for the analysis of working stations and industrial manual tasks with the main attempt to reduce and prevent the risk of overloads and injuries for the employees.

The International Organization for Standardization (ISO) is a worldwide federation of national standards bodies. International Standards are drafted by prepared ISO technical committees, in accordance with the ISO Directives rules. Draft International Standards adopted by the technical committees are shared with the member bodies for voting and the final publication as an International Standard requires approval by at least 75 %. The normative ISO 11228 was prepared by Technical Committee specialized in Ergonomics, Anthropometry, and Biomechanics. It generally appears under the name “Ergonomics – Manual handling”, but it is composed of three main independent parts:

- Part 1: Lifting and carrying
- Part 2: Pushing and pulling
- Part 3: Handling of low loads at high frequency

The three parts of ISO 11228 establish ergonomic recommendations and methods for risk evaluation for different manual handling tasks. In addition to the direct use in the industrial environment in order to prevent the occurrence of injuries and augmented risk of damages, the standards provide information for designers, developers, engineers, employers, and others involved in work, job, and product design. The normative is directly connected with ISO 11226, which deals with the determination of the acceptability of static working postures. For the current project, Part 1 and Part 3 have been considered and analyzed. Indeed, the exoskeleton prototype has been thought for the assistance of workers during lifting motions and repetitive tasks.

ISO 11228 Part 1. This part specifies the recommended limits for manual lifting and carrying tasks. It considers repetitive and homogenous lifting activities, performed by one worker and with both hands. The normative cannot be applied in case of lifting from sitting posture. The guideline allows the examination of the workstation, the assessment of the suitability of conditions and the analysis of common risk factors to verify that standard and secure limits are not overcome. It can be applied to manual handling of objects with a mass of 3 kg minimum. Based on the field of occupation, age and gender of workers, different limits for reference mass m_{ref} can be stressed, as reported in Table B.1:

Table B.1: Mass reference value.

Reference mass indication for manual handling and lifting tasks						
Field of application	m_{ref} (kg)	% of user population protected			Population group	
		Female & Male	Female	Male		
Non-occupational use	5	Not available data			Children and elderly	Total population
	10	99	99	99	General domestic population	
Professional use	15-23	95	90	99	General working population	General working population
	25	85	70	95	Adult working population	
	30-40	Specialized working population under special circumstances				

The weight limits reported in the table cannot be considered alone, because several other conditions may influence the suitability of the working task. One of the most important factors that can influence the allowable maximum weight of the object is the frequency of motion. Objects with higher total weight must be grasped and lifted in limited cycles. The normative supplies an important graph that relates the mass and the frequency, as depicted in Figure B.2.

Starting from the m_{ref} and the corresponding value of interest, it is possible to apply the equation proposed by the guideline in order to evaluate the level of risk of the analyzed task. The recommended limit of the total weight of the mass is strongly affected by other factors, that appears as multipliers in the following equation:

$$m_R = m_{ref} * h_M * v_M * d_M * \alpha_M * f_M * c_M$$

where:

- h_M considers the horizontal distance between the point of grasping of the object and the position of human hip joints;

- v_M considers the vertical position of the object during the grasping phase. The optimal condition has the object in correspondence to the hand position when upper limbs are in rest posture;

- d_M considers the vertical displacement of the object, that must be reduced. The optimal condition deals with the grasping and the release point at the same height;

- α_M considers the asymmetry of the human trunk, a combination of trunk rotation and trunk lateral bending. Optimal condition deals with the absence of human trunk movements outside the sagittal plane;

- f_M considers the motion frequency, combining repetition and velocity of the task;

- c_M considers the quality of grasping, the presence of an encumbrance, difficulty of grasping, unbalance of the object or dangerous structure of the load.

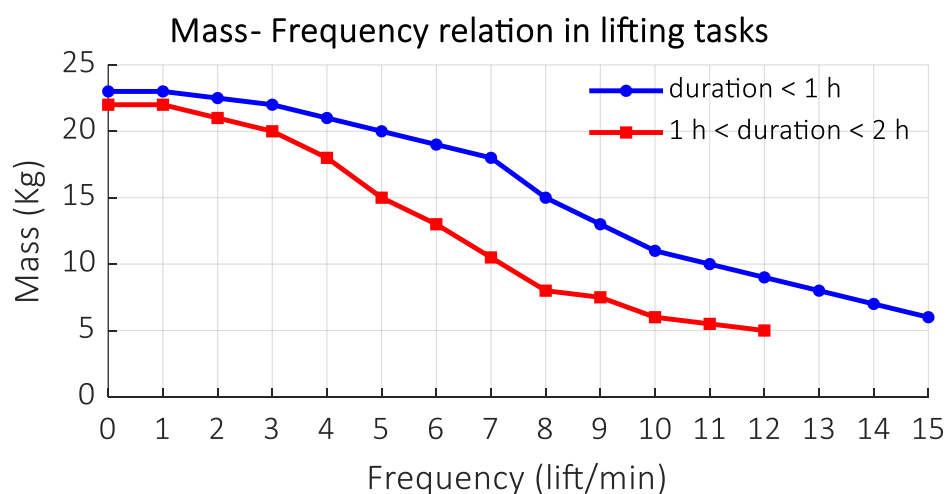


Figure B.2: Graph reported in the normative ISO 11228-Part 1 describing the relation between the mass of the external object and the frequency of grasping motion.

If the effective lifted mass (m_A) has a total weight less than the calculated recommended mass (m_R), the *Lifting Index* (m_A/m_R) results <1 and the general task condition could be considered acceptable. Table B.2 describes the classification of the *Lifting Index* based on the result and explains the value interpretation, as the consequences that must be adopted if overcoming the suitable conditions.

ISO 11228 Part 3. This part establishes ergonomic recommendations for repetitive work tasks involving the manual handling of low loads at high frequency. It provides guidance on the identification and assessment of the principal risk factors, therefore allows the evaluation of the related health risks to the working

population. Risk factors in repetitive work comprise the frequency of actions, exposure duration, postures and range of motion of body segments, forces associated with the work, demands on work output and level of training/skill. Additional factors can include environmental factors, such as climate, noise, vibration, and illumination. The current normative can be applied to evaluate working tasks that require repetitive movements of the human upper limbs. The evaluation of risk factors considers the Occupational Repetitive Action OCRA protocol. It consists of two methods, the first concerning the general investigation of principal mechanical and management conditions by a *checklist*, the second dealing with the analytical calculation of risk index and activity classification. The second method could be adopted because of the first method when necessary.

Table B.2: Classification of the Lifting Index in working manual and lifting tasks.

Classification of the Lifting Index (LI)			
Index	Level	Interpretation	Consequence
$LI \leq 1$	Acceptable	The condition is acceptable for most of the population	No consequence
$1 < LI \leq 2$	Presence of risk	A small part of the population might be exposed to the risk	Working tasks & workstations need to be reconfigured
$2 < LI \leq 3$	Presence of risk with high level	Most of the population might be exposed to a high level of risk	Working tasks and workstations need to be reconfigured as soon as possible
$LI \geq 3$	Presence of risk with very high level	The situation is unsuitable for all the working population. It can be performed only in special circumstances.	Working tasks and workstations have to be immediately reconfigured

The OCRA *checklist* allows a general initial screening of the working station and it considers five main risk factors: frequency of movement (numbers of actions for each minute), human body parts posture and movement (control of the limits of range of motion in the 3D space), force intensity (it represents the force required to perform the action), rest periods, and complementary effects (occasional physical and management working factors). All these factors are related to the exposition duration, which directly influences the evaluation of risk. The OCRA protocol supplies tables and a range of values that can be considered for the quantification of the risk. Based on the results, the risk can be classified into three sections: the acceptable risk that requires period controls, the possible risk that can be examined in depth by means of the second method, and the elevated risk that requires the immediate reconsideration of the task. Table B.3 depicts the risk assessment, the classification of the OCRA value and possible consequences.

Table B.3: Description of the OCRA classification of risk in case of repetitive tasks.

OCRA checklist evaluation		
Exposure Index	Classification	Consequence
value ≤ 5	Optimal	/
5.1 < value ≤ 7.5	Negligible	/
7.6 < value ≤ 11	Low	Check the task and reduce the risk
11.1 < value ≤ 14	Medium – Low	Find improvements
14.1 < value ≤ 22.5	Medium – High	Re-planning of working tasks and positions
value > 22.5	High	Re-planning of working tasks and positions

In case of possible or elevated risk, it is necessary to evaluate the *OCRA Index* with the attempt to quantify the risk. The *OCRA Index* can be defined as the ratio between the number of actions experimentally performed and the number of the maximum recommended actions (A_p/A_R). With “action” is intended the whole cycle of movements required for one elementary operation. The number of recommended actions (A_R) can be evaluated with the following equation:

$$A_R = \sum_{j=1}^n [k_f (F_{Mj} P_{Mj} R_{eMj} A_{Mj}) t_j] (R_{cM} t_M)$$

where:

- k_f is the frequency constant that deals with the number of the maximum recommended actions in initial condition (30 actions/min). Its value decreases based on the considered risk factors;
- F_{Mj} is the force factor evaluating the intensity of the required force;
- P_{Mj} is the postural factor describing the human body posture and joint motions;
- R_{eMj} is the repetitive factor;
- A_{Mj} is the complementary elements factor;
- t_j considers the total time of the repetitive movement;
- R_{cM} is the factor evaluating the rest period;
- t_M is the total time of the whole task;

Table B.4 describes the classification of the *OCRA Index* based on the result and explains the interpretation of value, as the consequences that must be adopted in the case of overcoming the suitable conditions. Due to the complexity, the impossibility to conduct the study in real-time and the long time required to complete the analysis, the OCRA protocol can be substituted by other semiquantitative and qualitative methods, as the *Strain Index* and the *Level of Manual Activity (HAL)*.

Table B.4: Classification of the OCRA Index.

Classification of the OCRA Index (OCRA_I)			
OCRA Index	Level	Interpretation	Consequence
$OCRA_I \leq 2.2$	Acceptable	The condition could be considered acceptable for most of the population	No consequence
$2.3 < OCRA_I \leq 3.5$	Presence of low risk	A small part of the population might be exposed to the risk of injuries at upper limbs	Working tasks and workstations have to be reconfigured based on posture, force, management aspects, ...
$OCRA_I \geq 3.5$	Presence of high risk	The situation is unsuitable for all the working population due to the high risk overloads	Working tasks and workstations have to be immediately reconfigured

C. Appendix: a standardized rating scale for subjective evaluation

During the past decades, the necessity to develop a shared evaluation scale for rating the subjective perception of working tasks has become fundamental because the more interest in how people feel, the type and level of their pain, how difficult the workers perceived their work. With a common measuring scale, it is possible not only to classify the analyzed effort variable but also to compare the results among several situations, between subjects or over time. Scientists and practitioners in health science and ergonomics agree on the important aspect of understanding the subjective evaluation. Therefore, specific methods for the quantification have been introduced. These methods should be equally applicable to most people regardless of gender, age, situations, and origin.

At the beginning, several so-called “ratio-scaling methods” have been proposed to measure perceptual intensities and exertion. One of these proposals is the “ratio production”, where the subject increases or decreases a specific stimulus parameter until he perceives a ratio or multiple of a standard stimulus. One of the most popular ratio-scaling methods is the “magnitude estimation”. In the occurrence of stimuli, the subject assigns numbers to them based on the perceived intensity. The first study of perceived exertion in heavy physical work was performed by Borg at the end of 1950’s, and a power function was proposed to relate the percentual variation with the physical intensity.

One of the most important drawbacks with ratio-scaling methods is the lack of interindividual comparisons. Acceptable general functions can be obtained for small groups, but the inter-subject assessment results are difficult due to the relative comparisons and the subjective choice of numbers for the classification. Borg developed a scale for ratings of perceived exertion with the attempt to overcome this limit. The first solution was a 21-grade category scale with a simple but direct estimation of the subjective intensity needed for the working task with specific verbal descriptions. A new category scale with a range from 6 to 20 was constructed by Borg in order to describe the high correlation between ratings of perceived exertion and heart rates and to increase the linearity of this relation. This proposed scale has become very popular and used in many studies, finding linear correlations also with other physiological variables. In a second moment, Borg improved the scale developing a category scale with ratio properties, increasing the accuracy and introducing a true zero. The verbal expressions have been placed in a correct position on a ratio scale for the accordance between verbal and quantitative meaning. The range of values has been defined from 0 to 10 for an easy and shared interpretation [107]. Figure C.1 depicts the Borg scale and the modified Borg scale with correspondence between number value and verbal descriptions. A color scale has been assigned with an attempt to correlate the numerical estimation to a color map, ranging from green color at low levels to red color at high levels.

There may not be one perfect scale for all kinds of situations and different scales might be used depending upon the purpose of the study. The newest category scale with ratio properties proposed by Borg could be used for testing the effectiveness of wearable systems, in particular, considering the subjective perceived exertion during the physical activities, with and without the device.

Rate of Perceived Exertion (Borg's scale)					
	COLOR	BORG'S SCALE	EXPLANATION	MODIFIED BORG SCALE	EXPLANATION
0					
1	GREEN	6	No exertion at all	0	At rest
2		7	Extremely light	1	Very easy
3		8			
4	YELLOW	9	Very light	2	Somewhat easy
5		10	Effort level where do not hear the breathing	3	Moderate
6		11	It is possible to talk and can run for a very long time		
7		12	Light (Building aerobic endurance)	4	Somewhat hard
8	ORANGE	13	Somewhat hard (it is quite an effort; feeling tired, but it is possible to continue)	5	Hard
9		14	Starting to hear the breathing		
10		15	It is possible to talk, but more challenging, use one or two-word answers	6	
11		16	Hard. It is considered as the steady state	7	Very hard
12	17	Very hard/strenuous. ANAEROBIC THRESHOLD			
13	RED	18	Breathing is vigorous, difficult to talk	8	
14		19	Extremely hard (counting the minutes until it ends)	9	
15		20	Maximal exertion	10	Very, very hard
16					

Figure C.1: Borg's scale and modified Borg's scale description. Explanation of the meaning of the different numbers in the ranges 6-20 and 0-10 respectively, that can be assigned by the subject during the evaluation.

In addition to the perceived exertion of intensity and activity, the other important parameter that needs to be considered is the comfort of a workstation, working mansion or interaction of workers with working tools or pieces of equipment. Indeed, the warning provided by the perceived discomfort is an indicator of the inadequacy of the examined working feature in correlation with the worker. The "industrial comfort" has been considered as a concept with a threshold level. Below this threshold, the operator would not be distracted from his work. For this reason, a measure of discomfort with a properly defined scale has become important. In 1976, Corlett adapted the technique proposed by Allen and Bennett for testing the comfort of pilots' seats for the evaluation of inadequate postures adopted during work. A case study of operators working with a machine was considered. The human body map was divided into several local areas. In intervals of the working period, the operators were asked to indicate on the diagram the human body parts most affected by discomfort and pain. At the same time, the evaluation scale was adopted to register an overall perception of discomfort. Some posture and machine changes were made during the experiment in order to verify any improvements or discomfort intensifications. The numerical value of the scale has been associated with a verbal explanation in order to simplify the user's

judgment. The case study highlighted the importance of the adopted technique to quantify the possible changes to the machine and posture for the operator in terms of limiting discomfort and pain [108]. Figure C.2 displays the discomfort scale used in the current study with a numerical range between 0 and 5 with each relative explanation. A color scale has been associated in order to depict a graphical color map of the investigated body subareas. A similar approach has been used for the implementation of a perceived pressure scale, with values range from 0 to 5. The perceived pressure scale might be fundamental for the investigation of the direct interface between the user and wearable systems. The subjective evaluation of perceived pressure could be related to the direct and objective measuring of interfacing forces through force sensors. It could be useful to identify pressure thresholds suitable for the developing of and improving wearable systems and supplied assistance. Human body maps of female and male manikins are reported in graphs A-B with the identification of different body subareas, while C-D show an example of assigned scale color to the singular body area (Figure C.2). The graphical and colored mapping can be adopted for both discomfort and pressure scales.

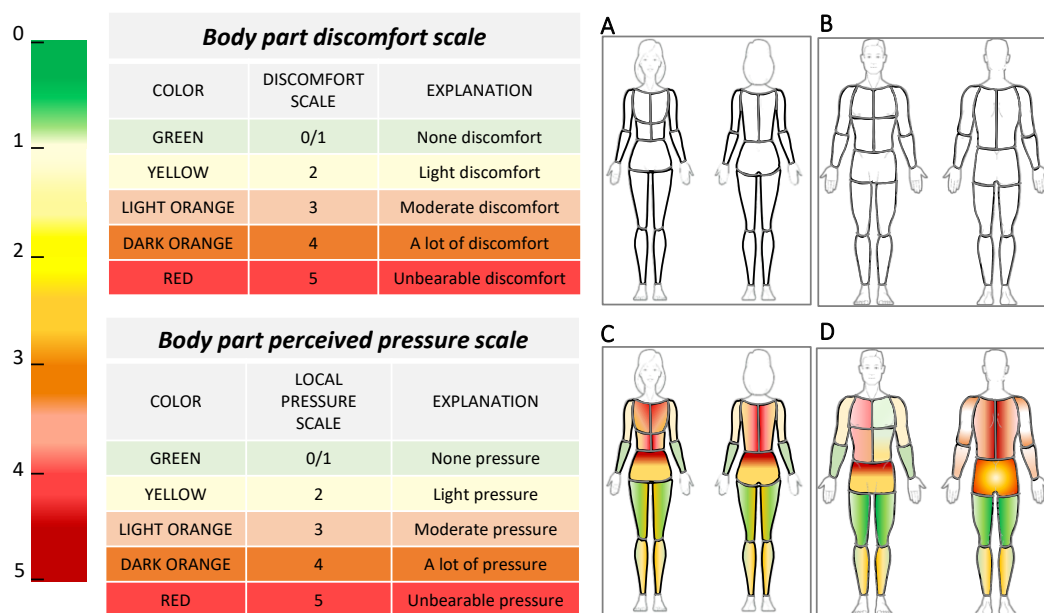


Figure C.2: Body part discomfort and perceived pressure scales description. Explanation of the meaning of the different numbers in the range 0-5 that can be assigned by the subject during the evaluation. Graphical maps of female (A-C) and male (B-D) human body with several body parts that can be used for the representation. A-B Graphs depicted the human body without mapping the evaluation while graphs C-D reported an example of colored mapping of local human body parts.